An investigation into the source and distribution of bromoform in the southern African and Southern Ocean marine boundary layer

Brett Kuyper

Thesis presented for the degree of
DOCTOR OF PHILOSOPHY
in the Department of Oceanography

UNIVERSITY OF CAPE TOWN

February 2014
This thesis is the author's own work.

Supervised by

Prof. C. J. C Reason
Dr. H. N. Waldron
Dr. C. J. Palmer
Mr. C. Labuschagne

Plagiarism Declaration

I declare that:

i the above thesis is my own unaided work, both in concept and execution, and that apart from the normal guidance from my supervisors, I have received no assistance except as stated below.

ii neither the substance nor any part of the above thesis has been submitted in the past, or is being, or is to be submitted for a degree at this University or at any other University, except as stated below.

- Parts of Chapters 2 and 3 have previously been published in scientific journals with reference below
  - Kuyper, B., Labuschagne, C., Philibert, R., Moyo, N., Waldron, H., Reason, C., and Palmer, C. (2012). Development of a simplified, cost effective GC-ECD methodology for the sensitive detection of bromoform in the troposphere. *Sensors*, 12(10):13583–13597.
- Part of Chapter 5 has been previously published as a Master's thesis at the University of Cape Town. M. Nguvava was responsible for the culturing of diatom species used in the nutrient limitation experiment.
  - Nguvava, M. (2012). The effect of nutrient limitation and oxidative stress on bromoform production from axenic cultures of marine diatoms. Master's thesis, University of Cape Town.

Abstract

Bromoform is a climatically important atmospheric trace gas. It is released by macro- and microalgae into the ocean, and rapidly transferred to the atmosphere, where bromoform undergoes rapid photolysis yielding bromine radicals. These bromine radicals are known to participate in catalytic destruction of ozone at all levels throughout the atmosphere. This is especially important in the lower stratosphere. This destruction of ozone results in changes in the oxidative potential and decreases the greenhouse effect of the troposphere.

A task-specific gas chromatograph with electron capture detector system, developed in-house, was used for the separation and quantitative detection of bromoform mixing ratios from environmental air samples. A custom thermal desorption unit was designed and built for use in this system along with a graphical user interface for the real-time collection and display of data. A limit of detection of 0.79 ± 0.09 ppt, with an overall precision of 12.7 % was achieved with this GC system and method.

The quantitative detection of bromoform mixing ratios was made at the Cape Point, Global Atmospheric Watch station over a one month period in early spring 2011. Bromoform mixing ratios detected ranged between 2.29 and 84.7 ppt with a mean of 24.7 ppt. These mixing ratios appear to be generally elevated compared to previous studies, however, were still within the maximum values published. Local kelp beds around Cape Point and possibly anthropogenic inputs from Cape Town are likely to have been the dominant source of bromoform measured there, caused by changes in wind speed.

A series of experiments were performed to explore the role of the bromoperoxidase enzyme in providing antioxidant protection in two diatom species (*Phaeodactylum tricornutum* and *Chaetoceros neogracile_cf*) under different oxidative stresses. Carbon dioxide and nitrate limitation were induced as oxidative stresses. The mean per cell bromoform concentrations during the growth phase of the carbon limitation were 2.73 x 10^{-17} and 8.68 x 10^{-18} mol cell^{-1} for *C. neogracile_cf* and *P. tricornutum*, respectively. This decreased to 2.94 x 10^{-18} and 3.87 x 10^{-18} mol cell^{-1} during the limited phase. Bromoform production decreased to zero for *P. tricornutum* during the nitrate limitation. These experiments suggest that in these species bromoperoxidase is not utilised as an antioxidant pathway when under these nutrient limiting conditions.

Acknowledgements

I would like to thank the following organisations for providing project funding and ensuring that the research aims were achieved:
The START Foundation for the initial start up funding and running costs of the gas chromatograph and laboratory.
The South African Weather Service for providing infrastructure, space and intellectual support.
CSIR for providing funding for the improvement of the gas chromatograph system.
The NRF for a Scarce Skills bursary and MA-RE for top-up bursaries.
The UCT Oceanography Wet Laboratory for providing general running expenses of the system and intellectual support.
ICEMASA Programme, who funded the equipment used in the laboratory experiments.

This project would not have been possible without the constant support of my supervisors Chris Reason and Howard Waldron from the Department of Oceanography, Dr Carl Palmer from ACCESS and Casper Labuschagne from the South African Weather Service. Thank you for all your time, effort and support over the years – your insights, support and guidance have seen this project to completion.

There are a number of people without whom this project would not have progressed – again I am thankful: Ernst Brunke at the South African Weather Service for his support in both time and equipment, encouragement and brilliant insights; Eva Bucciarelli, who supervised the culturing of axenic marine diatoms for experimentation – her support and insight proved invaluable; Sean Murray, Hayley McIntosh and Sherry Bremner for helping me with numerous bits of computer code; and Kobus Botha for practical assistance with integration of chromatography peaks in MATLAB. Brett Melville for all the work that they put in going over the thesis. Finally I would like to thank my mother, Sue Kuyper, for all the support over the many years. This has been a long and often tiresome journey, but it has come to fruition. Thank you for always being there!

A big thank you to Nicholas Moyo, Raïssa Philibert and Mariam Nguvava, the students who I have worked alongside who often provided valuable insights to the project. The development of the gas chromatography system might have floundered were it not for the support of the glass blower at UCT who tirelessly replaced broken bits of glassware and the Physics workshop who provided necessary tools and

excellent workmanship in the building of the permeation oven.

A final thanks to Ben Loveday, Hayley Evers-King, Theo Smith, Kate Larmuth and Leslie Roberson for many climbs and runs in the forest; Ian Tunbridge and Chris Warner for the numerous cycles all over the Cape. These helped keep me sane during the many hours of madness! Your support and friendship have proved invaluable along the road to completion. A final word of thanks go to Angela Forbes for standing by me and making life a happier place.

Contents

List of Figures

List of Tables

List of Abbreviations

°C	Degrees Celsius
^{63}Ni	Nickel radioactive isotope
^{222}Rn	Radon
1/Hk_a	Airside resistance
1/k$_w$	Waterside resistance
A	Amperes
AC	Alternating current
ADC	Analogue to digital conversion
Ap	Peak area
a.s.l	Above sea level
b	Base of triangle
BrO	Bromine monoxide
BrPO	Bromoperoxidase enzyme
Br$_y$	Inorganic bromine
BWD	Baseline wind direction, 170 – 320 degrees
CBD	Central business district
C$_{cell}$	Cell abundance per litre
CG	Carrier gas
CFCs	Chlorofluorocarbons
CH_2I_2	Diiodomethane
CH_3Br	Methyl bromide

$CHBr_3$	Bromoform
CH_2Br_2	Dibromomethane
$CHBr_2Cl$	Chlorodibromomethane
$CHBrCl_2$	Bromodichloromethane
Chl-a	Chlorophyll-$\boldsymbol{a}$
ClO	Chlorine monoxide
Cnx	$Chaetoceros\ neogracile\_cf$ x = replicate A, B or C
CO	Carbon monoxide
CO_2	Carbon dioxide
D	Molecular diffusivity
D	Cell diameter
DB	Dura Bond, column film
DC	Direct current
DMSP	Dimethylsulfoniopropionate
DOM	Dissolved organic matter
ECD	Electron capture detector
$\boldsymbol{F}$	Gas flux rate $(mol\ m^{-2}\ s^{-1})$
GAW	Global Atmospheric Watch
GC	Gas chromatograph
GUI	Graphical user interface
$\boldsymbol{h}$	Peak height
$\boldsymbol{h\nu}$	Determination of solar energy based on Plank's constant $\boldsymbol{h}$ and frequency $\boldsymbol{\nu}$
$\boldsymbol{H}$	Henry's Law constant
H_2O_2	Hydrogen peroxide
He	Helium
HCl	Hydrochloric acid
HCO_3	Bicarbonate

HO2	Hydroperoxy radical
HOBr	Hypobromous acid
hrs	Hours
HYSPLIT	Hybrid Single Particle Lagrangian Integrated Trajectory model
k	Gas transfer velocity
K	Kelvin
kPa	Kilopascals
LOD	Limit of detection
M	Molar concentration
MBL	Marine boundary layer
mBq	Millibecquerel
MFC	Mass flow controller
MODIS	Moderate Resolution Imaging Spectroradiometer instrument
MS	Mass spectrometer
mV	Millivolts
N	Number of theoretical plates
N_2	Nitrogen gas
$N_{2(l)}$	Liquid nitrogen
N_2O	Nitrous oxide
NO_3	Nitrate
NO_x	Nitric oxide and nitrogen dioxide (NO + NO_2)
nA	Nanoamperes
NaOH	Sodium hydroxide
$NaHCO_3$	Sodium bicarbonate
O_2	Oxygen
O_3	Ozone
OD	Outer diameter

OH	Hydroxyl radical
PAR	Photosynthetically active radiation
ppb	Parts per billion
ppt	Parts per trillion
PTFE	Polytetrafluoroethylene
Ptx	$Phaeodactylum\ tricornutum$ x = replicate A, B or C
R	Chromatographic resolution
RH	Relative humidity
ROS	Reactive oxygen species: superoxide O_2, H_2O_2 and OH
SAHP	South Atlantic High Pressure
SAWS	South African Weather Service
Sc	Schmidt number
TDU	Thermal desorption unit
TP	Temperature programme
t_m	Hold-up time
t_R	Retention time
t'_R	Adjusted retention time
μ	Specific growth rate
u	Wind speed
UT / LS	Upper troposphere / lower stratosphere
UV	Ultraviolet radiation
ν	Kinematic viscosity
V	Volts
V_{cell}	Cell volume, (μm^{-3})
VOCs	Volatile Organic Compounds
W m^{-2}	Watts per metre squared

Chapter 1

Introduction

Bromoform ($CHBr_3$) is one of a suite of biogenic halocarbons produced by macro- and microalgae in the surface ocean (Gschwend et al., 1985; Barrie and Platt, 1997; Carpenter and Liss, 2000; Tokarczyk and Moore, 1994) and is thought to be the dominant transport of organic bromine from the ocean to the atmosphere (Quack and Wallace, 2003). It is suggested that bromoform may be the largest source of inorganic bromine (Br_y) to the upper troposphere / lower stratosphere (UT / LS) region, where it is involved in catalytic ozone (O_3) depletion. Inorganic bromine in this region may account for a larger fraction of ozone depletion than chlorine radicals (Dvortsov et al., 1999; Carpenter et al., 2012). The measurement of bromoform both in the ocean and the atmosphere has mostly been constrained to the Northern Hemisphere with a few research cruises to the Southern Ocean (Ziska et al., 2013; Quack and Wallace, 2003). The Northern Hemisphere bias in measurements is largely due to a lack of physical infrastructure in the Southern Hemisphere, particularly in southern Africa with which to take measurements and skilled scientists who can run the relevant research programmes.

A modelling study of bromoform production in the tropics has suggested that the southern African region (south of 20° S), including the southern Benguela upwelling system, may be a significant source of atmospheric bromoform (Palmer and Reason, 2009). However, the validation for this and other atmospheric bromoform models suffer from a global lack of measurements (Palmer and Reason, 2009; Warwick et al., 2006). Variations in the nutrient concentrations may affect the quantity of bromoform produced, especially in upwelling regions such as the southern Benguela. It has been suggested that an increased ocean stratification due to climate change may result in decreased nutrient concentrations in the surface ocean (Behrenfeld et al., 2006; Carpenter et al., 2011). Nutrient limitation in macro- and microalgae results in an oxidative stress within the algae, possibly influencing the rates of bromoform production (Küpper et al., 2008; Vardi et al., 1999; Sunda et al., 2002).

This project focuses on three key areas in an attempt to address gaps in the global knowledge pool relating to the measurement of bromoform in the atmosphere and some of the possible conditions under which it is produced. The following gaps identified in the global knowledge are addressed by this project:

1. The development of a cost effective system and method for the sensitive quantitative detection of

bromoform in environmental air and seawater samples (Chapter 3).

Bromoform and halocarbons have not been measured on a long-term basis in the atmosphere around southern Africa. This lack of long-term measurement has been due to a lack of physical infrastructure, namely instrumentation with which to make measurements, and skilled scientific training necessary to operate instrumentation. The goal was to develop an instrument and method capable of quantitatively detecting bromoform in marine air samples. A secondary goal was to develop the human capacity in environmental analytical chemistry and ocean biogeochemistry to interpret and publish the results.

2. The detection and quantification of bromoform in the atmosphere at Cape Point and an examination of the mechanisms driving variability (Chapter 4).

Cape Point is a unique, remote location from which to measure bromoform mixing ratios in the atmosphere. The Global Atmospheric Watch (GAW) station, operated by the South African Weather Service (SAWS), receives air from the Benguela upwelling system, the Southern Ocean and occasionally anthropogenic influences from the city of Cape Town. The sub-tropical setting of Cape Point may make this an important atmospheric bromoform source. The project aimed to quantify the amount of bromoform found in the atmosphere at Cape Point and examine the likely sources. The measurements made of bromoform at Cape Point were also to highlight the importance of this under-sampled region and to demonstrate the ability of the system and method developed at the University of Cape Town to work in a field setting.

3. The examination of the effect of two oxidative stresses on the production of bromoform from microalgae in a laboratory setting (Chapter 5).

The variability of local sources such as the Benguela may be affected by changes in the rate of bromoform production by microalgae. Furthermore the exact mechanism of bromoform production remains unclear as do the reasons for production of this halocarbon in microalgae. To examine the role of oxidative stress induced by nutrient limitation, a series of laboratory culture experiments were performed. The cultures were subjected to carbon and nitrate limitations occurring in separate batches. It is hypothesised that the bromoperoxidase enzyme found in macro- and microalgae is responsible for the formation of bromoform as a mechanism of reducing local oxidative stress in the algae.

1.1 Background and literature review

1.1.1 Atmospheric bromine and ozone chemistry

The discovery of the 'hole' in the ozone layer in the 1980s has led to changes in the understanding of atmospheric chemistry (Farman et al., 1985). Stratospheric halide chemistry has become an important field in describing the processes involved in polar ozone depletion. Research initially pointed to a group of anthropogenically produced halogenated hydrocarbons (or halocarbons) called CFCs as the cause (Molina and Rowland, 1974; Crutzen, 2006). These photosensitive halocarbons, which accumulate through the winter, react strongly at polar sunrise causing massive ozone depletion to occur (Barrie and Platt, 1997). The halocarbons are photolysed, producing halogen radicals which are known to initiate catalytic ozone destruction (Reactions 1.1 and 1.2).

$$CFCl_3 + h\nu \rightarrow CFCl_2 + Cl \tag{1.1}$$

$$Cl + O_3 + h\nu \rightarrow ClO + O_2 \tag{1.2}$$

$$ClO + O_2 + h\nu \rightarrow Cl + 2O_2 \tag{1.3}$$

The extent of seasonal ozone depletion observed in Antarctica could not be supported by the anthropogenic halide chemistry alone (Jacob, 1999; Molina and Rowland, 1974). Examining hemispheric differences resulted in the discovery of self-reactions involving chlorine monoxide (C*l*O) and a second catalytic cycle involving bromine radicals (Jacob, 1999). Chlorine and bromine radicals both independently react with O_3 to form C*l*O and BrO and O_2 (Reactions 1.4 and 1.5). The bromine monoxide and chlorine monoxide then undergo a rapid reaction, releasing the halogen radicals back into the stratosphere and therefore resulting in the catalytic destruction of ozone (Reaction 1.6). Due to the high C*l*O concentrations found in the polar stratosphere, this catalytic depletion process accounts for approximately 30 % of the total ozone loss (Jacob, 1999).

$$Cl + O_3 \rightarrow ClO + O_2 \tag{1.4}$$

$$Br + O_3 \rightarrow BrO + O_2 \tag{1.5}$$

$$BrO + ClO \rightarrow Br + Cl + O_2 \tag{1.6}$$

When examining this catalytic destruction, the source of the chlorine and bromine radicals needs to be considered. Most of the inorganic chlorine is derived from the photolysis of CFCs. A concentration of the halogen radicals is reported to occur through the formation of polar stratospheric clouds in the winter. Long-lived halocarbons such as methyl bromide were thought to be the dominant source of inorganic bromine in the stratosphere (Jacob, 1999). However, recent attention has shifted to short-lived biogenically produced bromine halocarbons as a possibly significant source of additional halogen radicals to the stratosphere (Liu et al., 2011).

Due to the short atmospheric lifetime and slow mixing across the tropopause, biogenic halocarbons were initially discounted as a significant source of inorganic bromine in the stratosphere (Dvortsov et al., 1999; Warwick et al., 2006; Carpenter et al., 2012). There has been some debate regarding the proportional contributions to the inorganic bromine loading from long-lived halocarbons such as methyl bromide (CH_3Br) and short-lived biogenic halocarbons (Dvortsov et al., 1999; McGivern et al., 2002; Warwick et al., 2006). It was thought that the majority of biogenic sources such as bromoform were entirely photolysed in the lower troposphere. However, aircraft measurement and modelling studies have reported the detection of bromoform in the UT / LS region (Dvortsov et al., 1999; Hossaini et al., 2010; Sinnhuber and Folkins, 2005, 2006; Marécal et al., 2012).

Biogenic sources of bromine halogens may contribute 5 – 40 % of the bromine present in the atmosphere and are therefore of particular interest to atmospheric chemistry (Andrews et al., 2013). Bromoform is reported as the dominant biogenic source of inorganic bromine to the upper troposphere and the stratosphere; however, the main source of inorganic bromine in the lower troposphere (marine boundary layer) is thought to be the autocatalytic release of bromine from sea-salt aerosols (Quack and Wallace, 2003; Yang et al., 2005; Carpenter et al., 2012; Saiz-Lopez et al., 2012; Dvortsov et al., 1999). The longer atmospheric lifetime of bromoform suggests that it passes through the lower troposphere whereas inorganic bromine from sea-salt aerosol is formed directly from the aerosols. It has been noted, however, that the release of inorganic bromine is limited by the acidity of the sea-salt aerosol. In cases where the sea-salt aerosol acidity is low, limiting inorganic bromine, the release of inorganic bromine from the decay of bromoform may form the dominant source within the MBL (Quack and Wallace, 2003; Carpenter et al., 2012). Ozone contained within the marine boundary layer (MBL) was discovered in the late 1980s and it is thought that this ozone plays an important role in the oxidising capacity of the lower atmosphere (Barrie et al., 1988). Halocarbons released from macro- and microalgae were initially implicated in the marine boundary layer depletion of ozone; however, inorganic bromine from sea-salt aerosols is currently thought to play a dominant role (Barrie et al., 1988; Carpenter et al., 2012). In the polar troposphere it has been suggested that the interaction of inorganic bromine with sea ice results in the dominant depletion mechanism (Douglas et al., 2012; Sherman et al., 2012).

The bromoform measurements in the UT / LS region exhibit a large range of concentrations from less than 1 to more than 8 ppt (Marécal et al., 2012). Model estimates of the bromoform contribution to inorganic bromine loading in the lower stratosphere region cover a similar range at between 0.4 – 7.0 ppt (Dvortsov et al., 1999; Nielsen and Douglass, 2001; Sinnhuber and Folkins, 2006; Hossaini et al., 2010; Warwick et al., 2006; Tegtmeier et al., 2012). The variations in model estimates are primarily due to different assumptions regarding source chemistry and mechanics in the models, which makes direct comparison difficult (Aschmann et al., 2011). The global bromoform concentration is calculated in the models from either the known sink processes or extrapolated from limited surface measurements (Warwick et al., 2006). Modelling studies that have utilised the sink processes tend to estimate a lower global source strength than models based on the extrapolation of data (Warwick et al., 2006; Ziska et al., 2013). The limited measurements of bromoform across the globe and atmosphere result in great uncertainty within

model estimates (Nielsen and Douglass, 2001; Quack and Wallace, 2003; Aschmann et al., 2011; Andrews et al., 2013). It is therefore of great importance to close the gap of global measurements in order to improve the model estimates (Palmer and Reason, 2009; Andrews et al., 2013; Ziska et al., 2013).

Deep convection in the tropics is reported to rapidly transport bromoform to the UT / LS region (Dvortsov et al., 1999; Andrews et al., 2013). The reported ozone depletion potential of bromine is approximately 50 times that of chlorine, therefore, the low background bromoform mixing ratios reported (Sec. 1.4) may still make bromine halocarbons a significant source of inorganic bromine (Quack and Wallace, 2003). It has been contended that the bromoform source of inorganic bromine is strongest in the lowest portion of the stratosphere and upper troposphere (Nielsen and Douglass, 2001; Dvortsov et al., 1999). A model estimate suggests that bromoform contributes approximately 15 % to the total inorganic bromine loading in the stratosphere (Nielsen and Douglass, 2001). However, the contribution in the lower stratosphere is estimated at between 45 – 50 % (Nielsen and Douglass, 2001; Dvortsov et al., 1999). Unlike the more stable long-lived halons, bromoform begins to dissociate in the lowermost stratosphere, impacting this region significantly but not deeper regions, suggesting that biogenic halocarbons such as bromoform significantly impact the lower stratosphere (< 17 – 20 km) while source gases such as methyl bromine affect the upper layers (Dvortsov et al., 1999; Bridgeman et al., 2000; Sturges et al., 2000).

Inorganic bromine is released from bromoform via photodissociation and the reaction with hydroxyl radicals (OH), which results in bromoform atmospheric lifetimes of 25 – 35 and 100 days, respectively (Quack and Wallace, 2003; Carpenter and Liss, 2000; Liu et al., 2011; McGivern et al., 2002). These bromine radicals released from photolysis reduce ozone to oxygen in the presence of UV, forming bromine monoxide (Reaction 1.5). Then either through the catalytic reaction involving C*l*O outlined above, or reaction with HO_2, inorganic bromine is released and the catalytic destruction of ozone occurs (e.g., Reactions 1.6 and 1.7 – 1.9).

$$BrO + HO_2 \rightarrow HOBr + O_2 \tag{1.7}$$

$$HOBr + h\nu \rightarrow OH + Br \tag{1.8}$$

$$\text{Net:} \quad O_3 + HO_2 + h\nu \rightarrow 2O_2 + OH \tag{1.9}$$

Ozone in the upper troposphere is reported to contribute to the atmospheric radiative forcing (WMO, 2011). This radiative forcing may be decreased by approximately 10 W m^{-2} through bromoform mediated ozone depletion in this region. Atmospheric chemistry models suggest that the ozone removal rate in the tropical marine troposphere is larger than previously assumed by up to 30 %, and that this increased removal rate is due to local halogen chemistry (Saiz-Lopez et al., 2012). While the loss of upper troposphere and MBL ozone in the tropics due to halogen chemistry has only recently been shown to be significant (Read et al., 2008), biogenic halogens in the polar regions have long been implicated, particularly in spring (Berg et al., 1984; von Glasow and Crutzen, 2003; Warwick et al., 2006). This

suggests that halogen chemistry, including bromoform chemistry, in the tropical atmosphere may play a significant role in climate change, with increased bromoform possibly leading to a negative feedback. There is still much uncertainty regarding the global source strength of bromoform to the atmosphere and transport to the upper troposphere, thus creating the need for more measurements in this potentially important region (Warwick et al., 2006; Saiz-Lopez et al., 2012).

1.2 Sources of bromoform

Bromoform is predominantly produced biogenically by macro- and microalgae in the surface ocean. The majority of this bromoform is transferred to the atmosphere via sea-air gas exchange (Sec. 4.2). In this section we examine the reported sources of bromoform from macroalgae, microalgae and anthropogenic processes. Regional variations in the processes determining the bromoform rate of production and its transfer to the atmosphere results in an uneven global source distribution (Quack and Wallace, 2003; Ziska et al., 2013).

1.2.1 Macroalgae

The production of bromoform in macroalgae in the coastal oceans has long been reported (e.g., Gschwend et al., 1985; Manley et al., 1992). The bromoform produced by macroalgae may be delivered to the ocean water or directly to the atmosphere, in the case of inter-tidal species (Quack and Wallace, 2003). The production rates of bromoform are reported to be species dependent and dominated by red algae (Carpenter and Liss, 2000; Palmer, 2006). Measured bromoform production rates are reported to vary between 4 and 5000 pmol $CHBr_3$ h^{-1} (Manley et al., 1992; Nightingale et al., 1995; Pedersén et al., 1996). Due to the large global biomass, it is estimated that brown algae contribute a mean of 1.6 Gmol $CHBr_3$ yr^{-1}, or approximately 60 % of the total annual macroalgal production (Carpenter and Liss, 2000; Quack and Wallace, 2003). A higher rate of production is reported in tropical and subtropical species than in polar species. This may be an adaptation by tropical species to cope with the increased shortwave radiation found in this region (Laturnus, 1996; Quack and Wallace, 2003). The local environmental conditions, such as the amount of shortwave radiation or ozone, are reported to affect the production rate, which creates an uneven source distribution (Quack and Wallace, 2003). Within the global annual production estimate, the rate of production has been shown to fluctuate on a seasonal scale, with a maximum in summer and minimum during winter. These seasonal fluctuations in bromoform production rate are reportedly linked to variations in the bromoperoxidase enzyme (Itoh and Shinya, 1994). This suggests that the formation of bromoform is heavily dependent on this enzyme and its functional capacity (Carpenter and Liss, 2000; Quack and Wallace, 2003; Itoh and Shinya, 1994; Laturnus, 1996). The elevated bromoform emissions during summer are suggested to occur due to visible tissue decay (Quack and Wallace, 2003).

Physiological studies examining the distribution of bromoform production in macroalgae suggest that older sections of the thalli or blade are more prolific producers of bromoform than younger growing sections. Furthermore, the blade and the holdfast of selected Antarctic species were found to be the dominant

release points, possibly resulting in a subsurface maximum occurring in extensive kelp beds (Krysell, 1991; Laturnus, 1996; Quack et al., 2004; Nightingale et al., 1995). In this regard the surface may become depleted with respect to the subsurface through gas flux to the atmosphere, creating the above-mentioned concentration gradient. While bromine has been shown to be stored in the chloroplasts of certain species of red algae, bromoform has not been found. This suggests that bromoform is produced *de novo* and as required (van Hofsten and Pedersén, 1978; Nightingale et al., 1995; Pedersén et al., 1996; Collén et al., 1994). The seawater concentration of bromoform has been shown to vary between the coastal and the open ocean environments, with coastal concentrations up to 100 times those measured in the open ocean (Carpenter and Liss, 2000; Quack and Wallace, 2003).

1.2.2 Microalgae

Bromoform has been measured in the open ocean, away from known coastal sources and in upwelling systems. It has been suggested that this bromoform, measured in the open ocean, may be advected from areas of great production, such as coastal regions (Quack and Wallace, 2003). Although the horizontal advection of high concentrations of bromoform is possible, it is more probably the result of local microalgal production (Quack et al., 2004), which under laboratory conditions has been shown to occur (Tokarczyk and Moore, 1994). In this regard, upwelling regions and frontal boundaries are suggested to display elevated bromoform concentrations due to the abundant microalgal species found in these regions (Carpenter et al., 2009; Hughes et al., 2009). Coastal upwelling systems cover approximately 5 % of the world ocean surface and the Benguela is one of the most productive of such systems (Jennings et al., 2001; Kudela et al., 2005). A review of the literature shows that atmospheric mixing ratios above upwelling systems range from about 0.5 – 6.7 ppt with numerous reports indicating mixing ratios of between 2 and 5 ppt and a maximum of 24 ppt (Class and Ballschmiter, 1988; Quack and Wallace, 2003; Carpenter et al., 2007a).

The rate of bromoform microalgae in laboratory cultures has been shown to be dependent on the growth stage, with a maximum during the exponential growth phase. This production rate decreased by more than half during the senescent phase (Tokarczyk and Moore, 1994). Diatoms in microalgal blooms have been strongly linked with the release of bromoform (Tokarczyk and Moore, 1994; Hughes et al., 2009). In this regard, size fractionation studies of polar populations found that pico-plankton (0.4 – 3 μm) were the dominant bromoform producers (Quack and Wallace, 2003; Abrahamsson et al., 2004).

The global bromoform production rates by microalgal species is not well quantified. Bromoform measured in the open-ocean is often associated with upwelling regions and frontal boundaries. The production of bromoform by tropical species is reported to be low. In polar regions the dominant source of bromoform is reported from microalgal production (Quack and Wallace, 2003). Microalgae are therefore probably the dominant source of bromine to the polar atmosphere. Laboratory studies of cold water species found that the rate of production was linked to the stage of growth. The measured bromoform production rates for *Nitzschia sp.* and *Porosira glacial* were found to be 48.9 – 72 pmol $CHBr_3$ (mg Chl-

a)$^{-1}$ h^{-1} and 6 – 20.5 pmol $CHBr_3$ (mg Chl-*a*)$^{-1}$ h^{-1} during the exponential growth and senescent phases, respectively (Tokarczyk and Moore, 1994). While the per gram production rate of microalgae is reported to be significantly smaller than that of macroalgae, the larger global distribution of microalgae may make the annual contribution comparable between these sources. It is estimated that microalgae from coastal, polar and open ocean regions contribute a combined 0.6 Gmol $CHBr_3$ yr^{-1} (Quack and Wallace, 2003). Other authors have estimated a similar source strength from polar microalgae alone (Sturges et al., 1992). It has been suggested that further work is required to separate and understand the full relative contributions of macro- and microalgae to the atmosphere (Warwick et al., 2006).

1.2.3 Bacteria

The production of bromoform by marine bacteria has been shown to occur (Sturges et al., 1993). Previously, there are no other reports in the literature of bacterial bromoform production (Gschwend et al., 1985). The global contribution of bromoform from marine bacteria may prove to be a significant source (Wever and Van der Horst, 2013). Although an order of magnitude smaller than microalgae, it is estimated that cyanobacteria in the Baltic sea contribute 110 Mg $CHBr_3$ yr^{-1} to the global atmospheric bromoform source strength (Wever and Van der Horst, 2013).

1.2.4 Anthropogenic

While the majority of bromoform is thought to be biogenic in origin, there are a number of known anthropogenic sources to the atmosphere (Carpenter and Liss, 2000). Globally anthropogenic sources of bromoform are estimated to result in a flux of approximately 0.3 - 1.1 Gmol Br yr^{-1}, approximately 10 % of the global flux (Quack and Wallace, 2003). This fraction of the total bromoform is small in comparison to global natural sources; however, it may be significant on local scales (Quack and Suess, 1999; Quack and Wallace, 2003). The suggested dominant anthropogenic sources include the treatment of water, desalination of water, and the discharge from power plants (Yokouchi et al., 1997; Quack and Wallace, 2003; Liu et al., 2011).

Chlorination and ozonation are the main methods used for water treatment resulting in the formation of bromoform. In the case of the former, bromine, in the water, is oxidised by the added chlorine, forming hypobromite. Bromoform is then formed by the reaction of organic matter with the hypobromite. The production of bromoform from the treatment of water is estimated to produce 1 – 80 nmol l^{-1} $CHBr_3$ and 60 – 200 nmol l^{-1} $CHBr_3$ for fresh water and seawater, respectively. The higher production of bromoform in seawater is probably due to the large bromine and dissolved organic matter (DOM) concentrations (Quack and Wallace, 2003). The seasonal variation in DOM concentrations are thought to result in elevated bromoform concentrations during the summer. The majority of seawater treated by chlorination is to prevent biofouling and used for the cooling of coastal nuclear power plants. Globally coastal nuclear power plants use 142 km^3 seawater per year, resulting in an estimated annual source strength of 25 – 85 Mmol Br from these facilities. Water treatment for drinking and wastewater is estimated to globally contribute $\sim$0.35 Gmol Br yr^{-1}. This makes water treatment one of the largest

anthropogenic sources of bromoform to the atmosphere. Desalination of water, on the other hand, is estimated to contribute 2 Mmol $CHBr_3$ to the atmosphere annually. The majority (98 %) of the bromoform produced in the desalination process is liberated directly to the atmosphere (Quack and Wallace, 2003).

It has been suggested that biomass burning may be of importance to many atmospheric and biogeochemical cycles (Gregory et al., 1996; Andreae et al., 1996). The release of halocarbons and other important atmospheric gases might occur through either the direct release of these gases, or alternatively the precursors of these gases may be released during biomass burning (Gregory et al., 1996). The stage of the fire and duration in each phase may play a role in the release of different compounds associated with the varying stages, with halocarbons being preferentially released during the smouldering phase (Andreae et al., 1996). While biomass burning has not been shown to result in the production of bromoform, during a set of wild fires in Cape Town data collected suggested that fynbos, when burnt, might provide a source of bromoform to the atmosphere. The Cape Floral Kingdom covers an estimated 82 892 km^2 (Cowling and Pressey, 2003) and could prove to be a substantial source of bromoform to the atmosphere, if it is released during burning. This is especially pertinent as hundreds of square kilometres of fynbos are burnt on an annual basis. A small study was performed at the University of Cape Town to examine whether bromoform is released from burning fynbos. The results of the study were inconclusive (Moyo, 2010).

1.2.5 Factors affecting biogenic release

It has been found that the production of bromoform in macro-and microalgae is linked with exposure to oxidative stress. Through the formation of hydrogen peroxide, photosynthesis may dominate the oxidative stresses induced in algae (Collén et al., 1994; Pedersén et al., 1996). Removal of the intracellular hydrogen peroxide is thought to result in the formation of bromoform. Remnant intracellular hydrogen peroxide at the end of daylight may be responsible for the production of bromoform in the dark (Sec. 4.1.3).

Atmospheric exposure of macroalgae to H_2O_2, ozone, OH, and nutrient limitation have all been shown to result in the formation of bromoform (Collén et al., 1994; Carpenter and Liss, 2000; Palmer et al., 2005; Quack and Wallace, 2003). It has been suggested that stresses are maximised at low tide. The greater the tidal range the more macroalgae are likely to be exposed at low tide. The timing of the tide might affect the amount of bromoform produced through variations in the level of stress induced. The flooding phase of the tide has been linked to an increase in the production of bromoform in macroalgae in the North Sea. It is thought that in a desiccated state macroalgae are not able to produce bromoform, alternatively that production occurs extra-cellularly since bromine might not be stored for later use (Nightingale et al., 1995).

Algal exposure to surface ozone, typically at low tide, has been reported to result in increases in bromoform production (Palmer et al., 2005). This production is counteracted by the destructive effect ozone has on bromoform under sunlight. The hydroxyl radical (OH) might act in a manner similar to ozone and perform roles as both a stimulant and sink of bromoform. The oxidative stress as a function of

nutrient limitation (Sunda et al., 2002) has been shown in the literature to act through varying mechanisms. The effect of nutrient limitation on two species of phytoplankton is explored in Chapter 5.

1.3 Biogeochemical cycling of bromoform

Bromoform is the dominant halocarbon produced by micro- and macroalgae in the oceans and is important in the cycling of bromine through the Earth system (Quack and Wallace, 2003; Carpenter and Liss, 2000). This section examines the bromoform diurnal cycle, oceanic sinks and the sea-air gas flux. Full details on the biochemistry of bromoform formation are discussed in Chapter 5.

1.3.1 Bromoform diurnal cycle in the atmosphere

It has been suggested that in the atmosphere bromoform mixing ratios exhibits a strong diurnal pattern. An increase in mixing ratios has been recorded during the morning which is linked with increasing sunlight (Ekdahl et al., 1998). Bromoform concentrations in the ocean have been reported to increase in the morning (Carpenter et al., 2000; Abrahamsson et al., 2004). At Gran Canaria both oceanic and atmospheric measurements were taken. The atmospheric bromoform mixing ratios exhibit the same features as the oceanic concentrations, only on a shorter time scale (Ekdahl et al., 1998). This suggests that the oceanic diurnal cycle largely determines the atmospheric cycle. Consequently the mixing ratios decreased during the course of the afternoon. The rate of decrease in the afternoon was greater than the production rate in the morning. The mechanism responsible for the rapid removal has not been identified (Abrahamsson et al., 2004). In measurements taken over a diurnal cycle at two sites, Gran Canaria and in the Southern Ocean, an evening peak in bromoform mixing ratios has been noted (Ekdahl et al., 1998; Abrahamsson et al., 2004). It is thought that this night time increase in mixing ratios may be a function of either an accumulation of bromoform as the rate of photochemical production is decreased or a reaction from remnant intracellular hydrogen peroxide. Since the rate of photolysis decreases to zero at night this will result in an accumulation of bromoform released into the atmosphere as there is no destruction. This accumulation might be recorded as an increase in the bromoform mixing ratio. A complete account of the diurnal cycle of bromoform can be found in Chapter 4.1.3.

1.3.2 The relationship of bromoform and chlorophyll-*a*

Given the inherent difficulties associated with making bromoform measurements in the open ocean, numerous proxies such as Chlorophyll-*a* (Chl-*a*) have been suggested (Quack and Wallace, 2003). In this regard, some bromoform measurement studies performed in coastal upwelling and open ocean frontal boundary regions have found a direct positive correlation between bromoform and Chl-*a* (Carpenter et al., 2009; Manley and Barbero, 2001; Schall et al., 1996; Colomb et al., 2008; Paul and Pohnert, 2011). However, other measurement studies did not find any such relationship, or a tenuous one at best (Laturnus, 1996; Hughes et al., 2009; Palmer and Reason, 2009; Liu et al., 2011). It has been suggested that the link between Chl-*a* and bromoform might be masked by local anthropogenic contamination or by the horizontal advection of water containing elevated mixing ratios, especially in coastal regions (Quack and Wallace,

2003; Carpenter et al., 2000). The production of bromoform from macroalgal beds might be advected off-shore, particularly in upwelling regions, creating a remote source and hence masking local production by microalgae, thus obscuring a relationship between Chl-*a* concentration and bromoform (Carpenter et al., 2000). Therefore, until a greater understanding of the link between Chl-*a* and bromoform is achieved, the measurement of Chl-*a* does not make a reliable proxy for global bromoform concentrations. More global measurements of bromoform concentrations are required to achieve the above understanding and to reduce uncertainty within global chemistry models that rely on sparse data coverage (Warwick et al., 2006; Palmer and Reason, 2009).

1.3.3 Oceanic sinks of bromoform

The transfer of bromoform from the ocean to the atmosphere through sea-air gas exchange forms the largest known loss process. A number of degradation processes within the ocean have been proposed (Krysell, 1991; Quack and Wallace, 2003). The gas exchange is discussed in detail in Chapter 1.3.4. The oceanic degradation pathways discussed here include: hydrolysis, dehalogenation, halide exchange and photolysis. It has been suggested that these oceanic sinks of bromoform are much slower than sea-air exchange and therefore less prominent (Quack and Wallace, 2003; Manley et al., 1992).

The hydrolysis of bromoform occurs slowly, especially in cold water, with a half-life of the order of 1000 years at temperatures < 4 °C (Carpenter et al., 2007b). At higher temperatures (25 °C) the rate of reaction increases, resulting in a half-life of 30 – 50 years (Quack and Wallace, 2003). Based on a conservative assumption that a total oceanic concentration of 1.5 Gmol of bromoform exists, spread across the surface (10 pmol l^{-1}) and deep ocean (0.1 pmol l^{-1}), it is estimated that the total loss of bromoform from the surface and deep ocean, through this process, would amount to 3.4 – 5.5 Mmol $CHBr_3$ yr^{-1}. This makes the hydrolysis of bromoform in seawater an insignificant process especially in comparison to surface removal pathways (e.g., sea-air transfer of bromoform, which results in a half-life of hours to days and photolysis) described below (Quack and Wallace, 2003).

It is suggested that the decline in bromoform concentrations with increasing depth is a result of degradation by anaerobic bacteria or due to chemical reduction. Reductive dehalogenation would initially convert $CHBr_3$ to CH_2Br_2, which is itself an important transport of bromine to the atmosphere (Quack and Wallace, 2003). While bacterial degradation has been found to occur in other halocarbons, this process of bromoform removal has not been shown to happen. This mitigates bacterial degradation as a viable bromoform loss process (Goodwin et al., 1997). While the chemical reduction of several halocarbons has been shown to be related to oxygen concentrations, data for bromoform has not been shown. The higher redox potential of bromoform over the reported bromocarbons may make this an important loss process in the deep ocean, resulting in decreasing concentrations with depth (Tanhua et al., 1996). While this may be an important loss process below the euphoric zone, estimates of the magnitude of loss due to chemical reduction have not been made (Quack and Wallace, 2003).

The exchange of halogens in bromoform with either iodine or chlorine radicals is slow within the ocean, with a half-life of 5 – 74 years at temperatures between 25 to 2 °C, respectively (Hense and Quack, 2009; Goodwin et al., 1997). Based on measurements from the Atlantic, a reaction with chlorine is suggested to occur resulting in the formation of chloroform (Reactions 1.10 – 1.12, Class and Ballschmiter, 1988; Quack and Wallace, 2003). Although small quantities of $CHBrCl_2$ and $CHBr_2Cl$ have been reported to be produced directly from marine algae, the dominant source is thought to be the halogen exchange suggested above (Krysell, 1991; Sturges et al., 1997).

$$CHBr_3 + Cl^- \rightarrow CHBr_2Cl + Br^- \tag{1.10}$$

$$CHBr_2Cl + Cl^- \rightarrow CHBrCl_2 + Br^- \tag{1.11}$$

$$CHBrCl_2 + Cl^- \rightarrow CHCl_3 + Br^- \tag{1.12}$$

The loss of oceanic bromoform due to halide exchange is reported to be one to two orders of magnitude larger than hydrolysis. This suggests that an annual loss of between 20 – 100 Mmol $CHBr_3$ via halide exchange is expected to occur within the ocean (Quack and Wallace, 2003).

The photochemical decay of bromoform in the surface layer has been suggested to occur. The life-time of bromoform in the ocean as a result of photolysis is thought to be approximately 40 times longer than due to sea-air exchange rate. This suggests that about 2 % of the bromoform, that might have been transferred via gas exchange, may be degraded by photolysis prior to the loss by sea-air gas exchange (Carpenter et al., 2000; Quack and Wallace, 2003). It is reported that the UV (300 nm) penetration depth is approximately 10 cm (Carpenter et al., 2007b). The presence of UV in the surface layer and subsequent destruction of bromoform coupled with loss by gas flux might account for the observed subsurface maxima in bromoform concentration reported at depths of between 5 and 200 m (Quack and Wallace, 2003). Subsurface maxima have also been found to be associate with the presence of microalgae at the top of the thermocline (Quack et al., 2004).

1.3.4 Sea-air exchange

The surface ocean is the largest reservoir of bromoform (Krysell, 1991). The main bromoform loss mechanism from the ocean is to the atmosphere by means of sea-air gas exchange (Krysell, 1991; Carpenter et al., 2012). Volatilisation of bromoform results in an oceanic half-life of days to months, which is dependent on the water and air temperatures (Goodwin et al., 1997; Quack and Wallace, 2003). The wind speed and local relative concentrations are shown to affect the rate of transfer across the air-sea interface affecting concentrations (Carpenter et al., 2007a; Krysell, 1991). Measurements of the gas flux rate in the Southern Ocean found that the transport to the atmosphere was too small to support the amount of bromoform loss encountered within the ocean (Abrahamsson et al., 2004). The parameterisation of the gas flux and sea-air exchange models are explored in this section.

The estimation of the sea-air exchange rate presents a major uncertainty to biogeochemical and atmospheric chemical models (Nightingale et al., 2000). A number of gas transfer models, such as surface renewal, bubble mediated transfer and the role of waves and wave breaking, have been proposed to describe the transport of gases across the sea-air interface (e.g., Liss and Slater, 1974; Liss and Merlivat, 1986; Nightingale et al., 2000; Ho et al., 2006). However, the 'two-layer' model is often used in the calculation of air-sea gas transfer (Carpenter et al., 2012; Nightingale, 2009). While the 'two-layer' model is physically unrealistic in the environment, it has been widely used and provided a point of departure in understanding gas transfer processes. In this model we envisage that the two films, either side of the air-sea interface, are each well mixed and compounds are transferred across the interface by means of molecular diffusion (Liss and Slater, 1974; Nightingale, 2009). In this model the gas flux *F* (mol m^{-2} s^{-1}) is estimated as the product of the transfer velocity (*k*) and the difference in gas concentration across the air-sea interface (ΔC) (Equation 1.13; Liss and Merlivat, 1986; Wanninkhof, 1992; Nightingale, 2009).

$$F = k(\Delta C) \tag{1.13}$$

The chemical reactivity of the gas and turbulence in both micro-layers are the most important determinants to the magnitude of the transfer velocity (*k*). The gas and liquid interface layers form the main resistance to the transfer of gases and are defined by the reciprocal of the transfer velocity (Liss and Slater, 1974). The total transfer velocity is the sum of the transfer velocities though the air and water side micro-layers (Liss and Slater, 1974). The resistance is calculated by:

$$1/k_t = 1/k_w + 1/Hk_a \tag{1.14}$$

where 1/ k_t is the total resistance and *1/Hk*$_a$ and 1/ k_w are the air and water side resistance respectively. The Henry's law constant (*H*) is a measure of the solubility of a gas (Nightingale, 2009). The waterside micro-layer is the dominant resistance to the transfer of gases that are not highly soluble (high *H* value). For these gases the total transfer velocity (*k*) is approximated by the term 1/ k_w. The 1/ *Hk*$_a$ term dominates for gases that are highly soluble or rapidly react with water (Nightingale, 2009).

The near surface turbulence is dominated by wind speed. However, variables unrelated to wind speed, such as wave state, wave age, convective processes, surfactants, wave breaking and bubbles, have been found to impact the turbulence (Nightingale, 2009). While wind speed does not capture the entire variability, it is easy to measure and is therefore often used to parameterise *k* (Liss and Slater, 1974; Liss and Merlivat, 1986; Wanninkhof, 1992; Asher and Wanninkhof, 1998; Nightingale, 2009). The parameterisation of *k* by wind speed also utilises the Schmidt number (Sc) of a gas to scale the transfer velocity under varying environmental conditions and for different gases (Wanninkhof, 1992; Asher and Wanninkhof, 1998; Nightingale, 2009). The Schmidt number is a dimensionless value that relates the ratio of the kinematic viscosity (ν) to molecular diffusivity (*D*). As both kinematic viscosity and molecular diffusivity are temperature dependent, this results in a variability of the Schmidt number based on temperature (Liss and Merlivat, 1986). A common Schmidt number of 600 or 660 (Sc of CO_2 at 20 °C in

fresh and seawater, respectively) is used to normalise transfer velocities to aid in comparison (Nightingale, 2009).

The parameterisations of the air-sea gas transfer frequently relate wind speed (u) and the relevant Schmidt number for the gas of interest. One of the most widely used sea-air transfer parameterisation methods is that of Wanninkhof (1992), which suggests a quadratic relationship between u and Sc (Equation 1.15; Wanninkhof, 1992; Nightingale, 2009). Recent work at high wind speeds proposed a cubic model for the estimation of the transfer velocity (Equation 1.16; Wanninkhof and McGillis, 1999). This model achieves a better fit to the few measurements at high wind speeds, however the quadratic and linear equations of Wanninkhof (1992) and Liss and Merlivat (1986) have been suggested for low wind speeds (Palmer, 2006). The quadratic relationship of Nightingale et al. (2000) (Equation 1.17) provides results similar to those achieved by Wanninkhof and McGillis (1999) (Nightingale, 2009; Carpenter et al., 2012). However, while the Wanninkhof and McGillis (1999) parameterisation is best suited for high wind speeds, the Nightingale et al. (2000) model has been validated over a larger range of wind speeds (Nightingale et al., 2000).

$$k = 0.31u^2(Sc/660)^{-1/2} \tag{1.15}$$

$$k = 0.0283u^3(Sc/660)^{-1/2} \tag{1.16}$$

$$k = (0.222u^2 + 0.333u)(Sc/600) \tag{1.17}$$

In laboratory experiments three wind regimes of gas flux for increasing wind speed were found by Liss and Merlivat (1986). Increasing wind speed drives a greater flux of bromoform from the ocean to the atmosphere through changes in ocean state (Quack and Suess, 1999; Liss and Merlivat, 1986). Gas flux based on increasing wind speeds appears to break down into three regimes and can be linked with surface conditions (Liss and Merlivat, 1986). At low speeds (under 5 m s^{-1}) is the smooth phase that experiences low and slow gas fluxes, rough surface conditions are experienced at wind speeds between 5 – 10 m s^{-1} and above 10 m s^{-1} wave breaking and bubble formation begin to enhance transport from the ocean to the atmosphere (Liss and Merlivat, 1986). Liss and Merlivat (1986) propose gas flux equations for the three wind regimes (Equations 1.18 – 1.20) consider the different forces acting on the flux rate under the varying conditions, with the wind speed (u) playing an increasingly significant role.

$$k = (0.17u)(Sc/600)^{-2/3} \qquad \text{for } u \leqslant 3.6 \tag{1.18}$$

$$k = (2.85u - 9.65)(Sc/600)^{-1/2} \qquad \text{for } 3.6 < u \leqslant 13 \tag{1.19}$$

$$k = (5.9u - 49.3)(Sc/600)^{-1/2} \qquad \text{for } u > 13 \tag{1.20}$$

It is suggested that a number of possible techniques exist for the direct measurement of gas fluxes. These techniques include eddy correlation, relaxed eddy accumulation, gradient flux techniques and inertial dissipation (Nightingale, 2009). These techniques allow for the measurement of fluxes of smaller spatial (metres to kilometres) and temporal (minutes to hours) scales when compared to deliberate tracer experiments (Carpenter et al., 2012). Comparison of results between deliberate tracer experiments and

eddy correlation measurements are in good agreement (Nightingale, 2009). The results also indicate that solubility is an important variable in the determination of gas transfer velocity and needs to be incorporated into parameterisations (Nightingale, 2009).

Further work on the measurement of the gas transfer velocity by means of micrometeorological techniques may shed light on the role of variables such as solubility. Further developments in the parameterisation of gas transfer velocity may begin to account for other factors such as wave breaking and the presence of surfactants, which are not captured by wind speed alone. Atmospheric chemistry models would be greatly enhanced by improvements in the understanding and parameterisation of gas flux of trace gases between the ocean and the atmosphere, leading to correct atmospheric loadings of reactive gases.

1.4 Bromoform in the marine troposphere: a review of current measurements

Global ocean and atmospheric measurements of bromoform suggest a gradient of mixing ratios running from the tropics to the poles and from the coast toward the open ocean (Quack and Wallace, 2003; Carpenter and Liss, 2000). The global source strength of bromoform is estimated at between 2.0 x 10^{11} and 3.0 x 10^{11}g $CHBr_3$ yr^{-1} (Manley et al., 1992; Dvortsov et al., 1999; Quack and Wallace, 2003; Carpenter and Liss, 2000), based on the limited global dataset of bromoform measurements (Fig. 1.1). Approximately 10 % of this estimate is made from anthropogenic sources, resulting in a source strength of $\sim$0.2 x10^{11}g $CHBr_3$ yr^{-1} (Carpenter and Liss, 2000; Quack and Wallace, 2003). The source strength is shown to vary globally, based on macro- and microalgal extent, with costal regions typically being orders of magnitude greater than open ocean regions (Tables 2 and 3 in Quack and Wallace, 2003; Class and Ballschmiter, 1988, Table 1.1). The Southern Hemisphere is critically under-sampled, leading to errors in models and uncertainty in the variability of bromoform atmospheric mixing ratios. The source strengths vary with latitude and distance from the coast, with a maximum appearing in the coastal ocean (Quack and Wallace, 2003; Butler et al., 2007; Ziska et al., 2013).

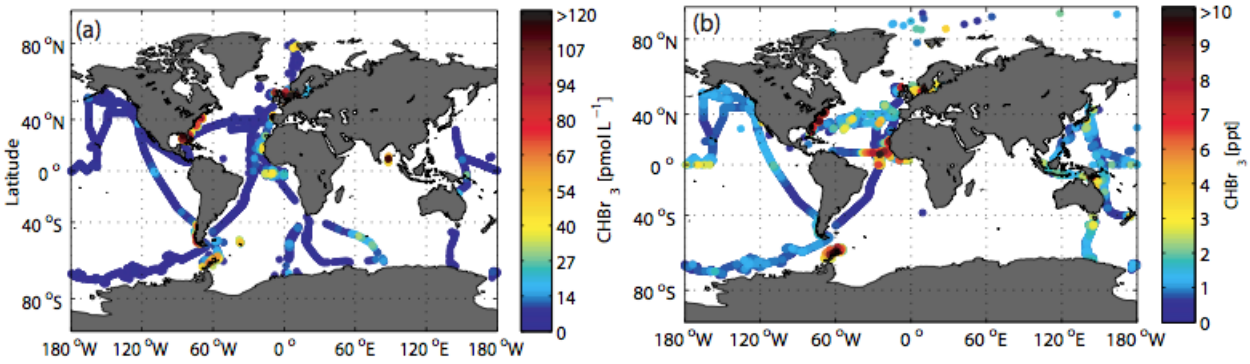

Figure 1.1: Global distribution of bromoform measurements in (a) air and (b) seawater. Adapted from Ziska et al., 2013.

Table 1.1: Selected previous atmospheric measurements of bromoform in coastal regions.

				$CHBr_3$ (ppt)			
Location	**Date**	**Latitude**	**min**	**max**	**mean**	**Reference**	**Region**
New Hampshire TF	Jun.-Aug. 2002-4	43.1° N	0.2	37.9	5.3-6.3	2	Coastal
San Cristobal Island	Feb.-Mar. 2002, 2003	0.92° S	4.2	43.6	14.1	3	Coastal
Christmas Island	Jan. 2003	1.98° N	1.1	31.4	5.6-23.8	3	Coastal
Cape Grim	Jan.-Dec. 2003	40.7° S	1.3	6.4	2.9	3	Coastal
New Hampshire AI	Jul.-Aug. 2004	42.9° N	0.9	47.4	14.3	2	Coastal
Cape Verde	May-Jun. 2007	16.8° N	2.0	43.7	4.3-13.5	4	Coastal
Borneo	Apr.-Jul. 2008	4.70° N	2-5	∼60		1	Coastal
Atlantic Ocean	Oct.-Nov. 2002	10° N	0.5	27.2		5	Open ocean

References: 1 Pyle et al., 2010; 2 Zhou et al., 2008; 3 Yokouchi et al., 2005 4 O'Brien et al., 2009; 5 Quack et al., 2004.

1.4.1 Atmospheric measurements

Measurements taken across the equator, mainly in the Atlantic (Fig. 1.1), suggest that an interhemispheric gradient of mixing ratios exists with slightly higher mixing ratios in the Northern Hemisphere. Locally, elevated mixing ratios in the order of 200 ppt have been reported; however, global background mixing ratios are suggested to be low, usually 0.5 - 1.5 ppt (Class and Ballschmiter, 1988; Quack and Wallace, 2003). Variations in sources and sinks may be the driver of the interhemispheric gradient. It is reported that Northern Hemisphere mean background mixing ratios are between 0.85 and 0.94 ppt compared to 0.58 and 0.74 ppt for the Southern Hemisphere (Quack and Wallace, 2003). An accumulation through the winter in the Northern Hemisphere, due to a reduction in sunlight and OH concentrations, might contribute to the difference in reported mean hemispheric mixing ratios.

1.4.2 Cape Town: a data poor region

Measurements taken globally indicate that atmospheric mixing ratios of bromoform are regionally highly variable (Table 1.1). The results of measurements taken from two coastal sites dominated by macroalgae show different atmospheric mixing ratios (e.g., Borneo, Pyle et al., 2010 and New Hampshire, Zhou et al., 2008). This highlights that given the common source and Northern Hemisphere setting there is much to be done to improve the understanding of variability of bromoform in the atmosphere. It is important to understand the variability in bromoform measurements as regional specific emissions may have a significant impact. In this regard the use of numerous, independent sampling sites provides an ideal mechanism for observing regional emission rates.

Long-term coastal measurements are important to atmospheric chemistry in understanding changes to the local and global source strengths. To date, the global estimate of bromoform source strength is heavily biased towards the Northern Hemisphere where the majority of measurements have been made, with

only a few cruises in the Southern Ocean and one site (Cape Grim) as a source for Southern Hemisphere measurements. Quantification and a greater understanding of the contribution of bromoform from southern Africa can help reduce this bias and further the global understanding of regional variability, making Cape Town an ideal region.

There is a general paucity of data from around southern Africa, which might conceal an important source to the global strength of atmospheric bromoform mixing ratios. Cape Point (34.5° S) is an ideal site from which to measure trace gases and bromoform, in particular, as air masses from the Southern Ocean, southern Benguela upwelling system, local macroalgae sources and the city of Cape Town are sampled (Brunke et al., 2010). A tropical bromoform production model suggests that the Benguela upwelling system may be a significant atmospheric source, located in the sub-tropics (Palmer and Reason, 2009). The strong upwelling found in the Benguela region may lead to increased bromoform in the stratosphere through deep convection. This region may contribute significantly to stratospheric loading of bromoform (Fig. 1.2). With growing interest in tropospheric and stratospheric ozone loss, understanding the full magnitude of this source is important (Hossaini et al., 2013). Transient research cruises have not shown the Southern Ocean to be a significant atmospheric source of bromoform (e.g., Carpenter et al., 2007b; Yokouchi et al., 2005; Butler et al., 2007). However, long-term sampling at Cape Point may reveal a seasonal signal, especially in winter when there are no ship measurements (Quack and Wallace, 2003; Ziska et al., 2013). Short-term studies, such as research cruises, are inadequate when examining the global bromoform source strength and in investigating any long-term trends.

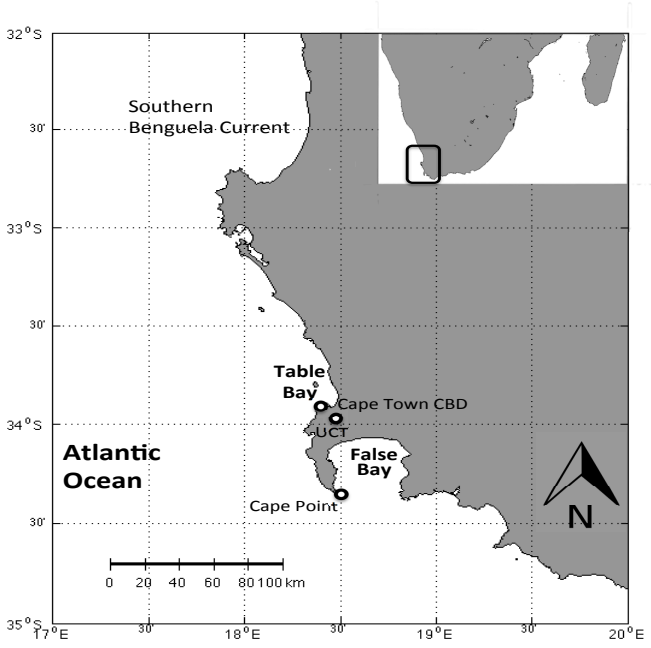

Figure 1.2: Map of the Cape Town area, highlighting the positions of Table Bay and False Bay, the southern Benguela Current region. Cape Town CBD is shown along with sampling sites at UCT and Cape Point.

1.5 Introduction to gas chromatography

Gas chromatography is an analytical chemistry process where mixed samples are separated into their constituent parts for independent measurement (Poole, 2003). Gas chromatography (GC) has a long history in atmospheric gas measurement due to the selectivity of the process (Lovelock, 1959, 1963; Quack and Wallace, 2003). In general a typical gas chromatography system for halocarbon measurement is built up of a number of general parts including a carrier gas supply to transport samples though the column that provides the separations. The column is housed in an oven and samples then pass onto a detector. The output from the detector is recorded on a computer (Fig. 1.3 and Urias, 2002). While paper integrators have been used to record the concentration of eluting compounds, with the advent of computers a move to digital data storage and analysis has been made. Specialised components may be added to the injector to allow for the pre-concentration of samples prior to injection or the injection of multiple samples automatically, especially for the quantitative detection of halocarbons (Poole, 2003).

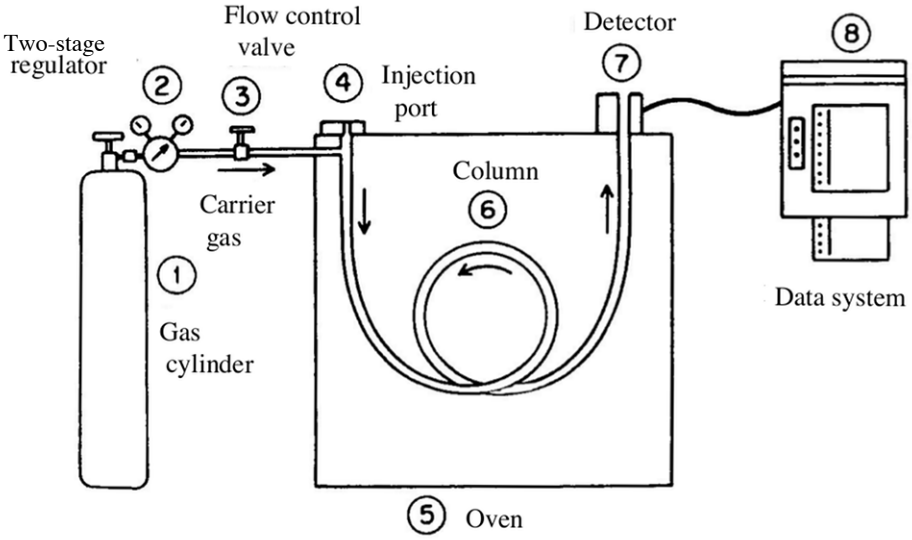

Figure 1.3: Layout and components found within a generic gas chromatography system. Adapted from Urias (2002).

The separation of mixed constituents into discrete components is achieved through chemical and mechanical processes within the column. The interaction between the mobile and stationary phases results in the separation of samples. The mobile phase is ideally an inert gas, usually hydrogen, helium or nitrogen, that carries samples through the column. Wall-coated open tubular columns, one of the five types commonly utilised in gas chromatography, are predominantly used in bromoform (halocarbon) analysis (Poole, 2003; Shaw, 2011). The stationary phase is a liquid film of between 0.10 – 5.0 μm bonded

directly to the internal column wall. Compounds in the sample may become temporarily attached to the stationary phase, retarding the flow of that molecule as it passes through the 25 – 100 m length of the column, under constant gas flow. Variations in the chemical properties of the stationary phase result in the eluting compounds adhering to the column wall. The duration of adherence of compounds is also varied in different columns (Christie, 1989). In general, the specific order of elution for a particular column and stationary phase is related to each compound's affinity for the stationary phase, molecular weight and boiling point. The typical Gaussian distribution of elution compounds is the outcome of Brownian motion of molecules within the column; not all the molecules of the same compound pass through the column at identical rates. The temperature of the oven is used to alter the rate of molecule adhesion to the stationary phase, with increasing temperature reducing the adhesion of heavier compounds (Poole, 2003; Urias, 2002).

In general the measurement of eluting halocarbons, including bromoform, is typically performed by either a mass spectrometer (MS) or electron capture detector (ECD) (e.g., Lovelock, 1963; Poole, 2003; Urias, 2002; Shaw, 2011). A mass spectrometer system measures the mass of the ions from the eluting compounds, which can be compared to libraries. This allows for the rapid identification of compounds. In the case of the ECD, free electrons are scavenged by polar compounds as they pass through the detector. The removal of these electrons alters the potential within the detector, which is accurately measured. Careful calibration is required with the ECD. The identification of eluting compounds is achieved by means of absolute and relative retention. The peak area of eluting compounds is proportional to the total concentration (Urias, 2002). The area of the peak can be calculated in a number of ways; however, popular methods include the triangle method (Fig. 1.4) and trapezium method. The two methods are reported to result in accuracy of integration ranging from 96.8 to 100.4 % for triangulation and trapezium methods respectively (Poole, 2003).

The typically low mixing ratios of halocarbons, including bromoform, found naturally in the environment makes the quantifiable detection and analysis of this gas particularly difficult (Carpenter and Liss, 2000). These low atmospheric mixing ratios necessitate a trapping phase for the pre-concentration of samples before analysis. Numerous methods for the trapping of bromoform from air samples have been suggested, these include cooled sample loops, and adsorbent beds within a thermal desorption unit. Once trapped, samples are thermally desorbed and transferred to the column for analysis (e.g., Quack and Wallace, 2003; Wevill and Carpenter, 2004; Khalil et al., 1983). The chromatography of the eluting compounds depends on a number of variables including the injection volume, column, carrier gas flow rate and oven temperature (Poole, 2003; Urias, 2002). The resolution (R) of the chromatography is calculated by the degree of separation between two adjacent peaks and given by:

$$R = \frac{2\Delta t}{W_1 + W_2} \tag{1.21}$$

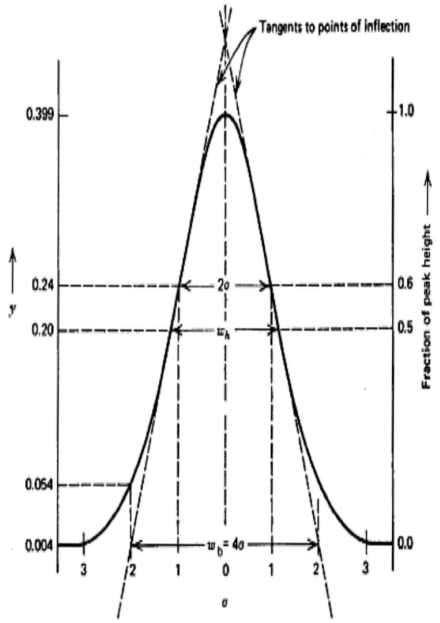

Figure 1.4: An idealised Gaussian elution peak, showing variations on the triangle integration method.

where Δt is the time interval between peaks, W_1 and W_2 are the widths at the base of the adjacent peaks. A baseline resolution requires a degree of separation of approximately 1.5 (Shaw, 2011; Urias, 2002). The temperature programme of the oven is important in ensuring the adequate separation of elutants, especially high molecular weight compounds. It can be used to vary the speed of elutants with higher temperatures increasing the elution rate, effectively shortening the total elution time and limiting the tailing of peaks due to band broadening processes. The consistency of carrier gas (CG) flow rate is important in ensuring repeatable separations and chromatograms. The rate of flow should be low enough to allow interaction between the compounds in the mobile phase and the stationary phase, while not allowing dead space to form. The choice of CG flow rate should maximise the resolution of separated peaks, while minimising the total elution time of samples. A CG flow rate of between 1 and 5 ml min^{-1} has been shown to result in the optimal separation for bromoform on gas chromatography systems (Wevill and Carpenter, 2004; Poole, 2003). Altering these variables results in changes to the chromatographic resolution.

Chapter 2

Methods

The main method employed in this work involved a GC-ECD system with a custom-built thermal desorption unit (TDU) interface. The methods used for the collection of bromoform measurements at Cape Point and in the laboratory culture experiments are discussed here. The GC was set up with a gas flow rate of 5 m*l* min^{-1} and a 5-step temperature programme between 30 and 200 °C. Nitrogen gas was added at 30 m*l* min^{-1} to the ECD which was maintained at 300 °C. Heating the TDU from -10 to 300 °C was achieved in 2 min 30 sec. This resulted in a bromoform detection limit of 0.73 ± 0.09 ppt from 15 minute trapped samples.

2.1 Gas chromatography system

A Shimadzu GC-8A that had previously been used by the South African Weather Service (SAWS) for the detection of nitrous oxide (N_2O) at Cape Point was employed with a PerkinElmer F-22 electron capture detector (ECD) for the measurement of bromoform. The numerous components were connected to the GC oven and ECD (Fig. 2.1). A brief overview of the operation of the GC is as follows: using a 3-way valve (Swagelok, SS-41GXS2) the air pump could be selected to draw air samples through the drying trap and mass flow controller before passing onto the adsorbent bed within the TDU. Switching the 3-way valve in the opposite direction allowed the trapping of nitrogen 'blank' samples or external calibration gas from the permeation oven. Nitrogen gas was split from the cylinder to pass through the permeation oven, to provide make-up gas and to act as a source for 'blanks'.

While the 6-port injection valve was in the 'load' position, helium carrier gas passed directly onto the column (Fig. 2.1, 2.2). When the position of the valve was switched, the helium carrier gas was passed through the TDU adsorbent bed, in the opposite direction to sampling, before passing onto the column. Once a sample had been directly injected, separation and subsequently detection occurred. A personal computer was used to collect and store detected results from the ECD (Fig. 2.1).

Cooling of the TDU was provided by an external water recirculation chiller, which was operated during sample trapping. Throughout the injection of a sample the TDU was electrically heated, desorbing the

trapped sample.

2.1.1 GC oven

Heating in the oven was provided by means of a high resistance heating element. A rotary fan in the back of the oven ensured a uniform heat distribution. The temperature of the element was manually adjusted and was able to achieve a maximum rate of heating of 65 °C min^{-1}. The oven temperature was regulated with an accuracy of $\pm$ 1 °C by a mechanical thermistor and an upper temperature of 300 °C was used for the removal of contaminants from the system. Samples were introduced into the oven through a port on the side of the oven, since the original ports had been blocked.

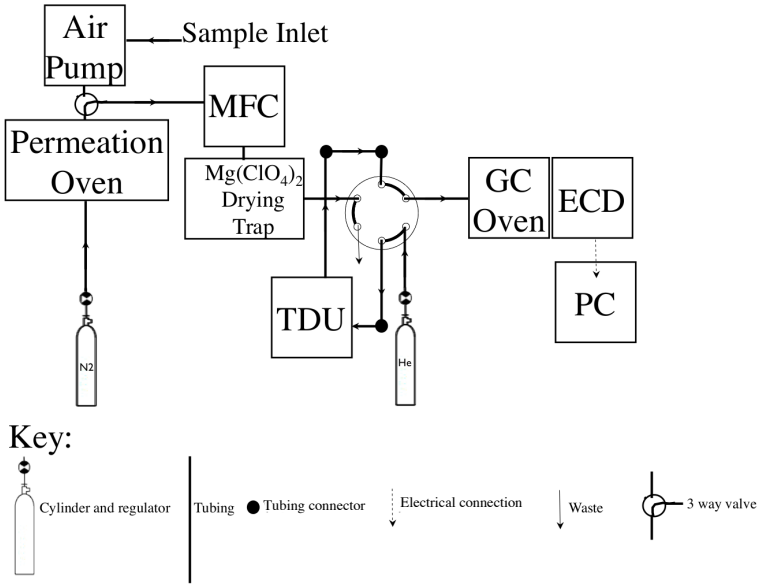

Figure 2.1: Schematic drawing showing the layout of the GC-ECD analysis system and associated gas and sample flows. Solid lines denote $\frac{1}{8}$" stainless steel tubing with the arrow denoting the direction of gas flow. The system is shown in the 'inject' position. Adapted from Kuyper et al. (2012).

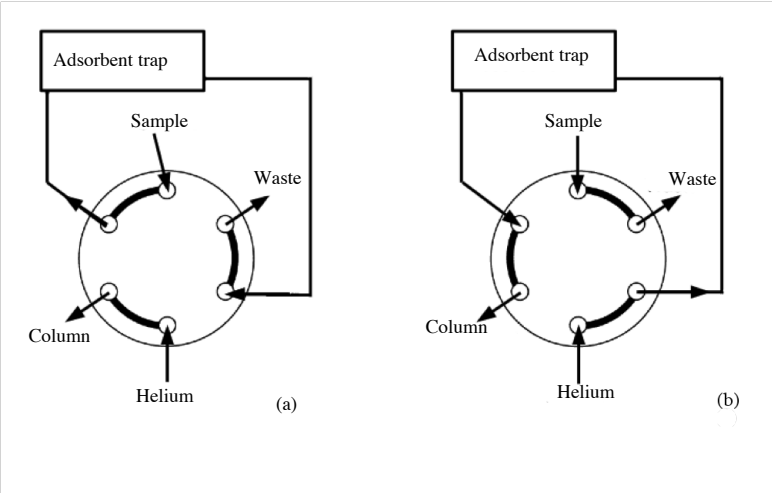

Figure 2.2: Gas flow control by means of a Valco 6-port gas valve. Two positions shown: (a) sample loading, (b) sample injection.

2.1.2 Temperature programme

The GC oven temperature was maintained at 30 °C during the injection of a sample and held for 5 minutes. Thereafter the temperature was increased at a rate of 65 °C min^{-1} every 5 minutes and held at 60, 90, 150, 200 and finally 220 °C respectively (Chapter 3.2.2). This temperature programme, on the DB-624 column, resulted in separating bromoform with a retention time (t_R) of approximately 14 minutes. A description of the development of the temperature programme can be found in Chapter 3.2.2.

2.1.3 Detector

A PerkinElmer F-22 ECD was attached to the left side of the GC oven as the original Shimadzu electron capture detector had failed. An external controller modulated the temperature of the ECD to a constant 300 °C via an injection cartridge. Operation of the detector at this temperature resulted in a low stable baseline signal of between 50 - 100 mV. A separate data controller collected and amplified the signal from the ECD. The signal from this controller in analogue format was then transmitted to a personal computer via a digital conversion process (Chapter 3.2.11).

2.1.4 Column

A J&W Scientific DB-624 (30 m x 0.32 mm and 1.8 μm, 5 % polarity film) capillary column was used for the separation of bromoform from mixed air samples. The column was housed entirely within the oven. A direct, splitless connection was made between the carrier gas and the column.

2.1.5 Carrier and make-up gas

Helium (He, Grade 5.0, Air Products / AirLiquide, Cape Town, South Africa) was used as the carrier gas within the system for the separation of samples. A constant back pressure of 200 kPa through the column during the elution of samples resulted in carrier gas flow rate of 5 m*l* min^{-1} at 30 °C. The back pressure was maintained by means of a TESCOM Dräger regulator fitted to the helium cylinder. Swagelok and Valco gas tight fittings were used to deliver the helium carrier gas directly to the head of the column.

A flow of 30 m*l* min^{-1} nitrogen (N_2, Grade 5.0, AirLiquide, Cape Town, South Africa) was added directly to the ECD. This addition of nitrogen was controlled by the back pressure on the cylinder regulator (100 kPa) and a mechanical Porter valve. A Swagelok needle valve (SS-ORS2) was used as a gas shut off. The effects of variation in carrier and make-up gas flow rate on bromoform detection and chromatography are discussed in Chapter 3.2.5.

2.1.6 Injection valve

As described above, a manually operated Valco 6-port valve was used for the injection of samples (Fig. 2.2). The valve controlled the direction of carrier and sample gas flow through the system (Fig. 2.1). In the 'load' position the carrier gas passed directly onto the column, while sample gas passed through the adsorbent bed and to waste (Fig. 2.2a). During an injection the valve was switched, resulting in the carrier

gas passing through the adsorbent bed, in the opposite direction to sample loading, before passing onto the column. Sample gas was passed directly to waste in the laboratory. Heater tape (RS Components) was added to the tubing between the end of the TDU and the head of the column to minimise condensation of compounds after desorption. The tape was run constantly at its maximum output, maintaining a temperature up to 200 °C. Power for the heater tape was drawn directly from the mains of the building.

2.1.7 Sample pre-concentration

A custom-built TDU (UniTemp, Cape Town) was used for the pre-concentration of air samples (Fig. 2.3). Two adsorbents, Carbopack X and Carboxen 1016 (9mg each) were housed in a glass tube restrained by glass wool. The adsorbents were packed such that an air sample was introduced to the less adsorbent Carbopack X first. During an injection the direction of gas flow was reversed ensuring samples were completely swept onto the column.

A Lauda RM-6 recirculation water chiller was used to circulate cooled glycol (-15 °C) through the external water jacket, maintaining a temperature of -10 °C within the adsorbent bed. Heating of the TDU was achieved using a high resistance coil regulated by a customised external alternating current (AC) controller. The TDU was heated from -10 to 300 °C in 2 min 30 sec.

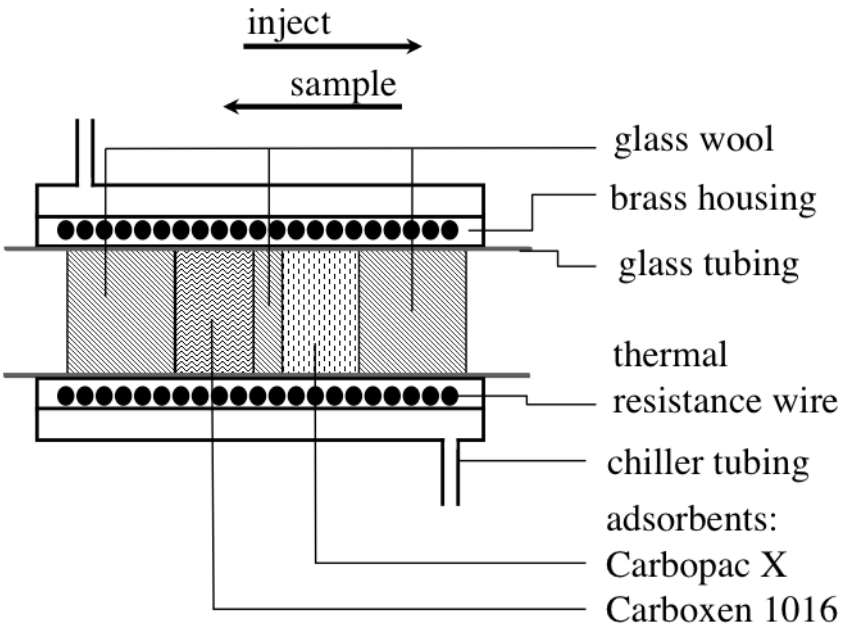

Figure 2.3: Plan view of the thermal desorption unit.

2.1.8 Mass flow controller

An ASM AFC-260 mass flow controller was connected in series after the magnesium perchlorate drying trap. The mass flow controller (MFC) limited the gas flow rate through the TDU adsorbent bed to a rate of 100 ml min^{-1}.

2.1.9 Air pump

A Rocker 400 piston air pump was used to draw external samples into the system and had a maximum air displacement rate of 400 ml min^{-1}. The pump was connected in-line to draw samples down the sampling line. Air samples were then pushed through the drying trap, mass flow controller and adsorbent bed. Excess air drawn down the sampling line was vented to the laboratory upstream of the mass flow controller and regulated by means of a Swagelok needle valve.

2.1.10 Drying trap

A custom-made glass trap with 8 mm glass tubes and a volume of approximately 20 ml filled with magnesium perchlorate was used to dry air samples. The magnesium perchlorate was held in place by a 1 cm plug of glass wool at each end of the trap. For a complete account of the chemicals and volumes tested see Chapter 3.2.10. Gas tight connections were achieved utilising silicone rubber ferrules with metal Swagelok reducing unions (Chapter 3.2.7.2).

2.1.11 Computer interface

Data output from the ECD was converted to a digital signal and recorded on a personal computer. A custom-built graphical user interface (GUI) was used to regulate the flow of data into the computer and record these data (Fig. 2.4). MATLAB provided the working support of the GUI and an internal script polled the serial (RS-232) port on the computer for data every 0.25 seconds. The digital signal read into the computer was displayed in real-time on a fixed set of axes. Time was displayed on the x-axis with detector response in millivolts on the y-axis. The data was recorded immediately and a figure was saved at the end of the sample measurement for later analysis.

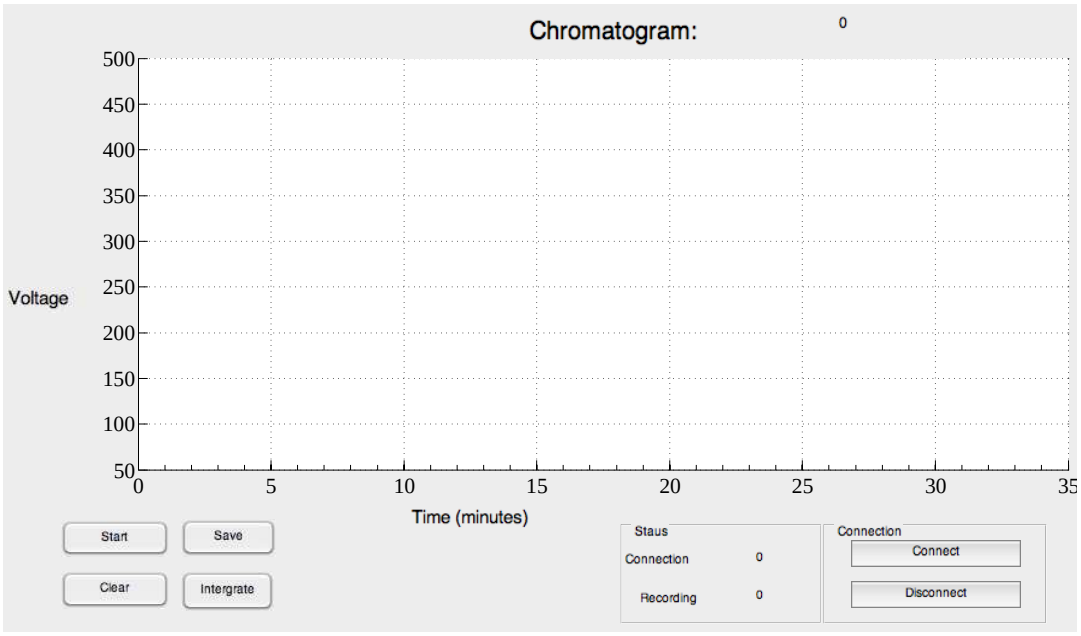

Figure 2.4: Custom graphical user interface developed in MATLAB, used to collect, display and save data from the ECD. The status of system figures was included in this GUI.

2.1.12 Permeation oven

A custom-built permeation oven was used for calibration of the GC-ECD system as per Wevill and Carpenter (2004). A commercially purchased bromoform permeation tube (HRT-003.00-4096/70, A&J Scientific, Cape Town) was housed in a glass trap within a heating block (Fig. 2.5). The aluminium heating block was kept at 70 °C by four injection cartridges (Hotwatt, Superwatt: HS37-1.5) and a temperature controller. The flow of nitrogen (Grade 5.0, AirLiquide Cape Town) was regulated through the oven system at a pressure of 100 kPa and rate of 100 m*l* min^{-1} by means of the cylinder pressure regulator and a mechanical Porter valve. A Swagelok needle valve (SS-ORS2) was added in-line as a shut off.

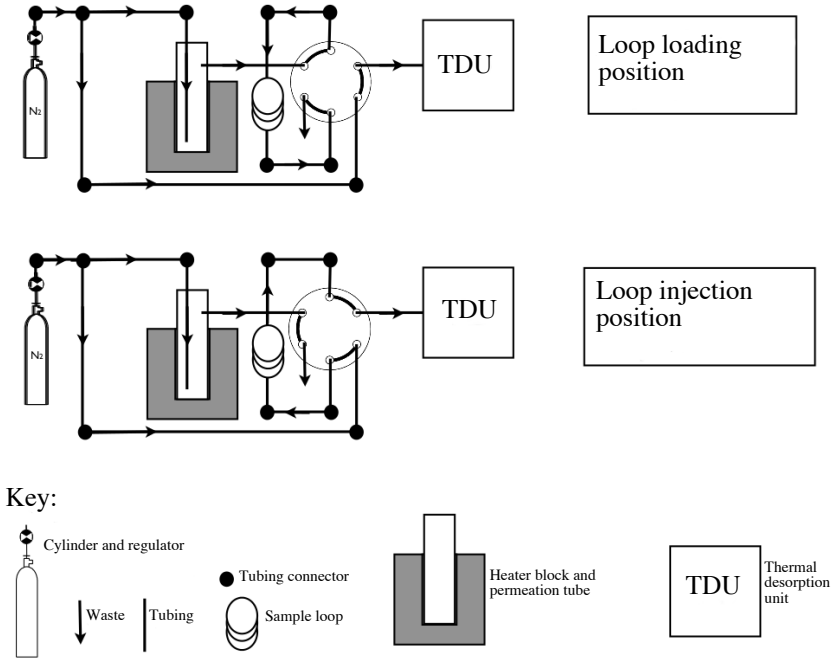

Figure 2.5: Plan view of the permeation oven unit used for the external calibration of the GC system.

Gas from the glass trap was continuously swept through a 100 μl sample loop (Valco) before passing onto a halocarbon trap. Heater tape (RS Components) was wrapped around all tubing downstream of the glass trap to ensure no loss of bromoform occurred through condensation. An electric 6-port sample valve (Valco) was used to inject samples from the 100 μl sample loop to the TDU adsorbent bed (Fig. 2.5).

2.2 Trapping of samples

All samples were trapped on the cooled TDU adsorbent bed. Selection of sample (air / N_2 and calibration) to be loaded on the adsorbent bed was achieved by means of a Swagelok 3-way valve (Fig. 2.1). Air samples were drawn into the TDU trap by means of a Rocker 400 piston pump. The flow rate of the samples through the TDU trap was regulated to 100 m*l* min^{-1} with an ASM AFC-260 MFC, while excess air was vented to the laboratory. A chilled adsorbent bed (9 mg each Carbopack X/Carboxen 1016) held

at -10 °C was used to pre-concentrate all samples prior to analysis (Fig. 2.1). The adsorbent bed was maintained at this temperature throughout the pre-concentration phase (Chapter 3.3).

2.2.1 Air samples

Air was drawn through the cooled adsorbent bed at 100 m*l* min^{-1} for 15 minutes resulting in a sample volume of 1.5 *l*. A description of sample and breakthrough volumes can be found in Chapter 3.3. The GC-ECD system was used to analyse air samples drawn via a purpose-built sampling mast at Cape Point (Chapter 4.3.4). Samples were chemically dried prior to loading on the adsorbent bed to prevent the accumulation of moisture within the trap, which would have had a negative effect on the column and chromatography (Chapter 3.2.10).

2.2.2 Nitrogen 'blanks'

A flow of nitrogen gas (Grade 5.0) was passed through the adsorbent bed at 100 m*l* min^{-1} for 15 minutes, in the same manner as described for air samples. The nitrogen gas was analysed with the system as described in order to demonstrate that a blank chromatogram was produced in the absence of bromoform or air samples. The analysing of nitrogen gas in this manner also demonstrated that the injection method was sufficient to clear the adsorbent bed and there was no accumulation of compounds, leading to so called 'memory effects'. A nitrogen 'blank' sample was trapped and run after each calibration point and every fifth air sample analysed, ensuring the system was ready for further sampling.

2.2.3 Calibration: permeation oven

An electronically activated switching valve was used to load 1, 2 or 3 sample loops of bromoform in the nitrogen stream from the permeation oven onto the TDU adsorbent bed for analysis (Figs. 2.1 and 2.5; Chapter 3.4). To avoid a possible loss of sample, the TDU adsorbent bed was pre-flushed with nitrogen gas and there was no gas flow through the adsorbent bed after the loading of bromoform loops.

2.2.4 Calibration: sparging flasks

A full description of all the sampling methods used during the laboratory diatom culturing experiments can be found in Chapter 5. A 100 m*l* aliquot of culture medium was transferred to a glass trap for immediate sparging. Samples were sparged with nitrogen gas (Grade 5.0) for 5 minutes at a flow rate of 100 m*l* min^{-1} and trapped on a TDU trap held at room temperature ($\sim$20 °C). The TDU traps were stored in the dark at approximately 0 °C and analysed within 6 hours.

2.3 Injection procedure

Once trapping of an air sample was complete, the TDU adsorbent bed was flushed with nitrogen gas for 5 seconds, removing any stagnant air, remnant in the trapping phase, prior to injection. The graphical user interface (GUI) was used to start recording data at the same time as the heating of the trap was initiated.

A small flask of liquid nitrogen ($N_{2(l)}$) was placed on the stainless steel loop just before the head of the column. The liquid nitrogen was used to cryo-focus the sample desorbed from the TDU adsorbent bed prior to analysis. The 'load / inject' valve was switched to the 'inject' position once the TDU trap had reached 15 °C, transferring the sample to the column. The injection valve was switched back to the 'load' position after 2 min 30 sec when the internal temperature of the TDU adsorbent bed had reached 300 °C. The flask of liquid nitrogen was rapidly replaced by a cup of boiled water. The cup of boiled water was held in place for 30 seconds, desorbing the trapped sample.

Following the injection of a sample, cooling of the TDU occurred through radiative transfer while a flow of 100 ml min^{-1} of $N_{2(g)}$ was maintained through the adsorbent bed. The cooling under a nitrogen flow resulted in the trap being purged ready for the next sample and the adsorbents were not degraded by reactions with air. Further cooling by chilled recirculated glycol was initiated once the TDU had cooled to below 50 °C. The risk of causing temperature shock damage to the TDU precluded the initiation of the glycol coolant immediately after the injection of a sample. The entire cooling cycle took 10 – 15 minutes to complete.

2.4 Calibration

An external calibration of the GC-ECD system was performed either by permeation oven or gas sparging of liquid aliquots. Details of the calibration technique used for the permeation oven can be found in Chapter 4 and for the sparging flasks in Chapter 5. Triplicates of three to five increases in bromoform concentration were analysed. The resultant peaks were integrated and collated into a calibration curve. This characterised the response of the detector to increasing concentrations, allowing for the determination of concentration or mixing ratio from the integrated peak area of samples.

2.5 Peak integration

The native MATLAB function *TRAPZ* was used to calculate the trapezium area between the inflection points of the detected bromoform peak ($t_R \approxeq 14$ minutes). For a detailed description of peak bromoform peak identification and integration see Chapter 3.4.1. The inflection points of the bromoform peak were manually identified by visual inspection and a straight line baseline height was computed for the area between the inflection points. A calculated rectangular area below the baseline was removed from the *TRAPZ* estimate peak area, to achieve constancy and to ensure only the true area of the peak was measured.

Chapter 3

Development of a gas chromatograph system and method for the sensitive and quantitative detection of bromoform

Gas chromatography (GC) has been used as the principal method of halocarbon measurement since the invention of the electron capture detector (ECD) in the 1960s (Lovelock, 1963; Poole, 2003). The high sensitivity and repeatability associated with GC systems and methods have made it a popular choice in halocarbon measurement. Different users across the globe are able to use variations of the same instrument and methods to achieve comparable results (Jones et al., 2011). The testing of components and methods for the separation of bromoform are explored in this chapter. The methods used for trapping and injecting samples as well as the instrumentation used are examined.

3.1 Gas chromatography

3.1.1 Fundamentals of separation

The time taken for a species to pass through or elute the column is known as the retention time (t_R), which is largely determined by the carrier gas flow rate and the partitioning between the carrier gas and the liquid column wall. The retention time is usually corrected by the hold-up time (t_m, Equation 3.1), which results in the adjusted retention time (t_R'). This is the time it would take a solute that does not react with the stationary phase to pass through the column (Poole, 2003).

$$t_R{}' = t_R - t_m \tag{3.1}$$

The partitioning of species between the phases is determined by distribution coefficient. The distribution coefficient relates the concentrations of the species in the two phases (liquid / gas). Species adhere to the column wall, thus retarding their progress and the greater retention time. The adhesion affinity of a species for the column wall can be adjusted with variations in temperature, thus affecting the retention time (Christie, 1989; Shaw, 2011).

3.1.2 Plate theory of chromatography

Under ideal conditions species should elute with a near Gaussian distribution. Band broadening is a process whereby tailing of the elution peaks occur. This is often the result of overloading or too great affinity for the stationary phase (Poole, 2003). The efficiency of a column can be determined through the estimation of the number of theoretical plates (*N*) within the column. Each plate can be considered a site of adsorption and desorption, partitioning analytes between the stationary and mobile phases. The number of theoretical plates is determined experimentally based on the adjusted retention time and peak width at half hight (Equation 3.2). The theoretical plate height is more commonly known as the the height equivalent to a theoretical plate height (HEPT), which is defined by the number of plates per length of column (Equation 3.3). The column efficiency is therefore directly proportional to the HEPT value (Shaw, 2011; Christie, 1989).

$$N = 5.54 \left(\frac{{t_R}'}{0.5 W_b} \right)^2 \tag{3.2}$$

$$HEPT = \frac{L}{N} \tag{3.3}$$

3.1.3 Rate theory

The rate theory provides a description of processes unaccounted for by the theoretical plate height theory (Shaw, 2011). Contributions to band broadening are considered through the effects of eddy diffusion, longitudinal diffusion and the resistance to mass transfer in rate theory. Band broadening is a major loss of chromatographic performance. It is influenced by a number of physical processes during the chromatographic separation, causing the peak width to increase. These factors affecting band broadening are generally described by the van Deemter equation (Equation 3.4).

$$HEPT = A + \frac{B}{u} + C \tag{3.4}$$

Where A represents the eddy diffusion term, B the longitudinal diffusion term and C the resistance mass transfer coefficients in stationary and mobile phases. The u term is the mobile phase velocity. From the van Deemter equations it was noted that an optimal mobile phase velocity existed. The optimal mobile phase velocity is determined by the longitudinal diffusion and resistance to mass transfer. This optimum mobile phase velocity is demonstrated by plotting HEPT against the mobile phase velocity in a van Deemter plot (Fig. 3.1). The choice of carrier gas affects the optimum mobile phase velocity, with lighter gases achieving higher flow rates (Shaw, 2011). Shorter separation times can be achieved by using mobile phase velocities above the optimal, but at the cost of resolution (Sec. 1.5, Poole, 2003).

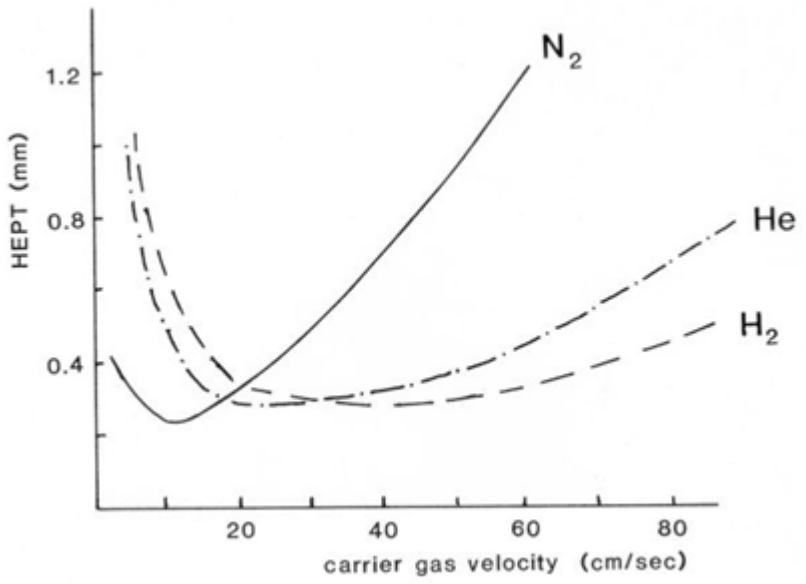

Figure 3.1: Van Deemter plot displaying the relationship between HEPT and carrier gas velocity for helium, hydrogen and nitrogen (Christie, 1989).

3.2 Gas chromatography system

The gas chromatography system was made up of a number of components commonly found in GC systems reported in the literature (e.g., Poole, 2003; Wevill and Carpenter, 2004). The low atmospheric mixing ratios of bromoform (Chapter 1.4) necessitated the need for sample pre-concentration. The pre-concentrated sample was then passed to the column in the oven for separation. A continuous gas flow (carrier gas) propelled the sample through the column where Brownian motion and molecular interaction with the coating on the column walls separated lighter molecules first, then heavier ones (Poole, 2003). While the measurement of the gas concentration in the eluting stream has been made with either an electron capture (ECD) or mass spectrometer (MS) detector, this study used an ECD (Wevill and Carpenter, 2004; Wada and Hama, 2012). The development of these components are discussed below.

3.2.1 GC oven

Testing of the oven was performed to establish the range and rates over which the oven was able to operate. The oven temperature was adjusted to preset limits, defined by the columns used and monitored over time. Thermal stability was assessed by monitoring variability of temperature over time at varying limits. This was performed at a number of predefined temperature limits. Testing indicated that the GC oven was able to maintain temperatures between 30 and 300 °C with an accuracy of $\pm$ 1 °C. To ensure consistency and control, due to hot laboratory conditions, a minimum operating temperature of 30 °C was maintained in the GC oven. A maximum of 300 °C was used to clear contaminants from the column and was the upper thermal limit of the columns utilised. The rate of temperature increase was tested by recording the time the oven took to adjust to a new predefined temperature. A maximum rate of heating of 65 °C min^{-1} was attained by the oven. The stability of the temperature regulation of the GC oven enabled the separation of bromoform. Apart from occasional, necessary reattachment of the heating coil, no work was done to the

GC oven.

3.2.2 Temperature programme

The aim of the temperature programme (TP) was to achieve the separation of bromoform from a mixed air sample, with a practical elution time, utilising a minimum number of adjustments. Bromoform elution times ranging from 9 – 38.8 minutes have been reported depending on the system specifications (Wevill and Carpenter, 2004; Bravo-Linares and Mudge, 2008). Air samples were run under isothermal and varying temperature programmes to determine the ideal conditions necessary to achieve bromoform separation. Between one and six adjustments of temperature were tested. The duration of the temperatures maintained between adjustments were varied in order to achieve the best separation of bromoform (Fig. 3.2). The fixed rate of heating achievable by the GC oven meant that temperature adjustments were based on time. The effectiveness of the temperature programme was determined by means of the resolution equation (Equation 1.21; Chapter 1.5).

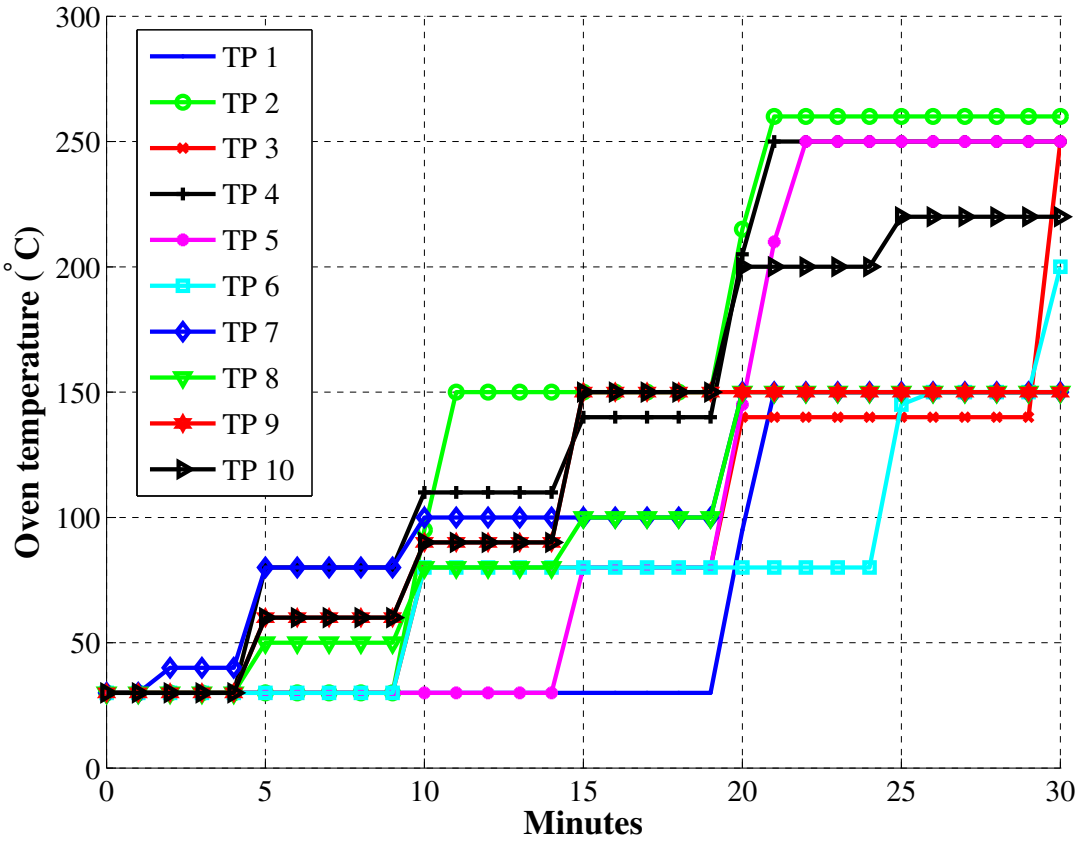

Figure 3.2: Different temperature programmes used with the GC system to achieve suitable separation. Programmes used between November 2008 and October 2011.

Isothermal and variations in temperature with time (ramped temperature programmes) were tested with the GC system to achieve the separation of bromoform. Ramped temperature programmes proved significantly better at achieving sample separation than an isothermal oven temperature (Table 3.1). The chromatography under isothermal temperature control displayed a raised baseline with few, poorly

separated peaks (Fig 3.3a). An improvement in the chromatographic resolution was achieved, over isothermal, with the introduction of three temperature ramps (TP 2 – 6). Oven temperatures were ramped from 5 minutes after injection to address the co-elution of peaks at retention times greater than 12 minutes (TP 7 – 10). The resultant chromatography showed better separation of peaks with chromatic resolution of the order of 7.5. Short temperature maintenance periods ($\leqslant$ 2 minutes, TP 7) were labour intensive and led to marginal improvements in chromatic resolution and challenges in method reproducibility.

Table 3.1: Resolution of chromatography based on temperature programme.

TP No. (Fig. 3.2)	Date	*R*
TP 1	November 2008	1.5
TP 2	June 2009	1.8
TP 3	August 2010	2.1
TP 4	September 2010	2.5
TP 5	March 2011	3.3
TP 6	May 2011	4.2
TP 7	May 2011	4.7
TP 8	June 2011	5.3
TP 9	August 2011	6.9
TP 10	October 2011	7.5

A temperature programme starting at 30 °C, was increased every 5 minutes and maintained at 60, 90, 150, 200 and finally 220 °C, was found to achieve good separation (Fig. 3.3k, TP 10). This final temperature programme effectively separated bromoform from mixed air samples and achieved a bromoform retention time of approximately 14 minutes with this temperature programme. The 220 °C temperature maintenance period at the end of the programme ensured a minimum of build up of contaminants. The TP was sufficiently simple to limit challenges to method reproducibility. The ability to vary the rate of heating or oven temperature more flexibly might have resulted in an improvement to the chromatographic separation.

3.2.3 Detector

Electron capture (ECD) and mass spectrometer (MS) detectors have been used extensively for the measurement of bromoform and halocarbons in the atmosphere (Lovelock, 1963; Wevill and Carpenter, 2004). The ECD is reportedly more sensitive to polar compounds such as bromoform than MS (Carpenter and Liss, 2000; Poole, 2003). However, careful calibration of the ECD is required for the identification of eluting compounds, whereas MS detectors provide mass spectra fingerprints for the identification of eluting compounds. The measurement of compounds in an ECD is achieved through changes in the electrical charge of a thermal electron plasma. The thermal plasma is created from electrons stripped off the carrier and make-up gas by the nickel (^{63}Ni) radioactive source in a heated environment up to 400 °C. When a polar or electron capturing compound enters the detector, electrons within the thermal plasma are

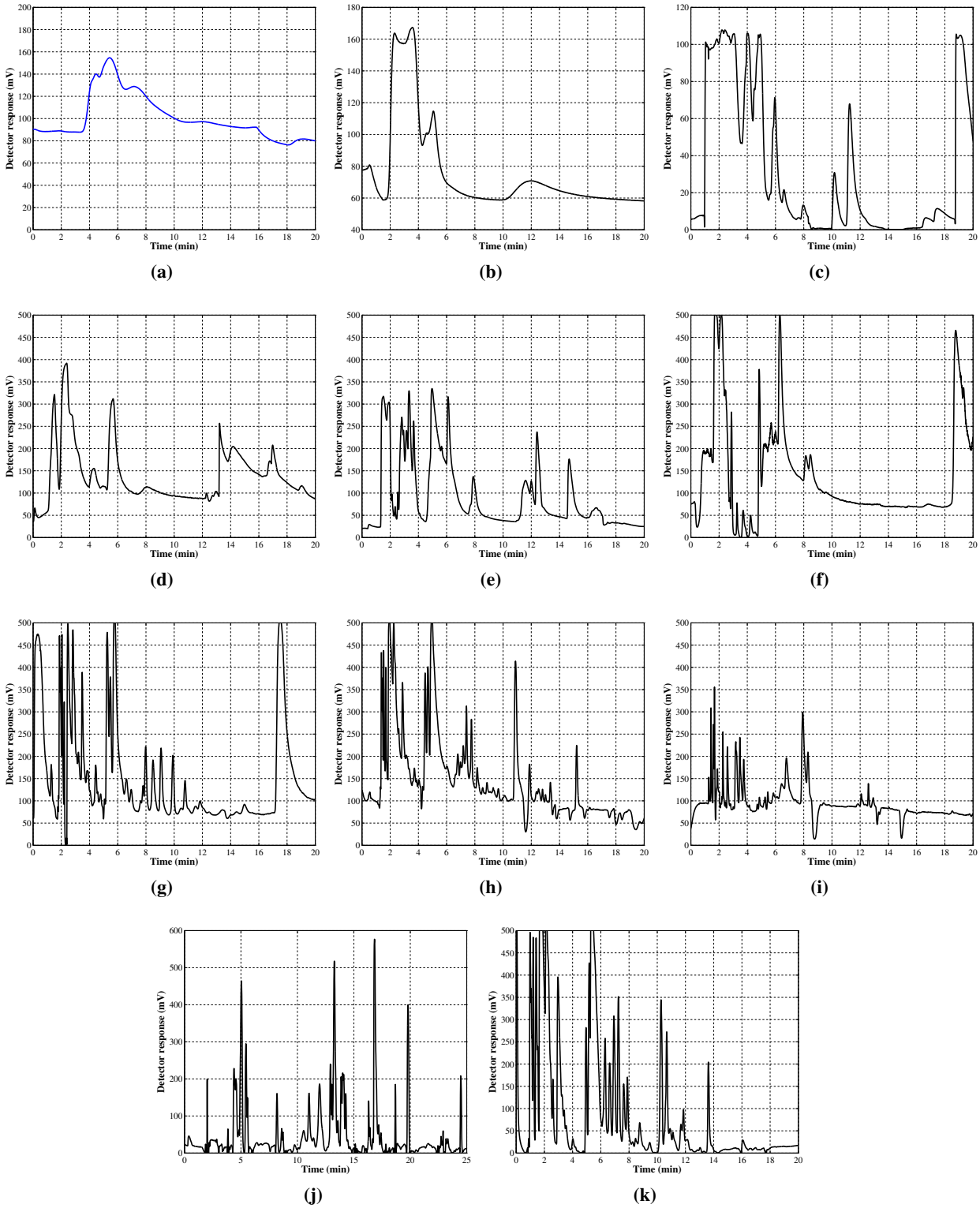

Figure 3.3: Air samples separated on GC-ECD system under different temperature programmes: (a) Isothermal temperature programme achieving poor separation and chromatography, (b) November 2008 TP1, (c) June 2009 TP2, (d) August 2010 TP3, (e) September 2010 TP4, (f) March 2011 TP5, (g) May 2011 TP6, (h) May 2011 TP7, (i) June 2011 TP8, (j) August 2011 TP9, and (k) October 2011 TP10.

removed, reducing the electro-potential between the source and the anode. This reduction in the electrical charge is measured by the detector (Poole, 2003). In contrast, the mass-to-charge ratio of ionised eluting

compounds is measured by MS detectors. Comparison of the generated mass spectrum against archived spectra, allows for the identification of eluting molecules. Previously unidentified compounds can be compared against a library of spectra and, following sets of rules, can be identified.

Combinations of either argon / methane (95 / 5 %) or helium / nitrogen have been suggested to result in the production of an ideal plasma within the ECD. The addition of make-up gas improves the sensitivity and response of the ECD. These are achieved through a reduction of the internal dead volume and a rapid deactivation of undesirable ionisation collisions. Early ECDs utilised wide bore columns, which provided a higher gas flow rate than the modern open tubular columns. The use of open tubular columns results in a lower flow and therefore greater dead volume within the detector. A make-up gas flow rate of 20 – 60 ml min^{-1} has been suggested for the optimal performance of the ECD (Emmert et al., 2007). While helium and argon make good carrier gases, the formation of metastable species from these gases results in them being poor make-up gases. Nitrogen and methane make-up gas rapidly remove ions formed from metastable species transferring excitation energy to solute vapours by means of collision. These collisions may result in undesirable ionisation effects within the detector. A standing square wave current places an electrical charge between the source and the anode, encouraging the electrons within the plasma to migrate toward the anode. A new set of electrons are required to replace the plasma. The introduction of a standing current within an ECD has been shown to eliminate daughter or decay reactants or products, improving the sensitivity and stability of the detector (Poole, 2003). Despite the advantage imparted through elutant identification by MS, an ECD was selected for its higher sensitivity to halocarbons, as well as its ease of use and maintenance.

The ideal operating protocols of the ECD with this system were determined by analysing the output under varying conditions. Variations to temperature, applied standing current and make-up gas flow rate were tested to determine these parameters. A low stable baseline and sensitive response of the detector were the desired result that would verify the cleanliness of the system. Nitrogen blanks (Grade 5.0) were passed through the GC-ECD at ECD operating temperatures of between 250 and 350 °C. Personal observation found that the measured baseline height increased as ECD temperatures departed from 300 °C. A stable and consistent baseline height of 50 mV was achieved with an ECD temperature of 300 °C, suggesting this as the ideal temperature at which to operate the system. A build up of contaminants within the detector, indicated by a general increase in the baseline height, was cleared by raising the ECD temperature to 400 °C for one hour, which resulted in a decrease of the baseline height back to 50 mV.

As repeated 1.5 l air samples were passed through the GC-ECD system, standing currents of between 0 and 2.0 nA were applied to the detector. This investigated the response and sensitivity of the ECD. While the baseline height varied greatly if no standing current was applied (Fig. 3.4a), it was found that the application of standing currents of 0.5 and 1.0 nA resulted in a stable baseline height, resting at 25 and 125 mV, respectively (Fig. 3.4b). Peaks generated in air samples under standing currents of either 0.5 or 1.0 nA were well resolved, displaying a good range of measurements without much noise. Under a standing current of 2.0 nA, the ECD became saturated, resulting in a fixed signal at 650 mV, which

is above the maximum set for the analogue to digital controller and thus rendering the ECD useless to detect samples. Determination of the make-up gas flow rate is discussed in detail below (Sec. 3.2.5). It was found that a make-up flow rate of 30 m*l* min^{-1} nitrogen achieved the best separation and sensitivity (Chapter 1.5).

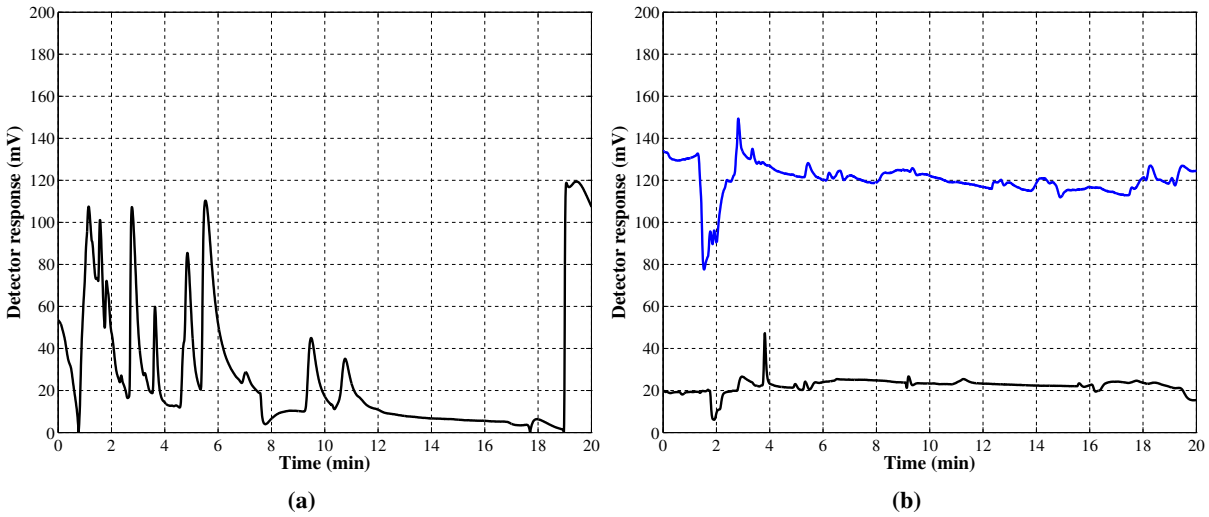

Figure 3.4: Varying standing currents effect on chromatography (a) N_2 blank with no standing current, (b) 0.5 (black) and 1.0 (blue) nA standing current applied to N_2 blanks.

The prerequisites required to operate the ECD were all consistent with previously published reports of operation (e.g., Lovelock, 1963; Simmonds et al., 1976; Poole, 2003). To achieve the best sensitivity and stability of the ECD a constant temperature of 300 °C was maintained, ensuring that condensation from the end of the column did not occur. Application of a 0.5 nA standing current ensured a low stable baseline from which detection of compounds was possible. A nitrogen (Grade 5.0) flow rate of 30 m*l* min^{-1} was constantly run through the ECD during sampling.

3.2.4 Column

Two J&W Scientific dura-bond (DB) PLOT columns were tested to determine which achieved the best separation of bromoform from mixed air samples in this system. Repeated 1.5 *l* air samples were passed through the J&W Scientific DB-5 (30 m x 0.25 mm and 1 μm film) and DB-624 (30 m x 0.32 mm and 1.8 μm, 5 % polarity film) capillary columns at varying carrier gas flow rates (Sec. 3.2.5) and under identical temperature programmes. Assessment of the chromatographic resolution (Table 3.1) was used to determine the efficacy of the columns at achieving the separation of air samples.

The testing of varying back pressures to achieve desired carrier gas flow rates is discussed below (Sec. 3.2.5). It was found that a carrier gas flow rate of 5 m*l* min^{-1} achieved the best separation on air samples in both columns. Due to the larger bore, a lower back pressure was needed with the DB-624 (0.32 mm *vs* 0.25 mm) column to achieve the desired 5 m*l* min^{-1} carrier gas flow rate. This lower back

pressure associated with the DB-624 resulted in improved separation of elutants, especially low molecular weight elutants (Fig 3.5b). Smaller sample volumes were injected into the DB-624 as a consequence of the lower back pressure. These smaller sample volumes resulted in a further improvement to the chromatography.

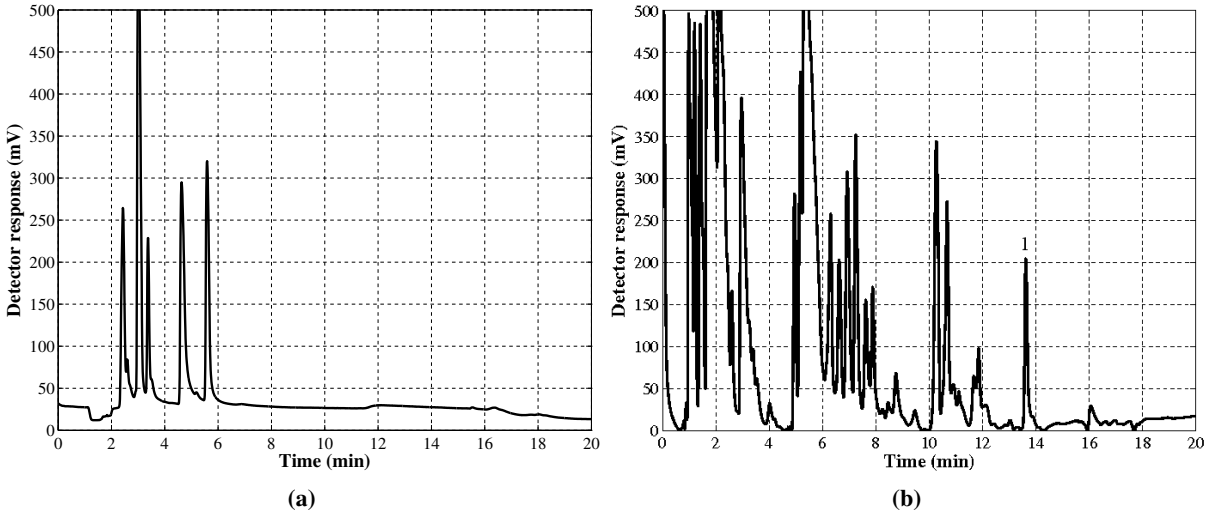

Figure 3.5: Comparison of the ability of columns to separate bromoform (1) from a mixed air samples using a similar method, (a) DB-5 bromoform not detected on this column and (b) DB-624.

The DB-5 column displayed greater thermal stability and a higher temperature limit than the DB-624, which proved important during the development as it was more durable under excess heating. The DB-5 column responded to changes in temperature more rapidly than the DB-624, due to the smaller bore. The thicker film in the DB-624 and lower required back pressure were instrumental in providing separations of low molecular weight compounds, which had co-eluted with heavier compounds from the DB-5 column (Fig. 3.5). Thermal stability of the bonded film in the DB-624 was lower than that of the DB-5, implying considerable care had to be taken to ensure that column bleed was kept to a minimum. The DB-624 displayed a lower maximum operating temperature than the DB-5; however, on this system, better chromatographic resolution was achieved with the DB-624. Therefore the DB-624 was used for the remainder of the study.

3.2.5 Carrier and make-up gas

The aim of the carrier gas is to provide a transport mechanism through the column for elutants at a rate that maximises separation and optimises total elution time. The carrier gas (CG) flow rate was regulated by the back pressure at the head of the column. A Varian digital gas flow meter was used to measure the CG flow rate from the ECD exhaust under different back pressures. Back pressures at the head of the column of between 100 and 1500 kPa were tested to establish the pressure relationship on flow rate. The results suggested an exponential relationship between pressure and flow rate. This allowed for the prediction of flow rate through the column based on back pressure.

The retention time of bromoform in air samples and calibration standards was measured under different back pressures. It was found that back pressures of 100 – 300 kPa achieved bromoform retention times of 25 – 12 minutes, respectively (Fig. 3.6a – c). A column head back pressure of 200 kPa was found to yield a 5 ml min^{-1} carrier gas flow rate, which resulted in bromoform retention time of 14 minutes (Fig. 3.6b). The chromatographic resolution of air samples run at 200 kPa was better than samples run at 100 or 300 kPa (Fig. 3.6a or c). An increase of back pressure to 300 kPa resulted in a decrease in the elution time of bromoform from 14 to 12 minutes (Fig. 3.6b or c). The raised pressure caused an increase in co-eluting of compounds at short retention times, making the identification of bromoform difficult. Air samples run at a column head back pressure of 100 kPa were found to exhibit a bromoform retention time in the order of 25 minutes (Fig. 3.6a). The lower back pressure resulted in poorer separation, which included peak tailing and an undiagnosed peak at 15 to 20 minutes. A total time of 20 minutes for all elutants of interest to pass through the column was achieved with a back pressure of 200 kPa, making it efficient for long-term sampling.

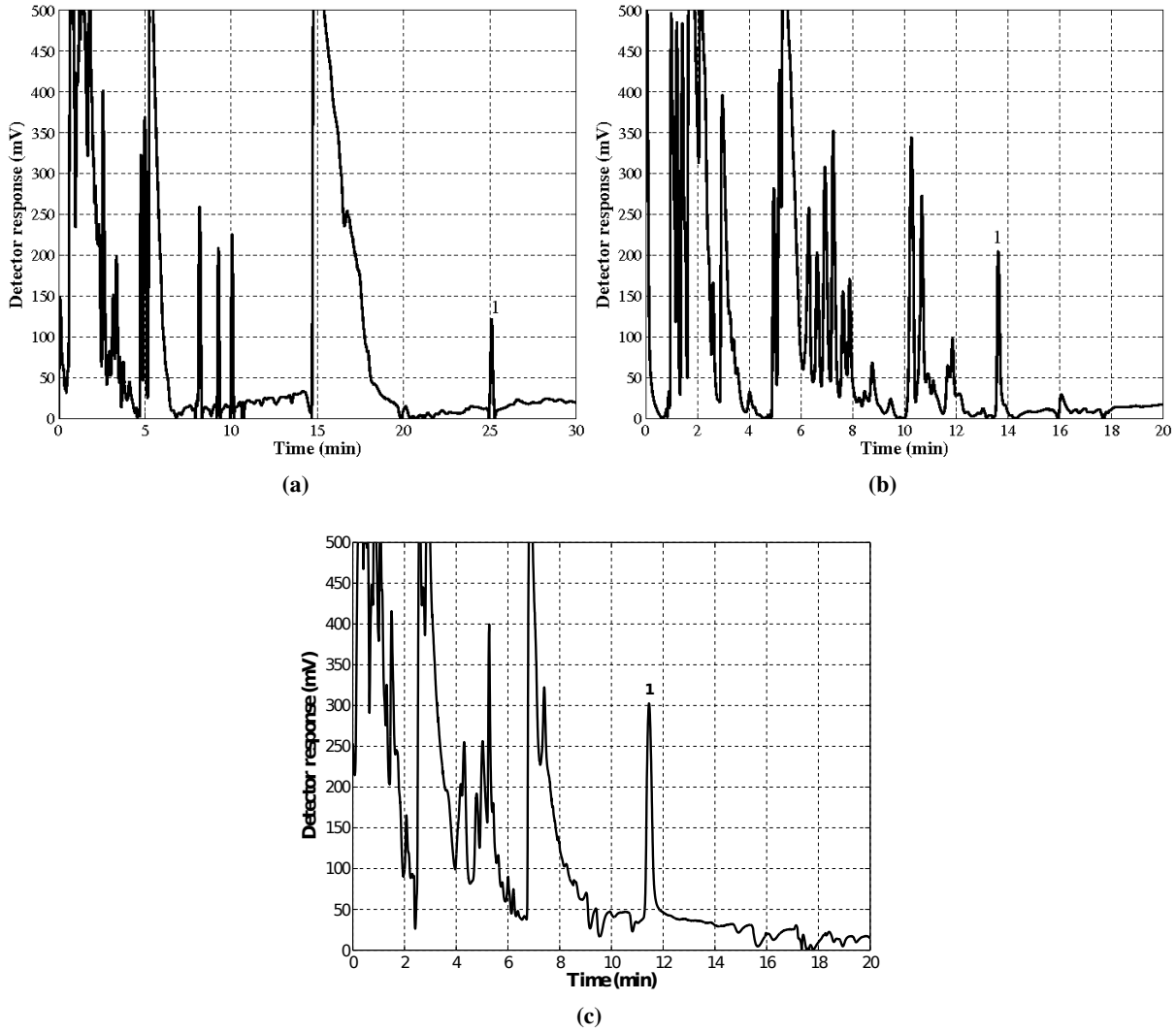

Figure 3.6: Chromatograms showing the pressure effects on the elution time of bromoform (1) with varying back pressure. Air samples run at: (a) 100 kPa back pressure, note the longer time axis (b) 200 kPa, and (c) 300 kPa back pressures.

A slight increase in the recorded baseline height was noted toward the end of the chromatographic runs. Testing of nitrogen blanks under isothermal and temperature programme conditions indicated that the rise in baseline height was related to heating. It is hypothesised that the rise in baseline height is due to either an increase in gas viscosity or column bleed. Gas viscosity has been shown to increase with temperature. The increased viscosity would decrease the carrier gas flow rate and therefore raise the baseline height. It has been suggested that higher temperatures result in the decomposition of the column stationary phase and elute with the sample (Poole, 2003). The decomposition of the stationary phase would reduce the efficacy of the column in separating samples. To address the change in gas viscosity associated with increasing temperature, the column head back pressure might be raised to ensure an entirely constant carrier gas flow rate (Poole, 2003). Since this rise in baseline height appeared to be neither masking important eluting peaks nor reducing the separating ability of the column, no further investigation was pursued. Neither the back pressure nor gas flow rate were adjusted during the analysis of a sample in order to address the rise in baseline height.

Helium (94 - 99 % purity) and nitrogen (Grade 5.0) were added directly to the detector at varying rates to determine which inert gas and what flow rate was needed to achieve the optimal stability and sensitivity of this system. The chromatography of repeated 1.5 *l* air samples was assessed while either helium or nitrogen make-up gas was added at varying flow rates. Make-up gas flow rates of between 10 – 38 m*l* min^{-1} were tested (Table 3.2). The flow rate of make-up gas through the detector was controlled by the cylinder pressure regulator and a Porter valve. A Swagelok needle valve was used as a daily shut off. It was found that nitrogen added at a rate of 30 m*l* min^{-1} resulted in a chromatographic resolution of 7.5 (Table 3.2). The ratio of 1:6 carrier to make-up gas appeared to produce an ideal plasma. The addition of make-up gas at flow rates < 30 m*l* min^{-1} resulted in the accumulation of metastable species, producing ionisation effects (Poole, 2003). The sensitivity of the system appeared to decrease at make-up flow rate above 30 m*l* min^{-1}. Samples were found to be diluted below the limit of detection (LOD) under high gas flow rates.

Table 3.2: Variations in chromatographic resolution (R) as a function of make-up gas flow rate.

Make-up gas (m*l* min^{-1})	**Baseline (mV)**	***R***	**Maximum (mV)**	**Minimum (mV)**
10	$\sim$ 50	0.5	175	55
12	35	1.1	500	35
15	35	2.4	500	35
20	50 – 100	3.1	500	10
25	25	4.7	500	10
28	35 – 50	5.3	500	0
30	50	7.5	375	0
33	25 – 150	5.1	500	10
38	$\sim$150	5.0	175	35

The chromatographic resolution showed a significant improvement with the addition of make-up gas (Fig. 3.7). This included an increase in the dynamic range of response to eluting compounds and a better separation of individual peaks (Fig. 3.7). The improvement in chromatography associated with the introduction of make-up gas was probably due to the increased flow rate through the detector. Eluting compounds stagnated in the detector under the low carrier gas flow, which negated the separating effects of the chromatography and allowed the accumulation of reactive metastable species. Nitrogen (Grade 5.0) replaced helium when ionisation effects within the ECD became too severe. The ionisation effects in the ECD made the detection of eluting compounds difficult and introduced large uncertainty (Fig. 3.7). A nitrogen gas flow rate of 30 ml min^{-1} through the detector was found to achieve the best chromatography, based on repeated 1.5 l trapped air samples (Table. 3.2). The improved detector range and ability to differentiate between eluting compounds, under the nitrogen make-up gas, stems from a decrease in the metastable species within the ECD. The nitrogen gas flow ensured eluting samples were not stagnated within the detector. Ions formed from collisions between metastable species and elutants were, consequently, rapidly removed (Poole, 2003). This ensured a minimum of ionisation effects limiting the detection of eluting compounds. The improvement in chromatography allowed for the identification of bromoform in the chromatograms. While bromoform was the primary trace gas examined the long-term aim was to be able to quantitatively detect a suite of related halocarbons in the atmosphere.

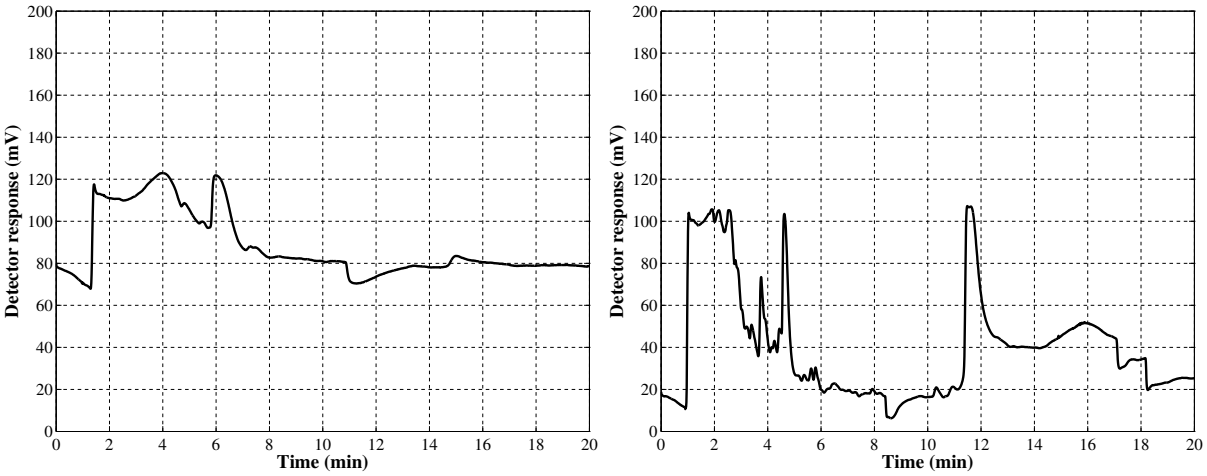

Figure 3.7: The effect of helium and nitrogen added to ECD as make-up gas. Chromatograms of air samples separated with the DB-5 column, (a) with helium make-up gas and (b) with nitrogen make-up gas. Note the improvement in sensitivity and detection with the addition of nitrogen make-up gas.

3.2.6 Injection valve

To maintain simplicity of the system a manual injection valve was utilised. A Valco 6-port injection valve was used to direct the carrier gas to either trap or inject samples to the column (Fig. 2.2). Gas plumbing through the valve was achieved by means of $\frac{1}{8}$" Swagelok fittings. It was found that a factor affecting the chromatography was a dead volume between the adsorbent trap and the head of the column. In an attempt to address this, the injection valve was placed as close as possible to the oven inlet, minimising the

amount of tubing required to bridge the gap between the trap and the head of the column (Fig. 2.1). The dead volume was further reduced by placing $\frac{1}{16}$" tubing between the valve and the head of the column. To achieve an absolute minimal dead volume between the trap and column, it has been proposed that a section of deactivated column be used (as at the University of York) for the transfer of compounds (C. Jones, University of York, pers. comm. 2009). The advantage of the deactivated column is the small dead volume achieved. Sample volumes were subsequently kept small and ensured a simple transfer to the column. Deactivated column for this purpose, is however, expensive and prone to breakages at the termination points. This suggested that a deactivated column transfer line was unsuited for this project. Heating this transfer line, to ensure that the sample did not condensation after desorption, would have posed a further challenge and expense. These complications made the use of a deactivated column impractical in this system. Improvement of chromatographic resolution was achieved through a reduction of dead volume with the addition of the $\frac{1}{16}$" tubing, as described earlier.

3.2.7 Sample pre-concentration

Background open ocean atmospheric mixing ratios of bromoform and halocarbons have been recorded in concentrations of low parts per trillion, while coastal mixing ratios in the tens of parts per trillion have been reported (Quack and Wallace, 2003; Pyle et al., 2010). These low mixing ratios make measurement an analytical challenge. Pre-concentration of air samples is essential in the measurement of bromoform mixing ratios. The literature suggests 'freezeout' trapping and thermal desorption as the main methods of sample pre-concentration of bromoform and other halocarbons (Khalil et al., 1983; Wevill and Carpenter, 2004; Poole, 2003). Both methods involve a cooling phase in order to achieve the trapping of bromoform from the air. The adsorbents used in a thermal desorption unit have been designed to trap bromoform from passing air samples at a range of temperatures, assisting in samples for analysis (Poole, 2003). The headspace above liquid nitrogen and recirculation of a cooled solution have been used for cold loop trapping, while Peltier plates have been used for cooling of adsorbent tubes in thermal desorption units. Desorption of the trapped samples by heating with boiled water and resistance coils or heater plates has also been reported for 'freezeout-loops' and adsorbent beds, respectively (Khalil et al., 1983; Wevill and Carpenter, 2004). 'Freezeout-loops' and adsorbed bed thermal desorption systems were tested to develop a simple, reliable method for the pre-concentration and injection of bromoform from air samples.

3.2.7.1 Stainless steel sample loop

Stainless steel loops (19.1, 14.4 and 1.0 cm^3) were cooled with a salted ice water solution. The salted ice water solution was stored in the freezer at -20 °C. The coil was cooled for 15 minutes during sample trapping. At the time of injection the cooling solution was rapidly replaced with a cup of boiled water. The heated water was held in place for 10 – 30 seconds to desorb samples from the 'freezeout-loop'. This trapping mechanism failed to produce a successful trapping of bromoform. The lack of detected bromoform might have been the result of the large trap volume, insufficient cooling or a lack of adsorption sites such as glass beads to assist in trapping. The large trap volumes may have limited the ability of the loop to adsorb bromoform from the passing air. The column may have become overloaded, due to the

large sample volume injected, resulting in an inability of the system to separate bromoform. Decreasing the 'freezeout-loop' volume did not appear to result in an improvement to the recorded chromatography or the ability for the system to trap and analyse atmospheric bromoform. The immersion of a stainless loop in liquid nitrogen (-183 °C) has been used for 'freezeout-loop' trapping and enrichment of air samples (Khalil et al., 1983; Kolb, 1999). This suggests that the salted ice water solution (-20 °C) may not have been sufficient to trap and hold bromoform.

3.2.7.2 Thermal desorption unit

Alternatively, two custom thermal desorption units (TDU) were built by UniTemp (Cape Town) for the cooled trapping of bromoform on an adsorbent bed. The TDUs were based on the design described by Wevill and Carpenter (2004). A brass or ceramic central tube, wrapped in a heating element, housed a 5 or 6 mm OD glass tube. Carbon adsorbents were held in place in the glass tube by means of glass wool plugs at either end of the tube. The whole unit was encased in a brass block and cooled by either an enclosed water jacket or spiralled coil surrounding the housing (Fig. 2.3 and 3.8). The literature suggests that a trap temperature of -10 °C is the most effective for charcoal adsorbents. It is also suggested that the flow rate of 100 m*l* min^{-1} is the ideal sampling rate (Wevill and Carpenter, 2004). A Lauda RM-6 recirculation water chiller was used to refrigerate pure glycol to -15 °C for the cooling of the TDU. The glycol solution was recirculated around the TDU, maintaining a temperature of -10 °C within the adsorbent bed. This temperature was maintained throughout the trapping phase.

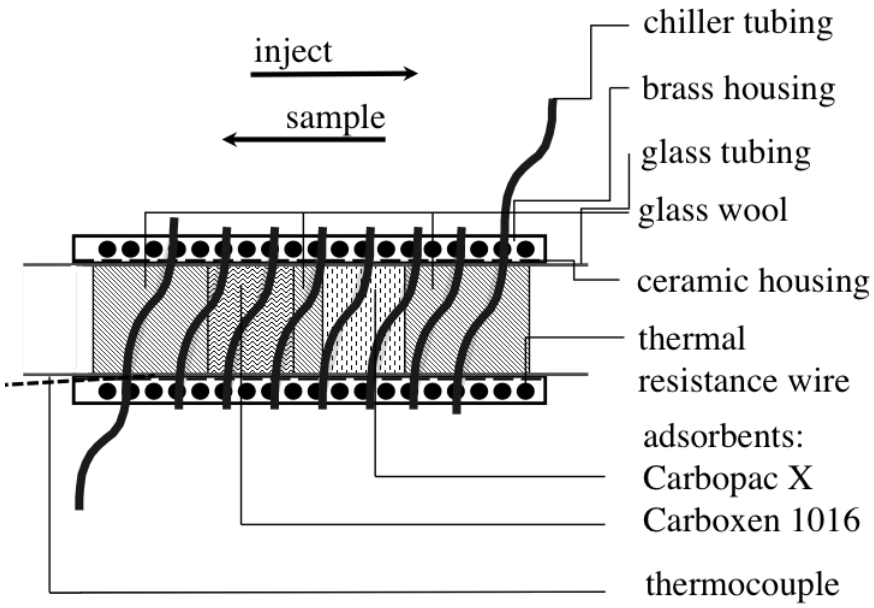

Figure 3.8: Schematic diagrams of thermal desorption unit with adsorbent bed.

The ceramic tube TDU had an inner diameter of 6 mm and length of 20 cm (Fig. 3.8). The high resistance coil was heated by direct current supplied at 28 V and 4.46 A *via* a Topward 3306D power supply unit, with temperature regulation achieved by means of an embedded thermocouple. The K-type

thermocouple was mounted in the brass housing, near the inner surface of the ceramic tube (Fig. 3.8). The unit was able to achieve a temperature of 300 °C within the adsorbent tube in 3 min 30 sec. The brass tube TDU was smaller with an internal diameter of 5 mm and length of 10 cm (Fig. 2.3). An alternating current resistance coil was used to heat the unit to 300 °C in 2 min 30 sec. A purpose-built controller with a temperature cutoff relay was used to power and regulate the temperature within the adsorbent bed of the brass TDU.

A decrease of inner tube width within the TDU resulted in a decrease in the injection time required to desorb samples (Fig. 3.9). The slope of rising temperature with time within the glass adsorbent tube increased from 1.4 to 2.0 (Fig. 3.9). This increase in the slope was linked to the change in tube material, the smaller dimensions and the power source, which all resulted in greatly improved chromatography. The ceramic inner tube exhibited a large thermal inertia, delaying the initial heating of the adsorbents. The transfer of heat to the adsorbents was greatly improved with the use of a brass inner tube, improving the desorption of trapped compounds. The smaller diameter of the brass TDU achieved a more uniform desorption of trapped compounds, transferring heat to the core of the adsorbent bed more efficiently. The change of heating coil from direct current (DC) to alternating current (AC) resulted in a more consistent internal temperature within the adsorbent bed. The consistent heating of the adsorbent bed across the full range of temperature (-10 – 300 °C) resulted in a more stable desorption, decreasing band broadening of detected peaks. The improved chromatography was demonstrated by the better separation and the limiting of band broadening of detected peaks.

During the cooling phase, the TDUs developed condensation and ice on the exposed outer surfaces. The tubing to and from the chiller also had a build up of ice (Fig. 3.10a). Ice on the TDU had a two-fold problem: (i) it slowed the heating rate of the unit during sample injection and (ii) water (condensation and ice melt) was able to enter the electronics of the trap and caused the unit to short circuit. This was particularly problematic with the ceramic tube TDU. The rate of heating of the trap when laden with ice was reduced as the ice and water created an additional thermal inertia to the heating of the trap. This build up of ice on the trap resulted in a decrease in the chromatographic resolution and consequently created tailing of the peaks detected. The insulation of tubing and metal surfaces with glass wool and high density foam (Fig. 3.10b) resulted in a significant decrease in the amount of ice build up. Insulation of the TDU also increased the rate of heating.

The adsorbent bed was contained within a glass tube and held in place with glass wool plugs (Fig. 3.8). Two adsorbents (Carbopack X and Carboxen 1016, Supelco) were used, in series, in the traps. The mass of adsorbents used was quantified by the testing of decreasing masses of adsorbents to achieve the best chromatography by the number of elutants separated (Table 3.3). The thermal inertia resulting from larger masses of adsorbents produced poor chromatography. The slow rate of heating resulted in an inadequate separation of peaks and strong band broadening. The non-uniform heating of the adsorbents was thought to be responsible for the band broadening through inconsistent desorption of elutants. Smaller adsorbed

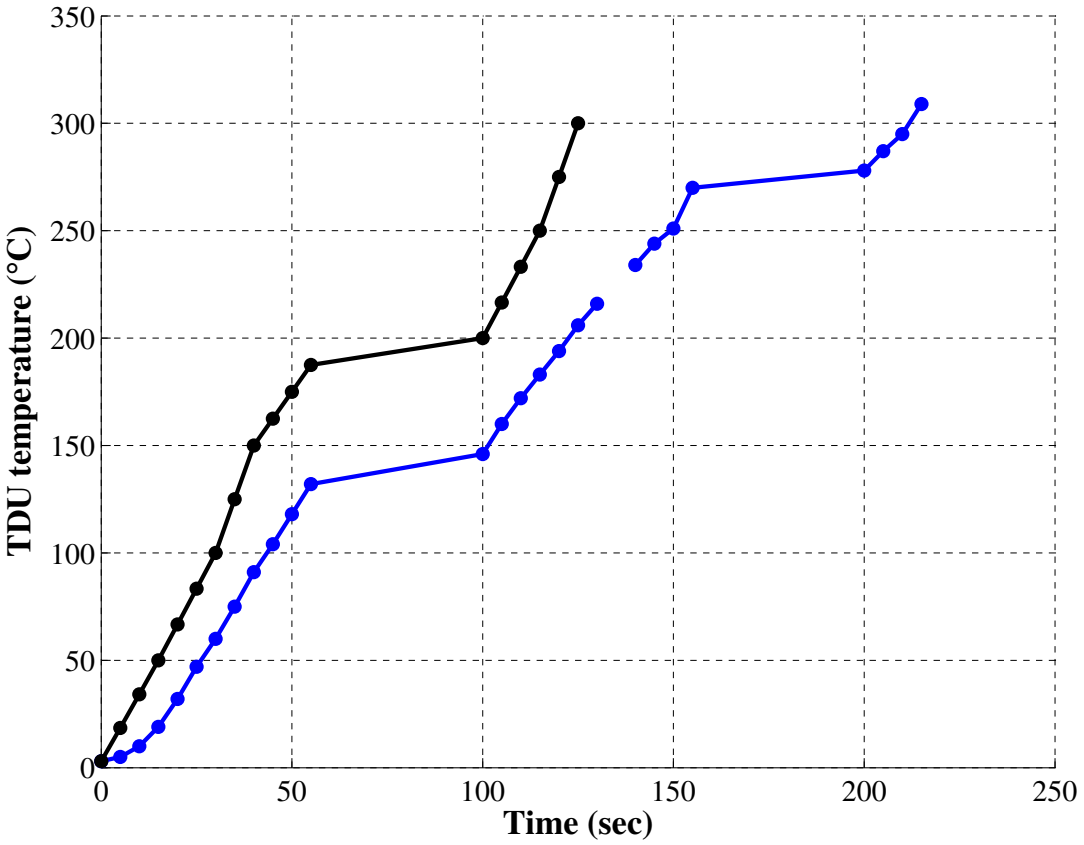

Figure 3.9: Temperature profiles for heating of TDUs. The all brass TDU (black) and ceramic inner tube TDU (blue).

beds and injected volumes were used in an effort to combat these problems. The smaller adsorbent bed volumes might result in a greater chance of sample breakthrough (Sec. 3.3).

Table 3.3: The number of peaks detected as a function of TDU adsorbent mass.

Carbopack X (mg)	Carboxen 1016 (mg)	Column	No. of peaks	TDU used
109	97	DB-5	0	ceramic
18	18	DB-5	5	ceramic
75	75	DB-5	10	ceramic
9	9	DB-5	25	brass
9	9	DB-624	50	brass

The DC power supply was, on occasion, left to heat the adsorbent bed and an internal temperature of between 400 – 700 °C was reached. Heating to this level resulted in the decay of the granular adsorbents to pellets of charcoal (Fig. 3.11). The pellets could not act as adsorbent in the drying trap as the number of active sites for adsorption was greatly reduced and the pellets did not cover the entire inner diameter of the glass tube. Consequently the adsorbent bed had to be repacked. A temperature driven feedback cut-off in the AC power regulator prevented the temperature in the adsorbent bed exceeding 350 °C.

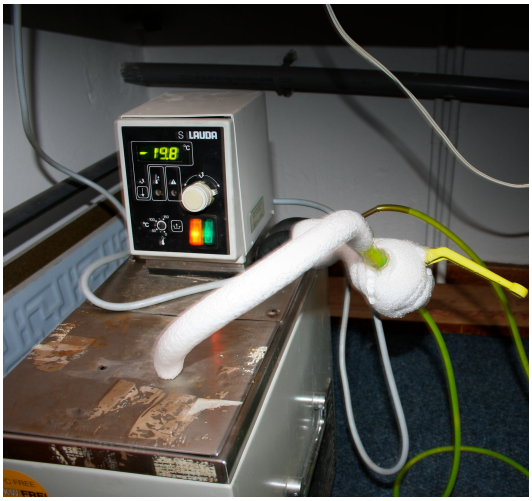

(a)

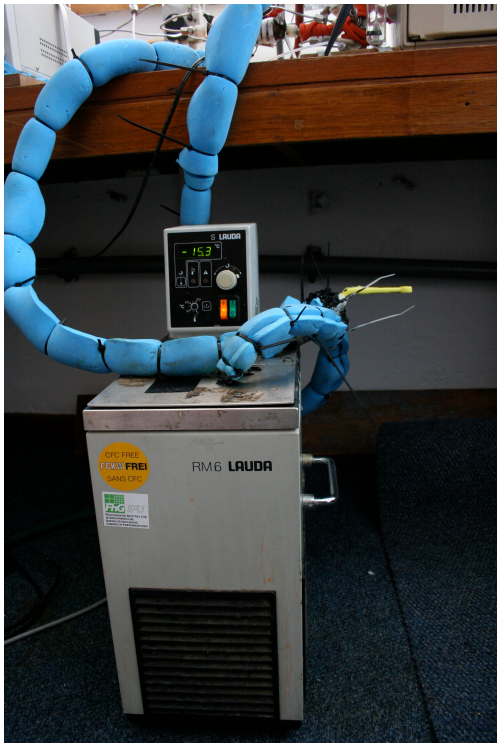

(b)

Figure 3.10: Build up of ice on exposed surfaces from the recirculation chiller, (a) accumulation of ice and (b) foam covering limiting accumulation.

In halocarbon measurement, glass is the best medium with which to work because volatile halogenated organic compounds (VHOCs) are not trapped by glass as they are with plastics (Moore, 2003). While useful, glass is brittle and the connection of glass to metal is a weak point. Metal nuts and ferrules crush glass tubes before a gas tight seal can be formed. Swagelok produce PTFE nuts and ferrules for use with glass in metal connectors. While limited in size range, an integrated PTFE nut and ferrule worked well on the TDU traps. The end of the glass tube had to be taped with PTFE tape to help achieve a gas tight seal between the tube and the union. This ensured that the glass tube was not crushed when the nut was tightened to complete the seal. On the drying trap a set of Swagelok PTFE nuts and ferrules were initially

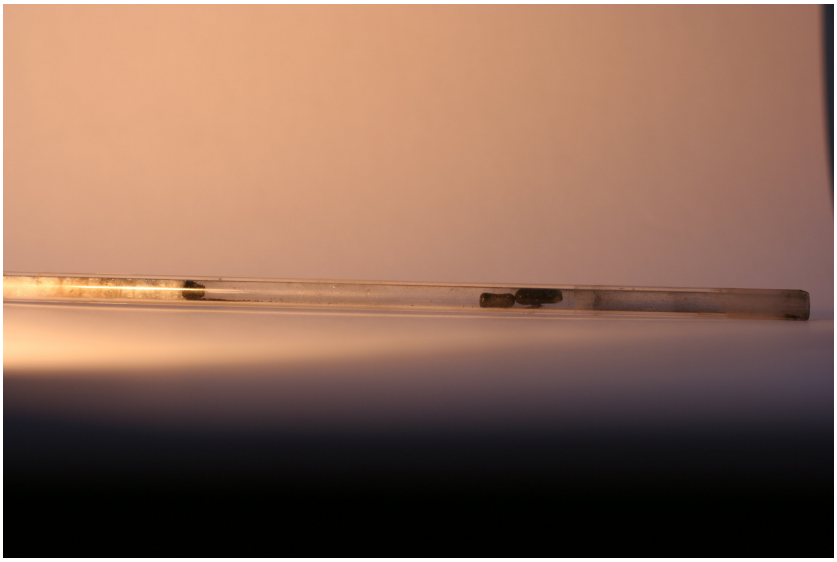

Figure 3.11: Thermally decayed adsorbents within the TDU when temperatures exceeded 400 °C.

used. The hard PTFE plastic was not malleable and often broke the tubing, if over-tightened. The nuts quickly lost shape and were difficult to fit onto the union without over-tightening. It was found that a short section ($\pm$ 5 mm) of silicone tubing approximately the same diameter as the glass tubing made an excellent gas tight seal. The silicone tubing was fitted over the glass tube where the ferrule would be seated and a metal nut could then be used to secure the glass tube in the union, providing a gas tight connection with minimal chance of collapse from the glass tube. The nut needed only to be finger tight to provide a gas tight seal up to 200 kPa.

3.2.8 Mass flow controller

A mass flow controller has been used in previous studies to regulate the sampling flow rate at 100 ml min^{-1} (Wevill and Carpenter, 2004; Palmer, 2006). Consistent gas flow rate through the sampling trap results in identical sample volumes. The all metal (stainless steel) ASM AFC-260 mass flow controller was tested at flow rates between 50 and 200 ml min^{-1} confirming that a sampling gas flow rate of 100 ml min^{-1} achieved the most consistent sample volumes. This flow rate minimised sampling time while limiting the chance of sample breakthrough from the adsorbent trap. The MFC was placed between the pump and the TDU (Fig. 2.1). This MFC placement was found to achieve the most consistent gas flow rate. The MFC was found to operate better in a 'push' rather than a 'pull' mode (Sec. 3.2.9).

3.2.9 Air pump

A Rocker 400 piston pump was tested for use in this system. This oils free mechanical pump was capable of displacing 400 ml min^{-1} of air, exceeding the requirement of the system. The air pump used for sample collection was tested in both a 'pull' and 'push' position within the sampling system. In the 'pull' position the pump was placed after TDU and air samples were effectively pulled through the system by the suction created by the pump. The pump was not able to generate a consistent suction through the sampling system, which resulted in a weak, fluctuating flow rate. The inconsistent flow rate introduced a large uncertainty

in the volume sampled, rendering it non-ideal. In the 'push' configuration the pump was placed upstream of the MFC and TDU and air was forced through the GC system. The build up of pressure in the pump by the MFC regulating the flow caused the pump to stall and excess air was vented to the laboratory. The pump was left in the 'push' configuration as this resulted in the best flow through the system.

3.2.10 Drying trap

Water trapped from air samples has been suggested to cause damage to the column and mask eluting peaks. Nafion tubes and chemical desiccants have been used to remove moisture prior to trapping on a chilled adsorbent bed (Moore and Groszko, 1999; Wevill and Carpenter, 2004; Poole, 2003). A loss of bromoform from samples was not reported with the use of these drying systems (Moore and Groszko, 1999; Wevill and Carpenter, 2004). A simple, cost effective method to dry air samples prior to trapping was developed for use during the present study. The initial expense of Nafion tubes and requirement of dry air precluded their use. Instead, a tube of magnesium perchlorate was used to dry incoming air samples prior to bromoform sampling (Moore and Groszko, 1999).

Glass pipettes (5 m*l*, ≈20 m*l*, and 25 m*l*) and glass tubing (8 mm OD, 150 mm length) were tested as the storage method for the magnesium perchlorate desiccant. These made up the drying traps in the system. The two commercial pipettes (5 and 25 m*l*) were conveniently shaped for use as drying traps. It was found that the desiccant was rapidly depleted from the 5 m*l* pipette, rendering it unsuitable for long-term use. The flow rate through the packed 25 m*l* pipette was severely reduced below 100 m*l* min^{-1}. Packing of these traps was a challenge due to the small diameter of the leading glass tubes. The non-standardised OD size of the tubes precluded the use of Swagelok fittings to make a gas tight connection. The traps were useful in establishing that a desiccant load between 5 and 25 m*l* was required to dry samples without restricting flow rate.

A custom-built glass drying trap (20 m*l*, 8 mm OD; Fig. 3.12) addressed the problems listed above. Packing of the trap was greatly simplified and gas tight fittings could be made. The magnesium perchlorate was held in place within the trap by means of glass wool plugs at either end. It was found that a vertical orientation of the tube achieved the best drying by ensuring that air samples passed through the desiccant. Air flow was restricted if the trap was filled with desiccant; however, it was found that a 75 % fill volume optimised both sample drying and limited gas flow restriction. A gas tight seal between the glass tube of the custom trap and metal fittings was achieved with a silicone ferrule, cut from a piece of tubing and fitted over the glass tube. A metal nut could then be used to close the connection, tightened finger-tight.

3.2.11 Computer interface

A custom graphical user interface (GUI) and analogue to digital conversion (ADC) system were developed such that the data output from the ECD could be read by a personal computer. Due to the age of the ECD (± 40 years, S. Britz, PerkinElmer S.A., pers. comm. 2008) the only available output was in the form of an analogue signal. Commercially available GC software has been designed and customised for modern

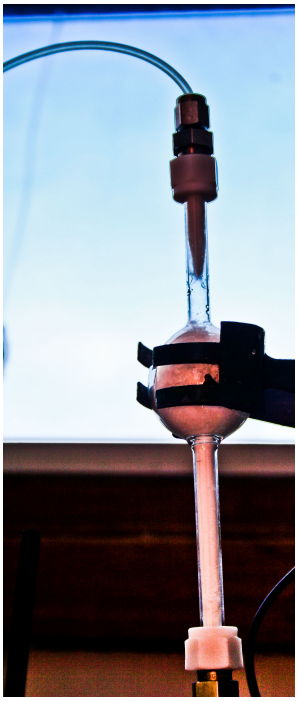

Figure 3.12: Custom glass drying trap used in the GC system.

hardware and specific configurations. This made these programs unsuitable for use in this project, which necessitated the development of an analogue to digital conversion system and a method of reading and recording data. ADC of data has been performed extensively by SAWS at the Cape Point GAW station and it was decided to use their prior experience in this respect.

The analogue output from the ECD controller was converted into a digital signal by means of Advantech ADAM 4017 and 4052 units. The ADAM units were connected in series to perform the analogue to digital conversion (ADC). Upon receiving the instruction, the ADAM 4017 converted the analogue signal to digital and transmitted it to the ADAM 4052. The latter unit acted as the communicator between the ADAM 4017 and the computer. The instructions transmitted to the ADAM 4017 from the computer via the ADAM 4052 were available in the ADAM manual. Text commands were sent through the RS-232 or serial communications port on the computer to the ADAM 4052 which communicated with the ADAM 4017 over RS-485 protocols through direct cable connection.

Adam.NET, Minicom and MATLAB software programs were tested for use as a computer interface. The program was required to: (i) read the output from the ADAM units, (ii) display the returned data in real-time and, (iii) record the data for later analysis. All three programs were able to establish a connection with the ADAM units and to read the string data returned. While the Adam.NET program had the capacity to display the returned data, the data was not stored. Within the software there were no mechanisms present for the storage or analysis of the returned data. Data read into the computer by Minicom was displayed as a list of strings that could not be saved. MATLAB was used in favour of Minicom and Adam.NET programs as it featured the ability to display, store and analyse the data returned from the ECD.

A custom graphical user interface (GUI) was developed in MATLAB using a set of commands to connect to and collect data from the ECD via the ADAM units (Fig. 3.13). Commands for the control and regulation of the ADAM 4017, obtained from Advantech, were passed through the ADAM 4052 from the computer. A single packet of data was returned at each request from the computer. Consequently, the code was looped to run through 5000 iterations with a 0.25 second pause between command cycles. This achieved a recorded chromatogram time of 35 minutes (Fig. 3.13). The first three, non-descriptive, characters from the returned data string were truncated and the datum point was added sequentially, with the concurrent sampling time, to a data file for later analysis. The data was displayed in real-time on a fixed set of axes with time in minutes on the x-axis and the detector response in millivolts on the y-axis (Fig. 3.13). Time for the chromatogram was calculated internally within MATLAB and started concurrently with the injection of a sample. The GUI simplified the data collection process, ensuring consistent data recording for later analysis.

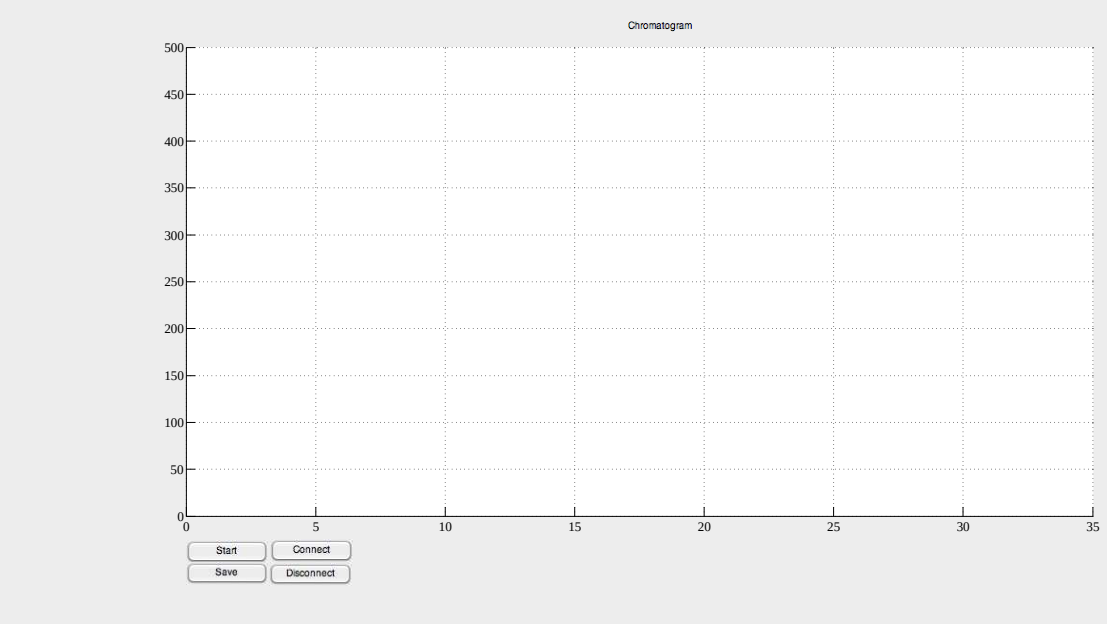

Figure 3.13: Custom-built MATLAB graphic user interface featuring a fixed set of axes for the real-time display of imported data. Operational buttons have been intuitively named and function as expected.

While the GUI made the collection and display of data more streamlined, there were occasional complications. The GUI and MATLAB would crash and have to be restarted if the wrong button was clicked or if the disconnect button was pressed while a chromatogram was running. This would result in the loss of the data for that experiment. The GUI was thus modified to address these problems. The ADAM activation buttons were moved to the opposite side of the fixed axes, lowering the chance of accidentally pressing the wrong button (Fig. 3.14). The code behind the GUI was modified to iteratively save the data as it was imported into MATLAB (see Appendix for full code). Iterative storage of data ensured that only a portion of the data was lost in the event of a power failure, breakdown of communication and / or software or hardware failure. Additionally, data was backed up on external hard drives on a regular basis.

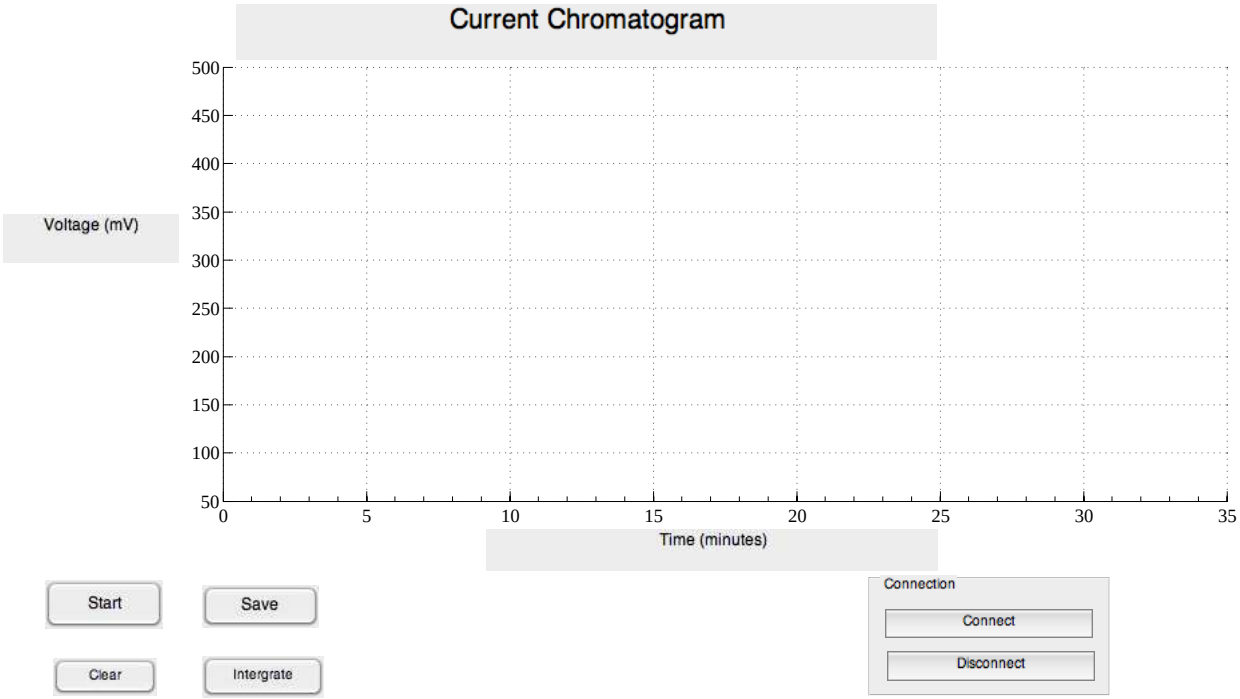

Figure 3.14: The improved layout of the MATLAB graphic user interface with separated operational buttons limiting operator errors.

Further modification of the GUI included the incorporation of system status update figures within the window (Fig. 2.4). A marked box indicated when a connection between the computer and the ADAM units had been established. The time and date stamp across the top of the axes made the recording of the laboratory conditions associated with a particular chromatogram simpler. The resolution of chromatograms was improved by increasing the number of data points recorded within a chromatogram. This was achieved by decreasing the delay between iterations from 0.5 sec to 0.25 sec, about the limit of the ADAM units.

3.3 Trapping of samples

Air samples were trapped on a cooled adsorbent bed held at -10 °C with a sample flow rate of 100 ml min^{-1} (Sec. 3.2.7). Local (UCT, Fig. 1.2) air sample volumes of between 1.0 – 3.0 l were trapped. Variations in trapped volume were analysed to establish the ideal sampling volume that resulted in a good pre-concentration of bromoform and limited chance of breakthrough. Analysis of the chromatography generated from varying sample volumes suggested that medium sized samples achieved the best chromatography (Fig. 3.15). Pre-concentration of bromoform in 1.0 l air samples was low, resulting in greater uncertainty within the measurement (Fig. 3.15). There was no noted benefit in trapping 3.0 l over 1.5 l samples (Fig. 3.15). The chromatography was not significantly better in the larger trapped sample volumes. Also the larger sample volumes required longer to trap, limiting the number of samples that could be performed in a day. Consequently, sample volumes of 1.5 l were used for the analysis of bromoform in this study. This achieved sufficient pre-concentration of bromoform for detection, while limiting the

chance of breakthrough (see below). Breakthrough of compounds from the adsorbent was more likely to occur at larger sample volumes, thus losing part of the sample.

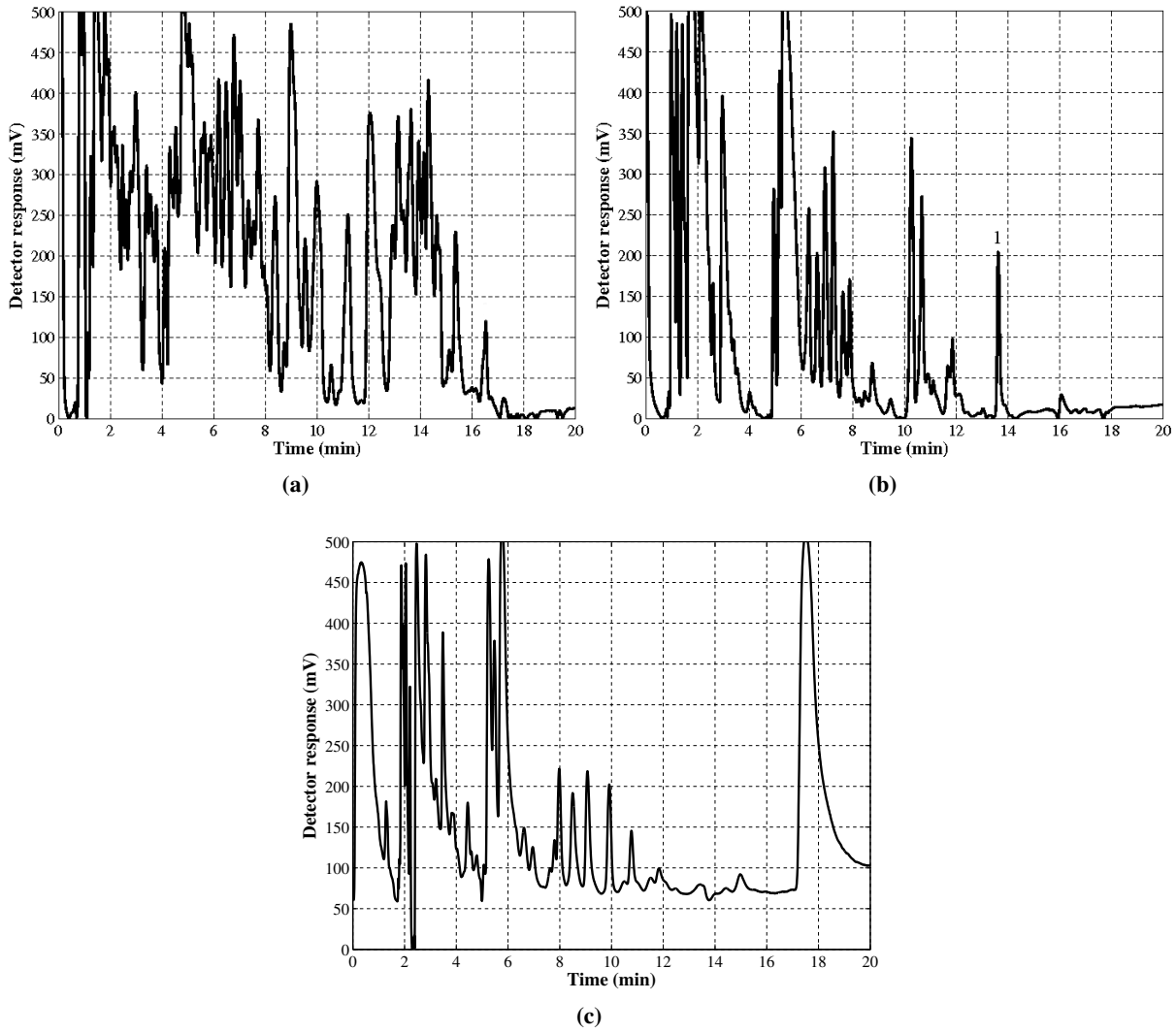

Figure 3.15: Variations in volume trapped (a) 1.0 *l* Bromoform not indicated (b) 1.5 *l* Bromoform (1) (c) 3.0 *l* Bromoform not indicated.

Trap breakthrough occurs when the adsorbent bed is no longer able to retain or adsorb a compound from the passing air stream (Poole, 2003). Verification of the breakthrough volume of bromoform on this system was achieved by passing 1, 3, and 5 *l* environmental air samples through two TDU adsorbent traps connected in series. The samples were collected in multiple cylinders filled at the same location in immediate succession. This suggests that the mixing ratios within the cylinders should be consistent. The traps were flushed at 100 m*l* min^{-1} with marine air collected from False Bay (Fig. 1.2). Environmental marine samples were selected for the breakthrough analysis over pure laboratory standards as the breakthrough volume may vary within a complex mixture compared to a single species chemical standard (Palmer, 2006). The environmental samples were collected in polished stainless steel flasks on a research cruise transect in False Bay (Philibert, 2010).

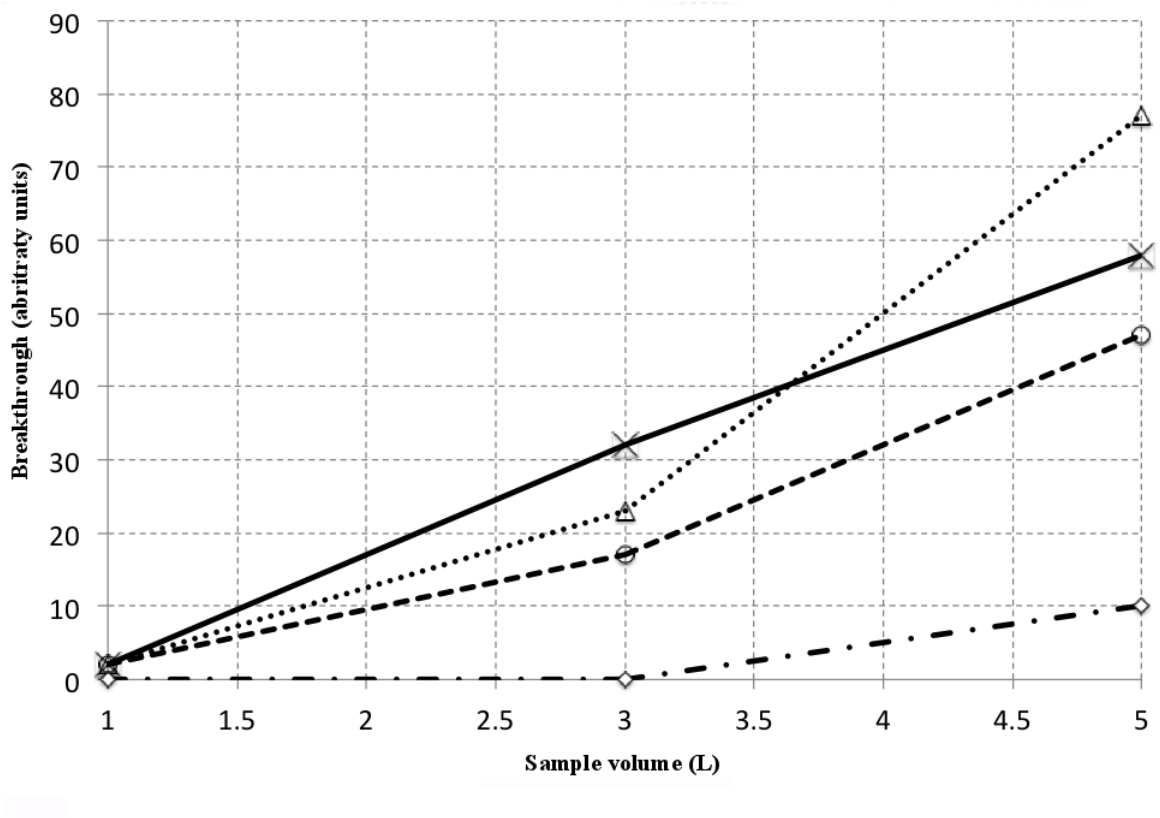

Figure 3.16: Trapping of varying volumes testing for breakthrough of packed adsorbent beds. The volume loaded on the primary trap and the cumulative peak area observed from the secondary trap are displayed on the X and Y-axes, respectively. Bromoform ($t_R \approx 14$ min) is denoted by the dot-dash line, while the other lines (dashed, dotted and solid) indicate unidentified volatile compounds (t_R = 2.4, 2.7 and 3.0 min, respectively), included here for comparison. Adapted from Kuyper et al., 2012.

The two TDU adsorbed traps connected in series allowed the testing of the secondary trap for breakthrough analytes without altering the setup. The primary trap, upstream of the secondary trap, was maintained at laboratory temperature (20 – 25 °C), whilst the secondary was cooled to -10 °C. This arrangement allowed the testing of the secondary trap to be performed without changing tubes. Air flow through the traps was stopped after 5 minutes and the secondary trap was analysed for breakthrough analytes using the thermal desorption unit and GC-ECD following the procedure described in Sec. 2.3. After the analysis was complete this secondary trap was cooled and the gas flow through both tubes resumed. Repeated flushing of the tubes provided conditions for the build up of up to 5 *l* on the primary trap, while the secondary was cleaned after each analysis. The volume of the sample that had to be passed through the primary trap in order to be detectable on the secondary tube defines the breakthrough volume of this system under these conditions. For this system, breakthrough of bromoform occurred at a volume of 5 *l* (Fig. 3.16). Two unidentified atomically lighter compounds had smaller breakthrough volumes than bromoform. Consequently additional work needs to be done to validate the system before sampling for lighter compounds. Note, however, that the 1 – 3 *l* sample volumes for bromoform exhibited no breakthrough.

3.3.1 Injection

Various heating methods, depending on the trapping mechanism used, have been suggested to thermally desorb trapped samples for analysis (Sec. 3.2.7). The use of heated oil and water have been reported for 'freezeout-loops', and electronic heating coils with an adsorbent bed have also been used (Wevill and Carpenter, 2004; Poole, 2003). The desorbed sample was passed to the column. A sample might be passed directly to the column through a splitless injector (directly) or a split injector. The splitless injector passes the entire sample directly to the head of the column. A split injector contains an extra gas stream, which splits the sample, both diluting it and reducing the gas volume injected to the column. The split injector has been used to dilute samples where high concentrations have been recorded. When a large volume is injected it can be reduced through a split injector as only a portion of the sample volume reaches the head of the column. A switching valve that swaps the direction of gas flow to the TDU has been used to inject samples and the carrier gas is passed through the TDU while heating. In automated systems, an electronic switching valve is used. The use of an electronic valve ensures that the sample volume injected is exactly replicated. The rate of switching is also faster in the electronic valves. Manual switching valves are cheaper and simpler to maintain; however, they make it more difficult to achieve exactly consistent injection volumes.

An injection procedure aims to deliver the trapped sample efficiently to the head of the column for separation. This should result in minimal band broadening and high quality chromatography. Following the trapping of samples on the cooled adsorbent bed, the TDU was heated and the sample was desorbed. The injection valve was switched to the 'inject' position (Fig. 2.2b) once the TDU had attained a temperature of 15 °C, transferring the sample to the GC for separation and analysis. A back pressure of 200 kPa helium carrier gas was maintained through the trap to ensure all the elutants were swept to the head of the column. Once the internal temperature had reached 300 °C (2 min 30 sec) the injection valve was returned to the 'load' position, returning N_2 flow through the trap. This cut off the He flow through the trap, which was passed directly to the column to maintain the carrier gas flow. The long injection times that occurred as a result of slow heating of the TDU produced poor resolution of the peaks in the chromatography. The poor chromatography was mainly due to band broadening effects (Poole, 2003). The resultant chromatograms showed little shape (Fig. 3.17a). The use of injection windows (Table 3.4) and second stage cryo-focusing (Fig. 3.17c) methods were explored as methods to address the problems of poor chromatography.

Injection windows limit the injection time to a short time-interval between two temperatures (Poole, 2003). The injection valve was switched for 10 seconds around the boiling point of bromoform (149 °C). The short window limits the size of the slug injected, improving the chromatography. Since lighter halocarbons would be flushed as the trap is being heated, this method precluded the chance of sampling for anything other than bromoform. Bromoform might also be mobilised prior to the valve switchover and thus lost. Since the loss would be non-quantifiable, it could bias the measurements and impact on accuracy.

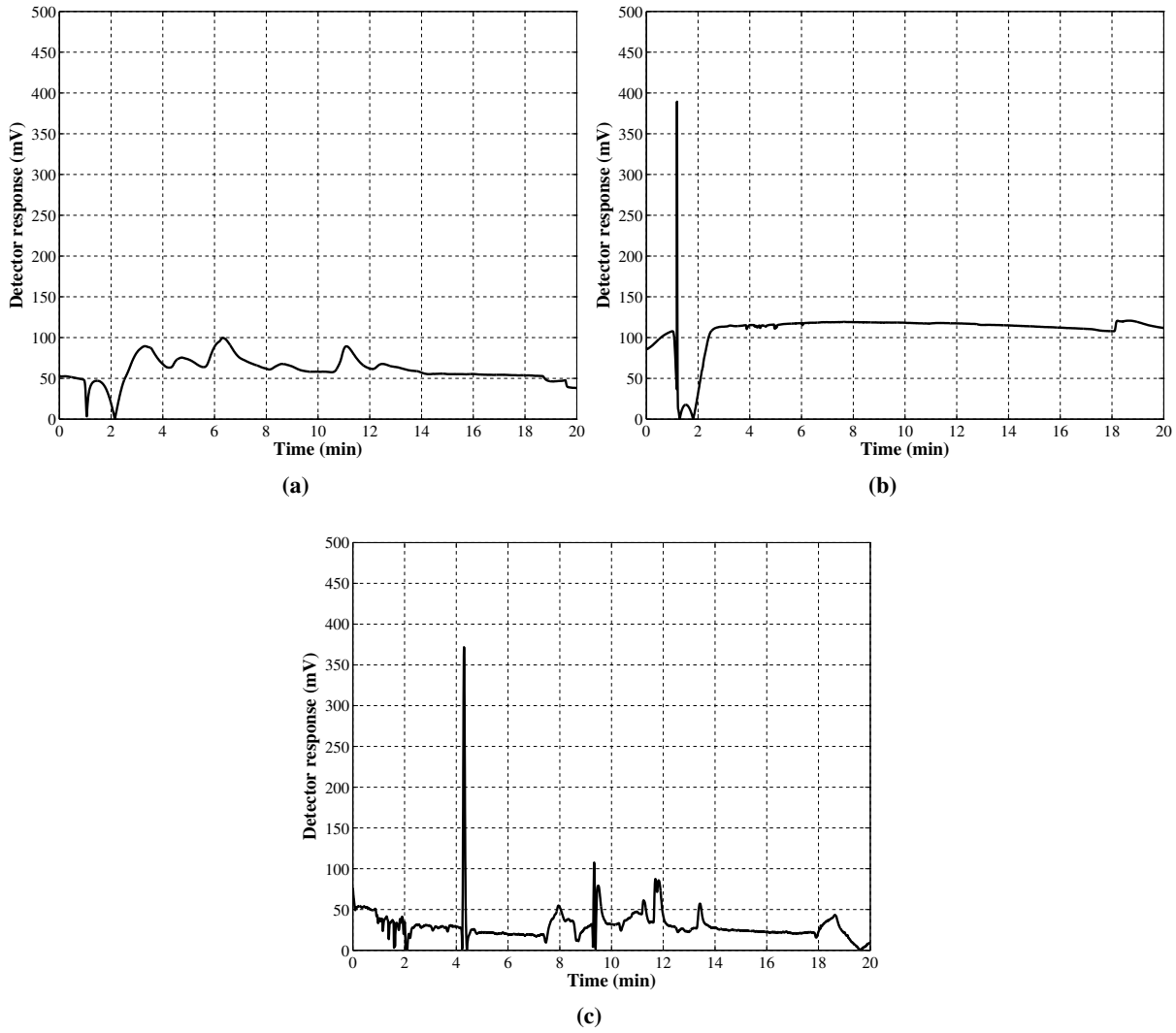

Figure 3.17: Improved chromatography as result of second stage cryo-focusing. (a) Salt-water ∼-20 °C, (b) $N_{2(l)}$ and chloroform mixture ∼-60 °C, (c) $N_{2(l)}$ -196 °C.

Desorbed compounds are re-trapped and desorbed at the head of the column, prior to separation and analysis, in a process known as second stage cryo-focusing (Poole, 2003; Wevill and Carpenter, 2004). The head of the column is cooled for the duration of the primary injection. This offered only limited improvement where the coolants were salted ice water (± -20 °C; Fig 3.17a) and a liquid nitrogen ($N_{2(l)}$) and chloroform mixture (± -60 °C; Fig. 3.17b), which were not sufficiently cold to trap the desorption slug of elutants. The mixture was expensive, consuming ($N_{2(l)}$) and chloroform. The use of liquid nitrogen as the cryo-focusing coolant resulted in the retention of the entire desorbed volume and minimised band broadening (Fig 3.17c). The $N_{2(l)}$ was held in place around the stainless steel loop for the duration of the initial desorption and rapidly replaced with boiling water to re-desorb the trapped sample. The concurrent use of injection windows and cryo-focusing to achieve excellent chromatography was not necessary (Table 3.4). The cryo-focusing was used as the method to limit band broadening with a full temperature injection from the TDU ensuring a full sample volume.

Table 3.4: Testing of various temperature windows as a method of limiting band broadening.

Month and Year	Start (°C)	End (°C)	Range (°C)
November 2008	10	150	140
November 2008	30	150	120
November 2008	15	154	139
November 2008	106	222	116
December 2008	15	98	83
December 2008	170	210	40
January 2009	170	185	15
March 2009	30	200	170
May 2009	5	180	175
May 2009	148	222	74
May 2009	0	180	180
June 2009	40	140	100
June 2009	50	150	100
July 2009	0	300	300
October 2009	0	200	200
November 2009	0	222	222
May 2010	0	300	300
August 2010	186	300	114
August 2010	186	202	16
September 2010	0	275	275
September 2010	100	250	150
March 2011	15	300	275
March 2011	25	300	265
April 2011	75	300	225
August 2011	15	300	275
September 2010	15	300	275

3.4 Bromoform identification

An external standard injection method was used to calibrate the ECD and determine the retention time of bromoform throughout the course of this project. The methods used to deliver external standards to the GC have been discussed above (Sec. 3.5). This section examines the methods used for bromoform identification, peak integration and the construction of the calibration curves.

3.4.1 Bromoform identification

The identification of bromoform in mixed air samples was based on the retention time. From repeated injections of bromoform from the permeation oven, a retention time of approximately 14 minutes was found to be optimal (Fig. 3.18b). A variability of the absolute retention time of the bromoform peak ($\sim$30 s) between samples was caused by the manual injection technique used. Slight variations to the exact time the sample selection valve was switched or, precisely when the hot water was placed on the second stage cryo-focusing trap, cause small changes in elution time of peaks. Also affecting the absolute timing

of recorded peaks is the exact time of chromatogram GUI initiation, especially in relation to the timing of injection valve switching and desorption. It has been found that the relative retention of peaks is not affected by the injection time or moment of desorption (Poole, 2003). Thus, based on the knowledge of approximate retention time and relative peak retention, bromoform was manually identified in air samples (Fig. 3.18c). Following the subtle shifts of the absolute retention time of bromoform, manual identification based on the similarity of chromatograms (relative retention) was performed.

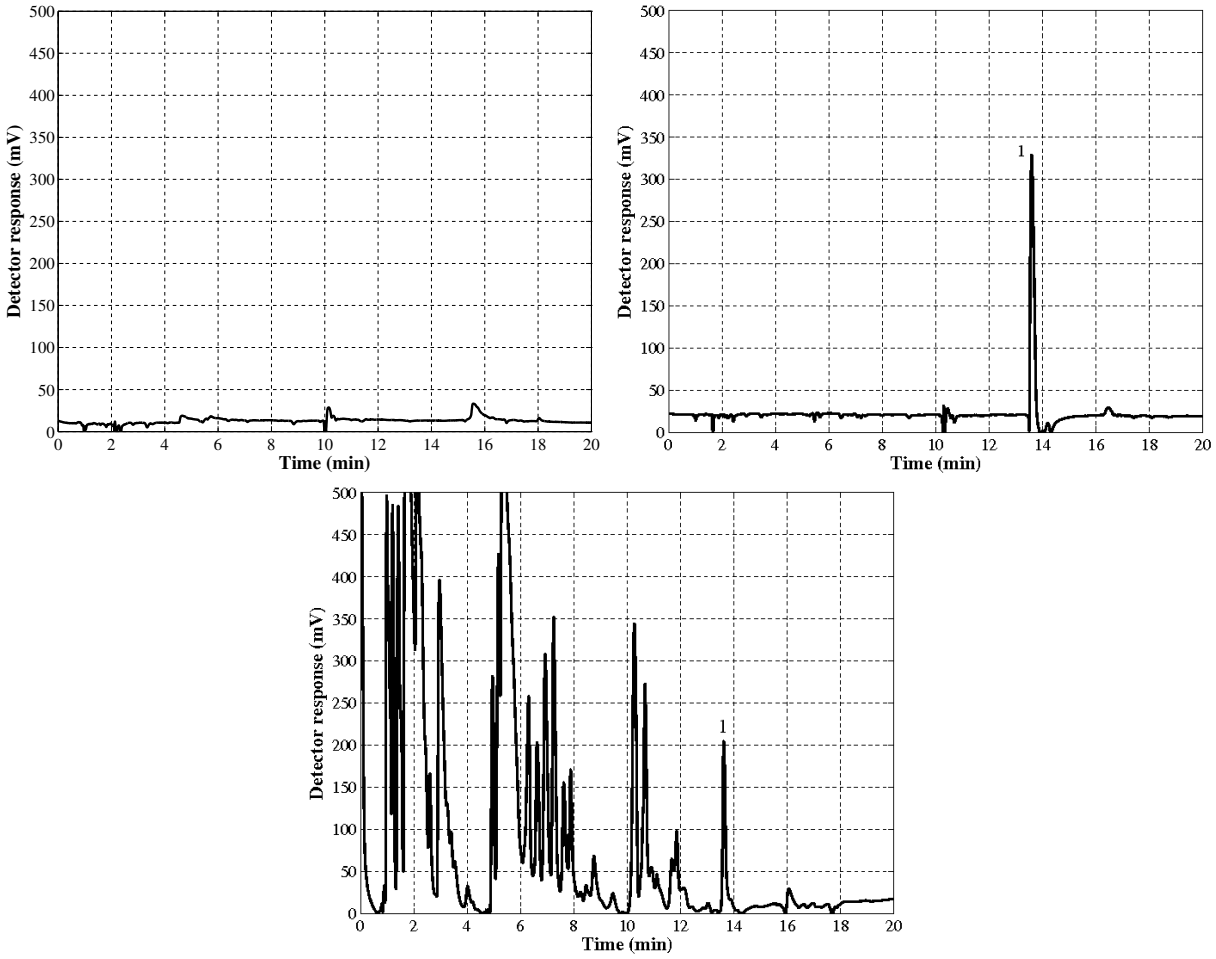

Figure 3.18: Identification of bromoform (1) in chromatograms. (a) Blank chromatogram indicating zero memory effect of TDU trap, (b) bromoform retention at 14 minutes in calibration sample 1 x 100 μl sampling loop, and (c) bromoform separated from a mixed air sample.

3.4.2 Peak area integration

The peak area, integrated from the chromatogram, is proportional to the concentration of the compound measured. A previous study estimated the area assuming it to be triangle or trapezium (Poole, 2003; Urias, 2002). Alternatively, a Gaussian or near Gaussian peak shape is assumed to exist for a number of the techniques. Testing of a Levenberg-Marquardt fitting routine, a manual triangulation method and the trapezium method was performed to ascertain which worked best for this system. The Levenberg-Marquardt fitting routine relied on mapping the chromatogram shape and was customised for simple chromatograms exhibiting a few well-defined peaks. As the chromatography improved and the complexity

and number of peaks present in the chromatograms increased, the Levenberg-Marquardt increasingly failed to accurately map the peaks. Consequently, this method was not able to provide an estimate of the peak area. A triangle was approximated within the recorded peak of the chromatogram (Fig. 1.4, Poole, 2003). The base (b) of the triangle was either defined as the distance between the inflection points or the width at half the peak height. Height (h) was measured from the baseline between the inflection points to the peak. The area (Ap) was calculated using the equation:

$$Ap = \frac{1}{2} b * h \tag{3.5}$$

The manual triangulation method was found to be laborious but estimated approximately 96.8 % of the true peak area and was best suited to Gaussian peaks (Poole, 2003).The larger the tailing the greater the error associated with this method. It also results in under sampling. Peak tailing occurred frequently in the early chromatograms of this study and estimates of area would have been impacted by these shortcomings.

The trapezium area has been shown to yield 100.4 % of the true peak area, even on tailing peaks (Poole, 2003). In MATLAB the native trapezium area estimation function *TRAPZ* was used to calculate the peak area. Manually identified inflection points of the bromoform peak were used as the base of the trapezium. A baseline was created between the inflection points. The *TRAPZ* function calculated the area of the trapezium from the base of the y-axis. Consequently the area of a rectangle, defined by the inflection points and the bottom axes, was removed from the calculated peak area. The removal of this rectangle ensured that the optimal peak area was calculated.

Outliers within the data were identified and removed by means of the inter-quartile range method (Underhill and Bradfield, 2005). The median and interquartile range of the data were calculated. Outliers are defined as values which are 1.5 times above or below the maximum and minimum of the interquartile range. Two values were found above the upper threshold of 85.0 ppt and no measurements below the minimum of 2.1 ppt. The values above the upper threshold were removed from the dataset.

3.5 Instrument calibration

One method of calibration of an ECD is by the introduction of an external standard (Poole, 2003). Internal standard calibration and relative retention methods can be used for calibration and compound identification (Poole, 2003; Wevill and Carpenter, 2004). These methods rely on a knowledge of the detector response to known compounds, the retention times of the compounds of interest and a consistent marker within the chromatograms (Poole, 2003). The relative retention of bromoform against carbon tetrachloride is an example that has been performed on specific research cruises (Shaw, 2011). The response of the detector to external standards introduced at varying concentrations enables the quantification of a compound from a mixed sample to be achieved. The identification of compounds detected by the ECD is primarily accomplished by retention time (Poole, 2003). For a given set of constant GC parameters, the retention time of a compound will be stable between different sampling runs. This makes the identification

of a compound from a clean external standard possible. The challenges identified through the development of the GC system in this study suggested that a simple external standard calibration method was preferable. This section examines the different methods of external standard delivery that were tested on this system. Three methods were tested as delivery mechanisms of bromoform standards to the GC system: headspace flasks, permeation oven and sparging glass trap flasks. As is discussed below, the permeation oven and sparging flasks proved to be effective, while the headspace flasks were unsatisfactory.

3.5.1 Volumetric solution and headspace method

Pure bromoform (99.5 %, Sigma) was dissolved in boiled deionised water to make calibration standards (Palmer, 2006). Serial volumetric dilution of bromoform was used to achieve parts per trillion concentrations within the standards. One microlitre (μl) of bromoform was diluted in 1 l boiled deionised water. One millilitre (ml) of this solution was further diluted in 1 l boiled deionised water, achieving a solution concentration of 1.14 x 10^{-8} mol l^{-1}. Aliquots of 10 – 50 ml were placed in a custom-built headspace flask, stored at 0 °C (Fig. 3.19). The flask was pre-flushed with nitrogen (Grade 5.0) to ensure no residual air remained in the flask, contaminating the calibration. A 30 minute period allowed the flask to come to equilibrium. Using the Henry's Law constant, the gas phase mixing ratio of bromoform was calculated, based on the volume of the working standard initially injected. The headspace of the flask was swept with nitrogen (Grade 5.0) to the TDU at 100 ml min^{-1} for 10 minutes to achieve a calibration point. Repeated flushing and variations in the volume of injected aliquots resulted in different trapped volumes of bromoform and allowed the formation of a calibration curve.

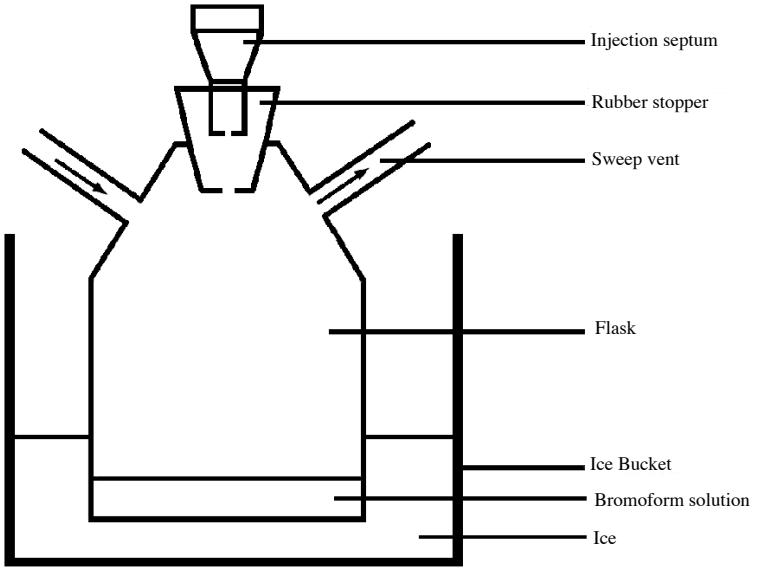

Figure 3.19: Schematic of headspace calibration bottle used for the calibration of bromoform in GC system.

While the retention time of bromoform was identified with this method, a full quantitative calibration was not achieved. Analytical obstacles associated with the volumetric preparation of the calibration standard were a probable cause. Liquid standards are frequently made up in methanol as this achieves

stability for up to a few months (Mattsson, 2013). Gas leaks to and from the headspace flask resulted in the sample either being lost or becoming contaminated. The arms of the headspace flask were a weak point in the design, as they often broke off during routine sampling. This created delays while the flask was repaired. For the reasons cited above, this method of calibration with this system was unsatisfactory.

3.5.2 Permeation oven

A permeation oven system was tested as a method of reliably delivering varying gas phase concentrations of bromoform to the GC system. An aluminium block maintained at 70 °C housed a glass trap (500 ml) containing a commercially purchased bromoform permeation tube (A&J Scientific, Cape Town, South Africa) in the custom-built permeation oven (Fig. 2.5), based on the same design used by Wevill and Carpenter (2004). The bromoform tube had a permeation rate of 373 ng hr^{-1} and when stored under a nitrogen gas flow rate of 100 ml min^{-1} resulted in parts per trillion (ppt) mixing ratios. Gas flow from the custom glass trap passed through a 100 μl sample loop and then onto a halocarbon trap. The continuously swept sample loop could then be used to inject specific volumes of bromoform to the TDU trap for calibration of the CG-ECD system (Fig. 2.5 and 2.1). The permeation tube was stored under a flow of nitrogen (Grade 5.0) in the glass trap. Gas flow of 100 ml min^{-1} through the custom glass trap allowed for the dilution of bromoform mixing ratios in the order of parts per trillion. A 100 μl sample loop was continuously swept with the diluted bromoform and this enabled increasing amounts of bromoform to be tested. A calibration curve was built through the analysis of repeatedly loading multiple loops on the TDU trap. The optimal time of 30 seconds required to completely flush the sample loop was established by repeatedly flushing the sample loop at varying times (Fig. 3.20). Repeated switching (1 – 3 loops) of the injection valve allowed for the accumulation of multiple sample loop volumes on the cooled TDU trap.

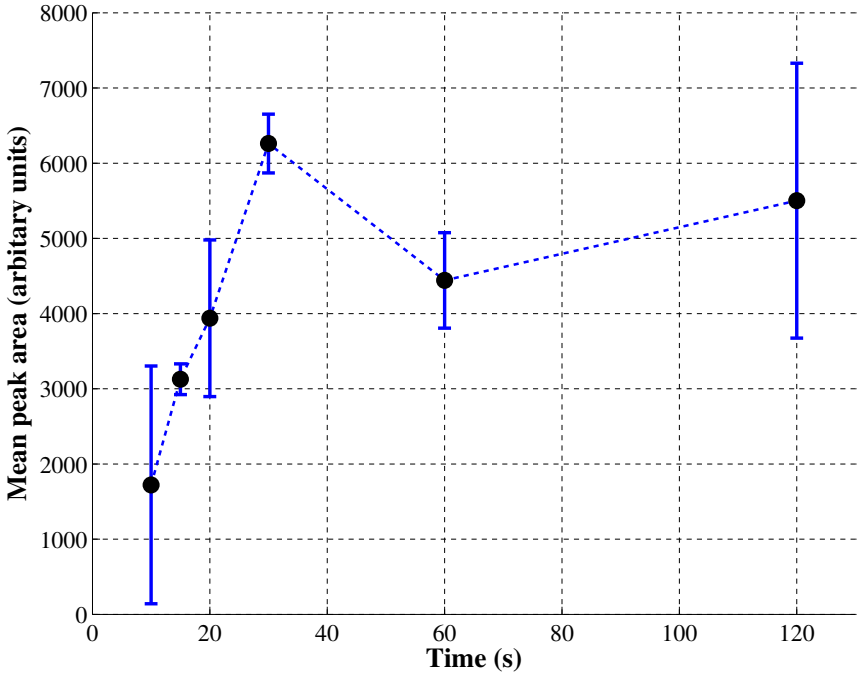

Figure 3.20: Detector response as a function of permeation oven sampling loop flushing time.

Analysis of triplicate injections of one, two and three sample loop volumes loaded on the TD trap allowed the construction of a calibration curve (Fig. 3.21a). The area of the peak produced by the ECD is directly proportional to the mixing ratio of bromoform or any compound detected. The peak area is thus proportional to the amount of bromoform loaded onto the adsorbent bed. Following the permeation rate of the tube in the oven (373 ng min^{-1} at 70 °C) and the known volume injected, the number of moles of bromoform trapped on the adsorbent bed can be calculated. The chromatographic peak area was then related to the known mixing ratio of moles of bromoform injected from the adsorbent bed. The mixing ratio of bromoform in air samples was calculated based on the sample volume and an assumed air number density of 2.5 x 10^{25} molecules m^{-3} (Nic et al., 1997). A complete calibration of the system was performed prior to the start of the bromoform sampling experiment. A daily calibration point of one, two or three loops was run to measure system drift, if any (Fig. 3.21b).

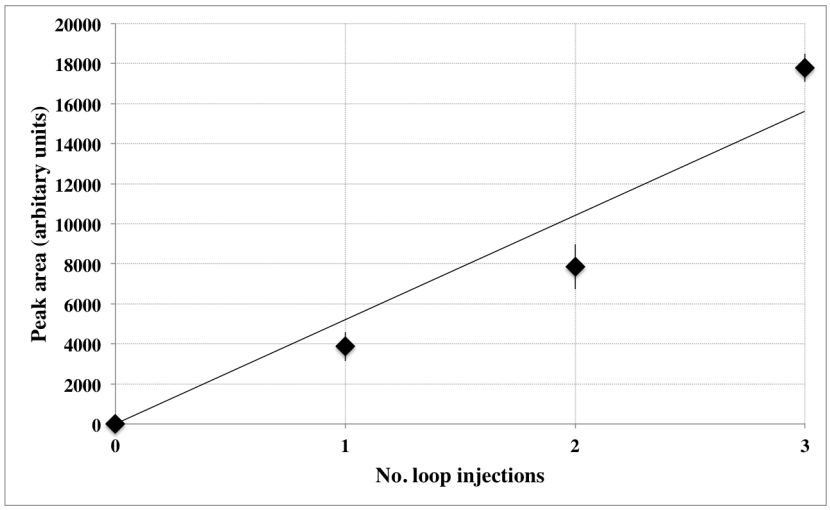

(a)

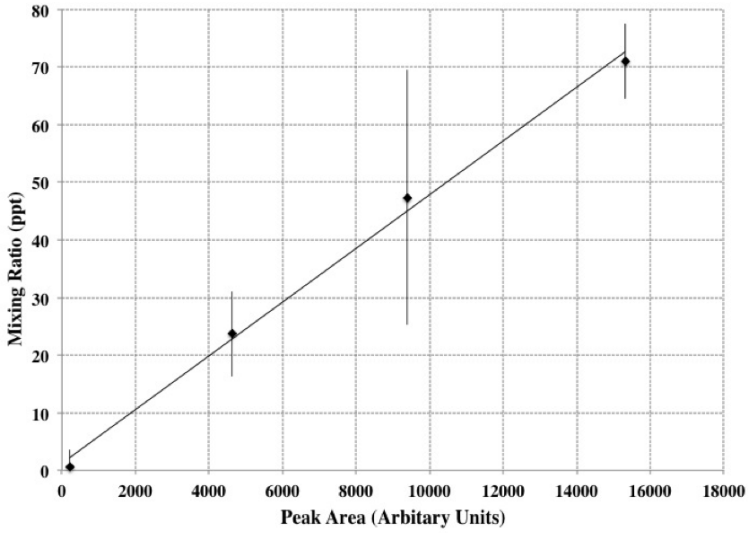

(b)

Figure 3.21: Calibration of the GC system at Cape Point, South Africa by means of the permeation system. (a) measured peak area as a function of the number of loops injected and (b) calculated air mixing ration of bromoform as a function of peak area.

3.5.3 Volumetric solution and gas extraction

Gas extraction of bromoform from water was achieved by means of bubbling pure nitrogen (sparging) through seawater or calibration standards during the laboratory experiments (Chapter 5). A sparging flask made from a 500 m*l* glass trap was developed in which to sparge samples to an adsorbent trap (Fig. 3.22). The connections between the flow regulator and the glass trap and between the glass trap and the adsorbent tube were made of PTFE tubing, while stainless steel tubing was used to connect the cylinder to the flow regulator (Fig. 3.22). These materials were used as they offered ease of use within the laminar flow hood and have been shown not to adsorb bromoform (Laturnus, 1996). A Porter valve flow regulator was used to achieve the desired flow rate of 100 m*l* min^{-1} through the sparging flask.

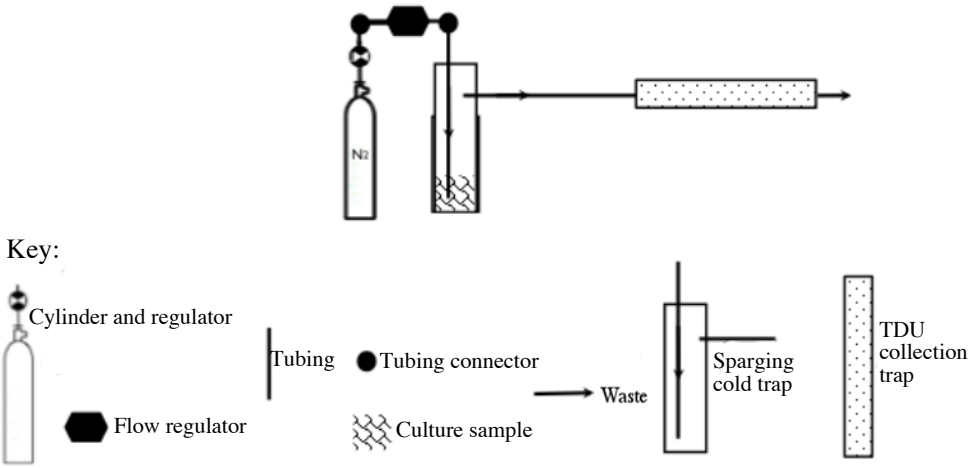

Figure 3.22: Glass trap sparging flask used for laboratory culture experiment calibration.

Using a fixed bromoform standard the ideal sparging conditions were tested. This included the volume of sample to sparge, sparging time and gas flow rate. Sample volumes of between 50 and 100 m*l* have been reported for the measurement of bromoform from laboratory cultures (Tokarczyk and Moore, 1994; Moore et al., 1996). On this system it was found that 100 m*l* samples resulted in a detectable quantity of bromoform sparged, while the quantification of bromoform concentration from 50 m*l* samples was at the limit of detection. It has been suggested that the sparging efficiency is affected by both the sparging time and chemical properties of the target compounds (Lee et al., 2001). The sparging efficiency was greatly improved for highly volatile compounds sampled over a shorter time period, while a longer time period achieved greater sparging efficiency for less volatile compounds such as bromoform (Lee et al., 2001). Sparging times of between 2 and 12 minutes were tested, with no benefit noted in the measurement of bromoform from samples, of the same initial concentration, that had been sparged for longer than 5 minutes. Gas flow rates through the sparging vessel of between 40 and 100 m*l* min^{-1} were tested to achieve the ideal extraction of bromoform from solution (Moore et al., 1996). Based on visual observation at low flow rates (below 50 m*l* min^{-1}) the bubbles produced were too large and infrequent to achieve adequate extraction of bromoform from the solution, which resulted in poor chromatography (Fig. 3.23a)

while the extraction at a flow rate of 100 ml min^{-1} achieved far better chromatography (Fig. 3.23b). It is possible that at the higher rate of sparging resulted in a breakthrough of the lighter compounds. This decreased peak area of lighter elements and increase in bromoform peak area resulted in easier quantification. This indicated a flow rate of 100 ml min^{-1} should be used for extraction. Based on personal observation, no benefit was noted in the extraction of samples at a higher gas flow rate, the bromoform area and chromatographic resolution were comparable to those extracted at 100 ml min^{-1}. This was not used since a higher gas flow uses more gas, which was limited.

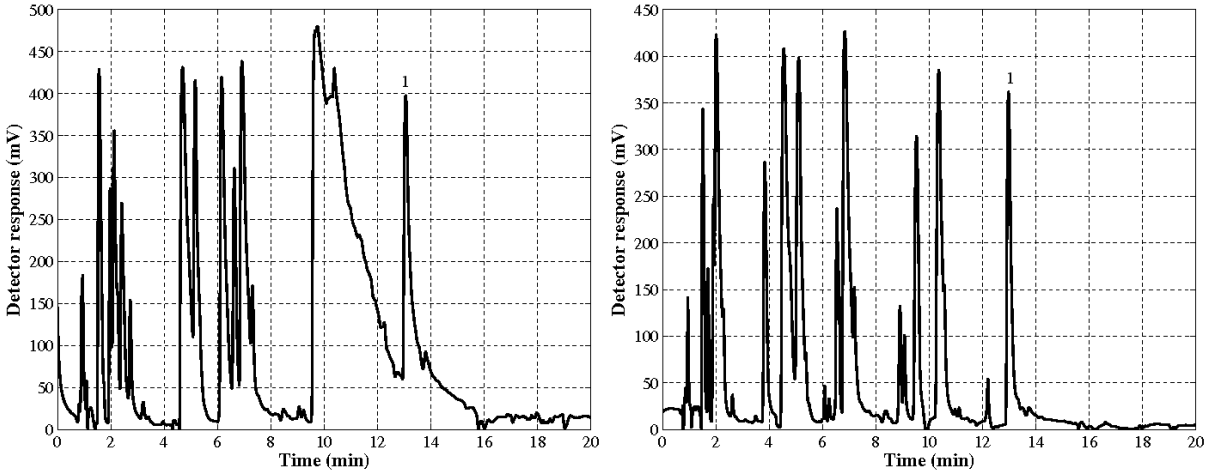

Figure 3.23: Sparging gas extraction of bromoform (1) for samples run for 5 minutes at (a) 50 ml min^{-1} and (b) 100 ml min^{-1}.

Two bromoform working standards (50 and 100 ppt) were made by the serial dilution of pure bromoform (99.5 %, Sigma) in methanol. Double and triple dilutions of 85 μl bromoform in 100 ml methanol resulted in the two bromoform working standards (50 and 100 ppt). Aliquots of between 10 and 50 μl of the working standard were injected into 100 ml, filtered (0.22 μm) and sterilised seawater. The seawater with bromoform was sparged with nitrogen (Grade 5.0) at 100 ml min^{-1} for 5 minutes. The exhaust gas from the sparging flask was trapped in an adsorbent tube (Carbopack X / Carboxen 1016) maintained at laboratory temperature (20 °C). The adsorbent tubes were stored in the dark at ∼4 °C and analysed on the GC within 6 hours.

Varying the volume of the injected working standard aliquot resulted in the development of a five point external calibration curve for use with sparged culture samples (Fig 3.24). The linear response of the ECD was tested with varied bromoform calibration concentrations of 0 – 50 nmol l^{-1}. This achieved a response of r^2 = 0.94. A calibration point was taken each day of sampling to ensure there was no drift within the system. The concentration of bromoform was determined based on the measured peak area. The difference between the measured sample and blank bromoform values was divided by the slope of the calibration curve, resulting in an estimate of the actual bromoform concentration. The peak area was manually measured using a trapezium method.

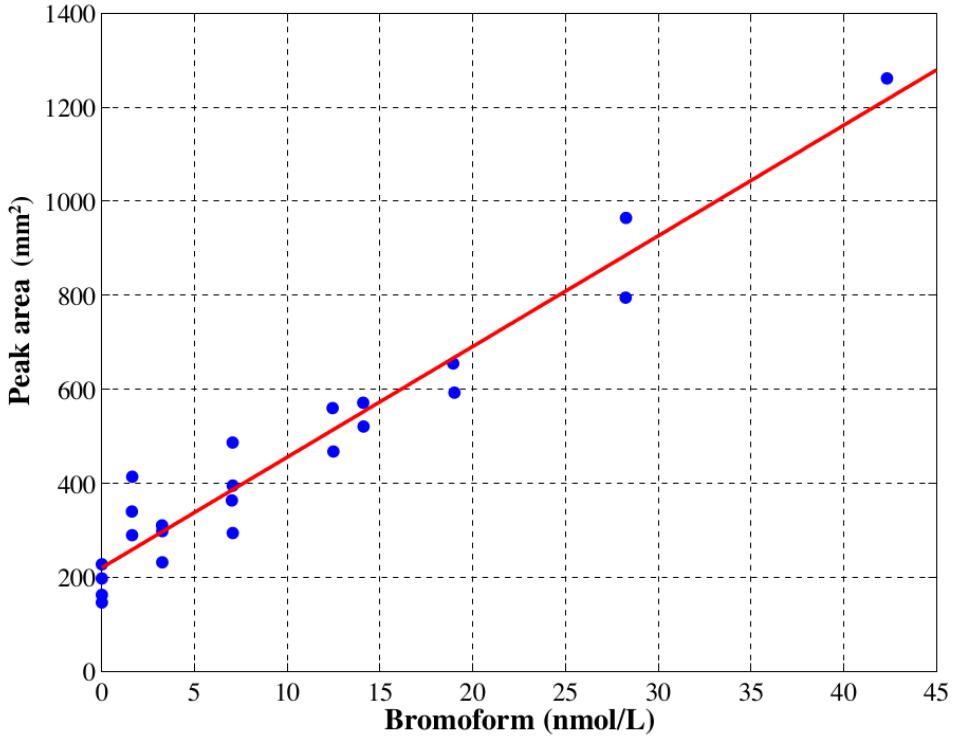

Figure 3.24: Calibration curve of ECD system from extracted headspace analysis.

3.5.4 Sensitivity and repeatability

The stability and sensitivity of the ECD and repeatability of the method were tested by repeat injections of bromoform standards. Analysis of repeated injections of bromoform from the permeation oven, indicated that the GC-ECD system exhibited a linear response within the range of mixing ratios of 5 – 90 ppt. The linear correlation relationship between measured peak area to mixing ratio for the system was found to be r^2 = 0.9 (Fig. 3.25). The system had a limit of detection (LOD) of 0.73 $\pm$ 0.09 ppt. Precision of the method was found to 12.7 % based on nine repeated 200 μl volume injections of bromoform standard on the TDU trap. This precision is similar to that reported by Wevill and Carpenter (2004) of approximately 8 % for bromoform and therefore practical for use in the quantitative detection of bromoform from air samples (Table 3.5). The slight elevation compared to other systems may be a result of the manual injection process used here (Table 3.5). Blanks were calculated to contain a mean concentration of 0.66 ppt. This is below the limit of detection (0.73 ppt) and therefore not of great concern. The value for the blanks was added to the calibration curve, thus removing this artefact from measurement. Mixing ratios in parts per trillion were determined by multiplying the measured peak area by the slope of the calibration curve (Equation 3.6).

$$mixing\ ratio = measured\ peak\ area * 0.0047 \tag{3.6}$$

The error contribution in ambient air samples may stem from a number of sources including variability in integration, blanks and sample volume. These errors should be considered as the overall precision and

Table 3.5: Comparison of system variables with other studies. All values reported at 1σ level unless otherwise stated.

Reference	Precision (%)	Accuracy (%)	Limit of Detection (ppt)
Wevill and Carpenter (2004)	$\sim$8	$\pm$15	0.05
O'Brien et al. (2009)	3.2	2.2	0.4
This study	12.7	$\pm$15	0.73
Zhou et al. (2008)	7.5		0.48 $\pm$ 0.04
Yokouchi et al. (2005)	<20		
Jones et al. (2011)	6.51 (2σ)		

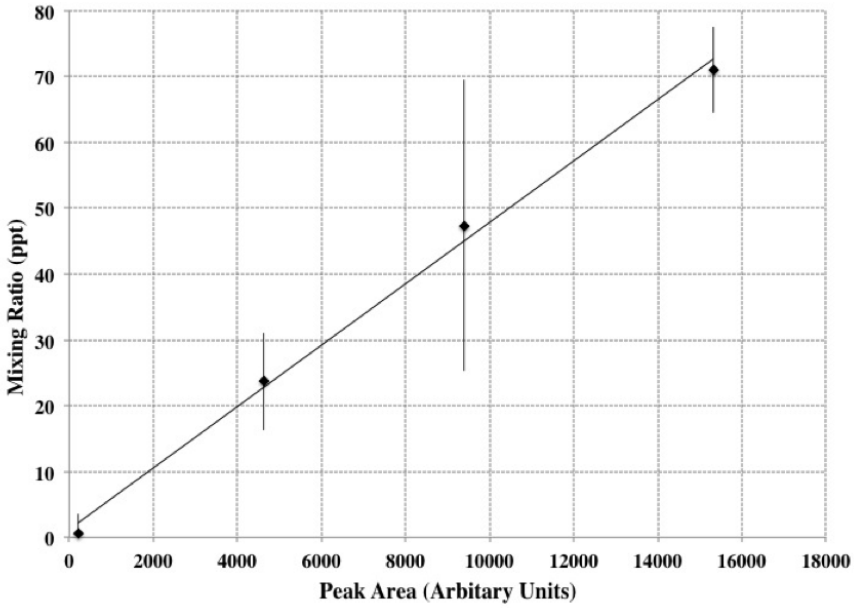

Figure 3.25: Calibration curve of ECD system from permeation oven. Adapted from Kuyper et al., 2012.

accuracy of the system may be substantially affect by these factors. This may be of particular concern under certain circumstances such as mixing ratios close to the LOD, large peak overlap and unstable peak areas. During these encounters the error of measurement may result in large errors (Plass-Dülmer et al., 2002).

3.6 Summary

Described here is the development of the GC-ECD system and method use for the analysis of bromoform from air and seawater samples at environmental concentrations. A Shimadzu-GC8A oven was used to house a J & W Scientific DB-624 capillary column. The GC oven was able to maintain set temperatures with an accuracy of 1 °C over a wide range of temperatures, resulting in the generation of a suitable temperature programme. The five incremental increases in temperature achieved the separation of bromoform from mixed air samples with a retention time of approximately 14 minutes. The simple

operation and maintenance of the PerkinElmer F-22 ECD ensured that running repairs could be made and that a relatively unsophisticated initial skill set was required. Helium carrier gas was passed through the DB-624 capillary column at a flow rate of 5 ml min^{-1} to achieve the separation of samples. The carrier gas was complemented with nitrogen make-up gas flow through the ECD at a ratio of 1:6. The manual injection valve used to direct gas flow through the TDU trap and to the column was simple to maintain and offered suitable injections. Precise injection volumes might have improved the chromatography further; however the cryo-focusing used resulted in limited band broadening of eluting peaks. Sample pre-concentration by means of an adsorbent bed within the TDU was used in this system. Samples were trapped from the air in the TDU adsorbent bed at a core temperature of -10 °C and flow rate of 100 ml min^{-1}. The trapped samples were desorbed upon injection by heating of the TDU to 300 °C by means of an internal resistance coil. Air samples were pushed through the adsorbent bed by a piston air pump and a mass flow controller regulated the sample gas flow rate through the trap. A chemical desiccant, magnesium perchlorate, was used to dry air samples prior to trapping on the adsorbent bed.

Moisture trapped on the adsorbent bed may possibly damage the column upon injection and lead to an increase in breakthrough from the trap. A breakthrough volume of 5 l was determined for this system. Samples were trapped on the adsorbent bed for 15 minutes resulting in a 1.5 l trapped sample volume. Bromoform should not have broken through the trap, base on these smaller sample volumes used. Calibration of the system was achieved by the introduction of external standards from a permeation oven or sparging flask. Calibration samples from either source were trapped on the adsorbent bed. The contents of a constantly swept 100 μl sample loop were repeatedly flushed onto the adsorbent bed for analysis. This resulted in mixing ratios between 5 and 90 ppt being analysed for calibration. The overall precision of the method was found to be 12.7 % with a limit of detection of 0.73 $\pm$ 0.09 ppt. While slightly elevated compared to previous studies, this is similar and therefore suitable for the quantitative detection of bromoform in air samples. Bromoform mixing ratios reported at Cape Point (Chapter 4) range between 2.29 – 84.7 ppt. The LOD below 1 ppt suggests that the GC system developed for this study was satisfactorily sensitive to quantitatively detect bromoform mixing ratios from environmental air samples.

A two-stage injection procedure was used to achieve high quality chromatography, with little band broadening and co-elution of compounds. Trapped samples were thermally desorbed from the adsorbent bed and re-trapped on a 'freezeout-loop' at the head of the column. Liquid nitrogen, used to achieve the trapping, was replaced by boiling water to desorb the sample for separation and analysis. The detected response from the ECD was recorded on a custom-built MATLAB GUI. The analogue output from the ECD was converted into a digital signal and read by the computer at rate of 4 iterations a second. Repeated injections of clean calibration slugs suggested that the retention time of bromoform in this system was approximately 14 minutes. Bromoform was identified in chromatograms based on retention time. A trapezium peak area integration method was used. The manually identified bromoform peak inflection points were used in the MATALB *TRAPZ* function. The method and system described here have been used in the subsequent chapters for bromoform measurements of air samples at Cape Point and water

samples obtained in a laboratory culture experiment.

Several of the components developed for the GC-ECD system described here are consistent with previously published reports, however they have been simplified here to reduce cost (Wevill and Carpenter, 2004; Moore and Groszko, 1999). The result of integration of these components is an instrument with the analytical capability to detect bromoform at ambient (ppt) environmental concentrations in the southern African region where there is currently neither a long-term dataset nor the availability of funding or skills to place a pre-existing instrument. The novelty of the system arises not from the individual components so much as the novel opportunity to contribute to science in a data-poor region. The long-term measurement of bromoform in the atmosphere or ocean has not been performed in southern Africa. This locally developed system and method provides the capacity for the routine quantitative detection of bromoform mixing ratios in environmental air samples along with possible culture studies.

Chapter 4

Bromoform measurements at Cape Point, South Africa

This study examines the character and possible mechanisms of variability of bromoform mixing ratios in the marine boundary layer, as measured at Cape Point. Measurements were performed in the austral spring of 2011. Bromoform mixing ratios were contrasted against local meteorological conditions at the time. Bromoform mixing ratios at Cape Point were found between 2.27 to 84.7 ppt with a mean of 24.7 ppt. The wind direction, drawing air from varying sources, appears to have been the dominant mechanism resulting in the observed bromoform variability.

4.1 Introduction

Globally, gaps exist in the spatial and temporal coverage of measurements of bromoform; particularly in respect of long-term measurements (Fig. 1.1). As discussed in Chapter 1, the Southern Hemisphere is particularly sparse in this regard, with southern Africa data being almost non-existent. Although some bromoform measurements around southern Africa exist they have mainly been made on periodic science cruises (Quack and Wallace, 2003; Carpenter et al., 2007a). This scarcity in global measurements of bromoform limits the ability to make an accurate estimate of global emission strength. The current global estimate is based on limited data, mostly from the northern hemisphere, therefore the source strength estimates are compromised by a hemispheric bias.

Bromoform is important in the biogeochemical cycling of bromine and ozone in the Earth system. The lack of a complete understanding of the strength of bromoform sources limits knowledge relating to the extent of its impact on stratospheric ozone. Bromoform not transported above the tropopause is known to play a role in varying tropospheric oxidative capacity through reactions with the hydroxyl radical (OH) and surface ozone (McGivern et al., 2002). Bromoform released in the tropical atmosphere is known to be an important source of stratospheric bromine (Andrews et al., 2013). The sub-tropical setting of southern Africa (south of 20° S) may mean that it is an important, hitherto unquantified source region of bromoform to the atmosphere, in particular the stratosphere.

It is contended that Cape Point is a crucial location to make such measurements in order to fill the knowledge-gap in respect of the global source strength of biogenic bromoform. Cape Point lies at the southernmost tip of the Cape Peninsula, approximately 50 km south of Cape Town (Fig. 4.1). A Global Atmospheric Watch (GAW) station operated by the South African Weather Service (SAWS) is housed at Cape Point (34° 21' S 018° 29' E, 230 m elevation). The GAW station is ideally situated to sample trace gases. It is positioned such that air samples from the Southern Ocean (baseline measurements), south Atlantic (coastal upwelling) and southern Africa (anthropogenic/biomass burning) regions are available. This permits measurement from different sources depending on wind direction. The baseline wind direction (BWD) at Cape Point, lies in an arc from 170 – 320 degrees capturing the Southern Ocean and South Atlantic but excluding local anthropogenic influences (Brunke et al., 2004).

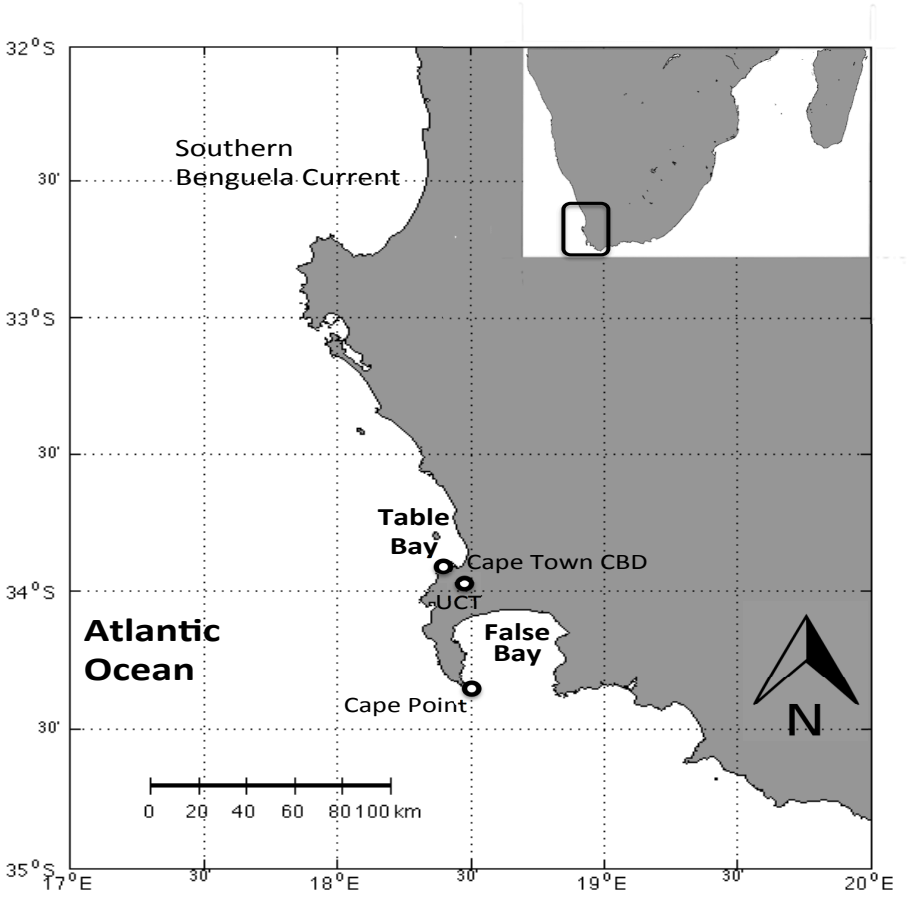

Figure 4.1: Map of the Cape Town area, highlighting the positions of Table Bay, False Bay and the Benguela Current region. The Cape Town CBD, UCT and Cape Point sampling sites are shown.

The synoptic meteorology in the region is principally driven by the strength and position of the South Atlantic High Pressure system (SAHP), yielding two dominant and seasonally dependent wind

patterns; from the southeast in summer and northwest in winter (Tyson and Preston-Whyte, 2000). In the summer months, the centre of the SAHP lies at a similar latitude to Cape Town, resulting in strong southeasterly winds. The southeasterly winds draw marine air in from the Southern Ocean. During the winter months, the SAHP shifts northwestward allowing extra-tropical cyclones to impact on Cape Town. These predominantly northwesterly winds draw air from the southern Atlantic and Benguela regions as a result of northwesterly dominant winds (Tyson and Preston-Whyte, 2000). Ahead of the fronts, northeasterly flow may draw air from the interior plateau as a föhn (locally known as a berg wind; Shannon and Nelson, 1996; Hutchings et al., 2009).

There are a number of potential local sources of bromoform in the atmosphere around Cape Point. The location is positioned to receiving bromoform from two dominant local sources: macroalgae beds surrounding Cape Point and anthropogenic sources within Cape Town and the greater Cape Flats region. A change in wind direction associated with season may determine the prevalent source. Through intra-diurnal changes in wind direction, a mixing of air from different sources is likely to occur, making Cape Point an interesting location at which to sample for bromoform because of the great number of potential sources. However, this can make sampling from such a site difficult due to the need to be able to sort and separate the different sources.

4.1.1 Local bromoform sources

As discussed earlier, bromoform mixing ratios from macroalgae, in the order of tens of ppt, have been recorded in laboratory studies and coastal sites (Palmer, 2006; Pyle et al., 2010, 2011; Zhou et al., 2008). Coastal regions often exhibit much higher mixing ratios than open ocean regions (Class and Ballschmiter, 1988; Quack and Wallace, 2003). The presence of macroalgae is limited by physical conditions, such as rock shores and nutrient concentrations, required to sustain them.

False Bay and the Cape Peninsula are home to a number of macroalgae species in extensive beds (e.g., Fig. 4.2). The dominant species around the Cape Peninsula include: *Ecklonia maxima* (Sea Bamboo), *Ecklonia radiata* (Spined kelp), *Macrocycstis angustifolia* (Bladder kelp), *Laminaria palilida* (Split-fan kelp), *Bifurcaria brassicaeformis* (Hanging wrack) and *Bifurcariopsis capenis* (Upright wrack) (Peschak, 2005; Branch et al., 2010). A number of these families have been linked to the production and release of bromoform (Palmer, 2006).

Water treatment by chlorination occurs with Cape Town for drinking water and to prevent biofouling at Koeberg coastal nuclear power station. They are distributed over a wide area of land extending 50 km to the east of Cape Town. Waste water from these facilities is discharged into False Bay at an approximate location $\pm$ 30 km NE of Cape Point. The proximity of this discharge to Cape Point might make it a significant source of bromoform. A nuclear power plant (Koeberg) is situated on the coast approximately 30 km and 75 km north of Cape Town and Cape Point, respectively. An intake of $\sim$78 m^3 s^{-1} of seawater is used to cool the plant, this is in-line with reported literature. This suggests that bromoform emissions

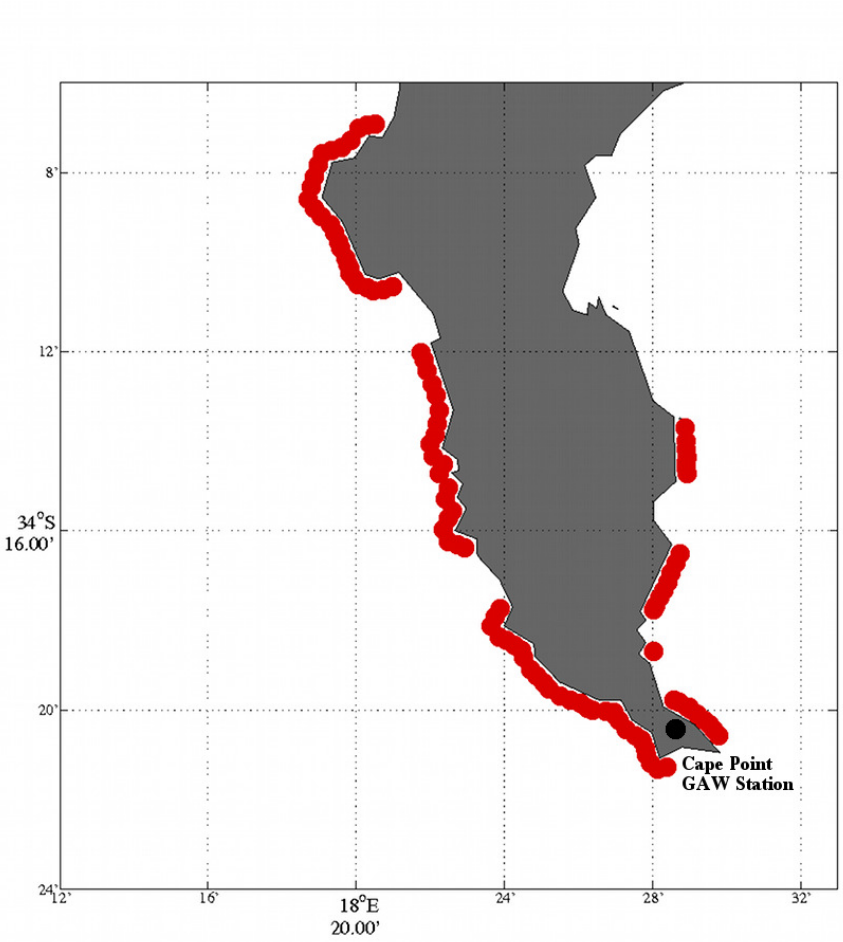

Figure 4.2: Approximate locations and distribution of macroalgae beds surrounding Cape Point based on satellite imagery (Google, 2014).

from Koeberg might be of the order of 34 Mmol Br yr^{-1} (Quack and Wallace, 2003). The discharge from Koeberg could, therefore, be a significant anthropogenic source of bromoform to the local atmosphere, similar to that reported in the literature (Quack and Suess, 1999). Air masses arriving at Cape Point from the north to northwest may contain a large anthropogenic bromoform bias. Bromoform from either Koeberg or the water treatment plants in Cape Town may make a significant contribution. Because of this, care is needed to separate the mixed signals from measurements. Other known anthropogenic sources of bromoform such as seawater desalination, rice paddies and inland power plants are not found in Cape Town.

4.1.2 Microalgae in the southern Benguela: a regional source?

The sub-tropical setting and strong productivity of the Benguela upwelling region (Kudela et al., 2005) might make this a globally important bromoform source (Palmer and Reason, 2009). Understanding the full magnitude of the Benguela as an atmospheric source of bromoform is important in closing the gap of knowledge regarding tropospheric and stratospheric ozone loss.

A modelling study of bromoform source strength suggest that the Benguela should be considered a potentially important source of bromoform to the atmosphere (Palmer and Reason, 2009). Extensive blooms with Chl-*a* concentrations in excess of 100 mg m^{-3} have been reported in the Benguela in summer and early spring (Fawcett et al., 2007). These blooms are typically dominated by diatoms and dinoflagellates, according to bloom succession (Pitcher et al., 1992).

It has been suggested that small phytoplankton sizes of less than 10 μm dominate the southern Benguela (Probyn, 1992). This implies the phytoplankton in the Benguela, when present, should be efficient producers of bromoform making it a significant source region. The species of phytoplankton found in the Benguela are known to vary at different times of the year depending mainly on nutrient concentration (Pitcher and Calder, 2000). Some species may be more efficient producers of bromoform than others, resulting in a variable source strength. There is much debate relating to the dominant source of bromoform in the ocean and atmosphere (Scarratt and Moore, 1996; Lin and Manley, 2012). While macroalgae produce orders of magnitude more bromoform than microalgae, the microalgae cover a much larger domain (Carpenter and Liss, 2000). Cape Point provides an ideal natural laboratory to answer some questions within this debate (Quack and Wallace, 2003; Manley and Barbero, 2001; Lin and Manley, 2012).

4.1.3 Diurnal variability of atmospheric bromoform

High frequency bromoform measurement studies at Mace Head, Grand Canaria and in the Southern Ocean all show bromoform mixing ratios increasing strongly through the morning, coupled with increasing sunlight (Ekdahl et al., 1998). A similar increase has been recorded in the ocean and possibly drives the atmospheric mixing ratios (Carpenter et al., 2000; Abrahamsson et al., 2004). The bromoform mixing ratios were found to peak at approximately local solar zenith, concurrent with the maximum photosynthetic rate (Carpenter et al., 2000; Quack and Wallace, 2003; Abrahamsson et al., 2004). The peak of this morning increase can be up to 400 % of predawn concentrations, which are usually the lowest in any day (Abrahamsson et al., 2004). A decrease in the sunlight throughout the afternoon results in a decline of bromoform mixing ratios to a minimum in the early evening (Carpenter et al., 2000; Abrahamsson et al., 2004). It has been suggested that in the Southern Ocean the rate of decrease in mixing ratios in the afternoon is too rapid to be explained by the loss of production by photosynthesis. Discovery and quantification of the mechanism(s) responsible for this observed bromoform loss still need to be investigated (Carpenter et al., 2000; Abrahamsson et al., 2004). Bromine present in the lower troposphere in the afternoon may account for between 30 – 50 % of ozone destruction during this time period (von Glasow et al., 2004).

A second diurnal peak of bromoform mixing ratios in the evening has been reported at Gran Canaria and in the Southern Ocean (Ekdahl et al., 1998; Abrahamsson et al., 2004), but not at Mace Head (Carpenter et al., 2000). The observed evening peak of bromoform mixing ratios may be linked with either respiration induced production of bromoform (Ekdahl et al., 1998; Abrahamsson et al., 2004; Collén et al., 1994) or

an atmospheric accumulation of bromoform due to the lack of photochemical degradation (von Glasow, 2008; Read et al., 2008; Goodwin et al., 1997). The production of intracellular hydrogen peroxide (H_2O_2) in macro-and microalgae as a by-product of the photosynthetic process, has been shown, in laboratory conditions, to occur under all light conditions (Collén et al., 1994; Pedersén et al., 1996). A small quantity of H_2O_2, approximately five times less, is produced by *Laurencia sp.* in the dark (Pedersén et al., 1996). Remnant intracellular H_2O_2 would be diffused, for approximately an hour, into the water column at the onset of darkness (Pedersén et al., 1996). As discussed it is possible that bromoform is produced as a defence mechanism against the scavenging of the hydrogen peroxide (Pedersén et al., 1996; Carpenter et al., 2000). The limited release of H_2O_2 might explain why there is an increase after sunset that peaks and then decreases. A lack of observed sea-air exchange of bromoform overnight might lend strength to the idea of a limited release of intracellular hydrogen peroxide (Abrahamsson et al., 2004).

The accumulation of bromoform in the atmosphere as a result of decreased rates of photolysis might result in the observed peak in evening mixing ratios. The rate of photochemical decay would initially drop to zero in the dark, allowing the bromoform produced to accumulate (von Glasow, 2008; Galbally et al., 2000; Saiz-Lopez et al., 2004). Atmospheric halocarbon mixing ratios above cold upwelling systems have been found to be inversely related to MBL height. Convection above the upwelling system was suppressed by a negative sensible heat flux driven by a positive ΔT (surface air temperature - sea surface temperature). This stable system has a reduced volume available for mixing and consequently exhibits elevated mixing ratios (Fuhlbrügge et al., 2013). Variations in wind speed might also play a role in this observed peak, increasing the sea-air flux to the MBL and the dilution of mixing ratios through the atmosphere once the flux decreases. The night time accumulation of bromoform in the atmosphere might be important in rapid ozone destruction, particularly in the polar regions. At polar sunrise the bromoform is rapidly converted to bromine radicals and catalytically destroys ozone (von Glasow, 2008; Galbally et al., 2000; Saiz-Lopez et al., 2004).

4.2 Sea-air gas exchange

The flux of gases across the air-sea interface may be estimated using bulk formulae that are based on the differences in the concentration between the two phases as well as wind speed. The solubility of a gas plays an important role in determining the movement of each compound and depends on in which phase it is found. The presence of waves and bubbles from breaking waves will increase the surface area of the air-sea interface and hence increase the flux strength. Microscale processes involving the waterside and airside control of compounds form the basis of gas flux models (Nightingale, 2009). Compounds in the bulk layers mix with the micro layers and transfer across the interface occurs between the two micro layers. The rate of transfer is compound specific based on solubility and the difference in concentration. For more details see Chapter 1.3.4.

4.2.1 Marine boundary layer

The marine boundary layer (MBL), the lowest section of the atmosphere, is pivotal with respect to air quality, weather and climate (Seibert et al., 2000; Seidel et al., 2010). The structure of the lower troposphere is directly influenced by the height of the MBL, which varies from a few 100s of metres to perhaps 1 – 2 km (Seibert et al., 2000). Momentum, water and trace gases are exchanged between the surface and the free atmosphere by processes within the MBL. These exchange processes and the height of the MBL contribute to the transport, dispersion and removal of surface released gases. The vertical extent of mixing, through turbulent, radiative and moisture processes, is limited by the MBL height (Seibert et al., 2000; Seidel et al., 2010). The height of the MBL determines the volume of the atmosphere into which surface released gases are mixed, influencing atmospheric mixing ratios (Seibert et al., 2000). Consequently, the MBL height may act as a natural pre-concentrator, elevating mixing ratios under a low MBL height, e.g., less than 100 m. The variability of bromoform measurements in the Mauritanian upwelling system have been linked to the height of the MBL (Fuhlbrügge et al., 2013).

The height of the MBL has been estimated from atmospheric profile measurements and/or models using both numerical and simple equations (Seibert et al., 2000). While newer remote sounding systems, such as LIDAR and Doppler profilers, were able to provide continuous measurements and have been deployed with increasing frequency, radiosondes still form a dominant vehicle for obtaining atmospheric profiles. Seibert et al. (2000) and Seidel et al. (2010) assert that the low temporal repeatability and vertical smoothing of measurements in radiosonde profiles, has been off-set by the routine nature of ascents and the length of each dataset. Utilising the atmospheric profiles generated from radiosondes numerous techniques have been reported for the estimation of MBL height. Traditional methods include: the ‘parcel method’, gradient of potential temperature, Richardson number, elevated inversion and surface based inversion (Seibert et al., 2000; Seidel et al., 2010). New techniques, based on remote sounding systems, include estimates of the level of minimum vertical gradient of relative humidity (RH), refractivity or specific humidity (Seidel et al., 2010).

Comparison between the ‘parcel’ and RH methods resulted in estimated MBL heights of 600 m to 2000 m respectively. Stable boundary layer conditions, a specific form of MBL, results in conditions for which most of the traditional techniques are unable to produce a result (Seibert et al., 2000). In these conditions, surface based and elevated temperature inversions along with Richardson number calculations are applicable depending on the quality of data available from radiosondes. Stable boundary layer conditions have been found to occur up to 60 % of the time at Cape Town (Seidel et al., 2010). Mean annual global estimates of MBL height, based on surface inversion, lie at approximately 250 m, while an elevated subsidence inversion has a mean height of between 1250 – 1500 m (Seidel et al., 2010).

4.2.2 Photochemistry of ozone, carbon monoxide and bromoform

This section examines the roles, interactions and importance of photochemical reactions of ozone (O_3), carbon monoxide (CO) and $CHBr_3$. It describes the relationships between the three gases, their sources

and sinks, and their impact on other chemical cycles.

Ozone in the troposphere is well documented and is a known naturally occurring surface pollutant. Being a key precursor in the formation of the hydroxyl (OH) radical, ozone plays a significant role in determining the oxidative capacity of the troposphere (Jacob, 1999; Kim et al., 2013; Chin et al., 1994). The catalytic cycling of HO_2 and CO (Reactions 4.1 – refeq:H) has been shown to initiate the formation of ozone in regions of sufficiently high NOx (Novelli et al., 1998). The two dominant sources of ozone in the troposphere are via photochemical production and subsidence from the stratosphere. The photochemical production of ozone occurs by reactions of NO_x and volatile organic carbons (VOCs) in sunlight (Reaction 4.3 –4.5). This formation process is thought to play a dominant role in determining the tropospheric ozone mixing ratios (Jacob, 1999; Kasibhatla et al., 1998). Photochemical production of ozone is thought to be the dominant source in the tropics, while subsidence from the stratosphere dominates in the polar regions (Vingarzan, 2004). Globally, the transport of ozone from the stratosphere is known to be slow and can only account for a fraction of the ozone in the troposphere (Jacob, 1999). Ozone found in the upper troposphere is reported to be a potent greenhouse gas (WMO, 2011). Variations in the mixing ratios of ozone at this level could therefore result in climate change feedbacks.

$$CO + OH \rightarrow CO_2 + H \tag{4.1}$$

$$H + O_2 + M \rightarrow HO_2 + M \tag{4.2}$$

$$HO_2 + NO \rightarrow OH + NO_2 \tag{4.3}$$

$$NO_2 + h\nu \rightarrow NO + O \tag{4.4}$$

$$O_2 + O + VOCs + h\nu \rightarrow O_3 \tag{4.5}$$

The oxidation of CO may, via reactions with OH, contribute a significant amount of O_3 to the tropospheric atmosphere (Kim et al., 2013). Without the OH radical, toxic species such as CO and methane (CH_4) would accumulate within the troposphere. The major sink of OH is due to reactions with CO, accounting for 75 % loss of the OH and for 90 – 95 % loss of CO (Granier et al., 2000; Novelli et al., 1998). CO is mainly anthropogenically produced with relatively well known sources (incomplete combustion and hydrocarbons) (Chin et al., 1994; Kim et al., 2013). Based on a reaction with OH, CO has an atmospheric lifetime of about two months (Jacob, 1999). This makes it an excellent tracer of anthropogenic emissions. CO is more abundant in the northern hemisphere winter due to lower amounts of the OH radical in that season. The Southern Hemisphere background mixing ratio has been shown to be between 35 – 70 ppb (Novelli et al., 1998). Detection of CO mixing ratios above this range in the Southern Hemisphere are, therefore, highly indicative of anthropogenically influenced air (Novelli et al., 1998).

The relationship between O_3 and CO is considered complex (Jacob, 1999; Chin et al., 1994). Varying atmospheric conditions can cause different local concentrations of each (Voulgarakis et al., 2011). Positive

and negative correlations between O_3 and CO are known to exist (Kim et al., 2013; Jacob, 1999). Positive and negative correlations between O_3 and CO relate to different ozone production locations. A positive correlations highlights a tropospheric ozone source, while a negative correlation suggests a stratospheric source (Chin et al., 1994; Kim et al., 2013). The ozone-CO relationship has been used in tropospheric studies to distinguish between photochemically produced and stratospheric ozone vertically transported to the surface (Kim et al., 2013). It has been suggested that positive correlations indicate tropospheric production of ozone, possibly through the destruction of CO (Kim et al., 2013). While negative correlations, on the other hand, have been shown to occur in the absence of photochemistry (Chin et al., 1994) and act as an indicator of the vertical transport of stratospheric ozone (Kim et al., 2013). Understanding the ozone-CO correlation may shed light on the ozone source and local atmospheric chemistry present.

Bromine radicals, released from the photolysis of bromoform, react catalytically with ozone, causing its removal. Details of the reactions of bromoform with ozone in the troposphere and stratosphere can be found elsewhere in this thesis (Chapter 1.1.1). Through reactions with OH radicals in the atmosphere bromoform has an atmospheric time in the order of 100 days. Following the initial removal of the hydrogen atom from bromoform, the resulting tribromomethyl compound should react with molecular oxygen. This reaction will ultimately lead to release of bromine radicals, which are known to catalytically destroy ozone. While the decomposition rate has not been estimated, it is expected to be rapid (McGivern et al., 2002).

4.2.3 Determination of air mass origin

The determination of air mass origin is important in distinguishing source regions of trace gases in the atmosphere. This determination is of particular importance for atmospheric bromoform measurements at Cape Point (Brunke et al., 2004). CO and radon (^{222}Rn) gas tracers and the HYbrid Single Particle Lagrangian Integrated Trajectory model (HYSPLIT, Draxler, R. R. and Rolph, G. D., 2013)[1] and back trajectory analysis were applied to bromoform and meteorological measurements at Cape Point to determine the source region of air masses.

The HYSPLIT model is based on a joint effort by the National Oceanic and Atmospheric Administration (NOAA) and the Australian Bureau of Meteorology. Time integrated, three dimensional trajectories of the position of air parcels based on meteorological data are generated through either forward or backward time steps in the model. The model can be used in a 'forward' capacity to show how a chemical distributes in the atmosphere, or in a 'backward' capacity to investigate the origin of an air parcel. Vertical movement of parcels in the model is integrated through constant pressure (isobaric) or temperature (isentropic) surfaces or is calculated from the vertical velocity field within the meteorological data.

[1]HYSPLIT model access via NOAA ARL READY Website: http://ready.arl.noaa.gov/HYSPLIT.php.

CO and ^{222}Rn measurements at Cape Point were used to identify samples which had a strong anthropogenic and terrestrial signal as opposed to the maritime samples. The terrestrial source and rapid decay of radon (half-life: 3.824 days) makes it an ideal tracer to indicate the relative age of an air mass with low mixing ratios for aged marine air (Brunke et al., 2004). The concentration indicates whether an air parcel has had recent contact with a landmass, making ^{222}Rn measurement a powerful indicator determining whether air has been influenced by land or coastal processes. CO, as already discussed, is anthropogenically produced (Sec. 4.2.2), making it an ideal tracer for anthropogenic contamination of air samples.

4.3 Methods and materials

4.3.1 Cape Point, Global Atmospheric Watch

The Cape Point GAW station monitors several climate relevant gases including CO, O_3, carbon dioxide (CO_2), methane (CH_4), ^{222}Rn, gaseous mercury and halocarbons (CFCs). In addition, standard meteorological measurements, including wind speed, direction, shortwave radiation, air temperature and relative humidity are continuously taken and autonomously collected. The 30m high sampling mast, on top of the station, is used to draw air from three sampling heights: 4, 10 and 30 m. Air for sampling is continuously drawn into the station by means of a metal bellows pump. The air is dried by sequential cold trapping at -5 and -40 °C before being passed to the detectors.

Shortwave radiation is measured by means of a Kipp & Zonen pyranometer (CMP3). The pyranometer is stationed on the roof on the northern side of the sampling mast. A measurement of incident light falling on the detector is taken every 5 minutes. These measurements are averaged to 30 minute means.

For the purpose of this study, air was drawn from 4, 14 and 30 m heights on the sampling mast for ozone measurement. Three Thermo Electron 49C analysers were used to perform ozone measurements based on the ultraviolet (UV) detection technique. Daily zero and span measurements were used to assess long-term stability of the detectors. A TEI 49i-PS ozone calibrator was used every two months to verify the measurements from the Thermo Electron instruments. The air samples were drawn off a continuous gas flow every minute. Half-hourly mean values were generated from the one minute samples.

The CO mixing ratio was measured using an RGA3 (Trace Analytical, Inc., USA). The system is based on a gas chromatography process to separate the sample. The detector uses reduction of mercuric oxide (HgO) to determine the concentration of CO (Brunke et al., 2004). Measurements are made every 15 minutes with a calibration occurring every 2 hours. The CO measurements were cleaned for non-background influences. Consequently a background only CO dataset was used during the analysis of bromoform variability at Cape Point.

An Australian Nuclear Scientific & Technology Organisation (ANSTO) two-filter radon detector is used at Cape Point (Brunke et al., 2004). The detector works by measuring the decay products of

radon under controlled conditions. All the decay products are initially scrubbed from the air as it passes through the first filter. Air is then passed through a decay chamber where daughter products are allowed to collect on the second filter. The number of collected daughter products is proportional to the radon concentration (Whittlestone and Zahorowski, 1998). Detection is performed by a photomultiplier examining the second filter, which is usually made up of a scintillator *viz* zinc sulphide. The count rate is proportional to ambient ^{222}Rn concentrations (Brunke et al., 2004). Monthly calibration is achieved by the addition of a known radon source. The limit of detection for a one hour count is 36 mBq m^{-3} (Brunke et al., 2004). Samples, drawn from the top of the mast, are recorded half hourly (Brunke et al., 2004).

4.3.2 HYSPLIT back trajectories

Single particle HYSPLIT back trajectories valid for the days of bromoform sampling were obtained from the NOAA ARL READY-HYSPLIT website. The back trajectories were generated for 72 hours prior to bromoform mixing ratio measurement. The backward particle trajectories utilised model vertical velocity to estimate changes in height during transit of the air parcel. End point arrival height was set to the elevation of Cape Point GAW station (230 m a.s.l). For the estimation of trajectories, the model uses meteorological conditions from the GDAS1 dataset. Default settings were used in the remaining fields.

The NCEP Global Data Assimilation System archived model output (1997 – present) was used in this study. Single particle back trajectories for the 72 hours preceding bromoform measurements were generated for all observations. The trajectories were generated with a termination height of 230 m (a.s.l), the height of the GAW station and the model was used to generate plots showing the back trajectory of sampled air for the preceding 72 hours. Single back trajectories were taken at one height level only (230 m surface). This represented the surface wind direction and would best show where air had been in close proximity to the ocean surface, hence maximising the bromoform mixing ratio. The data were sorted based on CO and ^{222}Rn gas concentrations which highlighted different regions or sources. Back trajectories give an indication of the path and height an air parcel has travelled adding further information regarding source region.

4.3.3 Tidal height

Simon's Town is the harbour nearest to Cape Point. Located about 20 km to the north of Cape Point, it is a suitable proxy for tidal height. Unfortunately, the tidal gauges at Simon's Town and Cape Town harbours were broken for the duration of the experimental period. Therefore, predicted tidal heights were obtained from the Navy Hydrographic Office (http://www.sanho.co.za/). An hourly tidal height measurement is provided. Variations from the predicted tide could be caused by changes in atmospheric pressure, wind direction and coastally trapped waves. With the exception of storm events, the variation would, typically, be less than 25 cm (approx. 12 % of tidal range; H. N. Waldron, University of Cape Town, pers. comm. 2012). Gaps in the predicted height, due to hourly predictions, are interpolated using MATLAB. Actual and predicted tidal heights for Port Nolloth (west coast) and Mossel Bay (south coast) were obtained for comparison purposes. These two harbours are the closest to Simon's Town for which

actual measurements exist. Comparison of predicted tidal heights against actual heights was performed (Sec 4.4.4). This analysis gives an indication of reliability of the predicted tidal height as a proxy for actual tidal height over the bromoform sampling period.

4.3.4 Bromoform measurements

Measurements of bromoform were taken in austral spring, October to November 2011, at the Cape Point GAW station. A quasi-discrete sampling pattern was achieved for bromoform measurements during the experimental period. Attempts to match sampling time on various days was hampered by the manual nature of the method and occasional technical difficulties with the system. Measurements were intensively collected in batches over three day periods during the bromoform experimental periods. Following trapping on the adsorbent bed air samples were analysed immediately on the GC-ECD instrument and data acquisition system (Kuyper et al., 2012 and Chapters 2 and 3). Meteorological measurements, concurrent with bromoform sampling, were obtained from the Cape Point GAW station. This provided concurrent ancillary data for the analysis of variability observed within the bromoform measurements.

Due to differences in infrastructure availability and increased relative humidity at Cape Point compared to the University of Cape Town, minor modifications to the sample inlet were necessary for sampling. Two modifications to the GC system were necessary for this sampling. These were: a new sampling line being fitted and the installation of additional drying traps for the removal of moisture prior to the quantitative detection of bromoform in air could be made (Fig. 4.3).

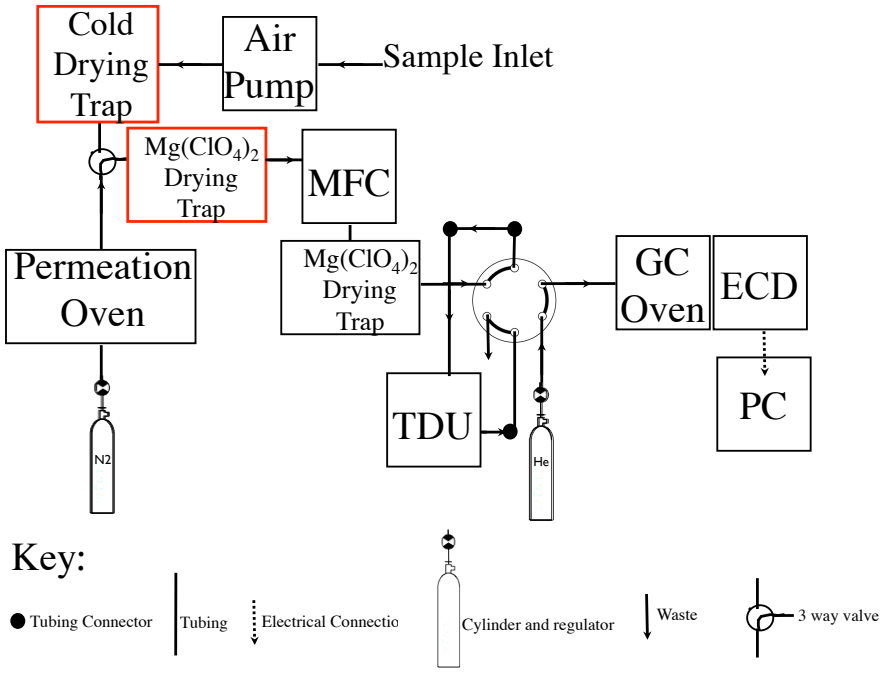

Figure 4.3: Modified bromoform sampling system at Cape Point, South Africa. Items in red denote new system components.

Previously at UCT, samples had been drawn in through 10 m of $\frac{1}{8}$" PTFE tubing. A longer section of tubing at Cape Point was required to connect to a sampling mast and avoid contamination from any local sources. A small sampling mast, in the form of a clean wooden pole, was built on top of the of the chimney of an adjacent building as there was no way to draw air from the existing main sampling mast (Fig. 4.4).

Figure 4.4: Modified bromoform sampling mast at Cape Point, South Africa.

Dekaron tubing (30 m x $\frac{1}{4}$") was attached to the short mast and roof and run into the GC. The larger diameter tube ensured that the sample flow rate through the desorption trap was not affected by the longer sampling line. To prevent particle accumulation and direct moisture, the inlet was bent over to point down and covered with a plastic bottle. (Fig. 4.4).

A greater humidity was experienced in the air at Cape Point than at the University of Cape Town, which overwhelmed the magnesium perchlorate trap. A cold trap was placed in the recirculating glycol bath (-15 °C) with a large magnesium perchlorate trap (15 x 2.5 cm) upstream of the MFC. Air samples passed through the cold trap immediately after being pumped into the system. A second smaller magnesium perchlorate trap (10 x 0.6 cm) was kept in-line between the MFC and sampling trap, ensuring that both calibration and air samples were run through at least one chemical drying trap (Fig. 4.3).

4.3.5 Marine boundary layer

Radiosonde atmospheric profiles were obtained from the SAWS station based at Cape Town International Airport ($\pm$ 45 km NE of Cape Point). Gaps in the profiles were smoothed by means of interpolation in MATLAB prior to the estimation of MBL height. Surface and elevated temperature inversion techniques were used to estimate the MBL height at Cape Point (Seibert et al., 2000; Seidel et al., 2010). Temperature profiles from the twice daily (noon and midnight) radiosonde releases were examined to identify the presence of a temperature inversion (Seibert et al., 2000). If no temperature inversion was found at $<$ 2000 m, well-mixed conditions were assumed to exist and consequently no MBL was present and therefore no value was attached.

4.3.6 Satellite remotely sensed data

Remote sensed datasets for the Benguela were obtained for Chlorophyll-*a* (Chl-*a*), sea surface temperature (SST), photosynthetically active radiation (PAR), and wind speed and direction during the Cape Point sampling period. Daily (24 hour) mean composite data for Chl-*a* and SST were used in conjunction with back trajectories to generate a daily value for each day of sampling. The Chl-*a* and SST data were derived from the MODIS satellite at 1 and 4 km resolution respectively and was obtained from the Marine Remote Sensing Unit (http://www.afro-sea.org.za). Back trajectories of air parcels arriving at Cape Point were overlaid on the Chl-*a* and SST daily mean composite data (Fig. 4.5). The mean of the Chl-*a* and SST values lying below the HYSPLIT back trajectories were extracted, resulting in a representative measurement for that day. Cloud cover on a number of days in the Benguela region limited the effectiveness of this method to extract meaningful values of Chl-*a* or SST. In these events, the day before or after the bromoform mixing ratio measurement was examined provided there was less cloud cover. Phytoplankton blooms extend for 10s of kilometres from the coast and cover the length from Cape Columbine to Lüderitz, Namibia. A temporal stability of hours to days for the blooms in this region have been reported (Hutchings et al., 2009) This variability implies that conditions are able to change rapidly and consequently the measured values from non-synoptic days are not representative. The few days for which a Chl-*a* image correlated with bromoform produced statistically weak results.

Analysis of back trajectories, for the bromoform experimental period, suggested that those transiting over the Benguela passed dominantly through an area south of Cape Columbine (33 – 34.5° S and 16.5 – 15.5° E; Fig. 4.6). Daily PAR and wind speed and direction estimates for the Benguela were generated from the mean of values occurring within this area. The Cross Calibrated Multi-platform (CCMP) winds at 0.25° x 0.25° resolution were obtained from the Po.DAAC website (http://podaac.jpl.nasa.gov). MODIS Photosynthetically Active Radiation (PAR) at a 4 km resolution was obtained at a daily time scale from Ocean Color Data website (http://oceandata.sci.gsfc.nasa.gov/MODIST/L3BIN/2011/). The level 3 (L3) data of these datasets was largely cloud free, resulting in more consistent data for the bromoform experimental period.

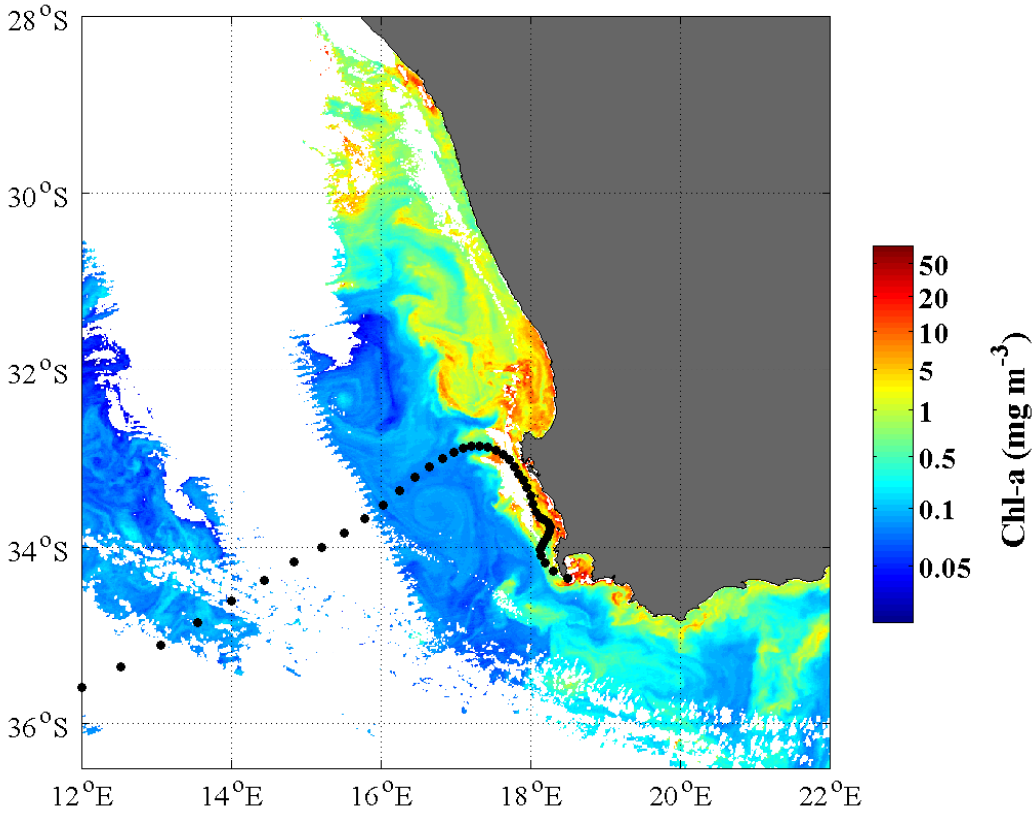

Figure 4.5: MODIS Chl-*a* daily composite with single HYSPLIT back trajectory overlaid.

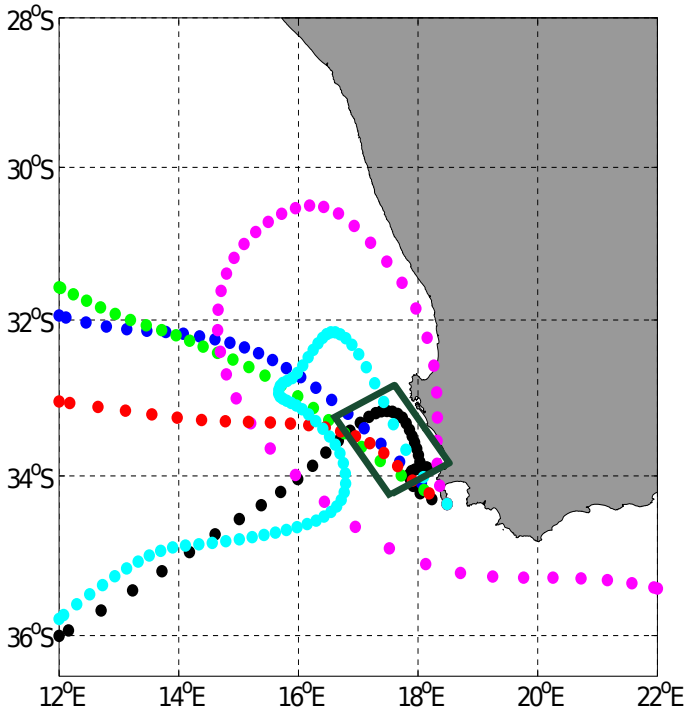

Figure 4.6: HYSPLIT back trajectories passing over an area adjacent to Cape Columbine.

4.4 Overview of meteorological and natural environmental conditions

The meteorological conditions at Cape Point during the bromoform measurement experimental period are examined in this section. The spring climatology for Cape Town exhibits a mixture of summer and winter conditions. Mean air temperatures ranged between ∼13 and 18 °C, night and day, respectively during the experimental period. The occurrence of sub-tropical cyclones were typical for this time of year. Weather patterns are dominated by migratory anticyclones called cold fronts (Tyson and Preston-Whyte, 2000). Selected elements were extracted and examined in greater detail for their impact on the variability in the bromoform mixing ratio.

4.4.1 Wind speed and direction

The wind speed at Cape Point varied between still air to an upper limit of 24.3 m s^{-1} (Fig. 4.9) during the experimental period. The variability in wind speed is primarily driven by local changes in pressure and wind direction with higher wind speed from the east to southeast (15 – 25 m s^{-1}) compared to westerly winds (10 – 15 m s^{-1}; Fig. 4.9). The change in wind speeds is possibly caused by local topographic features.

The wind direction measurement at Cape Point becomes unreliable at speeds of < 4 m s^{-1} and so these measurements were removed from the dataset before analysis (E.-G.Brunke and C. Labuschagne, SAWS, pers. comm. 2011). Two dominant wind directions were experienced at Cape Point during the experimental period (Fig. 4.7), one from the west-southwest (WSW) to northwest (NW) and one from the east (E) to southeast (SE). There were a greater number of days with direction from WSW-NW than E-SE. The two dominant wind directions found at Cape Point are driven by synoptic conditions (Brunke et al., 2004). The southeasterly directions are driven by the presence of the SAHP, which is more indicative of summer conditions, while westerly winds are driven by cold fronts associated with extra-tropical cyclones that are mainly a winter phenomenon in Cape Town (Hutchings et al., 2009). Cut-off low pressure systems occur predominantly during the transition seasons (Singleton and Reason, 2007). These episodic low pressure systems are known to result in significant rainfall, often leading to flash-flooding. Cut-off low pressure systems have been linked with stratospheric-tropospheric exchange, resulting in the draw down of ozone (Singleton and Reason, 2007).

The variation in wind speed coupled with changes in direction may be an important driver of the observed variability in bromoform mixing ratios measured at Cape Point. Changes in speed providing conditions for the accumulation or dispersion within the MBL (Quack and Suess, 1999; Liss and Merlivat, 1986), and direction determining source region of the air mass.

4.4.2 Air temperature, relative humidity and shortwave radiation

Air temperature was relatively stable with a daily mean of 14.4 °C and a range of 10.5 – 21.5 °C (Fig. 4.8). The lack of correlation between wind speed and air temperature suggests an absence of local land or

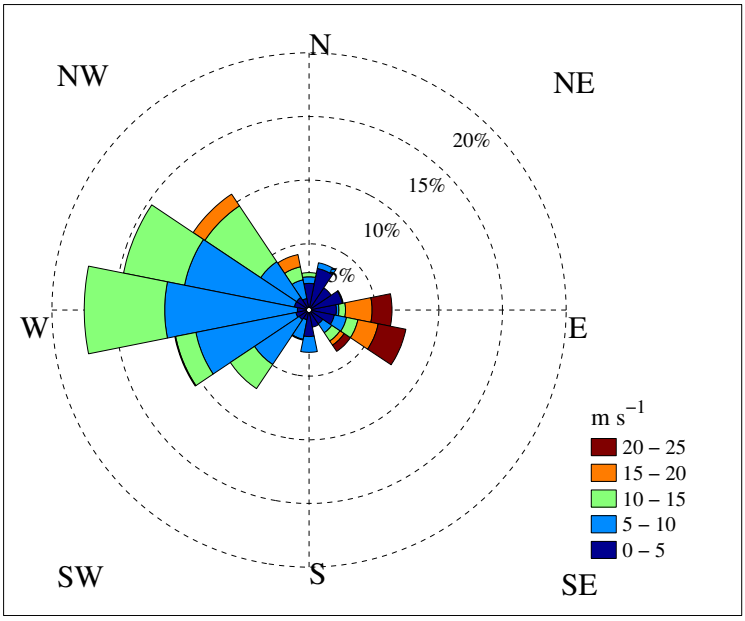

Figure 4.7: Wind speed and direction frequency plot for Cape Point during the bromoform experimental period.

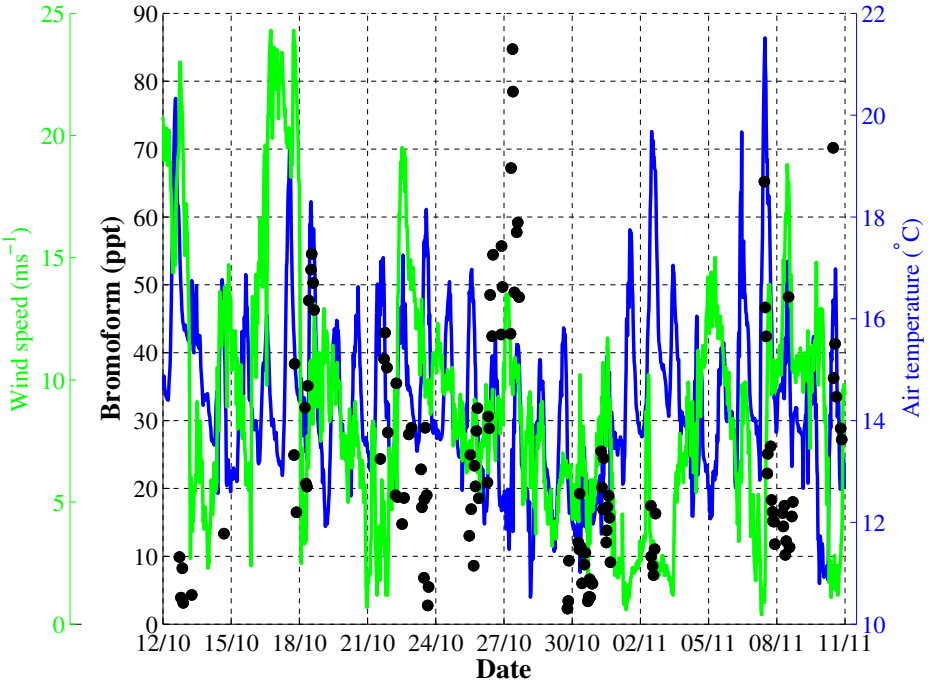

Figure 4.8: Comparative graph of wind speed (green), air temperature (blue) and bromoform mixing ratios (black) at Cape Point during the bromoform experimental period.

sea breezes. However, land and sea breezes may have occurred on certain days and played a role in moderating local mixing ratios of bromoform in a manner similar to that experienced by Carpenter et al. (2000).

Shortwave radiation exhibited a mean daily maximum of approximately 973 W m^{-2}. Light from the moon does not seem to have impacted on measured global radiation despite many cloudless nights. The

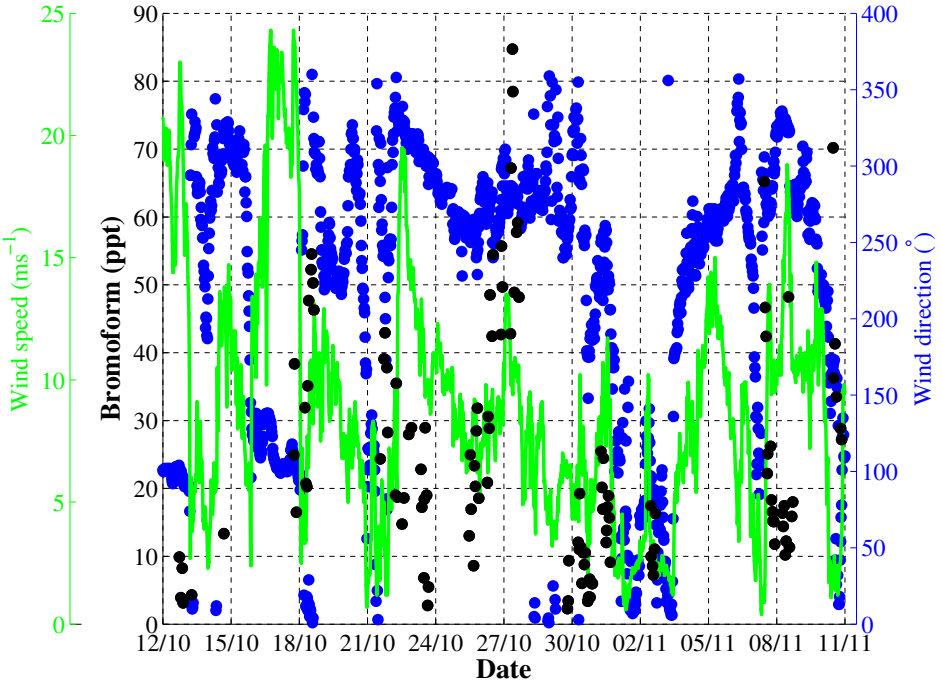

Figure 4.9: Time series of wind speeds (green) and direction (blue stars) with bromoform mixing ratios (black) at Cape Point during the bromoform experimental period.

proximity of the GAW station to the lighthouse at Cape Point might explain the raised radiation values at night. Local cloud events caused a decrease in the maximum radiation received at ground level. Six cloudy days were recorded at Cape Point during the experimental period, decreasing shortwave radiation values from ∼1000 W m^{-2} to between 400 and 800 W m^{-2}.

Relative humidity (RH) values exhibited a cyclical variation with values ranging between 80 and 95 % during the experimental period. Two departures from this occurred during 26 and 28 October and 7 to 8 November where RH values remained low at 60 – 70 % and < 50 %. The depreciated RH values may have been due to changes in wind direction and consistent wind (Fig. 4.9). While RH and air temperature showed a weak negative (r = -0.32) relationship, they displayed a concomitant variability, exhibiting a strong diurnal cycle. RH and shortwave radiation showed a moderate negative correlation (Fig. 4.10).

4.4.3 Marine boundary layer height

The MBL height at Cape Point showed some large variations, ranging from lows of 91 m (night time surface inversions) to highs of ∼2000 m as well as days with no apparent MBL, suggesting well mixed conditions. The estimated MBL heights do not seem to be correlated with any of the meteorological measurements taken at Cape Point (Fig. 4.11). A roughly diurnal pattern can be discerned from the estimated heights, suggesting that shortwave radiation and air temperature mechanisms may be driving the variability, despite the lack of correlation (Seibert et al., 2000). The spatial inconstancy of measurement may be the reason for an inability to rigorously identify driving mechanisms.

4.4.4 Tidal height

A comparison of predicted *versus* actual tidal height for Port Nolloth (west coast) and Mossel Bay (south coast) during the bromoform sampling period found no significant difference in the heights or timing,

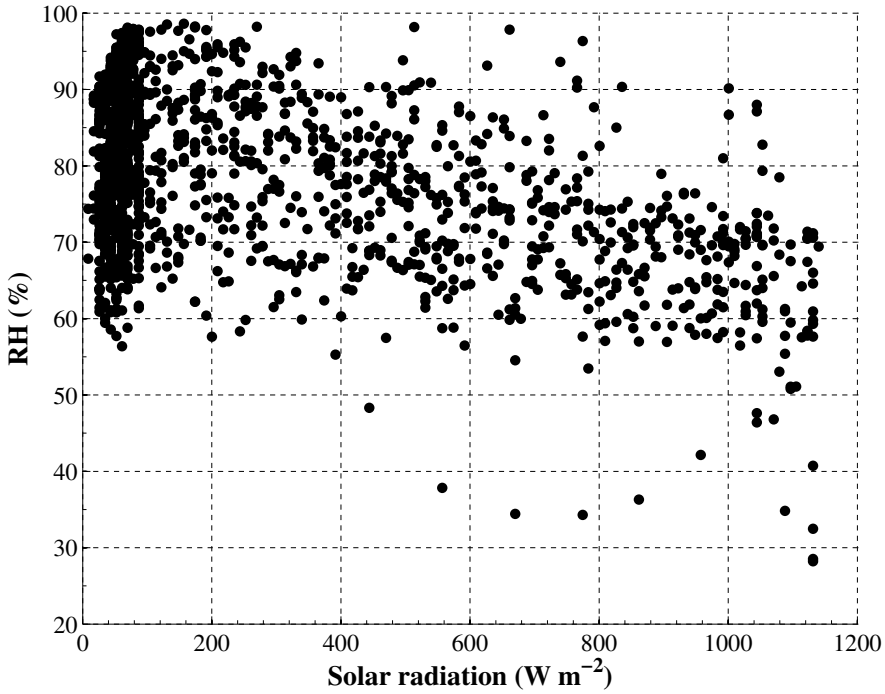

Figure 4.10: Comparative graph of relative humidity and incoming shortwave radiation at Cape Point during the bromoform experimental period.

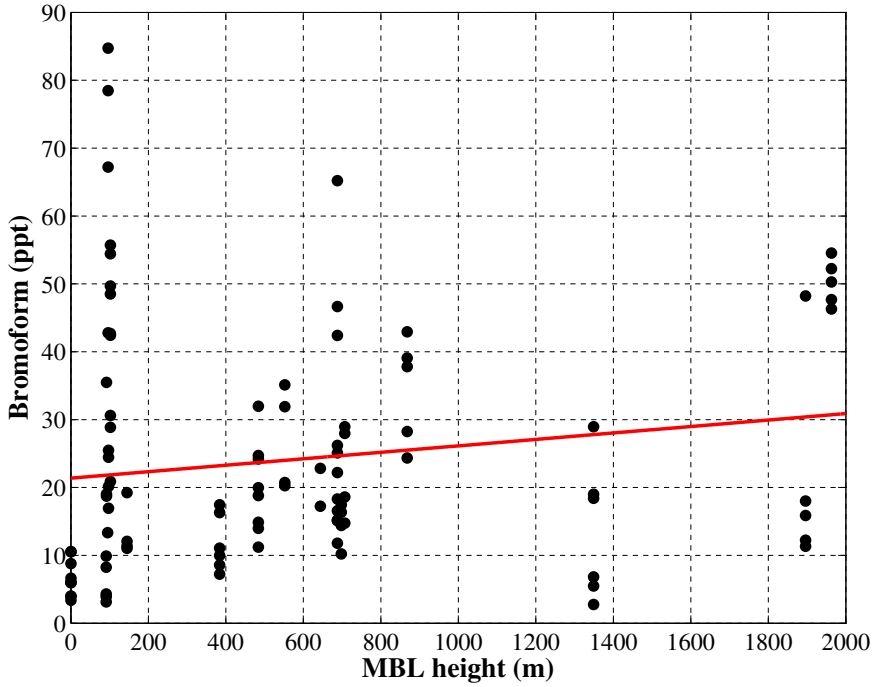

Figure 4.11: Estimated boundary layer height at Cape Town International airport as a proxy for MBL at Cape Point. The linear relationship between MBL height and bromoform is shown by the red line.

implying that the tides were not influenced by internal or coastal trapped waves (Fig. 4.12). Correlations of the predicted to actual height were 1 and 0.94 for Port Nolloth and Mossel Bay, respectively. This generated confidence in the use of the predicted tidal heights for Simon's Town as a proxy for the actual tidal height at Cape Point.

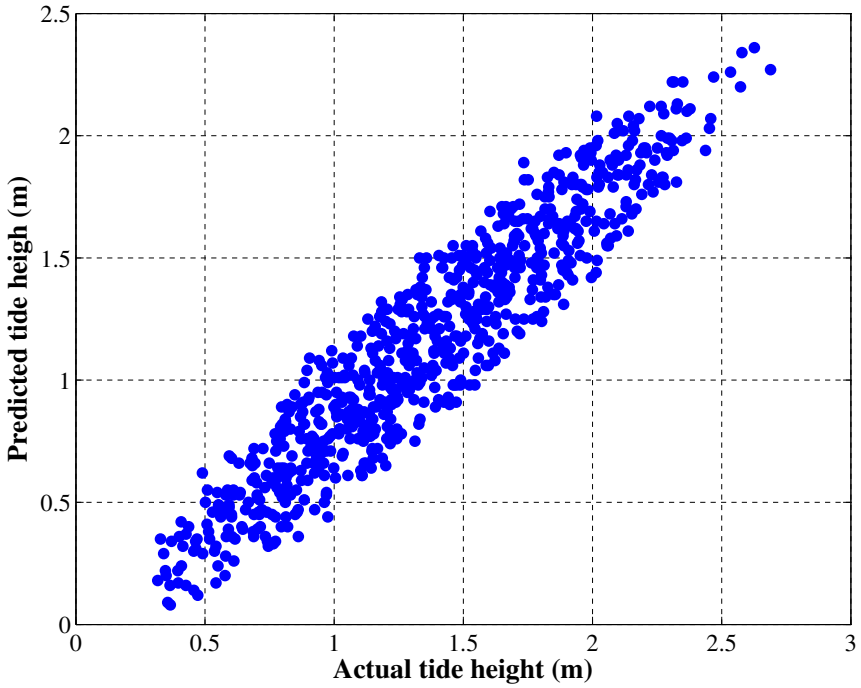

Figure 4.12: The predicted *versus* actual tidal heights for Mossel Bay are shown.

The predicted tidal height record for Simon's Town showed a maximum range of 1.93 m (26 October 2011) and a minimum of 0.56 m (21 October 2011). Sampling started on a spring tide. The time of the first low tide on the day in the semi-diurnal pattern shifted from 9 am to an earlier 3 am during neap tides (Fig. 4.13). The timing and range of the tide may affect the variability of bromoform mixing ratios through the extent of exposure and amount of photosynthetic stress induced. A larger tidal range is likely to expose a greater mass of macroalgae to the atmosphere possibly initiating the release of bromoform. If the macroalgae is exposed with increasing shortwave radiation, this may induce a greater photosynthetic stress in the macroalgae, affecting the amount of bromoform release. The neap tides occurred on 21 October and 2 November 2011, while the spring tides occurred on 26 October and 10 November 2011.

4.4.5 Gas tracers

Ozone (O_3) mixing ratios at Cape Point exhibited a cyclical pattern with a mean of approximately 28 ppb. Between 16 and 19 October 2011 mean O_3 mixing ratios were elevated to approximately 32 ppb (Fig. 4.14). Observed CO mixing ratios displayed stability on a diurnal scale, however fluctuations over the course of days occurred (Fig. 4.14). CO mixing ratios remained low between 46 and 58 ppb during the experimental period. The observed background monthly means of CO at Cape Point during October and November amounted to 55.9 $\pm$ 2.0 ppb and 51.6 $\pm$ 3.0 ppb, respectively (E.-G. Brunke, SAWS, pers. comm. 2014).

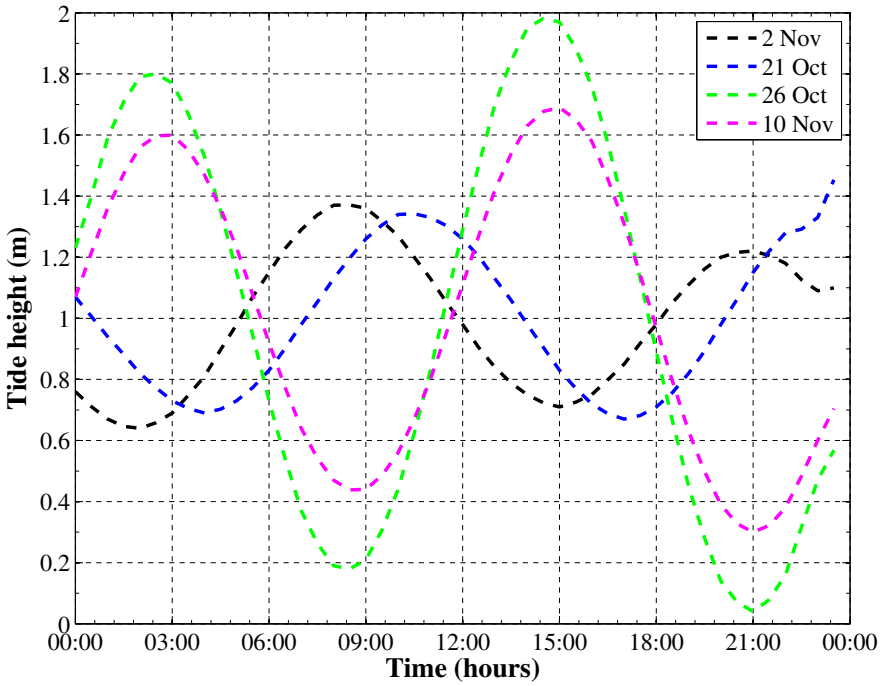

Figure 4.13: Four tides at Simon's Town, near Cape Point: 2 spring (black and magenta) and 2 neap (blue and green). Reflecting the range, timing and variability of the tides during bromoform experimental period.

This confirms that during the experimental period approximately 55 % of the CO concentrations observed fall within this background range. Therefore, the majority of air samples recorded at Cape Point during the experimental period were of a marine origin.

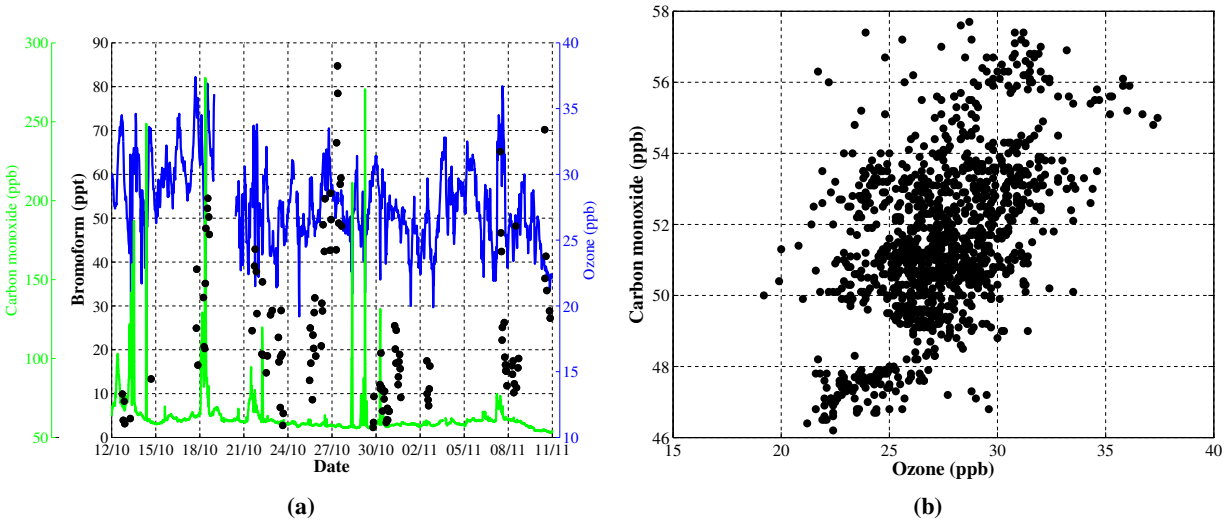

Figure 4.14: Comparative graphs of background CO (green) and O_3 (blue) (a) over time with bromoform indicated in black, and (b) correlation of CO and O_3 at Cape Point during the bromoform experimental period.

The cyclic variability of O_3 and background CO values appeared to be concomitant ($r = 0.51$, Fig. 4.14), however, the CO mixing ratios observed at Cape Point decreased for a number of days on four separate occasions (Fig. 4.14). This created departures between the O_3 and CO records, reducing the ozone-CO

correlation. The O_3 mixing ratios remained constant during these periods (Fig. 4.14). The variability of CO at Cape Point is sensitive to anthropogenic influences. The decreased CO values may be due to changes in wind direction resulting in a decrease in anthropogenic input. A positive relationship between ozone and CO was observed (O_3 / CO; 0.38 – 0.68), during the experimental period. This suggests local photochemical production was the dominant source of the ozone observed at Cape Point.

The strength of the relationship between O_3 and CO decreased (r = 0.33) when air samples from the baseline wind direction (BWD, 170 – 320°) were considered in isolation. The decrease in the ozone-CO relationship strength in marine air samples (BWD) suggests an influence of anthropogenically contaminated air at Cape Point through a reduction in CO mixing ratios. Most of the air samples arriving at Cape Point during the bromoform experimental period were of clean marine origin with ^{222}Rn mixing ratios below 350 mBq m^{-3} (Fig. 4.15). A few days contained mixed air samples that had come into contact with landmasses (600 – 1000 mBq m^{-3}) and an almost equal number of anthropologically enhanced air samples occurred (> 1200 mBq m^{-3}, Fig. 4.15). Cape Point mainly received clean marine air with occasional days or events of mixed or anthropogenic influence. Increases in CO mixing ratio appear to be linked with changes in air mass type from clean marine air to urban air (Fig. 4.15). The higher CO values might, therefore, imply an anthropogenic source. However, CO mixing ratios were uncorrelated with ^{222}Rn and occurred over a wide range of ^{222}Rn values, probably due to the fact that background CO values were used.

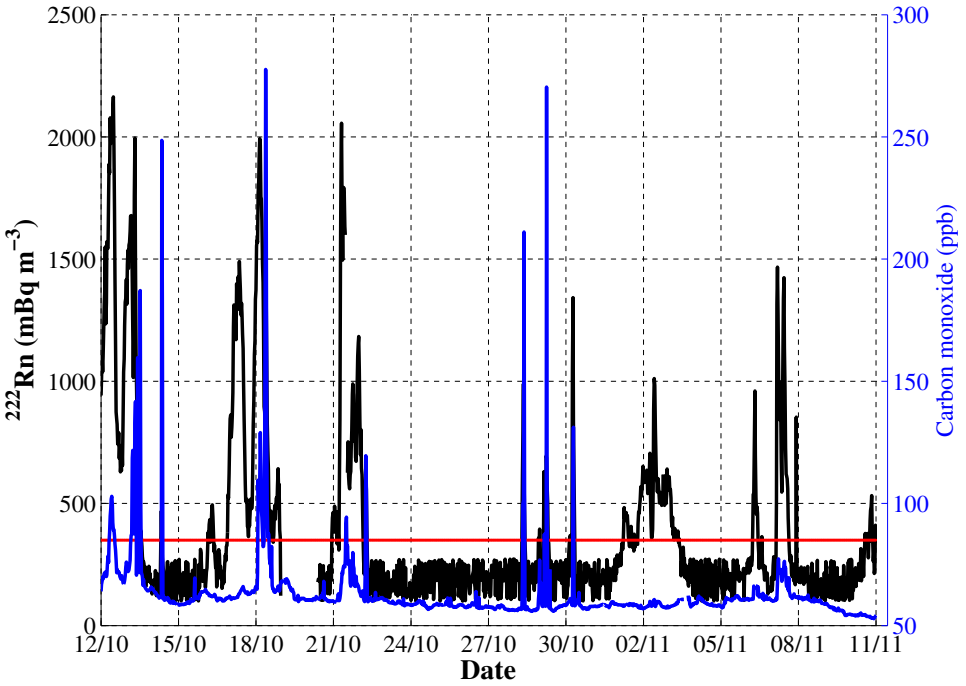

Figure 4.15: The time evolution of ^{222}Rn and CO measurements at Cape Point during the bromoform experimental period show concurrent elevation events, possibly the introduction of anthropogenically enhanced air masses. Gaps in both data sets are due to the removal of bad data through quality control checks applied by SAWS. Clean marine airs samples are shown by measurements occurring below red line (350 mBq m^{-3}).

4.5 Results and discussion

In this section, the bromoform mixing ratios observed at Cape Point are discussed in relation to meteorological conditions. These measurements are examined in the context of mechanisms that may explain the variability observed.

4.5.1 Bromoform measurements at Cape Point

Bromoform mixing ratios observed in air samples at Cape Point ranged between 2.29 to 84.7 ppt with a mean of 24.7 ppt (Fig. 4.16). The measurements appear to have followed a cyclical pattern of variability and half the measurements occurring below the median (19.0 ppt), with 25 % of the measurements observed at mixing ratios larger than 33.1 ppt (75 th percentile). The distribution of measurements is biased to lower values with a few large mixing ratios. This distribution is thought to stem from mainly low mixing ratio sources with a single nearby source of elevated bromoform mixing ratios; most probably the local macroalgal beds.

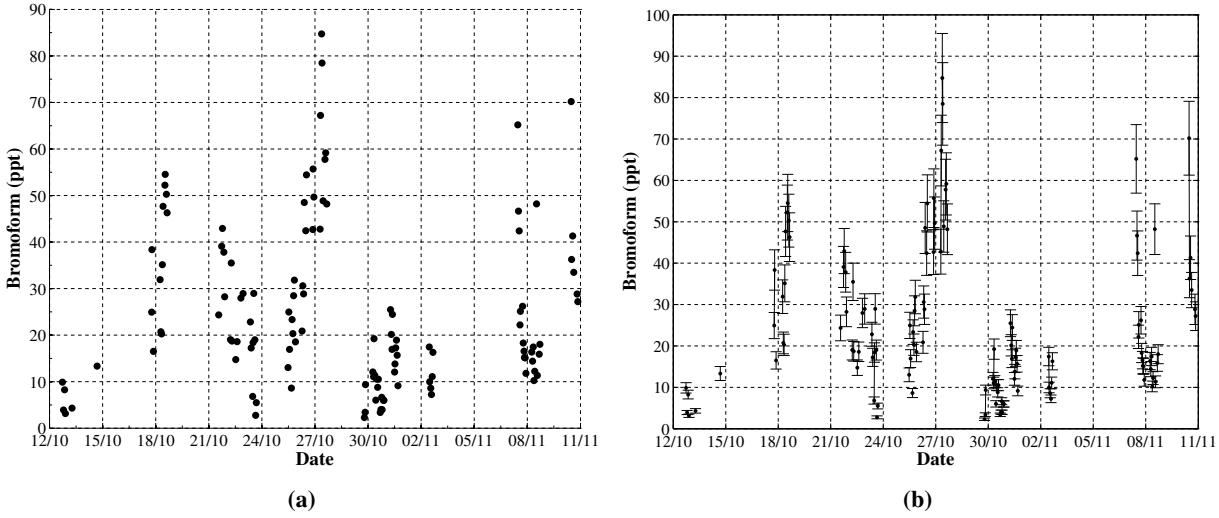

Figure 4.16: Bromoform mixing ratios (ppt) taken at Cape Point, South Africa. Taken between October and November 2011. (a) Time series plot of mixing ratio on specific days. (b) Time series plot of mixing ratios including uncertainty of measurement.

Cape Point is a unique location, receiving air masses from a mixture of independent sources: anthropogenic Cape Town, local macroalgae beds, the Benguela upwelling system, the interior via berg winds and the Southern Ocean (Brunke et al., 2004). Measurements from New Hampshire, USA (43° N) and Borneo (4.5° N), both macroalgae rich coastal environments, have been recently published (Zhou et al., 2008; Pyle et al., 2011). The mixing ratios presented in these reports are similar to those found at Cape Point (Table 4.1). The maximum mixing ratios present are 47 and 60 ppt with means of 14.3 and < 5 ppt, respectively, suggesting that similar processes occur at Cape Point (Table. 4.1). The most closely matched locations to Cape Point, in latitude and sources from macro-and microalgae, are probably Cape Grim, Tasmania (40.5° S) and Gran Canaria, Canary Islands (27° N). These two locations are influenced by

local macroalgae beds and phytoplankton sources. Cape Grim is located on the northwestern edge of Tasmania and receives clean marine air from the Southern Ocean (Cox et al., 2005). Consequently mixing ratios are typically < 5 ppt (Yokouchi et al., 2005).

Table 4.1: Selected previous atmospheric measurements of bromoform in coastal regions.

			$CHBr_3$ (ppt)				
Location	**Date**	**Latitude**	**min**	**max**	**mean**	**Reference**	**Region**
New Hampshire TF	Jun.-Aug. 2002-4	43.1° N	0.2	37.9	5.3-6.3	3	Coastal
San Cristobal Island	Feb.-Mar. 2002, 2003	0.92° S	4.2	43.6	14.1	4	Coastal
Christmas Island	Jan. 2003	1.98° N	1.1	31.4	5.6-23.8	4	Coastal
Cape Grim	Jan.-Dec. 2003	40.7° S	1.3	6.4	2.9	4	Coastal
New Hampshire AI	Jul.-Aug. 2004	42.9° N	0.9	47.4	14.3	3	Coastal
Cape Verde	May-Jun. 2007	16.8° N	2.0	43.7	4.3-13.5	5	Coastal
Borneo	Apr.-Jul. 2008	4.70° N	2-5	∼60		2	Coastal
Cape Point*	Oct.-Nov. 2011	34.5° S	2.29	84.7	24.7	1	Coastal
Atlantic Ocean	Oct.-Nov. 2002	10° N	0.5	27.2		6	Open ocean

References: *This study 1 Kuyper et al., 2012; 2 Pyle et al., 2010; 3 Zhou et al., 2008; 4 Yokouchi et al., 2005; 5 O'Brien et al., 2009; 6 Quack et al., 2004.

4.5.2 Wind direction

The synoptic variability that dominates at Cape Point resulted in a bimodal distribution of wind directions during the bromoform experimental period. The two dominant directions were from the WSW-NW and E-SE (Fig. 4.7). This results in air being drawn from different source regions, thus influencing the variability of bromoform mixing ratios observed at Cape Point. The bromoform mixing ratios, sorted by wind direction, display a strongly dominant source to the W-WNW followed by sources to the north and south, with low mixing ratios associated with all wind directions around Cape Point (Fig. 4.17). The highest recorded mixing ratio occurred from the west and is of biogenic origin (Fig. 4.17). Elevated bromoform mixing ratios in air masses from the northwest to north that contain ^{222}Rn above 600 mBq m^{-3} are thought to be influenced by terrestrial processes.

The mean mixing ratio of bromoform from the westerly sector (238 – 328°) was 27.5 ± 18.9 ppt, which was similar to measurements from the north (340 – 20°, 30.1 ± 15.6 ppt). Mixing ratios from the southerly sector (160 – 200°) exhibited a lower mean of 19.7 ppt but a much larger range of variability with a standard deviation of 24.0 ppt. This suggests that, during the bromoform experimental period, the northerly and westerly sectors were the main sources of bromoform to Cape Point. Southerly wind transports appear to be sporadically large and may draw elevated mixing ratios from the macroalgal beds rather than the low baseline measurements recorded at other times. The westerly sector is probably influenced by the macroalgae beds surrounding Cape Point, while the Benguela and Cape Town anthropogenic sources affect the northerly sector and the Southern Ocean impacts the southerly wind sector.

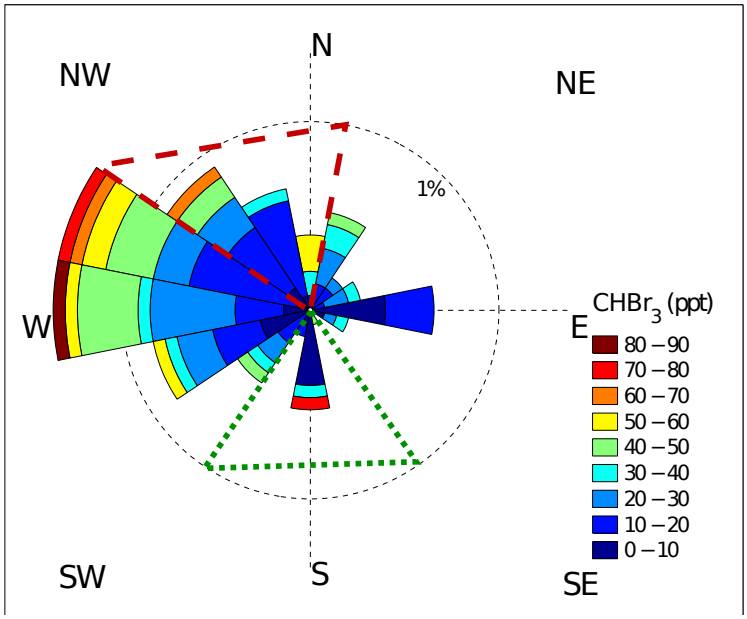

Figure 4.17: Wind rose diagram of bromoform measurements taken at Cape Point, South Africa between October and November 2011. The red triangle (dashes) to the north denoting inputs from the Benguela and the green triangle (dots) to the south denoting air from the Southern Ocean

The status quo referred to above probably results from the macroalgae beds to the west (0.5 km) and north (1.5 – 8 km) of Cape Point (Table 4.2). Species of *Ecklonia*, *Laminaria*, *Macrocycstis* and *Bifurcaria* are all found in the False Bay region. These species, especially *Ecklonia*, *Laminaria* and *Macrocycstis* have been linked to the release of bromoform. The specific release rate of the macroalgae at Cape Point may be greater than those previously published for similar species, which might explain some of the elevated mixing ratios observed (e.g., Laturnus, 1996; Nightingale et al., 1995; Carpenter and Liss, 2000). Shortwave radiation levels, nearly double those of Mace Head, may contribute to the local macroalgae producing bromoform at higher rates and concentrations (Carpenter et al., 2000). See section 4.4 for a description of the conditions affecting Cape Point and consequently the macroalgae beds in the surrounding areas during the bromoform sampling period.

Table 4.2: Varying distances to sampling sites of bromoform measurements in coastal regions.

				$CHBr_3$ (ppt)		
Location	**Distance**	**Latitude**	**min**	**max**	**mean**	**Reference**
New Hampshire TF	24 km	43.1° N	0.2	37.9	5.3-6.3	2
New Hampshire AI	200 m	42.9° N	0.9	47.4	14.3	2
Cape Verde	∼200 m	16.8° N	2.0	43.7	4.3-13.5	3
Borneo	∼50 km	4.70° N	2-5	∼60		1
Mace Head	∼100 m	53.3° N	2	23	4	
Cape Point*	0.5 km	34.5° S	2.29	84.7	24.7	5

References: 1 Pyle et al., 2010; 2 Zhou et al., 2008; 3 O'Brien et al., 2009; 4 Carpenter and Liss, 2000;5 This study and Kuyper et al., 2012.

The synoptic conditions that draw air from the west might result in two additional atmospheric sources of bromoform at Cape Point. Extra-tropical cyclones, that dominate through winter, produce deep mixing of the surface layers and deposit large amounts of macroalgae on the beaches. It has been shown that within macroalgae beds a subsurface maximum of bromoform exists (e.g., Krysell, 1991; Laturnus, 1996). Deep mixing of the surface layers by extra-tropical cyclones might bring this sub-surface bromoform to the surface and hence would enhance the gas flux. This would result in an increase in atmospheric bromoform loading, raising mixing ratios as observed. The macroalgae washed ashore during winter storms is left on the beaches to decay, possibly releasing bromoform or precursors in the process. This may provide an additional contribution of bromoform to the local atmospheric loading (Quack and Wallace, 2003).

It is likely that, air masses arriving at Cape Point from the north (340 – 20°) would have entrained bromoform from either anthropogenic sources in Cape Town or the Benguela. It has been suggested that anthropogenic sources of atmospheric bromoform may be locally significant (Quack and Wallace, 2003). Koeberg nuclear power station, along the west coast, and water treatment facilities within Cape Town present possible sources of anthropogenic bromoform. The measurement of radon is used as an indicator of the cleanliness and quality of air recorded at Cape Point (Brunke et al., 2010). Measurement of bromoform at radon mixing ratios > 600 mBq m^{-3}, suggest that anthropogenic sources due north of Cape Point contributed a mean of 24.0 $\pm$ 9.40 ppt bromoform with 6.60 $\pm$ 2.90 ppt from mixed air sources. Anthropogenic sources at Cape Point are significant and may require close attention as an important global source. A cleaned CO dataset not containing any non-background values were not used during the analysis of bromoform measurements. This precluded the use of CO values as a sorting term within the bromoform dataset.

Table 4.3: Mean bromoform mixing ratio (ppt) sorted by ^{222}Rn (mBq m^{-3}) / air mass type / mean CO and wind speed (m s^{-1}) and direction (deg.). Values in brackets denote standard deviation.

Air mass type	$CHBr_3$	CO	Speed	Direction	No. of Samples
Clean (0 – 350)	24.3 (18.2)	59.1 (4.71)	8.76 (3.94)	250.0 (67.5)	85
Mixed (600 – 1000)	23.2 (14.4)	52.3 (2.80)	8.84 (7.63)	154.0 (101.0)	16
Anthropogenic (> 1200)	17.3 (11.8)	no data	12.4 (7.18)	127.1 (90.9)	4

Southern Benguela Chl-*a* values regularly reached concentrations of approximately 50 mg m^{-3} on a repeated basis during the bromoform experimental period (Fawcett et al., 2007). Persistent cloud cover over the Benguela limited the extraction of data. No statistically significant relationships could be established between the limited extracted remotely-sensed data and variability of bromoform measured at Cape Point. The lack of correlation between Cape Point bromoform measurements and the Benguela Chl-a does not imply a weak or insignificant source. The signal may be reduced through dilution during transport as it approached Cape Point. Transport of air toward the open ocean may have occurred during upwelling events resulting in a low recorded signal. Shortwave radiation levels exhibited a gradient,

decreasing between Cape Point and the Benguela. The lower shortwave radiation levels in the Benguela were thought to be due to the persistent cloud cover, which may have resulted in lower bromoform production response. Increasing shortwave radiation levels toward Cape Point may have raised the rate of photolysis, suppressing a signal of bromoform from the Benguela upwelling system.

A mean of 14.4 $\pm$ 2.66 ppt bromoform was estimated to emanate from maritime air (^{222}Rn < 600 mBq m^{-3}) over the Benguela (328 – 340°). This suggests that the Benguela is a source comparable in strength to that of anthropogenic sources within Cape Town. Transient measurement of bromoform from a passing research vessel reported an austral spring mean bromoform mixing ratio of 24 ppt in the Benguela (Class and Ballschmiter, 1988). It has been postulated that there is a seasonal cycle in the rate of bromoform production due to variability in the bromoperoxidase enzyme (Quack and Wallace, 2003) and further, that this cycle of bromoperoxidase enzyme activity peaks in late boreal spring and summer (e.g., Itoh and Shinya, 1994). The data presented here and other studies in the Benguela suggest the bromoform concentrations in this region peak during the austral winter (Table 4.4). It is possible that microalgae react in an identical manner across the globe, although this is highly unlikely. Itoh and Shinya (1994) proposed a near inverse relationship between temperature and bromoperoxidase enzyme in macroalgal cultures. It is therefore possible for an austral winter peak of bromoform to occur as the water warms from a minimum in summer. The summer SST minimum is driven by local upwelling in the Benguela region. While the production of bromoform by bromoperoxidase has been shown for macroalgae, it has not yet been shown to occur in all microalgal species and is therefore highly speculative at this stage. The longer distance, and therefore time, between source region and measurement in this study compared to the research cruise in the Benguela upwelling region may result in the lower mixing ratio recorded in this study.

Table 4.4: Seasonal influence on bromoform in the Benguela.

Reference	$CHBr_3$ (ppt)	Month
Class and Ballschmiter (1988)	24.0	August
Chuck et al. (2005)	2.13 (1.13 – 3.88)	Feb / March & Sept / Oct
Carpenter et al. (2007a)	1 – 5	October / November
This study (2011)	14.4	October / November

4.5.3 Wind speed

The mixing ratios of bromoform showed no direct relation to the variability of wind speed measured at Cape Point. Bromoform mixing ratios were sorted into bins of incremental increase in wind speed, from all wind directions (Fig. 4.18). Mixing ratios decreased from a mean of 65 ppt to 8 ppt between 0 and 5 m s^{-1} wind speed. Thereafter the bromoform mixing ratios peaked at a mean of 30 ppt with increasing wind speed to 10 m s^{-1}. A decrease in measured mixing ratios occurred between wind speeds of 10 – 12 m s^{-1}. Above 12 m s^{-1}, bromoform mixing ratios decrease to approximately 20 ppt and

displayed no significant distribution thereafter (Fig. 4.18). The use of all wind directions results in the inclusion of anthropogenic sources, which might mask biogenic interactions of wind speeds and bromoform mixing ratios. A part from less variability, bromoform mixing ratios from the baseline wind direction exhibited a similar distribution of measurements and order of magnitude. This suggested that anthropogenic sources were not masking variability in the relationship between bromoform mixing ratios and wind speed at Cape Point.

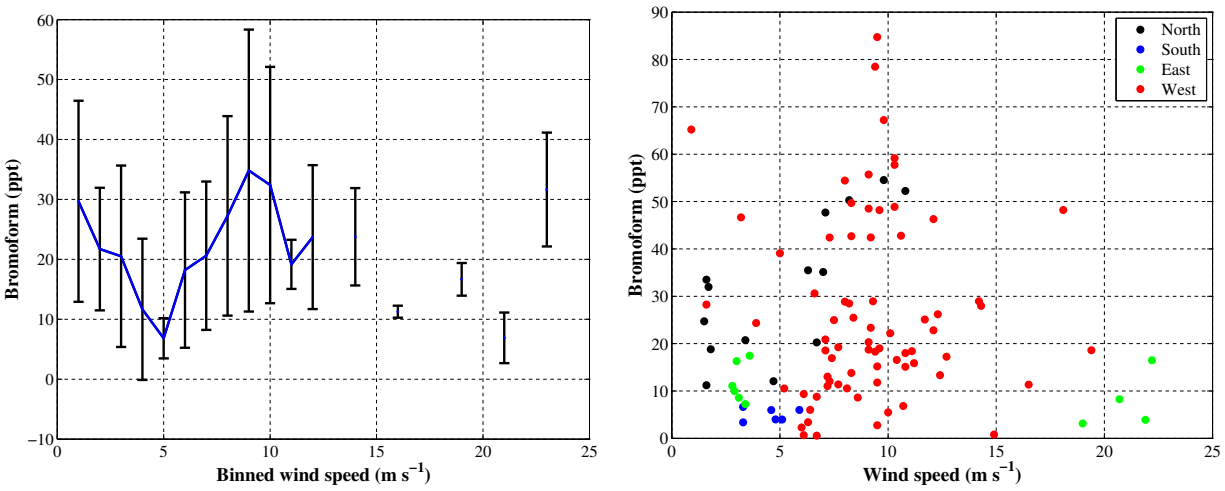

Figure 4.18: Bromoform mixing ratios: (a) binned by increases in wind speed. Thin black lines indicate standard deviation. (b) Bromoform mixing ratio as a function of wind speed form different wind directions.

The sea-air gas transfer rate is dependent on a number of physical and chemical processes (Sec. 1.3.4; Nightingale, 2009). These processes act at numerous spatial and temporal scales, resulting in challenges to the estimation of sea-air fluxes (Palmer, 2006). However, wind speed appears to capture the complexity of sea-air gas transfer in a single easily measured variable (Nightingale, 2009). One model of understanding of the sea-air flux suggests that three ocean surface regimes have been associated with varying wind speeds (Liss and Merlivat, 1986). Smooth surface conditions were found with wind speeds below 5 m s^{-1} and gave way to wave formation and a broken surface at 5 – 10 m s^{-1}. Above 10 m s^{-1}, a rough surface regime exists, associated with wave breaking and bubble formation. In conjunction with an understanding of these three surface regimes, wind speed measurement might also be used to separate coastal from open ocean sources in mixed air samples (Quack and Suess, 1999). It has been found that lower wind speeds (< 5 m s^{-1}) were associated with coastal sources, acting over a small fetch with little dilution. It was further suggested that increased wind speeds dilute the local atmosphere, decreasing mixing ratios and trace gas concentrations to those measured in the open ocean (Quack and Suess, 1999). A larger fetch and increased gas flux rate were observed at higher wind speeds. Different models of gas flux and atmospheric accumulation possibly dominated at varying speeds, resulting in the distribution of measurements observed at Cape Point (Fig. 4.18).

At extremely low wind speeds (< 2 m s^{-1}) the dilution of bromoform from the local atmosphere is virtually zero. The lack of bromoform dilution within the atmosphere would account for the elevated mixing ratios observed, despite the low gas flux rate at low wind speeds (Fig. 4.18). The local atmospheric dilution effect and gas flux rate would have increased concurrently with wind speeds above 2 m s^{-1}. The bromoform mixing ratio may have decreased due to the increasing dilution effect at wind seeds between 2 – 5 m s^{-1} (Fig. 4.18). Although the gas flux rate may have increased with the wind speed, the rate across the smooth ocean surface found at these wind speeds would not have been sufficient to sustain local atmospheric mixing ratios, resulting in the observed decrease in bromoform.

The formation of waves at wind speeds between 5 – 10 m s^{-1} would have promoted an increase in the gas flux rate. Waves increase the surface area through which gas exchange may occur. Based on the two film gas exchange model (Sec. 1.3.4), wave action might increase the mixing of the surface with bulk layers either side of the interface, stimulating greater gas flux rates (Liss and Merlivat, 1986; Nightingale, 2009). The increase in bromoform mixing ratios observed at Cape Point may have been supported by larger sea-air gas fluxes. While the local dilution effect would have been greater, the significance of this was offset by an increased gas flux in the local environment.

The significantly larger fetch over air masses at high wind speeds (10 – 15 m s^{-1}) would result in the decreasing bromoform mixing ratios observed (Fig. 4.18). The higher wind speeds may have produced a greater gas flux through wave action and breaking; however, this would have occurred over the open ocean. The open ocean has been reported as a significantly smaller source of bromoform than the coastal environment (Carpenter and Liss, 2000). The observed decrease in bromoform mixing ratio was thus considered due to an open ocean dominated source, rather than local coastal source. Increased dilution of bromoform a in larger volume of the atmosphere may have also reduced the bromoform mixing ratios observed.

The difficulty associated with making accurate measurements of gas flux rate at wind speeds in excess of 15 m s^{-1} has resulted in a poor understanding of the physical processes that affect the gas flux rate at these speeds (Nightingale, 2009). The measurements of bromoform, at Cape Point, displayed no significant relationship with wind speeds above 15 m s^{-1} (Fig. 4.18). This distribution of bromoform measurements may have resulted from varying physical processes, such as changes in wave dynamics and the introduction of air over an ever increasing fetch. The bromoform mixing ratios may have decreased as wind speed increased from 15 – 20 m s^{-1} as bubble enhanced transport abated while waves built to their peak heights. Above 20 m s^{-1}, wave breaking, which would create bubble enhancement and sea spray, may explain the rise in bromoform mixing ratios observed (Fig. 4.18). The lack of relationship relationship between bromoform mixing ratios and wind speed observed at Cape Point might be explained by variations in local dilution and wave breaking. The decrease in bromoform mixing ratio between 15 – 20 m s^{-1} may be due to the dilution of the local atmosphere. Included in the large fetch, increased wave breaking at the coast may release more surface bromoform, resulting in the increased mixing ratios observed at wind speeds above 20 m s^{-1} (Fig. 4.18).

The emission of bromoform from natural sources is neither uniform nor consistent. This makes the interpretation of results, especially from short-term studies such as this one, particularly difficult. Observations from fixed measuring stations such as Cape Point would allow for more in-depth analysis of recorded mixing ratios as the data can be filtered for particular conditions. Transient measurements such as from ship cruises may report highly different results for the same ocean region as they may miss or pass through a highly productive area. Better statistical results will be achieved with with longer datasets and the simplest way to achieve this is through long-term measurements at fixed observatories.

4.5.4 Diurnal cycle

An estimated diurnal cycle of bromoform variability was formulated from measurements on numerous days. Bromoform measurements from separate days were averaged in hourly bins and placed on a 24 hour time axis (Fig. 4.19). Morning (6 am – midday) bromoform mixing ratios increased from 12.7 ppt to a peak of 31.8 ppt by 11 am with a mean of 25.9 $\pm$ 6.10 ppt. Bromoform mixing ratios decreased throughout the afternoon (midday – 6 pm) to a minimum of 19.1 ppt with a mean of 23.0 $\pm$ 3.41 ppt by 6 pm. A second peak of 22.7 ppt was found to occur in the evening at approximately 9:30 pm. Despite this peak, mean bromoform mixing ratios (19.3 $\pm$ 2.45 ppt) were found to be generally lower in the evening than during the day (6 pm – 11 pm).

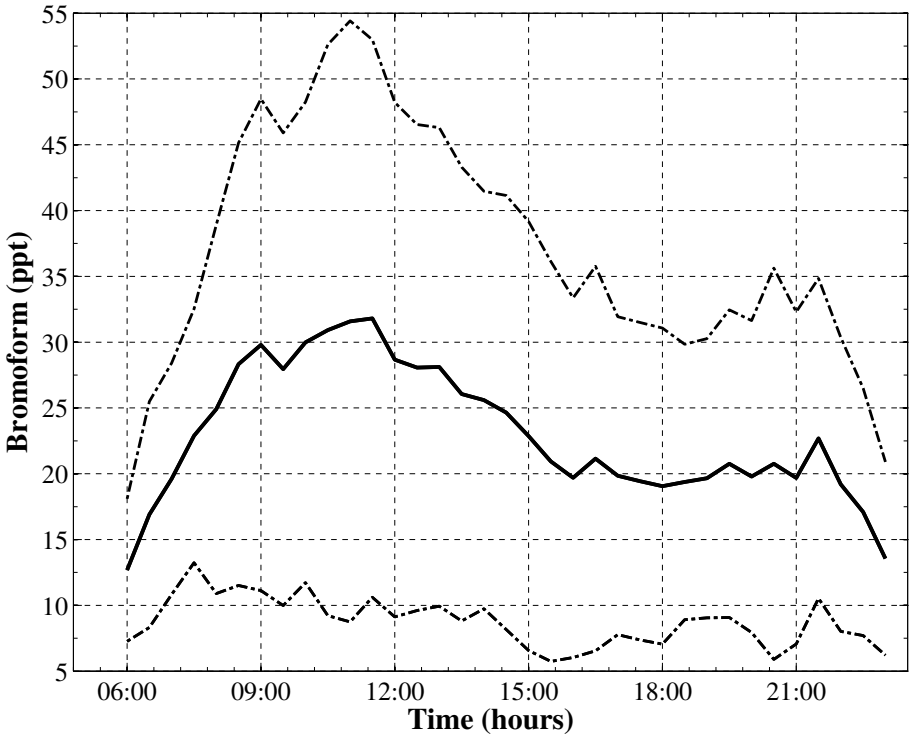

Figure 4.19: The mean diurnal pattern measured at Cape Point. Grey lines indicate 1 standard deviation.

The estimated diurnal pattern of bromoform mixing ratios observed at Cape Point were consistent with previously published daily patterns of variability (Ekdahl et al., 1998; Carpenter et al., 2000; Abrahamsson et al., 2004). Increases in light intensity have been reported to result in an amplification of bromoform

mixing ratios measured over rock pools and in laboratory studies (Ekdahl et al., 1998; Collén et al., 1994; Pedersén et al., 1996). It has been suggested that the amplification of bromoform mixing ratios was associated with increased photosynthetic rate, which peaks at the local solar zenith (Abrahamsson et al., 2004). It is suggested that the increased photosynthesis through the morning resulted in the rise in bromoform mixing ratios observed at Cape Point. The mixing ratios observed at Cape Point showed a main diurnal peak at 11 am, one hour earlier than previously (Ekdahl et al., 1998; Carpenter et al., 2000; Abrahamsson et al., 2004). This discrepancy may derive from the differences in sampling location, particularly elevation. Sampling sites at Mace Head and Gran Canaria were located at sea level, while the Cape Point GAW station is situated 230 m above sea level (Carpenter et al., 2000; Ekdahl et al., 1998; Brunke et al., 2004). The atmospheric lifetime of bromoform is estimate to be approximately 26 days (Hossaini et al., 2010). Given the high levels of solar radiation found at Cape Point, this atmospheric lifetime may shorter than previously published. The additional height, creating a longer path length from the ocean to measurement, may have resulted in the destruction term of bromoform becoming significant. It is, however, more probable that dilution of the sample occurred along this path from the ocean to sampling station. The destruction of bromoform by direct photolysis and reactions with ozone may increase in the afternoon under the intense shortwave radiation, suppressing the bromoform mixing ratio signal, despite increased production with photosynthesis. These reactions may become dominant after the local solar zenith, when the photosynthetic and production rates decrease (Fig. 4.19). The bromoform that was released might be impacted upon by changes in local photochemistry (Abrahamsson et al., 2004), decreasing local mixing ratios through the afternoon.

The peak observed in the evening (Fig. 4.19) is consistent with previously published reports from a rock pool in Gran Canaria and the Southern Ocean (Ekdahl et al., 1998; Abrahamsson et al., 2004). Previous work suggests that the release of bromoform in the dark may be a function of the respiration process (Carpenter et al., 2000; Ekdahl et al., 1998; Chapter 4.1.3). Remnant intracellular hydrogen peroxide (H_2O_2), a by-product of photosynthesis, results in the formation of bromoform through a haloperoxidase reaction (Collén et al., 1994). The high shortwave radiation levels experienced at Cape Point, twice those found at Mace Head, may lead to increased intracellular H_2O_2 concentrations, resulting in the peak of bromoform observed (Carpenter et al., 2000). The supply of remnant intracellular H_2O_2 may be limited, thus providing a mechanism for the minimal peak observed. As the intracellular H_2O_2 became depleted the production of bromoform would rapidly cease. A low wind speed would be sufficient to provide dilution of the local atmosphere, possibly causing the observed rapid decrease in bromoform mixing ratios at night. At night the photochemical degradation of bromoform may have been reduced to nearly zero, allowing for an accumulation of bromoform in the atmosphere. This decrease in photolysis rate and respiration production may have resulted in the observed evening peak. As the intracellular H_2O_2 was depleted, the respiration based production would have decreased, reducing the rate at which atmospheric bromoform was replaced and therefore lowering observed mixing ratios. At night, the photochemical degradation of bromoform would be reduced to virtually zero, allowing an accumulation of bromoform in the atmosphere.

The diurnal variability of the bromoform mixing ratios at Cape Point were contrasted against those of the meteorological and physical variables measured. Shortwave radiation, air temperature, particle counts and CO displayed the strongest positive relationship but relative humidity exhibited a strong negative relationship (Fig. 4.20a and b). The variability of CO measured at Cape Point may be associated with changes in wind direction coupled with anthropogenic inputs from Cape Town. The high shortwave radiation levels found at Cape Point might induce a large particle and bromoform response from macroalgae as an anti-oxidant pathway (Küpper et al., 2008; Palmer et al., 2005). There is a strong correlation between bromoform and particles ($r = 0.82$, $p < 0$) observed at Cape Point, suggesting that bromoform and iodinated halocarbons formed in response to ROS may rapidly form particles. This is particularly noticeable during the morning (Fig. 4.20) suggesting a photochemical production of bromoform and iodinated halocarbons that rapidly form particles, increasing the local particle counts.

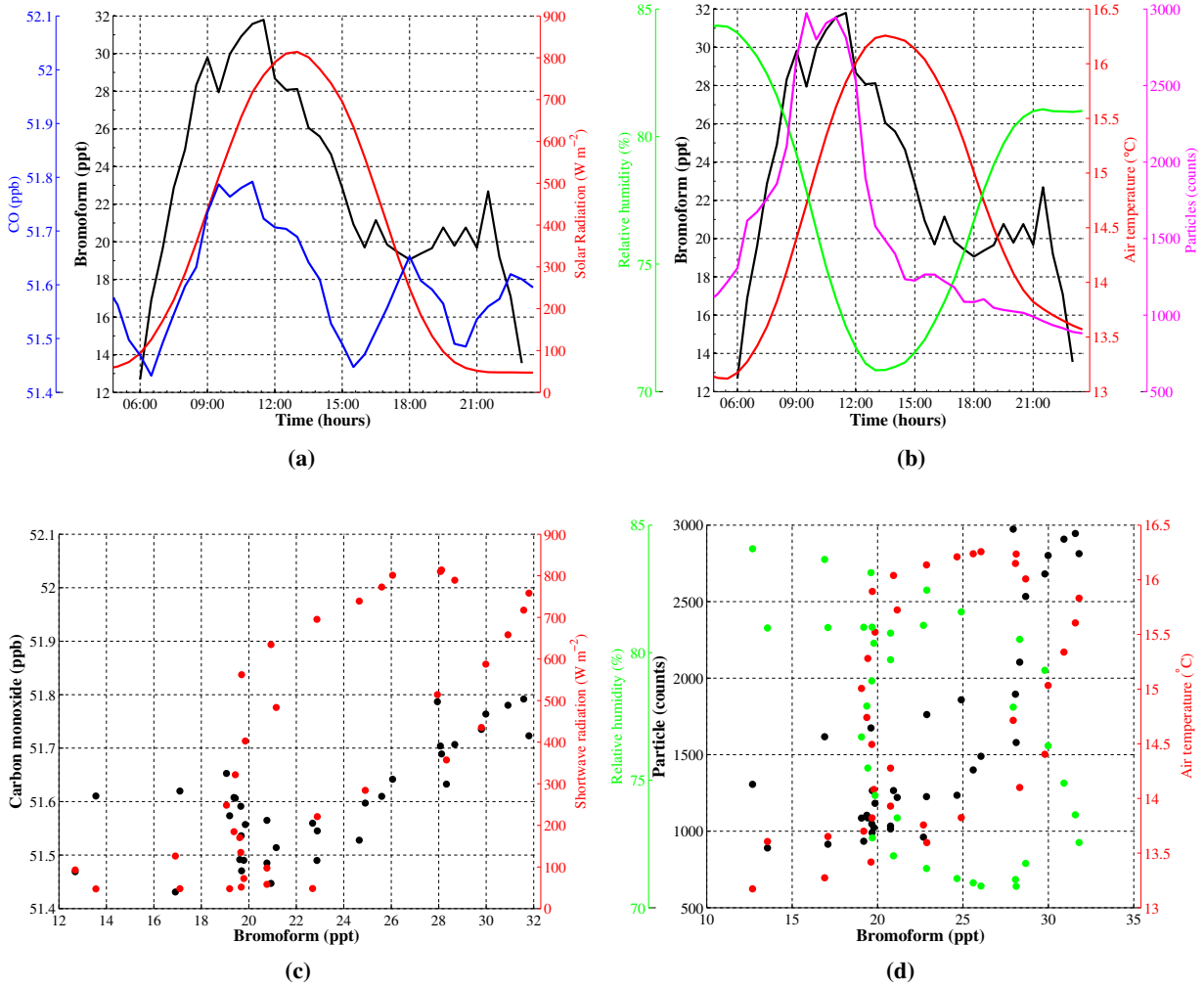

Figure 4.20: Mean diurnal cycles at Cape Point during bromoform experimental period: (a) bromoform, CO, and shortwave radiation, (b) bromoform, air temperature, RH and particles. Correlation plots of variables compared in mean diurnal cycles: (c) same variables as used in a, (d) same variables as compared in b.

4.5.5 Regression analysis

A regression model was developed in an attempt to better understand the patterns of variability in the bromoform mixing ratios observed at Cape Point. A multiple linear regression of the meteorological data against bromoform mixing ratios was performed. A number of significant correlations were expected between bromoform mixing ratios and physical variables such as tidal height, sunlight, ozone and MBL height (Fuhlbrügge et al., 2013; Palmer et al., 2005; Carpenter et al., 2000). Robust correlations were not observed and only a few weak relationships could be established. The strongest correlations found were for surface atmospheric pressure, RH and gaseous mercury ranging from r = -0.24 to r = -0.28 at $p < 0.05$ (Fig. 4.21). Harmonic terms were added to the linear regression constants of the meteorological variables measured at Cape Point. The addition of the harmonic terms was to account for possible diurnal processes affecting bromoform variability.

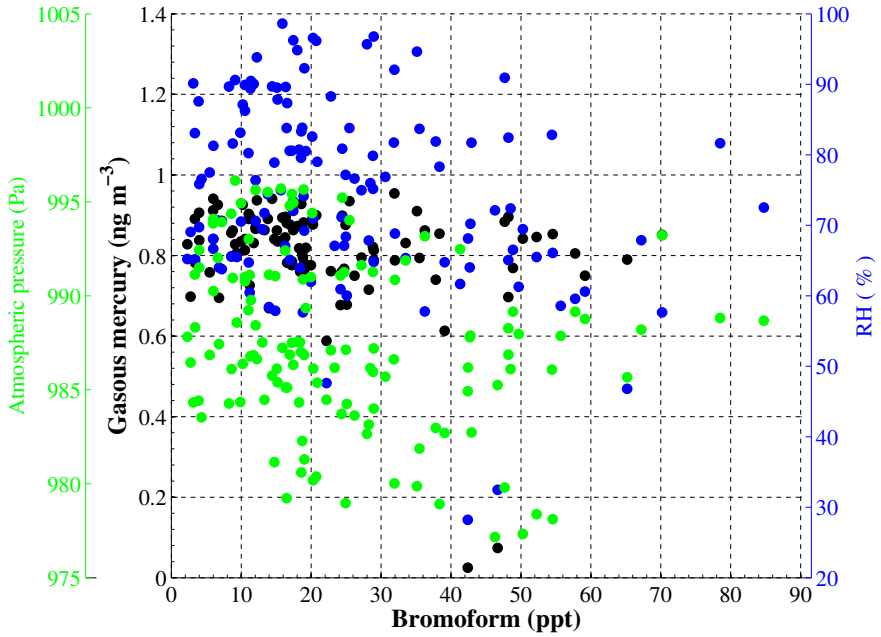

Figure 4.21: Chart displays the relationship between bromoform mixing ratio (x-axis) and RH, air pressure and gaseous mercury. Colours are associated to the axes. The chart highlights the strength of relationships between bromoform mixing ratio and selected meteorological data.

Time lags between bromoform and meteorological measurement were introduced to improve and refine regression outputs. Lags of between zero and five hours were tested, resulting in an improvement to correlations between bromoform and certain meteorological variables (Table 4.5). The lead and lags are probably important to the model in that they allow for the model to adjust, accounting for time dependent biological reactions. The correlation of variables that occur before the bromoform measurement is made are likely to be a precursor or initiator variable, while those occurring after, are considered to be reactions with bromoform and therefore sinks. An increase in bromoform is typically noted with increasing incident sunlight, however it is not an instantaneous reaction. The physical parameters act on the macroalgae at different time scales and sometimes may have either additive or counteracting effects on bromoform

mixing ratios. Variability within the modelled bromoform was achieved by parameterising changes in meteorological and physical processes known to affect bromoform mixing ratios. The regression coefficients for gaseous mercury, ozone, current pressure, relative humidity, tidal height, shortwave radiation and air temperature were used. The lag between bromoform and the measurements of the variables might identify the time required for production and destruction reactions of bromoform within the atmosphere to occur. The aim of the model was to describe the mechanisms of bromoform variability

Table 4.5: Important covariates of bromoform incorporated into the regression model.

Variable	**Zero lag***	**Lagged corr***	**Lag time****
Gaseous mercury	-0.42	0.02	-0.29
Shortwave radiation	0.74	0.00	0.64
Radon	0.35	0.03	-0.71
Air temperature	0.52	0.00	0.60
Pressure	0.41	0.01	0.53
Particles	0.82	0.00	0.44
RH	-0.52	0.00	-0.50
CO	0.65	0.00	0.63
Ozone		0.42	
MBL		0.63	

* $p < 0.05$ for all data
** Positive values occur after bromoform measurement and negative values occur before, i.e. negative values bromoform is a precursor while positive values are reactions

at Cape Point. The model is built up of regression constants multiplied by harmonic terms. Successive harmonic terms are then added together and stepped through at half hour intervals. The model follows the form (Chatfield, 2003) :

$$y_i = \beta_0 + S_i * \beta_i + C_i * \beta_{i+1} + ei \tag{4.6}$$

where: $S_i = \sin(i * (2 * \pi * (t/48)))$
$C_i = \cos(i * (2 * \pi * (t/48)))$
β is the linear regression constant
i is the number of the harmonic
j is the regression term
ei is the error term.

The time was taken as the real time of measurements used in the regression. It was assumed that a 24 hour period existed within the data. Since data points for every 30 min were available, it was necessary to use a time frequency of 48 cycles per day, giving a daily frequency of 24 hours. An increasing number of harmonic terms can be added to the model to allow for a more complicated diurnal pattern.

The use of eight harmonic terms (gaseous mercury, shortwave radiation, air temperature, radon, pressure, RH, ozone and tidal height), coupled with the regression constants of meteorological variables accounted for ∼29 % of the variance observed in the bromoform measurements at Cape Point (Fig. 4.22). The harmonic terms in the model produced three peaks that captured the extreme events observed at Cape Point (Fig. 4.22). The model appears to be unresponsive to smaller changes, failing to capture variance in mixing ratios below 30 ppt. The extreme events may have upwardly biased the results and lowered the sensitivity of response within the model. It was assumed that the timed response of meteorological variables was identical. Diurnal cycle differences between meteorological variables may partially account for the low variability of the reported bromoform measurements. While the inclusion of a varying time length of harmonic terms may have improved the overall model output, this was beyond the current available resources to achieve. The predicted timing of peaks within the model was satisfactory, being within 30 minutes of the measured peak, however resolution of troughs at low mixing ratios was poor at 2 – 4 hours either side of measurements. The lack of rapid response at low bromoform mixing ratios results in the model missing an important element of variability. The distribution of the residuals, i.e. subtraction of calculated model output from measurements, was found to be Gaussian, suggesting that the model reasonably approximates the variability and is not being biased by one of the terms.

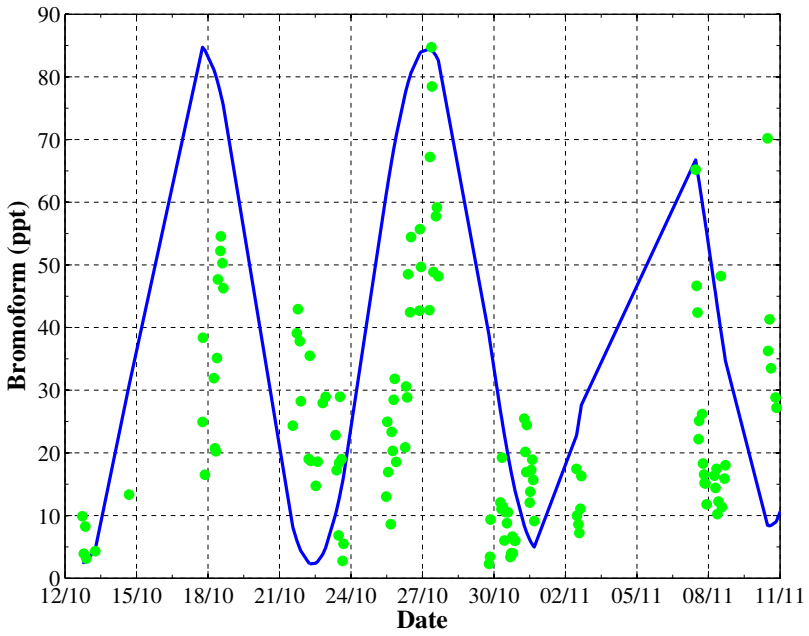

Figure 4.22: Output from the harmonic model (blue) overlaid with bromoform measurements (green).

The harmonic model failed to describe the full range and variability of the measurements made at Cape Point. This failure of the model may be the result of three shortcomings: lack of measurements, inadequate data or the quasi-discrete nature of the sampling. The meteorological variables used in the regression model might not have included the pivotal variable or all the variables of significance. This suggests that a descriptive variable might be missing. A missing descriptor variable might be the key to improving the output of the model. There may not be enough information in the bromoform mixing ratio measurements

taken to fully describe the cyclical pattern. One month of data does not describe a full seasonal cycle making a diagnostic predictive model difficult. A more extensive bromoform mixing ratio dataset might show that auto-correlation found in the measurements is lower, to the point of non-existence, indicating that there is no cyclical pattern in the measurements of bromoform. Furthermore, this season may have been atypical. The time interval between samples was irregular, which made most statistical analyses very difficult. A longer time series, giving the seasonal cycle, would result in a better understanding of the variability of bromoform mixing ratios. This would either negate the need for a harmonic model or highlight the ability of the model to predict local mixing ratios.

4.5.6 Case study: back trajectory and parcel transit height

Seibert et al. (2000) and Seidel et al. (2010) suggested that the MBL may act as a concentrating mechanism for surface released gases or as a barrier to mixing with upper layers in the atmosphere. Although MBL height and bromoform mixing ratios at Cape Point exhibited no direct relationship, an indirect mechanism may exist. The MBL height might have acted as barrier to mixing of surface released gases with trajectories that passed above the MBL and may account for a large portion of the observed variability in bromoform mixing ratios. Analysis of back trajectories indicated that the air parcels exhibited one of three behaviours: they remained below the MBL, remained above the MBL, or traversed the MBL. Those that remained below the MBL height should have the highest bromoform mixing ratios, depending on the sources traversed, as the parcel would have been allowed the largest time to entrain bromoform. Air parcels that remained above the MBL would have the lowest recorded bromoform mixing ratios as the parcel would have been separated from all bromoform sources for the duration of the transit. Traversing across the MBL, air parcels would be expected to contain moderate bromoform mixing ratios that would be entrained while the parcel was below the MBL. Thus, the vertical position of the parcel transit might account for a portion of the bromoform variability observed. The impact on bromoform mixing ratio at Cape Point based on parcel transit height in relation to the MBL height was explored through the examination of four mixed source (^{222}Rn $\approx$ 1000 mBq m^{-3}) air samples (Fig. 4.23). Two high and two low MBL and bromoform mixing ratio days were selected for comparison.

On certain days air parcels appeared to have arrived at Cape Point from a similar north to northwesterly direction (Fig. 4.23b, c and d), however the entrained bromoform mixing ratios varied. On 13 and 18 October and 7 November (Fig. 4.23b, c and d) air parcels passed over the southern Benguela and Cape Town before arriving at Cape Point. Since the path travelled was similar, the source loading should have been similar. The difference in MBL height on two of the 18 October and 7 November (Fig. 4.23c and d; 91 and 668 m, respectively), may explain the difference in bromoform mixing ratios observed (Table 4.6). The transit height of the air parcels on both days was elevated at between 500 – 3000 m. The low MBL height on 13 October 2011 (Fig. 4.23b) resulted in a small local entrainment of bromoform. The air parcel remained above the marine MBL for the duration of the transit, dropping below just before the air parcel arrived at Cape Point. The short duration below the MBL allowed a small entrainment of bromoform, thought to be from the local macroalgae beds. The higher MBL on 7 November 2011 (Fig. 4.23d) resulted

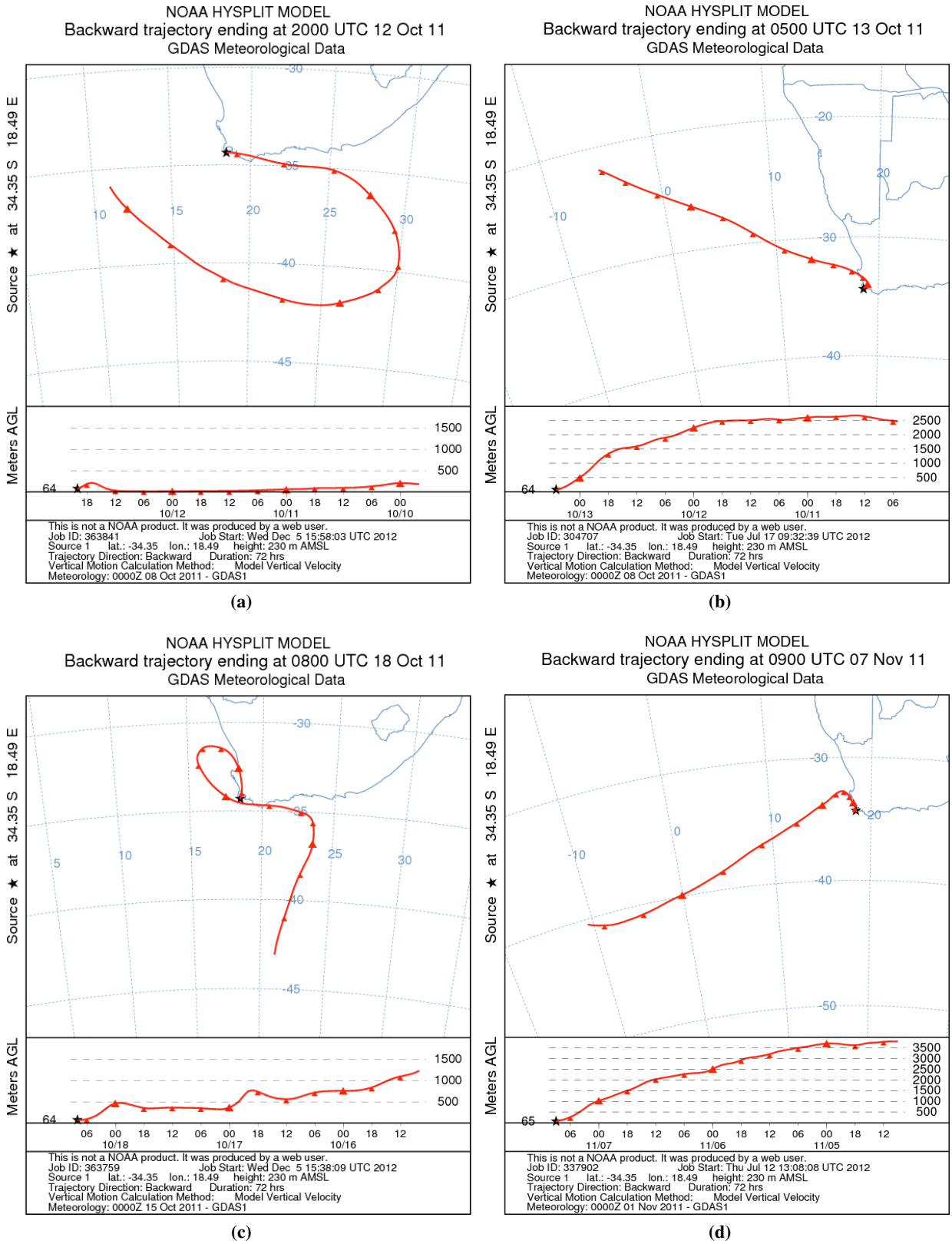

Figure 4.23: HYSPLIT back trajectories of mixed air masses. (a) False Bay, minimal macroalgae at low level. (b) Benguela and Cape Town at high level. (c) Benguela and Cape Town low level. (d) Benguela and coastal impact, maybe Koeberg.

in the parcel passing below the top of the MBL approximately 8 hours prior to being analysed. This transit below the top of the MBL resulted in the entrainment of bromoform along the west coast and in the vicinity of Cape Point. The low wind speed on 7 November 2011 (Fig. 4.23d) may also have induced a stronger coastal influence, resulting in the higher recorded bromoform mixing ratios. The 18 October 2011back trajectory (Fig. 4.23c) highlights a case where the air parcel remained below the top of the MBL, exhibiting large bromoform mixing ratios (Table 4.6). The bromoform sources and the air parcel trajectory also impact on the entrained mixing ratios. The 12 October trajectory (Fig. 4.23a) showed low bromoform mixing ratios despite remaining below the MBL for the duration of the trajectory. It was thought that the parcel did not pass over any of the few sources to the east of Cape Point.

Table 4.6: Arrival direction and height as drivers of bromoform mixing ratio variability. Bromoform mixing ratio in ppt, ^{222}Rn in (mBq m^{-3}) and wind speed in (m s^{-1}).

Fig no.	Date	$CHBr_3$	^{222}Rn	Wind Speed	Direction (°)	MBL (m)	Arrival Height (m)
4.23a	12 Oct 11	3.13	1091	19.0	95	91	< 500
4.23b	13 Oct 11	4.31	1212	4.90	334	91	500 – 2000
4.23c	18 Oct 11	47.7	1038	7.10	29	1963	∼500
4.23d	7 Nov 11	65.2	1138	0.90	306	688	500 – 3500

The transit height of an air parcel in relation to the MBL height seems to provide a mechanism to describe the fluctuations of bromoform mixing ratios observed at Cape Point by determining the amount of possible entrainment. Samples passing over similar source regions, (Fig. 4.23b and d) at different heights, resulted in a variation of observed bromoform mixing ratios. The sources, if any, found below the trajectory seem to play an important role in determining the bromoform mixing ratios observed at Cape Point. Air sample back trajectories below the MBL were probably resulted in the elevated bromoform mixing ratios through increased entrainment when the air parcel passed over strong sources (Fig. 4.23a and c). Surface released gases are mixed through the atmosphere to the height of the MBL, therefore the top of the MBL may act as a barrier preventing mixing with the atmosphere above (Seibert et al., 2000). Air parcels passing through the atmosphere above the top of the MBL would be separated from the surface by the top of the MBL and thus contain lower bromoform mixing ratios. While the height of the top of the MBL might not act as a pre-concentrator at Cape Point, the impact through the top acting as a barrier may account for some of the variability observed in air samples arriving from similar directions. This kind of analysis helps to explain the lack of clear correlations within the data presented here. This is a dynamic region and air parcels may be influenced by a number of processes, even when arriving from similar directions.

4.5.7 Hypothesis testing

The mechanisms of variability described in the literature should be applicable at Cape Point as the measurements of bromoform mixing ratios made at Cape Point were consistent with global measurements

(Table 4.1). To understand the variability in bromoform mixing ratios observed at Cape Point and to determine the mechanisms that may drive the fluctuations observed, there was a testing of hypotheses (Table 4.7). The hypotheses developed, based on mechanisms of variability reported in the literature, explore relationships within the data. It is possible that there are a number of thresholds of variables relating to each other, interacting on different time scales. Previous studies have shown a single physical variable dominating or describing a majority of the variability found in measurements (e.g., Carpenter et al., 2000; Fuhlbrügge et al., 2013; Nightingale et al., 1995). Precursor processes were explored within the data through the introduction of time lags. The quasi-discrete nature of bromoform mixing ratio sampling at Cape Point might be a limiting factor in identifying elements driving the observed variability. While no clear indication of the processes involved in driving the bromoform mixing ratio variability observed at Cape Point, the hypotheses did suggest some possible mechanisms. The combination of multiple variables was devised to illuminate processes resulting in the fluctuations of bromoform mixing ratios. Hypotheses that included two concurrent variables *viz* when the tide is low and the shortwave radiation is high, or when the tide is low and ozone mixing ratios are high, were explored. The limited dataset of bromoform mixing ratios at Cape Point resulted in a paucity of data points for a significant correlation of double sorted variables.

Table 4.7: Hypotheses of factors causing variability in bromoform mixing ratios at Cape Point during the experimental period.

No.	Hypothesis	Theory	Result	Conclusion
1	The Benguela is a larger source than the Southern Ocean (low ^{222}Rn NW vs. SE winds)	Stronger and more constrained upwelling found in the Benguela may make it a more important source.	Mean [$CHBr_3$] were 19.1 $\pm$ 11.8 (Benguela) and 19.7 $\pm$ 24.0 ppt (Southern Ocean)	Source strengths from the Benguela and Southern Ocean might be approximately equal. However the Southern Ocean displays a greater degree of variability.
2	As air temperature increases $CHBr_3$ increases	Increased air temperature promotes photosynthetic response in plants[1] and affects gas flux rates[2]	A weak positive correlation between $CHBr_3$ and air temperature could be found.	Increased air temperature may promote the formation of $CHBr_3$.
3	As shortwave radiation increases so [O_3] increases	Tropospheric ozone can be produced by photochemical pathway (equation 4.3).	Shortwave radiation is not a predictor of O_3 at Cape Point. No relationship was established.	Ozone at Cape Point was dominated by stratospheric draw down rather than local production.

Table 4.7 Continued from previous page

No.	Hypothesis	Theory	Result	Conclusion
4	Increasing shortwave radiation results in increased [$CHBr_3$] through increased photosynthesis	Shortwave radiation incites production of bromoform through photosynthesis (Sec. 1.2.5)	No direct relationship could be found. [$CHBr_3$] produced in the dark range from zero to 58 ppt. A 5 hr bromoform lag produces a marginally negative relationship.	The photosynthetic production of bromoform was likely not instantaneous nor dominant in this region. The production of $CHBr_3$ in the dark should be further investigated.
5	MBL height acts as a pre-concentrator	Lower MBL hight suggests smaller atmosphere in which to mix bromoform	A non-significant positive relationship between MBL and $CHBr_3$ was found (r = 0.13 p = 0.17) at Cape Point	This suggests that at Cape Point the MBL might be a slight pre-concentrator of $CHBr_3$
6	Increasing atmospheric pressure will result in increased [$CHBr_3$]	Increasing atmospheric pressure implies subsiding air consequently trapping surface released gases, possibly lowering the marine boundary layer.	A weak negative relationship was found to exist between [$CHBr_3$] and atmospheric pressure.	The increasing pressure may lower the MBL, however low pressure at Cape Point implies NWly wind directions. This suggests the Benguela or Cape Town city as the source region.
7	The [O_3] should vary as either a precursor or as a function of atmospheric [$CHBr_3$]	O_3 stimulates biogenic production of $CHBr_3$[3]. Catalytic destruction of O_3 as a result of $CHBr_3$ is also known to occur[4, 5, 6]	$CHBr_3$ and O_3 correlate at r = 0.04 p = 0.20. Highest $CHBr_3$ (67.2 – 84.7 ppt) occur at 27.8 – 28.6 ppb O_3. $CHBr_3$ and O_3 consistently exhibit positive relationship, even when O_3 lags $CHBr_3$.	O_3 was not leading stress, nor being destroyed. Possibly a process affecting both weakly or a strong process causing dilution so we don't observe these on the spatial and temporal scales of this experiment.

Table 4.7 Continued from previous page

No.	Hypothesis	Theory	Result	Conclusion
8	Low tides produce more $CHBr_3$ than high tides	Low tides expose the greatest extent of the macroalgae bed to the atmosphere.	Mean [$CHBr_3$] were found to be larger at low tide. Tidal ranges < 1 m have a maximum [$CHBr_3$] of $\pm$ 30 ppt.	Low tides at Cape Point appeared to result in higher [$CHBr_3$] than high tides. Larger tidal ranges appear to be important.
9	Particle and $CHBr_3$ concentrations will increase with oxidative stress	Kelp have been shown to release particles[7] and bromoform[8] as an anti-oxidative mechanism	Particles count and ($CHBr_3$) show a weak positive relationship (r = 0.32) up to counts of 2000, thereafter the relationship becomes negative. Higher particle counts tend to result in higher [$CHBr_3$], with particles leading by $\sim$2 hrs.	The formation of reactive oxygen species (ROS) may increase [$CHBr_3$] and halocarbons and consequently result in particle formation.
10	Increasing [$CHBr_3$] will decrease atmospheric gaseous mercury	Halocarbons have been implicated in the destruction of atmospheric mercury[9].	$CHBr_3$ leads gaseous mercury by 5 hours on all data r = -0.48. BWD immediate correlation r = -0.42.	Increasing [$CHBr_3$] might therefore contribute to decreases in mercury. The decay products of bromoform might destroy gaseous mercury or bromoform may trigger an unidentified destruction pathway.

References: 1. Monson et al., 1982; 2. Nightingale, 2009; 3. Palmer, 2006; 4. Carpenter and Liss, 2000; 5. Cota and Sturges, 1997; 6. Read et al., 2008; 7. Küpper et al., 2008; 8. Palmer et al., 2005; 9. Sorensen, 2011.

The upwelling driven phytoplankton blooms (> 100 mg m^3 Chl-*a*) found in the Benguela upwelling system (Fawcett et al., 2007) are more productive and more constrained than in the Southern Ocean. The Benguela is also very close to Cape Point, suggesting that atmospheric attenuation of bromoform

would be lower than samples from the Southern Ocean. Hypothesis 1 (Table 4.7) suggests that due to the proximity and limited destruction, the Benguela presents a larger source of bromoform to the atmosphere at Cape Point than the Southern Ocean. The mean bromoform mixing ratios recorded from the two regions (Fig. 4.17) were shown to be statistically similar at the 95 % confidence level. The greater variability displayed in the measurements from the Southern Ocean may stem from the highly dynamic conditions experienced in this region. This suggests that the Benguela may be a more dominant source of bromoform to Cape Point over time. The two regions might alternate in dominance with changes in wind direction associated with season (Fig. 4.17). It is suggested that this would result in elevated bromoform mixing ratios when Cape Point was influenced by both sources in quick succession.

The photosynthetic processes in plants have been reported as being stimulated and promoted through increases in air temperature (Monson et al., 1982; Robarts and Zohary, 1987; Abrahamsson et al., 2003). The rate of photosynthesis has been shown to increase with temperature to a maximum at approximately 25 °C (Monson et al., 1982). It has been suggested that algal species may produce halocarbons in varying rates proportional to temperature (Abrahamsson et al., 2003). This suggests that the photosynthetic rate, and consequently bromoform production, should be high (Fig. 4.8; hypothesis 2 Table 4.7). A weak positive relationship between air temperature and bromoform mixing ratios was found at Cape Point. This suggests that air temperature plays a small, non-dominant role in determining the variability of bromoform in the atmosphere at Cape Point. Influencing the photosynthetic rate in plants with higher temperatures may provide a large source during austral summer.

Lower air temperatures, resulting in condensation, have been suggested to produce a decrease in the gas flux rate of up to 30 %. Increased stratification due to cooler temperatures, suppressed mixing between the surface and bulk layers, decreasing the gas flux rate. Higher air temperatures produce a skin surface cooling of up to 0.3 °C, which results in a 4 % decrease in gas flux rate (Nightingale, 2009). Air temperatures recorded at Cape Point were not cool enough to result in condensation (Fig. 4.8). The gas flux rate would therefore not have been suppressed via this mechanism, suggesting elevated bromoform mixing ratios. The weak relationship between bromoform mixing ratio and air temperature established at Cape Point suggests that gas flux variability model might explain a portion of the variability observed. Gas flux rates might have been marginally suppressed at cooler temperatures, masking a complete relationship or other processes influencing the gas flux rate or bromoform mixing ratio variability.

Photosynthesis has been shown to result in the production of bromoform (Collén et al., 1994; Sec. 1.2.5). It is therefore asserted in hypothesis 4 (Table 4.7) that bromoform mixing ratios should increase with shortwave radiation. The high levels of shortwave radiation found at Cape Point (Sec. 4.4.2) suggest that photosynthetic processes should be comparably strong, which should produce elevated bromoform mixing ratios from local macroalgal sources. The variability in bromoform mixing ratios was not found to be linked directly with shortwave radiation. This might be due to an instantaneous production of bromoform from photosynthetic processes. Through the introduction of time lags, allowing for reactions, did not achieve an improvement in association between bromoform and shortwave radiation. It is possible that in

this region photosynthesis is not a dominant oxidative stress in the macroalgae, thus limiting production through this mechanism. The production of bromoform in the dark via respiration (Sec. 1.2.5) might mask the diurnal production of bromoform from photosynthetic processes.

The height of the MBL has been suggested as a mechanism for natural pre-concentration of surface released gases (Seibert et al., 2000; Seidel et al., 2010; Fuhlbrügge et al., 2013). It is suggested that lower MBL heights will result in elevated bromoform mixing ratios by means of trapping the surface released gases (Fuhlbrügge et al., 2013; hypothesis 5, Table 4.7). The MBL height *per se* does not seem to affect the variability of bromoform mixing ratios at Cape Point. This lack of influence of the MBL on bromoform mixing ratios might arise from the atmospheric profile measurements being made at Cape Town International airport and not at Cape Point. The inland setting of the airport and distance from Cape Point might make the airport measurements a poor proxy for variations in MBL height at Cape Point (Jury, 1984). The bromoform mixing ratios and calculated MBL height at Cape Point exhibited a weakly positive relationship, which is counter to the finding of Fuhlbrügge et al. (2013). The discrepancy in findings might be explained by the different techniques used to estimate MBL height. A difference in the sampling location might lead to different synoptic conditions driving the mixing ratios. While the Mauritanian upwelling system may also include samples influenced by the open ocean, it is predominantly a shelf upwelling region, albeit wide. Cape Point is influenced by local coastal, upwelling and open ocean sources. Modelling of MBL height at Cape Point might better highlight the local interaction between the MBL height and the bromoform mixing ratios.

In hypothesis 6 (Table 4.7) it is suggested that surface atmospheric pressure at Cape Point might influence bromoform mixing ratios in a manner similar to the MBL. Higher surface pressures may act as a concentrator of surface released bromoform through the subsidence of air. The weak negative correlation observed between bromoform and atmospheric pressure at Cape Point suggests that the subsidence, pre-concentration theory does not apply here. Strong southeasterly winds at Cape Point (Fig. 4.7) associated with ridging anticyclones may have diluted the bromoform in the MBL, thereby lowering the mixing ratios. While westerly to northwesterly winds, associated with low pressure systems, were fewer and possibly drew in air from wider sources resulting in higher observed bromoform mixing ratios (Fig. 4.7). The lower wind speeds associated with W-NWly winds may have resulted in a dominance of coastal sources and therefore, higher bromoform mixing ratios (Sec. 4.5.3). Atmospheric pressure, therefore, did not act as a pre-concentrator, however it may be an indicator of wind direction and therefore source strength.

Ozone in the lower troposphere has been reported as an oxidative stress in macroalgae (Palmer et al., 2005; Palmer, 2006) resulting in the production of bromoform, which has been reported to catalytically destroy ozone (Carpenter and Liss, 2000). The variability of atmospheric bromoform may be described by the presence of ozone through either a production or destruction process (hypothesis 7, Table 4.7). Hypothesis 3 (Table 4.7) contends that ozone mixing ratios should increase on a diurnal scale under the influence of shortwave radiation. Tropospheric ozone having two sources: local photochemical production

and vertical transport from the stratosphere (Jacob, 1999; Kim et al., 2013). During the bromoform sampling period it was found that ozone and shortwave radiation at Cape Point shared a weak relationship ($r = 0.24$, $p = 0$). No simple relationship between bromoform and ozone at Cape Point could be established, regardless of lead or lag times. Ozone measured at Cape Point is dominantly sourced from the vertical transport from the stratosphere rather than local photochemical production (E.-G. Brunke, SAWS, pers. comm. 2012). This provides a mechanism of stability observed in the ozone record (Fig. 4.14). The consistent ozone mixing ratios found at Cape Point might act with other processes such as reactions with OH or auto-catalytic destruction under the strong sunlight found at Cape Point. Thus removing O_3 from the local atmosphere and resulting in the episodic high bromoform mixing ratios observed. The interaction between ozone and other, unidentified processes, may explain the lack of strong relationship to bromoform observed.

A greater proportion of macroalgae is exposed to the atmosphere at low tide. Hypothesis 8 (Table 4.7) suggests that the greater atmospheric exposure of macroalgae at low tides results in increased production of bromoform (Palmer, 2006). The mean bromoform mixing ratios at low tides (27.2 ppt) were higher than those at high tide (23.5 ppt). Applying a t-test to the data indicates that the difference in mixing ratio between the tidal heights was not significant. Higher bromoform mixing ratios were found to occur concurrently with greater tidal ranges. Such conditions may result in increased exposure of the macroalgae to the atmosphere at low tide, which may trigger an elevated production response. The time of low tide occurrence may play an important, but not independently sufficient, role in the variability of bromoform mixing ratios at Cape Point. The highest bromoform mixing ratios observed at Cape Point occurred during spring tides. The exposure of the macroalgae beds at mid-morning (Fig. 4.13) may have increased bromoform production through photosynthesis and anti-oxidant pathways from exposure to the atmosphere. This exposure may account for the elevated bromoform mixing ratios on these days compared to neap tide days.

The variability of bromoform mixing ratios was not fully explained by the tides and the signal may have been suppressed through a combination of processes. The elevated position of the GAW station (230 m a.s.l), from which measurements were made, may result in an increase in the photochemical loss term, suppressing a tidal signal. The tidal range found at Cape Point was approximately half that reported for Mace Head, Ireland (Carpenter et al., 1999). Despite the smaller tidal range found at Cape Point (< 2 m), bromoform mixing ratios were similar to reported values (Table 4.1). This suggests that the tides might play a minor role in the variability of bromoform at Cape Point, which may be influenced by remote sources. The dominant species of *Ecklonia* and *Laminaria* found around Cape Point have large floats, ensuring that their fronds are always in the upper layers near the surface, possibly reducing the effect of tides on their exposure and thereby suppressing a tidal signal. The consistent exposure to the atmosphere may account for the elevated bromoform mixing ratios observed during spring tides and low wind speeds.

Oxidative stresses such as sunlight, ozone and exogenous hydrogen peroxide have been reported to elicit the production of halocarbons from macroalgae species (Palmer et al., 2005; Küpper et al., 2008). Particles

are formed as a by-product of the release of iodinated anti-oxidants (Küpper et al., 2008). Following hypothesis 9 (Table 4.7) it was found that the measured particle counts exhibited a moderated correlation with shortwave radiation (r = 0.24, p <0) and a weak negative correlation with ozone (r = -0.15, p = 0.04). The limited particle measurements made during the bromoform experimental period may mask stronger relationships with oxidative stresses at Cape Point. The stronger relationship found between particles and bromoform (r = 0.32, for particle counts up to 2000) suggests a concomitant driving mechanism. Above counts of 2000, the anti-oxidant processes of particles may limit the production of ROS from macroalgae and consequently retard the formation of bromoform.

Atmospheric gaseous mercury at Cape Point is known to become periodically depleted and halogens have been suggested as a possible cause of the depletion (Brunke et al., 2010; Sorensen, 2011). It has been suggested that atomic bromine may be the dominant oxidant of gaseous mercury. In the polar regions the gaseous mercury depletion events are reported to occur concurrently with an ozone depletion event (Sorensen, 2011). The mercury depletion events are, however, dominated by an alternate as yet unidentified chemical pathway. Concurrent ozone and mercury depletion events have not been recorded at Cape Point (Brunke et al., 2010). This unidentified chemical process resulting in mercury depletion may be initiated by local halide chemistry, including bromoform (E.-G. Brunke, SAWS, pers. comm. 2014). It is hypothesised that bromoform (not previously measured) in the atmosphere may initiate the episodic mercury depletion events observed at Cape Point as described in hypothesis 10 (Table 4.7). Bromoform mixing ratios at Cape Point exhibit a medium strength of association to gaseous mercury. A lag of 5 hours between measurements bromoform and gaseous mercury at Cape Point results in the strongest relationship. This suggests that a destruction process of gaseous mercury might be triggered by the presence of bromoform. While one mercury depletion event was recorded during the bromoform sampling period (7 November 2011), the full mechanisms were not explained from this study. Depletion events did not occur on every occasion bromoform was present, therefore bromoform might be an important but not independently sufficient cause of the mercury depletion.

4.6 Conclusions

The measurements of bromoform mixing ratios taken at Cape Point, presented here, represents the first extended record taken in southern Africa. The GAW station operated by the SAWS at Cape Point is an important location in these types of study, receiving air masses from numerous local and regional sources. The dominant wind direction at the station being from the Southern Ocean provides an ideal site for the sampling of background mixing ratios of trace gases. The bulk of bromoform measurements made at Cape Point appear to be sourced from the local surrounding macroalgae beds and display a maximum of approximately 30 ppt, consistent with recently published coastal locations (Table 4.1). An episodic, simultaneous influence of the diverse sources of bromoform in the atmosphere surrounding Cape Point may result in the few extreme events of bromoform mixing ratios of the order of 60 – 80 ppt that were recorded. Some key variables affecting bromoform mixing ratios are considered below.

The north-westerly (NW) and south-easterly (SE) wind directions that dominated during this period were consistent with the wind directions expected at Cape Point (Tyson and Preston-Whyte, 2000). This combination of air masses allows the analysis of open-ocean, coastal and anthropogenically contaminated air masses from a single location. These two dominant wind directions brought bromoform from distinctly different sources; local macroalgae beds and the Benguela in the NW and Southern Ocean from the SE. The different sources influenced the variability of the bromoform mixing ratios. The macroalgae beds surrounding Cape Point appear to have been the dominant source of bromoform to the marine atmosphere. While the mean mixing ratios contributed by the Benguela and the Southern Ocean were comparable, the increased number of NW wind days suggests that the Benguela upwelling system and Koeberg coastal peer plant contributed more bromoform to the atmosphere during this study. The anthropogenic influence of bromoform from the NW, on air masses at Cape Point was less than that of biogenic origin, however, it could still pose a significant impact on long-term studies.

Bromoform mixing ratios at Cape Point responded to changes in wind speed through a number of processes. From the hypothesised dynamics suggested in previous studies, the two most likely dominant processes are: changes in surface state causing varying mixing between surface and bulk layers, and variations in coastal and open ocean sources via diluting effect of the local atmosphere (Liss and Merlivat, 1986; Quack and Suess, 1999). Low wind speeds were dominated by an accumulation of bromoform in the air despite low mixing ratios through a lack of dilution, resulting in elevated mixing ratios. A decrease in bromoform mixing ratios occurred as wind speed increased through dilution of the local atmosphere. Gas flux rates were not thought to be sufficient to support the previously observed bromoform mixing ratios. Rough surface conditions resulting in strong mixing of the surface layers and the formation of bubbles produced no significant distribution of bromoform measurements with wind speed. It is contended that this resulted from variations in surface mixing and bubble formation.

The variability of the bromoform mixing ratios at Cape Point were investigated through the testing of a number of hypotheses based on previous studies. Hypotheses based on previously found relationships between bromoform and physical variables were explored. These processes included the role of shortwave radiation and ozone in affecting the variability of bromoform at Cape Point. Photosynthesis in algae results in the formation of H_2O_2, a ROS, which are detrimental to the algae. As discussed in Chapter 5, the bromoperoxidase enzyme may be used in algae to reduce the stress caused by ROS. A number of weak relationships were discovered (hypotheses 2, 5, 6, 9, 10 and 11, Table 4.7) suggesting mechanisms that may each explain a portion of the variability of bromoform mixing ratios observed. The hypotheses were not able to describe the full range of variability. However, the hypotheses may provide clues to further work that could shed light on the mechanisms affecting bromoform mixing ratios at Cape Point.

The calculated diurnal pattern of variability in bromoform mixing ratios was consistent with previously published reports (Ekdahl et al., 1998; Carpenter et al., 2000; Abrahamsson et al., 2004). The processes affecting variability were, therefore, likely to be similar. Bromoform mixing ratios increased during the morning with increasing shortwave radiation and then decreased in the afternoon, probably as a result

of local dilution processes or a regime shift. A second peak in bromoform mixing ratios was observed, driven by a formation through respiration processes or an accumulation through reduced destruction. Bromoform mixing ratios were well correlated with CO, shortwave radiation and particle counts. The correlation of particles and bromoform at Cape Point may be the result of shortwave radiation inducing a comparable particle anti-oxidant and photosynthetic response in the macroalgae at Cape Point. These processes may be limited by the high levels of shortwave radiation experienced, thus peaking before local solar zenith. The relationships between the other variables was probably driven by the diurnal cycle of shortwave radiation.

The harmonic terms incorporated into the regression model were able to explain approximately 29 % of the variance of the bromoform mixing ratios observed at Cape Point. The model captured the extreme bromoform mixing ratios but failed to capture the variability at lower mixing ratios. In order to capture the extreme events accurately, the model sacrificed the variability at low mixing ratios. Harmonics of varying frequencies and an insufficient number of bromoform measurements is thought to have limited the effectiveness of the model in this case. The work described here demonstrated that this may be a viable method for modelling bromoform mixing ratios, which could be important in areas where measurements are sparse.

MBL and back trajectory analysis provides a possible explanation of the variability observed. Air parcels that transited above the MBL typically contained lower bromoform mixing ratios than those below. While the MBL at Cape Point did not appear to act as a natural pre-concentrator, its presence as a barrier, capping surface released gases is notable as mechanism driving variability in bromoform mixing ratios at Cape Point. These gases are then prevented from mixing with air masses in the atmosphere above the top of the MBL. This mechanism could explain the reason for variability between air samples passing over the same sources, making the arrival height and direction relative to the MBL height an important consideration in bromoform variability.

The measurements of atmospheric bromoform taken at Cape Point are generally consistent with previous reports. The unique setting of Cape Point has air masses arriving from multiple, varied sources. These sources include local macroalgae beds, the Benguela upwelling system to the north and the Southern Ocean to the west and south. It is possible that interaction of multiple, simultaneous sources resulted in the episodic elevated bromoform mixing ratios above 60 ppt, observed at Cape Point. While the testing of hypotheses shed light on processes occurring at Cape Point, they were not ultimately instrumental in determining the driving mechanisms of observed bromoform variability. The quantitative detection of bromoform at Cape Point could make an important contribution to global knowledge by helping to validate chemistry models. Model output data has shown the Benguela to be an important atmospheric bromoform source (Palmer and Reason, 2009). Sparse sampling in this region has, however, prevented adequate validation to date. A longer time series is needed for the southern African region to tease out the variability of bromoform mixing ratios here. This may go toward describing the possible causes of the variability observed in the bromoform mixing ratios.

Chapter 5

Effects of oxidative stress on the production of bromoform by two marine diatom species

This study examines the role of nutrient limitation on the production of bromoform in two axenic diatom species. The cultures were grown in laboratory conditions and nutrient limitation was achieved by the addition of sodium hydroxide or starvation. The bromoform per cell concentrations increased during the exponential growth phase, but displayed significant decreases during the limited phases of the experiments. The work presented here was a collaborative effort with the diatom culturing being performed by Mariam Nguvava, as part of her MSc (Nguvava, 2012).

5.1 Introduction

Microalgae are an important source of bromoform to the global atmosphere (Quack and Wallace, 2003; Weinberger et al., 2007). However, the role of halocarbons and bromoform in macro- and microalgae and the reason for its release remains unclear (Laturnus, 1996; Paul and Pohnert, 2011; Palmer et al., 2005). A number of triggers have been suggested for the release of bromoform including: grazing, through an allelopathic response (Collén et al., 1994; Laturnus, 1996; Gschwend et al., 1985; Goodwin et al., 1997), oxidative stress (Palmer et al., 2005; Küpper et al., 2008) or as the by-product of the photosynthetic process (Pedersén et al., 1996; Manley and Barbero, 2001). While the evidence for an allelopathic release response is ambiguous (Gschwend et al., 1985), an oxidative burst of reactive oxygen species (ROS) was reported in macroalgae to an oligoguluronate solution, which was used to simulate grazing, may result in the formation of bromoform (Küpper et al., 2008). Various chemical compounds have been reported to be released from macro- and microalgae in response to grazing and bacterial attack (Gschwend et al., 1985). It is often suggested that this may be a reason for release of bromoform from macro- and microalgae (Gschwend et al., 1985; Collén et al., 1994; Pedersén et al., 1996; Laturnus, 1996). However, the evidence for the release of bromoform as a defence mechanism is unclear. In a laboratory experiment the periwinkle (*Littorina littorea*) avoided macroalgae that contained CH_2I_2. The presence

of bromoform in the agar plates did not seem to affect the grazing by the snail (Gschwend et al., 1985). No conclusions can be drawn from this single study. Although there is little evidence to support the theory, it has been suggested that bacterial attack might elicit a bromoform release response from macro- and microalgae (Quack and Wallace, 2003; Wever et al., 1991; Moore et al., 1996; Küpper et al., 2008; Palmer et al., 2005). In this regard, it is therefore unlikely that bromoform is released as a defence mechanism against grazing or bacterial attack. Numerous studies have demonstrated increased bromoform release from micro- and macroalgae placed under various different oxidative stresses including increased irradiance, increased concentrations of ozone, oligoguluronates and hydrogen peroxide (Palmer et al., 2005; Pedersén et al., 1996; Manley and Barbero, 2001).

The mechanisms of formation of bromoform in macroalgae are not clearly understood (Quack et al., 2007; Palmer et al., 2005; Weinberger et al., 2007). While an abiotic formation process has been proposed, such as the irradiance of seawater with UV, the main formation process suggested centres around the oxidation of bromine atoms by the bromoperoxidase enzyme (BrPO) and the subsequent reaction with dissolved organic matter‘(Quack and Wallace, 2003; Class and Ballschmiter, 1987). The partial decay of the brominated dissolved organic matter via the haloform reaction results in the formation of bromoform (Wever et al., 1991; Pedersén et al., 1996; Paul and Pohnert, 2011; Manley and Barbero, 2001; Wever and Van der Horst, 2013; Palmer et al., 2005; Hill and Manley, 2009). While the presence of the bromoperoxidase enzyme has long been known in macroalgae (Wever et al., 1991), it has only more recently been shown in microalgae (Tokarczyk and Moore, 1994; Moore et al., 1996). Bromoperoxidase catalytically oxidises halide anions (Br^-) in the presence of hydrogen peroxide (H_2O_2) which results in the formation of hypobromous acid (HOBr). The HOBr rapidly reacts with dissolved organic matter (DOM) near the ocean surface, producing unstable brominated intermediaries. The intermediaries decay via the haloform reaction, which results in the formation of bromoform (Reactions 5.1 – 5.3; Hill and Manley, 2009; Wever and Van der Horst, 2013; Paul and Pohnert, 2011). The rate of reaction between HOBr and DOM is of the order of milliseconds. In many species of marine algae BrPO enzymes have been shown to exist both intra- and extracellularly, proving a mechanism to cope with intra- and extracellular hydrogen peroxide (Wever and Van der Horst, 2013; Paul and Pohnert, 2011).

$$H_2O_2 + H^+ + Br^- \xrightarrow{BrPO} HOBr + H_2O \tag{5.1}$$

$$HOBr + DOM \rightarrow DOM(Br) \tag{5.2}$$

$$DOM(Br) \rightarrow CHBr_3 + DOM \tag{5.3}$$

Increased light intensities have often been linked with elevated rates of bromoform production (e.g., Hill and Manley, 2009; Mtolera et al., 1996; Wever and Van der Horst, 2013; Carpenter et al., 2000; Pedersén et al., 1996; Collén et al., 1994; Palmer et al., 2005). During daylight hours hydrogen peroxide is produced during photosynthesis by means of the Mehler reaction. Mitochondrial respiration at night produces hydrogen peroxide, though at a much lower rate than photosynthesis (Pedersén et al., 1996; Collén et al.,

1994; Hill and Manley, 2009). The intra- and extracellular H_2O_2, which is poisonous to algae (Pedersén et al., 1996; Collén et al., 1994), results in oxidative stress within the algae (Hill and Manley, 2009). It is suggested that the formation of H_2O_2 results in the bromoform diurnal cycle described previously (Chapter 4.1.3). Increased light intensities have also been suggested to result in the decay of algal tissue during the summer period. This decay has been linked with a peak in measured bromoform mixing ratios during the summer period (Goodwin et al., 1997; Quack and Wallace, 2003). Carbon limitation has been shown to result in an oxidative stress similar to that induced by sunlight (Mtolera et al., 1996 and references therein). Some laboratory studies have shown a relationship between bromoform concentration and pH (Mtolera et al., 1996). The decreasing acidity as pH increases might favour the formation of bromoform through one of the steps of formation (Reactions 5.1 – 5.3).

The releases of reactive oxygen species (ROS, hydrogen peroxide (H_2O_2), hydroxyl radical (OH), superoxide (O_2^-)) is a well documented defence trigger in macro- and microalgae (Küpper et al., 2008; Palmer et al., 2005). It is suggested that the ROS may be rapidly released from the plant in an oxidative burst (Küpper et al., 2008). The sudden influx of oxidative species may result in the rapid formation of bromoform. The bromoform would be produced as a by-product of the BrPO enzyme scavenging the ROS and then reacts with DOM and is reduced via the haloform reaction as discussed. Although not necessarily allelopathic, the formation of bromoform may therefore be the by-product of algal defence against grazing (Küpper et al., 2008).

Seasonal variations in the rate of production of bromoform have been observed in multiple locations (Laturnus, 1996; Carpenter et al., 2000; Zhou et al., 2008). The seasonal variation might be influenced by changes in sunlight, DOM concentrations or ocean temperature associated with the different seasons (Laturnus, 1996; Itoh and Shinya, 1994; Carpenter et al., 2000). The rate of photosynthesis in algae would be affected by changes in light intensity with the seasons, resulting in a maximum in summer and minimum in winter. In theory the decrease in photosynthetic rate would result in less H_2O_2 being formed, thus producing less bromoform. The local concentrations of DOM have been reported to vary through the seasons with a maxium in summer (Quack and Wallace, 2003). Variations in the DOM would affect the formation of bromoform by limiting the amount of matter that can react with HOBr to form intermediaries (Reaction 5.2). The rate of efficiency of the BrPO enzyme has been shown to be inversely related to sea surface temperature (Itoh and Shinya, 1994; Laturnus, 1996). Variation of the efficiency of the BrPO enzyme might limit the formation of HOBr, resulting in a limitation of bromoform (Reaction 5.1).

The effect of oxidative stress in the form of nutrient limitation on bromoform production from two sub-tropical marine diatoms, cultured in axenic conditions (i.e. with no bacteria present), was explored in this project. Because bacteria have also been shown to produce bromoform (Manley et al., 1992; Quack and Wallace, 2003), this creates a complication of attributing the production of bromoform to the microalgae or bacteria present in phytoplankton laboratory cultures contaminated by bacteria and in mixed community environmental samples (Tokarczyk and Moore, 1994). Mixed community environmental

samples are also rarely done so this necessitates the need for laboratory microalgal culture experiments to be run under axenic conditions (Tokarczyk and Moore, 1994). After being grown under continuous light, the diatom species here were first subjected to carbon (CO_2) limitation, which has been shown to induce oxidative stress in microalgae (Vardi et al., 1999; Sunda et al., 2002). It is thought that an increased amount of bromoform will be produced as a result of a natural allelopathic mechanism of the microalgae. In a second experiment, one of the diatom species was grown under nitrate limitation. Increased upper ocean stratification and temperature, as a result of climate change, are reported to result in the decrease in ocean productivity in the tropics (Behrenfeld et al., 2006; Carpenter et al., 2011). This stratification limits the nutrient availability, placing increasing strain on micro- and macroalgae found in these regions. The increased stress induced by the natural changes in CO_2 and nutrients may result in an increase in bromoform production, despite an overall decrease in productivity. The increased bromoform atmospheric mixing ratios might have a significant impact on ozone concentrations and lead to positive climate change feedbacks. It is of great importance to understand the mechanism of variability within microalgae as they may be the largest global bromoform producers (Quack and Wallace, 2003).

5.2 Methods and materials

5.2.1 Experiment details

Axenic, unialgal clones of the diatoms *Phaeodactylum tricornutum* (CCMP 633) and *Chaetoceros neogracile_cf* (CCMP 1425) were purchased from the National Center for Marine Algae and Microbiota (NCMA, http://www.ncma.bigelo.org), Bigelow Laboratory, USA. The cultures were grown at 21 $\pm$ 1 °C under a continuous cool white light (BioSun NL® T858W/965), resulting in an irradiance flux of 180 μmol photons m^{-2} s^{-1} (Nguvava, 2012). Batches of each culture were grown in duplicate and triplicate for the nitrate and carbon limitation experiments respectively. Duplicates of blank medium (filtered and sterilised seawater) as controls were stored under and treated in an identical manner to the culture batches (Moore et al., 1996; Colomb et al., 2008; Manley and Barbero, 2001). A standard f/2 medium was used to sustain and support the cultures in 1 *l* Duran® glass bottles (Guillard, 1975; Guillard and Ryther, 1962). The culture vessels were maintained with zero headspace and sealed with gas tight PTFE lids to minimise gas exchange and loss (Colomb et al., 2008). All glassware and equipment was either purchased sterile or autoclaved.

The f/2 medium was made in-house from enriched False Bay seawater (Guillard, 1975). The False Bay seawater, collected in acid washed plastic carboys, was filtered through a 0.22 μm glass fibre filter to remove any bacteria present. The seawater was sterilised by boiling in a microwave for 8 minutes (Keller *et al.* 1988). Due to outgassing of CO_2 during the sterilisation by boiling, the seawater pH rose from 8.0 to 8.3. The pH of the medium was regulated at $\sim$7.8 for the exponential growth phases by the addition of hydrochloric acid (HC*l*) and sterile sodium bicarbonate ($NaHCO_3$) as a buffer (Nguvava, 2012). Sterile macronutrients, trace metals and vitamins were added to the filtered and sterilised seawater to achieve the desired f/2 medium (Table 5.1).

Table 5.1: Macronutrient concentrations found in the f/2 seawater medium.

Component	Element	Seawater (μM)	f/2 (M)
Macronutrients	N	5.4 ± 1.5	8.82 x 10^{-4}
	P	0.5 ± 0.4	3.62 x 10^{-5}
	Si	8.6 ± 1.0	1.06 x 10^{-4}
Trace metals	Fe		1.17 x 10^{-5}
	Cu		3.93 x 10^{-8}
	Mo		2.60 x 10^{-8}
	Zn		7.65 x 10^{-8}
	Co		4.20 x 10^{-8}
	Mn		9.10 x 10^{-7}
Vitamins	B_1		2.96 x 10^{-7}
	H (Biotin)		2.05 x 10^{-9}
	B_{12}		3.69 x 10^{-10}

Two separate oxidative stress experiments were performed on the diatoms to test the antioxidant response of the bromoperoxidase enzyme. The oxidative stress induced within the culture species through the experiments was achieved by the limitation of carbon (CO_2) and nitrate (NO_3). During the exponential growth phase the cultures were kept with sufficient nutrients to ensure growth. The carbon limitation within the culture batches was induced on the 4^{th} day of exponential growth by the addition of 5 M sodium hydroxide (NaOH) (Sunda et al., 2002). This was noted by an increase in the pH recorded in the sample flasks. The nitrate limitation was achieved on the 6^{th} day of growth. The addition of phosphate and silicate after each sampling ensured that these macronutrients never became depleted. The pH was maintained at < 8.3 for the duration of the sampling period by adding HC*l* and sterile $NaHCO_3$ as a buffer (Nguvava, 2012).

5.2.2 Sampling and analysis

The diatom cultures were grown for ten generations prior to the commencement of sampling. Daily 65 m*l* aliquots of medium were drawn from each of the culture batches for the analysis of physical cell variables and nutrient properties. The extracted volume was immediately replaced with fresh blank medium to ensure a zero headspace (Sunda et al., 2002; Bucciarelli et al., 2007). A correction for dilution was applied to all the data collected. The culture bottles were gently overturned or reversed 50 times to uniformly mix the cells before the aliquots were drawn. Axenicity of the cultures was achieved through the use of a laminar flow hood. The flow hood and gloved hands were washed in ethanol (25 %) to ensure both were sterile. Aseptic preparation of media and transfers for sampling were done under the laminar flow hood (Scarratt and Moore, 1996).

Physical cell variables examined included maximum cell volume (V_{cell}, μm^{-3}), cell abundance (C_{cell}, l^{-1}) and the presence of bacteria. Cell volume and abundance in the medium was measured using a 2-2 Multistar Coulter counter, set at 100 μm aperture size and 20 – 150 μm^{-3} particle volume range. Samples were run through the Coulter counter within 20 minutes of being drawn. Due to the mechanics of the Coulter counter and the difference in cell shape between the diatom species, only the cell volumes for the spherical *C. neogracile_cf* were measured. Cell volumes of *P. tricornutum*, which is pennate in shape, were estimated following Bartual et al. (2008):

$$V_{cell} = \frac{\pi}{6} D^2 H \tag{5.4}$$

Ranges for the diameter (*D*) and length (*H*) of the *P. tricornutum* cells were obtained from the NCMA website (http://ncma.bigelow.org/node/1/strain). The cell volume for *P. tricornutum* was estimated at between 60 and 330 μm^3, based on a mean diameter and length of 3 – 5 μm and 13 – 25 μm, respectively. The specific growth rate (μ, d^{-1}) for the diatoms was determined by dividing the difference of the natural logarithm of the cell abundance by the difference in days, after Sunda and Huntsman (1995):

$$\mu = \frac{ln(N_2) - ln(N_1)}{t_2 - t_1} \tag{5.5}$$

Bactopeptone was used to test the culture media axenicity. Approximately 1 m*l* of culture medium was pipetted into 5 m*l* sterile bactopeptone medium (1 g l^{-1}) and kept in the dark at laboratory temperature (20 °C) in a test tube for 7 days. If present, bacteria formed a white cloud in the test tube within 7 days. If a culture batch was found to be contaminated with bacteria, the batch was discarded. Nutrient concentrations and pH were measured from the daily drawn aliquots. A HANA HI 9125 pH/ORP meter was used to measure 2 m*l* of culture medium from each batch. The measurement of pH was performed within 10 minutes, at laboratory temperature.

The maintenance of axenicity in the culture vessels is of great importance. The potential production of bromoform by the bacteria may hinder the interpretation of production by diatoms (Manley et al., 1992; Scarratt and Moore, 1996). Certain oceanic bacteria and microorganisms are able to remineralise urea and ammonia, the waste products of microalgae, back into nitrate (Alonso-Sáez et al., 2012; Wuchter et al., 2006; Martens-Habbena et al., 2009). Under nitrate limitation experiment this could be of concern as one would effectively have no control over nitrate concentrations in the cultures (E. Minor, University of Minnesota, pers. comm. 2012).

A sterile disposable 0.2 μm filter and 25 m*l* syringe were used to filter samples for the analysis of nitrate, phosphate and silicate in the culture medium. Samples were stored in 50 m*l* plastic bottles and in a fridge for up to 3 weeks. Manual colourimetric analysis of the filtered media samples was used to determine nutrient concentrations. Chemicals added to the seawater samples resulted in the formation of coloured compounds, which were proportional to the nutrient concentration. A spectrophotometer was

used to measure the absorbance of light at specific wavelengths to determine the concentration (Grasshoff et al., 1983, 2009).

The concentration of nitrate in the culture media was determined through the reduction to nitrite and subsequent measurement (Strickland and Parsons, 1965). Samples were run through a cadmium column in order to reduce the nitrate to nitrite. Background nitrite concentrations were determined by analysing samples that had not been reduced. The addition of sulphanilamide followed by N-(1-naphthyl) ethylenediamine dihydrochloride resulted in the development of a red coloured compound in the solution. Concentration of nitrate was determined from a seven-point external calibration curve based on the absorbance of nitrite at 540 nm wavelength.

Phosphate concentrations were determined by means of a colourimetric absorbance method after Greenfield and Kalbar (1954) and Murphy and Riley (1958). Ammonium molybdate, ascorbic acid and, sulphuric acid and potassium antimonyl tartrate were added to the aliquots of culture medium in the form of a single reagent. The resulting solution was reduced to a blue phosphomolybdic acid by the later addition of ascorbic acid. External calibration of nine data points measured at 880 nm wavelength resulted in the determination of phosphate concentrations.

A blue coloured compound was developed in the media samples by the reduction of siliconmolybdic acid by ascorbic acid for the determination of silicate in water samples. The silicomolybdic acid is formed from ammonium molybdate and sulphuric acid, after Dienért and Wandenbulcke (1923). Interference from reactions with phosphate in the solution were limited by the addition of oxalic acid. The silica concentration was determined from the absorbance of the solution at 810 nm wavelength.

5.2.3 Bromoform sampling

Measurement of the cultures for bromoform occurred once a day at approximately the same time every day (9 – 11 am). A daily sample from each replicate was taken to measure change in bromoform concentration. Two sampling days were performed during the exponential phase, while three days of sampling during the limitation phases were performed for each limitation experiment. A sample of the controls was taken on a daily basis to form a baseline of background bromoform concentrations within the medium. Unfiltered culture and medium (100 m*l*) was carefully poured into the calibrated custom-built glass trap (Glasstech, Cape Town) for gas sparging. The glass trap was calibrated by repeated pouring of 50 and 100 m*l* deionised water into the trap. The height of the water was marked by etching the glass trap. To ensure axenicity of the culture flasks the samples were poured in the laminar flow hood.

As described in Chapter 3, the culture samples were sparged with nitrogen (Grade 5.0) at 100 m*l* min^{-1} for 5 minutes at laboratory temperature (< 20 °C) to achieve gas extraction (Tokarczyk and Moore, 1994). Bromoform sparged from the 100 m*l* culture samples was trapped on thermal desorption unit adsorbent traps (9 mg each Carbopack X and Carboxen 1016, Chapter 2). The adsorbent tubes were stored in the

dark at 4 °C and analysed within 6 hours. The samples were analysed on a GC-ECD system, as per method described in Chapter 2 and Kuyper et al. (2012). Nitrogen was passed through the setup for 2 minutes between sample points to remove moisture from the PTFE tubing. The measurement of bromoform was normalised to mol cell^{-1} for each duplicate analysed.

5.3 Results and discussion: changes in diatoms and bromoform response

This section examines the conditions surrounding the growth of the cultures through the different phases of the experiments and the associated variations in bromoform concentrations. These conditions include the physical and physiological states of the diatoms during the exponential growth phase and the two oxidative stress phases. Examination of the bromoform response in the diatoms to oxidative stress via nutrient limitations is explored.

5.3.1 Culture growth

The cultures were initially incubated for one week to ensure that the diatoms were healthy and well adapted to the culture conditions. Mean specific growth rates recorded for *P. tricornutum* and *C. neogracile_cf* were μ = 1.08 and 1.48 d^{-1}, respectively. These specific growth rates were consistent with previously reported studies under saturating light for diatoms of equivalent cell volumes (Sarthou et al., 2005). The cultures were grown through an exponential phase for each limitation experiment prior to the limitation either by induction (carbon) or nutrient depletion (nitrate).

The pH in the culture medium was maintained at below 8.3 and 8.5 for *P. tricornutum* and *C. neogracile_cf*, respectively (Table 5.2). A pH of greater than 8.5 has been suggested as the threshold for the onset of carbon limitation (Goldman et al., 1982; Scarratt and Moore, 1996). A favourable maximum growth rate was achieved through the range of pH measured in the culture vessels. The calculated assimilation rates of nutrients by the diatoms were used to ensure that macronutrient concentrations were not limited during the exponential growth phase (Table 5.2). The cultures were thus able to achieve a maximum rate of growth and were not limited by nutrient concentrations nor pH during the exponential growth phase (Table 5.2).

Table 5.2: Macronutrient concentrations (μmol l^{-1}) during the exponential growth phases 1 (CO_2 limitation) and 2 (NO_3 limitation), reported as minimum and maximum.

	Exponential phase 1		**Exponential phase 2**	
Nutrient	***P. tricornutum***	***C. neogracile_cf***	***P. tricornutum***	***C. neogracile_cf***
Nitrate	596 –745	715 – 841	253 – 858	603 – 760
Phosphate	23 –31	22 –29	23 – 46	29 – 52
Silicate	110 – 132	75 – 129	127 – 182	139 – 233
pH	7.9 – 8.3	7.8 – 8.5	8.0 – 8.3	8.0 – 8.3

Mean specific growth rate of μ = 1.29 $\pm$ 0.0 and 1.35 $\pm$ 0.13 d^{-1} for *P. tricornutum* (Fig. 5.1a) and *C. neogracile_cf* (Fig. 5.1b), respectively, was recorded over the duration of the first exponential growth phase. A second exponential growth phase, for the nitrate limitation experiment, resulted in mean specific growth rates of μ = 1.32 $\pm$ 0.0 and 2.08 $\pm$ 0.0 d^{-1} for *P. tricornutum* (Fig. 5.1c) and *C. neogracile_cf* (not shown), respectively. Due to the accidental addition of nitrate to the *C. neogracile_cf* cultures at the end of the exponential growth phase the cultures were run into nitrate poisoning instead of limitation. The quantification of bromoform in this exponential growth phase was used in conjunction with the CO_2 limitation experiment growth phase. However, since the cultures were never run into nitrate limitation there is no data present for *C. neogracile_cf* for this experiment.

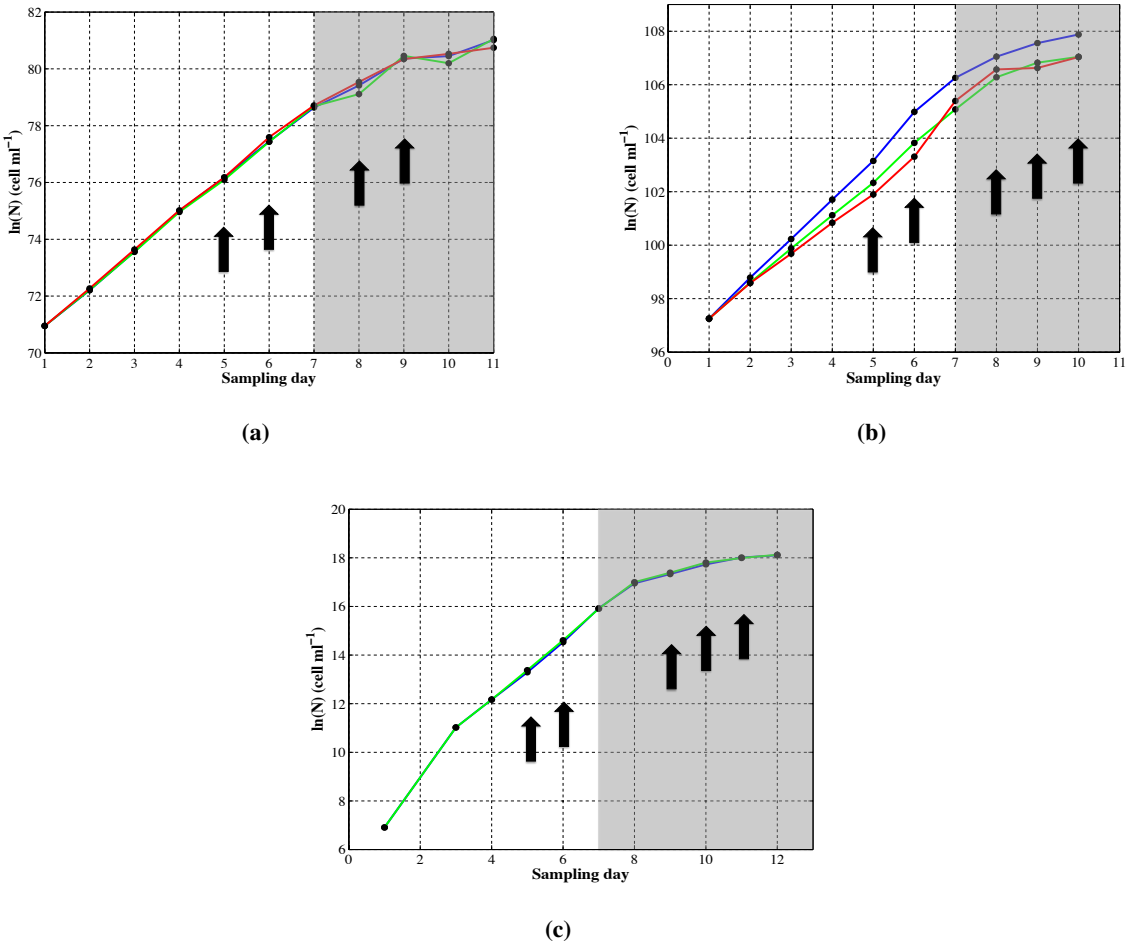

Figure 5.1: Specific growth rate curves for (a) *P. tricornutum* and (b) *C. neogracile_cf* during CO_2 limitation and (c) *P. tricornutum* during NO_3 limitation. The exponential growth phase is is visible days 1 – 6 with nutrient limitation days 7 – 10 (shaded). The slope indicates the specific growth rate. Varying colours represent the different replicate culture batches grown. Black arrows mark bromoform sampling days.

The specific growth rates for all the cultures exhibited a two- to five-fold decrease following the onset of nutrient limitation (Fig. 5.1a, b, c). This resulted in mean specific growth rates of μ = 0.56 $\pm$ 0.0 d^{-1} and 0.46 $\pm$ 0.0 d^{-1} for *P. tricornutum* and *C. neogracile_cf*, respectively during the carbon limitation, while the specific growth rate of *P. tricornutum* ranged between μ = 0.28 and 0.30 d^{-1} for the duplicates

during the nitrate limitation. Carbon limitation was induced in the cultures by the addition of 5 M NaOH on the 5th day of exponential growth. A measured increase in pH from 8.3 to 9.17 $\pm$ 0.0 and 9.38 $\pm$ 0.2 for the *P. tricornutum* and *C. neogracile_cf* cultures respectively, was used to confirm the CO_2 limitation. Although the pH was allowed to increase after the initial addition of NaOH, macronutrient concentrations were maintained to ensure that the cultures were not limited by multiple sources. Following the initial exponential growth phase the cultures were grown into nitrate (NO_3) limitation. Nitrate concentrations decreased from the initial values of 859 and 734 μmol l^{-1} in duplicates for *P. tricornutum*. Nitrate concentrations recorded were at the lowest on the 8th day of sampling, suggesting that full limitation occurred from the 9th day. Sampling in the limited phase commenced on this day. Other macronutrients (phosphate and silicate) and pH in the culture vessels were kept in balance through the duration of the NO_3 limitation to ensure that only a single limitation was affecting the cultures.

5.3.2 Bromoform measurement

The measurement of bromoform from the culture samples occurred during the exponential and nutrient limited phases (Fig. 5.1 and 5.2). Bromoform concentrations recorded in the exponential phase were used as a baseline against which concentrations recorded in the nutrient limited phase were compared. The controls exhibited elevated bromoform concentrations relative to the cultures (Fig. 5.2). The elevated bromoform found in the controls was thought to originate from the False Bay seawater used for culture medium. The False Bay seawater was collected from near a macroalgae bed, in order to ensure low nitrate concentrations. However, in an oversight the water was not properly sparged prior to the culturing and possibly contained large quantities of bromoform from the macroalgae bed. The seawater was sterilised by boiling which should have lowered the bromoform concentrations. The project was not simply repeated due to limited equipment and cost. It is possible that the bromoform in the seawater controls was formed via an abiotic process (Lin and Manley, 2012). Hypobromous acid (HOBr) may be formed from the reaction of molecular bromine and seawater, possibly in the presence of extra-cellular BrPO. Bromoform might then be formed by the partial decay of brominated dissolved organic matter, which had been brominated by reaction with HOBr (Reactions 5.1 – 5.3; Lin and Manley, 2012). It is possible that an increase in the bromoform concentration within the seawater controls would be synoptic of the presence of the above abiotic formation pathway. While elevated, during the nitrate limitation experiment the the bromoform concentration in the seawater controls was not found to increase (Fig. 5.2b). The mean bromoform concentration in the control was found to vary at the same rate as the *C. neogracile_cf* cultures. This increase may be due to a concurrent abiotic production in both the control and the culture. During the limitation phase of the experiments (after day 7) much lower bromoform production rates in *C. neogracile_cf* were recorded than during the exponential rate. Thus any abiotic production in the blank may match that of the cultures.

Due to the elevated bromoform concentration recorded in the controls it was important to determine whether measurements from the cultures were significant. Using a permutations test the variability between the controls was found to be small (Fig. 5.3a) and were found to be statistically similar (α =

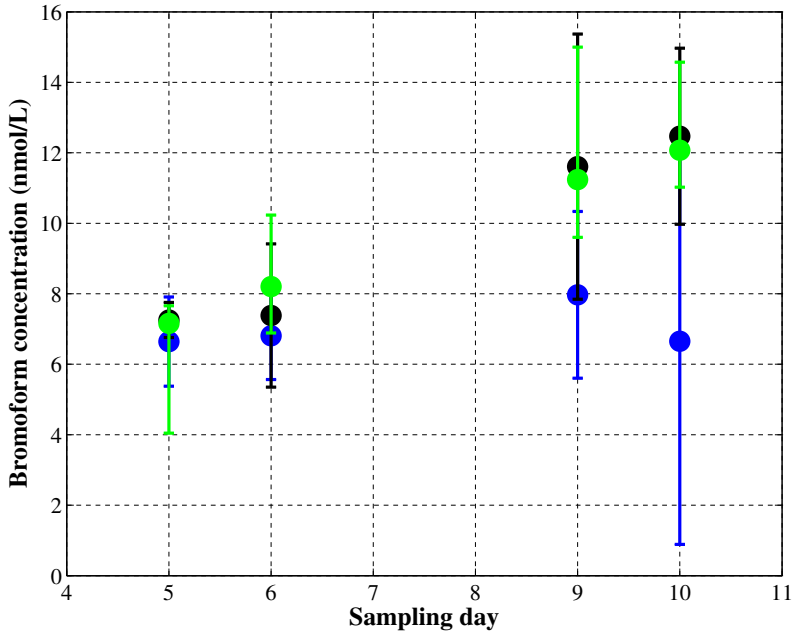

Figure 5.2: Mean measurements of bromoform concentration (nmol l^{-1}) with (a) displaying *P. tricornutum* (blue), *C. neogracile_cf* (green) and controls (black) for CO_2 limitation experiment and (b) *P. tricornutum* (blue) and seawater control (black) for NO_3 limitation experiment. Error bars denote 1 standard deviation.

0.05; Oatley and Underhill, 2001). A permutation test runs a small sample set through numerous, in this case 10 000, iterations of different combinations of the data. This allows a limited dataset (less than 10 points) to be tested robustly. The mean, standard deviation and 95 % confidence interval of bromoform concentrations (nmol l^{-1}) were calculated for the culture samples and the seawater controls. Significant measurements of bromoform were determined from the the calculated confidence interval of the seawater controls. The calculated mean bromoform concentration in the seawater controls was subtracted from

the measured concentration in the culture and the result was compared to the confidence interval. If the seawater confidence interval was larger than the calculated difference between the mean of the control and the culture measurement then the data point was removed. The significant bromoform concentrations recorded for each species were pooled for the exponential phase and the respective nutrient limitation phase.

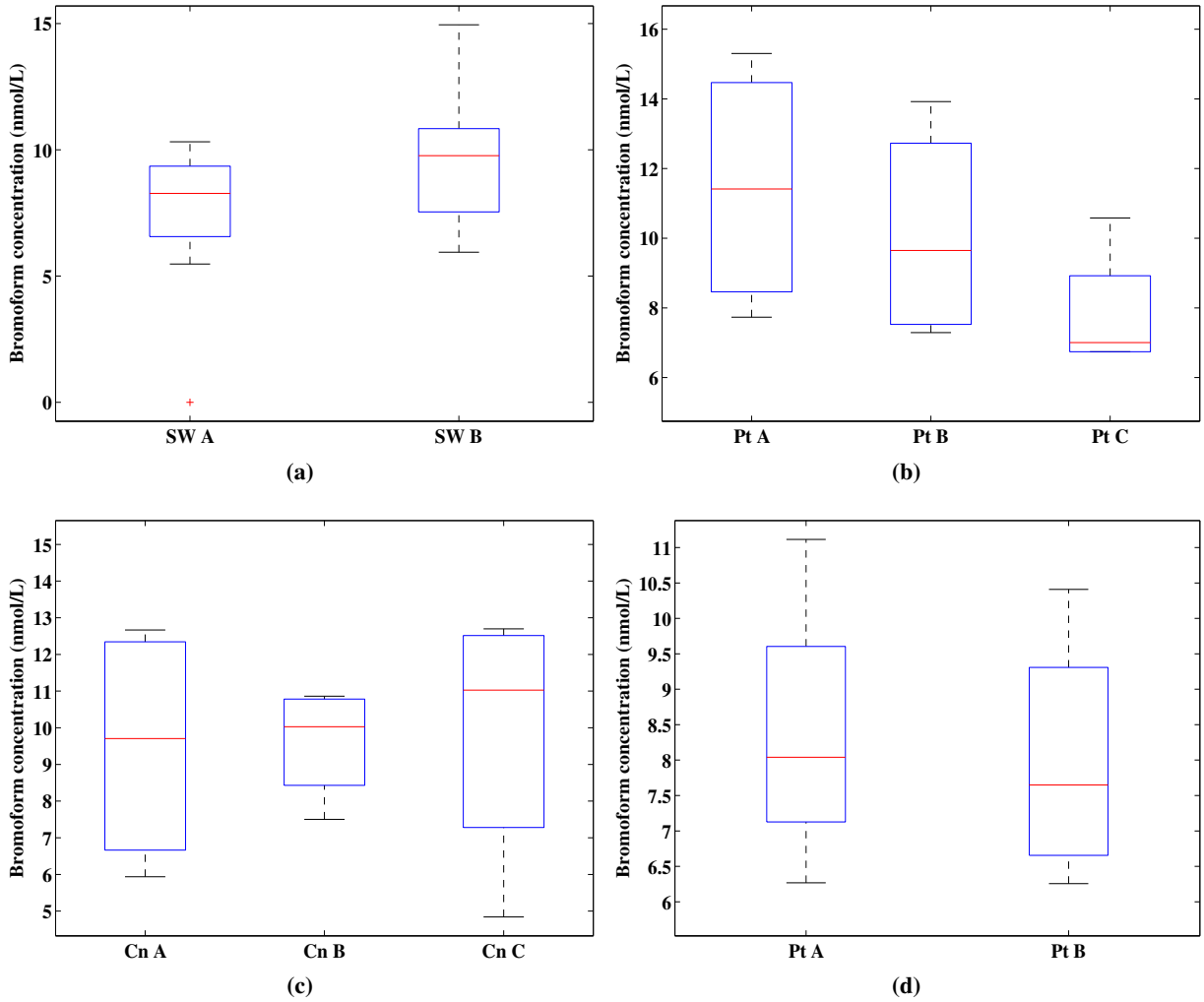

Figure 5.3: A comparison of the variability in bromoform measurement between replicates during the exponential and CO_2 limited phases for (a) seawater controls (b) *P. tricornutum* and (c) *C. neogracile_cf* (d) *P. tricornutum* duplicates over the exponential growth and NO_3 limited phases.

The significant measurements of bromoform in the cultures were standardised by calculating the concentration per cell. The production of bromoform per cell was calculated for the different species over the duration of the experiments (Table 5.3). The production rate of bromoform per cell was found to be approximately three times larger for *C. neogracile_cf* than *P. tricornutum*. The difference in the rate of production was found to be significant based on a paired Student's t-test ($p < 5$). The two species of diatoms achieved different specific growth rates during the exponential growth periods, with that of *P. tricornutum* being lower than *C. neogracile_cf*. It is possible that the size differential between the species produced the varying specific growth rates. The cells of *C. neogracile_cf* are reported to be up

to three times smaller than *P. tricornutum* and are thus able to assimilate nutrients faster (Sarthou et al., 2005). The smaller cells and greater specific growth rate of the *C. neogracile_cf* may account for the elevated bromoform concentrations per cell compared to *P. tricornutum*. The larger amount of bromoform produced by the smaller cells may be due to faster photosynthetic processes than are found in the larger *P. tricornutum* cells.

Table 5.3: Bromoform per cell concentration (x 10^{-18} mol cell^{-1}) and production per cell (x 10^{-18} mol cell^{-1} d^{-1}) during the exponential phases, significant data combined.

	per cell concentration		**production per cell**	
Nutrient	***P. tricornutum***	***C. neogracile_cf***	***P. tricornutum***	***C. neogracile_cf***
Mean	5.3 – 12.4	4.4 – 40.7	7.0 – 15.6	8.5 – 57.0
Range	9	16.5	11.4	280
Standard deviation	2.7	3.8	3.4	5.3
n	5	5	5	5

The quantity of bromoform produced by the diatom species tested here is of the same order of magnitude as previously published (Fig. 5.4; Tokarczyk and Moore, 1994; Moore et al., 1996). The species used by Tokarczyk and Moore (1994) (red) and Moore et al. (1996) (blue) were both of polar origin, while the species used here are of a sub-tropical origin. Given that polar diatom species are reported to be larger producers of bromoform than tropical or sub-tropical species it is a little surprising to see such similar quantities of bromoform produced (Fig. 5.4; Tokarczyk and Moore, 1994). The similar amounts of bromoform produced by the two different groups of microalgae may be related to the amount of light exposure. The polar species were grown under a saturating cool white light at either 12 or 40 μmol photons m^{-2} s^{-1} during the low and high light experiments (Tokarczyk and Moore, 1994; Moore et al., 1996). The sub-tropical species grown for this study were therefore saturated under light intensity approximately 4.5 or 15 times greater than the polar species (Sec. 5.2). If we assume a linear increase in bromoform concentration with light intensity and that the photosynthetic system is not impeded by the additional light, then under a similar light used here, it is estimated that the polar species would produce between 90 x 10^{-18} and 270 x 10^{-18} mol cell^{-1} of bromoform during the exponential growth phase. This range is approximately three to 27 times the amount produced in this study. When scaled by light intensity, it is apparent that the sub-tropical species produce significantly less bromoform per cell than the polar species, which suggests that there is a bromoform production gradient in microalgae running from a high in polar species to a low in tropical species (Tokarczyk and Moore, 1994; Quack and Wallace, 2003). The measured bromoform production is, however, of the same order of magnitude and so could be significant over the large frontal areas across which the sub-tropical species may be found.

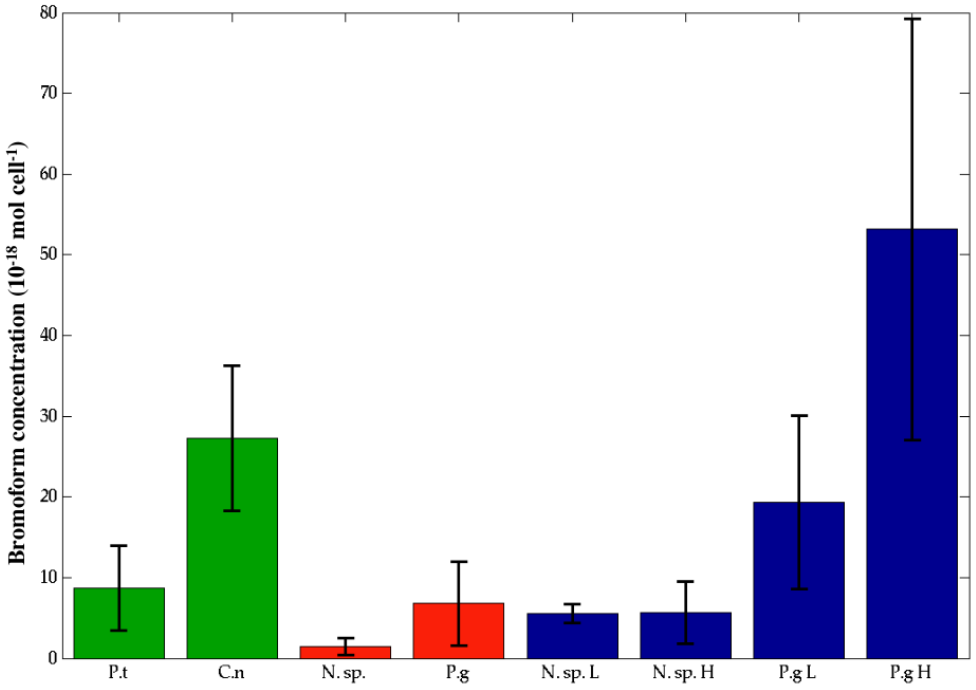

Figure 5.4: Comparison of bromoform production during exponential growth phase. P.t = *P. tricornutum*, C.n = *C. neogracile_cf* (this study, green), N.sp = *Nitzschia sp.*, P.g = *Porocira glacialis* (Tokarczyk and Moore, 1994, red), N. sp. L = *Nitzschia sp.*, N .sp. H = *Nitzschia sp.*, P.g L = *Porocira glacialis*, P.g H = *Porocira glacialis* (Moore et al., 1996, blue). H denotes high light while L denotes low light experimental conditions.

5.3.3 Carbon and nitrate limitation

The growth rate of microalgae may be dependent on the internal concentration of a limiting nutrient. Nutrient limitation is reported to result in decreased growth rates (Bucciarelli and Sunda, 2003). While the growth rate decreased during the limitation phases, growth continued probably due to internal stores of CO_2 or nitrate (Bucciarelli and Sunda, 2003). The diatoms continued to grow for longer after the onset of CO_2 limitation than for nitrate limitation. This may be due to a greater store of carbon, allowing for continued growth.The nitrate limitation was created by not replacing the used nitrate. The diatoms might have become increasingly stressed as the nutrient concentrations decreased, which would have possibly resulted in smaller intracellular stores of nitrate and slowed the growth rate prior to the full onset of the nitrate limitation.

The per cell concentration of bromoform decreased during the CO_2 limitation experiment. Mean bromoform concentrations decreased in the *C. neogracile_cf* culture vessels from 2.73 x 10^{-17} to 2.94 x 10^{-18} mol cell^{-1} (Fig. 5.5a), whereas the mean per cell concentration of bromoform produced by *P. tricornutum* decreased from 8.68 x 10^{-18} to 3.87 x 10^{-18} mol cell^{-1} during the carbon limited phase (Fig. 5.5b). The depreciated amount of bromoform in cultures was above the detection limit and that of the controls. The difference in production between the diatom species was not found to be significant. However, the amount of bromoform between the phases was found to be significantly different ($\alpha = 0.05$) different for *P. tricornutum*, and non-significantly different for *C. neogracile_cf*.

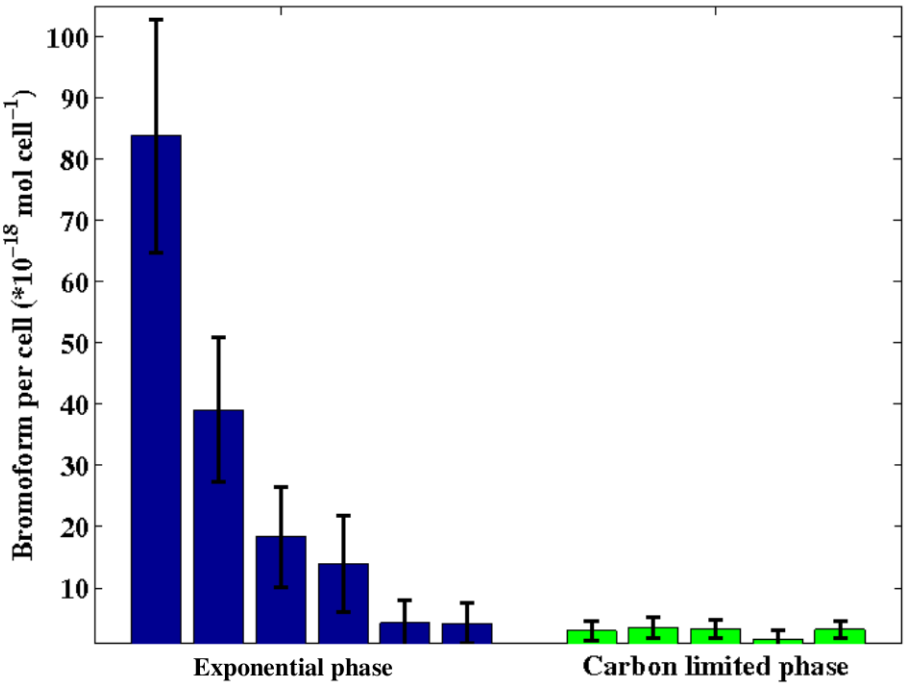

(a)

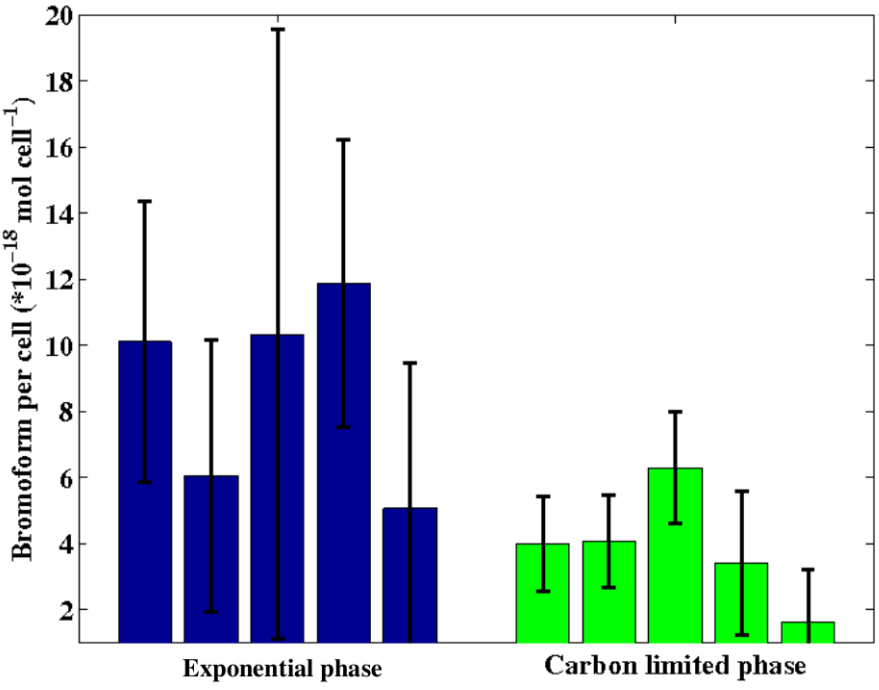

(b)

Figure 5.5: Bromoform concentration taken on different days during exponential growth phase (blue) and the CO_2 limitation phase (green) for
(a) *C. neogracile_cf* and (b) *P. tricornutum*.

The active transport of inorganic carbon within the cells during CO_2 limitation increases the cellular demand for energy. Carbon dioxide is created from HCO_3 at the cell surface. The conversion of HCO_3

requires the presence of the carbonic anhydrase enzyme, which requires nitrogen in order to be produced. Since both enzymes require nitrate, the intracellular formation of the bromoperoxidase enzyme may become limited if there is an increased cellular demand for the anhydrase enzyme (Bucciarelli and Sunda, 2003). This suggests that under CO_2 limitation cells may favour the formation of anhydrase enzyme in order to convert HCO_3 as a source of energy over the use of bromoperoxidase to reduce oxidative stress.

Should an oxidative burst of ROS, as has been observed in macroalgae occur in microalgae, then this would probably result in the formation of elevated concentrations of bromoform (Küpper et al., 2008). An increase in the concentration of ROS has been measured with CO_2 limitation for species of *Preidium gatunense* and *Thalassiosira pseudonana* (Vardi et al., 1999; Sunda et al., 2002). While a measurement of bromoform concentration was not taken on the day of nutrient initiation, an elevated concentration was not recorded the following day during analysis (Fig. 5.2). This suggests that a single large effusion of bromoform as a result of an oxidative burst or in response to the increased oxidative stress did not occur. The culture vessels were maintained with zero headspace and sealed with gas tight PTFE lids. The known mechanisms of loss within water (Chapter 1.3.3) result in aquatic bromoform half-lives of more than years. This suggests that were an elevated quantity of bromoform produced, it would have been detected the following day. Since a large amount of bromoform was not detected the following day, it is probable that it was never released.

In response to the nitrate limitation in the culture vessels the production of bromoform showed a marked decrease (Fig. 5.6). Nitrate was added to the *C. neogracile_cf* culture vessels on the fifth day of sampling. Consequently the cultures were not in nitrate limitation and no further bromoform measurements were taken for *C. neogracile_cf*. The total amount of bromoform measured from each of the duplicate flasks decreased to a mean of 6.71 mol l^{-1} from the mean of 8.88 mol l^{-1} recorded during the exponential growth phase. The continued growth in the number of cells during this limitation period resulted in a near zero per cell concentration of bromoform by *P. tricornutum*. The negative bromoform per cell values attributed to *P. tricornutum* in the nitrate limited phase are not significant. Elevated bromoform concentrations in the seawater controls masked any possible production by the diatom *P. tricornutum* under nitrate limitation. The masking of bromoform in the culture vessels suggests that this diatom probably did not produce any bromoform while under nitrate limitation.

An inverse relationship between bromoform and nitrate was observed in the Arctic (Krysell, 1991). It is suggested that this relationship arises from different sources within the region, namely pelagic and benthic microalgae. The low nitrate values occur as a result of microalgal bloom growth, hence producing elevated bromoform mixing ratios (Krysell, 1991). The nitrate concentrations reported by Krysell (1991) seldom drop below 5 μM and so while interesting are not applicable to this study other than during the exponential growth phase.

Different phases of the bloom cycle have been linked with varying bromoform release rates. A maximum production rate is reported for the exponential growth phase with a decrease during the senescent phase of

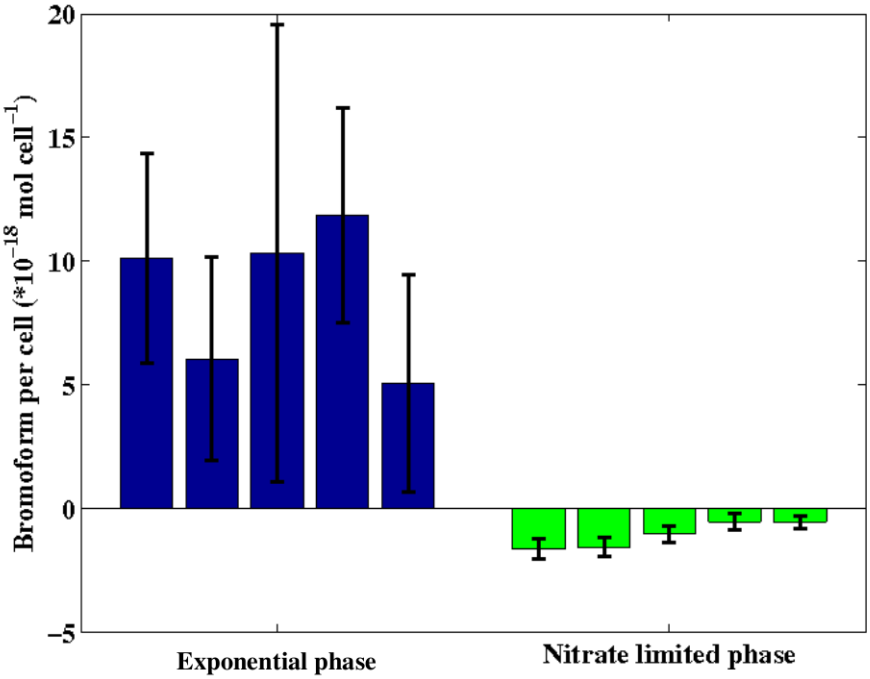

Figure 5.6: Bromoform concentration taken on different days during exponential growth phase (blue) and NO_3 limitation experiment (green) for *P. tricornutum* cultures.

the bloom cycle (Roy et al., 2011; Tokarczyk and Moore, 1994; Quack and Wallace, 2003). The specific growth rates for the *P. tricornutum* and *C. neogracile_cf* diatoms grown for this study decreased during the limitation phases; however, the species remained growing. It is suggested that nutrient limitation might force cells to enter premature senescence (Kuilman et al., 2010), which may account for a portion of the decreased bromoform recorded during the nitrate limitation experiment. The decreased growth rate may be due to imbalances in certain metabolic pathways within the microalgae. These affected pathways include photosynthesis, CO_2 fixation, increased energy demand, and a reduced ability to eliminate oxidative stressors (Bucciarelli and Sunda, 2003). A decrease in the rate of photosynthesis due to nutrient limitation will result in an increase in ROS concentrations including H_2O_2 and therefore should raise bromoform concentrations. The biochemical pathway described above (Reaction 5.1 – 5.3) may be limited by the concentration of either H_2O_2 or DOM (Lin and Manley, 2012). Although ROS concentrations were elevated during the nitrate limitation experiment almost no bromoform was produced by *P. tricornutum* during the this phase. This suggests that the BrPO enzyme pathway is not utilised during this stress as it is dependent on limited resources required for growth.

An increase in the bromoform per cell concentration would be expected if bromoperoxidase was used as an anti-oxidant in these cells during the two oxidative stress experiments. BrPO is used in cells to remove reactive oxygen species, notably hydrogen peroxide (H_2O_2) generated from photosynthesis. The lack of increase in bromoform may be due to these species not utilising the enzyme for this purpose. Bromoperoxidase is a large enzyme that requires a great deal of nutrients in order to function efficiently, particularly nitrate (Littlechild et al., 2009; Johnson et al., 2011). The carbon and nitrate limitations

may impede the efficiency of this enzyme, or in the face of nutrient limitation, cells may opt not to use BrPO as a defence mechanism against the oxidative stress. An alternative anti-oxidant pathway might be utilised during these limitation oxidative stress experiments. Testing of well known anti-oxidants such as ascorbate peroxidase, iodine, glutathione or alternate anti-oxidants such as DMSP should be done to elucidate the full anti-oxidant mechanisms of microalgae (Bucciarelli and Sunda, 2003; Küpper et al., 2008).

It has been suggested that the BrPO enzyme is found near the surface of the microalgae and not buried deep within the workings of the cell (Wever et al., 1991). It has further been suggested that this BrPO may be released to the ocean upon cell death or lysing of the cells, releasing the BrPO into the ocean. It has been argued that this BrPO may react with DOM in the ocean providing an abiotic source of bromoform to the atmosphere. In the coastal Pacific the maximum abiotic rate of production of the order of 1000 $f$mol l^{-1} hr^{-1} has been recorded (Lin and Manley, 2012; Wever et al., 1991). The total and per cell production rates of bromoform recorded during the limitation experiments were found to decrease with increasing limitation. If abiotic production were occurring it would be noted by an increase in the total amount of bromoform and possibly in the controls. An increase in the controls was not noticed. Therefore, it can be concluded that in this experiment the dominant form of bromoform production occurred via biotic pathways involving BrPO.

Due to increased warming of the ocean surfaces, it is suggested that the ocean is becoming increasingly stratified (Behrenfeld et al., 2006; Carpenter et al., 2011). The ocean stratification will probably lead to a decrease in the primary production by diatoms that relies on nutrients, which will not be replenished. The increased oxidative stress caused by nutrient limitation may have a significant impact on global bromoform production, especially in the tropics. As discussed in the Chapters 1 and 4, bromoform produced in the tropics is reported to be a significant source of inorganic bromine in the upper troposphere and lower stratosphere (Dvortsov et al., 1999; Quack and Wallace, 2003; Carpenter et al., 2012). A decrease in bromoform from this region would lead to a positive feedback in climate change which could be significant. Although these experiments suggest that bromoform production decreases under nutrient limitation, other species may display an alternate response. Alternate anti-oxidant systems such as iodine or DMS may also be used instead of BrPO when diatoms are placed under oxidative stress. These anti-oxidant systems may be linked with climate change through the formation of new particles and the CLAW hypothesis, respectively (Küpper et al., 2008; Bucciarelli and Sunda, 2003; von Glasow, 2007).

5.4 Conclusions

The production of bromoform by two diatom species placed under nutrient limitation and under axenic conditions is described here. Carbon and nitrate limitation were used to induce an oxidative stress in the diatoms *Phaeodactylum tricornutum* and *Chaetoceros neogracile_cf.* The cultures were grown in a f/2 medium under a saturating cool white light at approximately 21 °C. Seawater collected from False Bay was filtered and sterilised in order to make the f/2 medium. Gas tight glass bottles were used to culture

the diatoms to ensure bromoform was not lost to the atmosphere. During the exponential growth phase macronutrients were added on a daily basis to ensure the maximum possible growth rate. The nutrient limitations were achieved by the addition of 5 M NaOH to induce CO_2 limitation and the cultures were grown into nitrate limitation. The axenicity of the cultures was assessed daily by testing a small aliquot of culture in bactopeptone. The cultures remained bacteria free for the duration of the nutrient limitation experiments. Bromoform concentrations were measured at discrete points in the exponential growth and nutrient limited phases.

The accurate measurement of bromoform in the culture vessels was limited by the high bromoform concentrations recorded in the seawater controls. This reduced the precision of the measurement of bromoform in the cultures during these experiments and therefore makes the drawing of conclusions difficult. However, statistically significant concentrations of bromoform were quantified during the exponential growth stage of the two species of diatoms tested. Furthermore, the per cell concentration of bromoform decreased for all species during the nutrient limitation. The decrease was statistically significant (α = 0.05) for *P. tricornutum* in both limitation experiments with virtually no bromoform produced by this species under nitrate limitation.

During the exponential growth phase the per cell production of bromoform was lower but at the same order of magnitude as previous studies on polar species (Fig. 5.4). A higher rate of bromoform production was recorded for *C. neogracile_cf* than *P. tricornutum* during the exponential growth phase, which is probably due to the smaller cell size and faster growth rate of the former. The rate of production was found to be similar between the species during the carbon limitation experiment.

The dominant mechanism of bromoform production in red and brown macroalgae is thought to involve the bromoperoxidase enzyme. It is a pity that monetary and time constraints did not allow for the investigation of the existence and function of vanadium BrPO in these species of microalgae. The BrPO enzyme reduces hydrogen peroxide and in the process releases HOBr, which reacts with dissolved organic matter producing brominated-DOM. The partial decay of the DOM(Br) results in the formation of bromoform. The experiments here aimed to induce an oxidative stress on two species of bromoform-producing diatoms (*P. tricornutum* and *C. neogracile_cf*) by means of nutrient limitation. The cultures were grown in gas tight glass bottles under saturating light. The response in bromoform production was during the exponential growth phase and nutrient limitations was monitored.

The decrease in bromoform production may be a function of decreased photosynthetic rate in response to the nutrient stress. The bromoperoxidase enzyme requires a great deal of nitrogen in order to function effectively. This study suggests that the diatoms used in this experiment do not utilise the BrPO as an anti-oxidant under these nutrient limiting experiments. An alternate anti-oxidant pathway that is less dependent on carbon or nitrate such as DMSP or iodine might be utilised to mediate the effect of the oxidative stress. It is of importance that the mechanisms regulating the production of bromoform be understood. Increasing stratification in the ocean is thought to lead to reduced microalgal abundance due

to decreased nitrate in the upper ocean. The reduced nitrate may initially result in an oxidative stress on the microalgae and therefore, as observed in this study, reduce bromoform concentrations leading to a positive feedback to climate change.

Chapter 6

Discussion and summary

6.1 Introduction

Bromoform plays a central role in the biogeochemical cycling of bromine through the Earth system. Following the formation of bromoform in the surface ocean by macro- and microalgae, the dominant proportion is rapidly transferred to the atmosphere. Bromoform, particularly in the tropical atmosphere, is thought to be the dominant source of inorganic bromine in the upper troposphere / lower stratosphere region, and contributes to the catalytic destruction of ozone at this level. Inorganic bromine at the tropopause is thought to have a greater ozone depletion potential than CFCs and long-lived halocarbons. This suggests that bromoform may result in a negative feedback to climate change through the destruction of ozone in the upper troposphere (Dvortsov et al., 1999; Saiz-Lopez et al., 2012). Bromoform production around southern Africa could, consequently, be of great global interest and importance. Globally the contribution of bromoform from macro- and microalgae are thought to be similar and result in a mean annual source strength of 10 (3 – 22) Gmol $CHBr_3$ (Quack and Wallace, 2003). This estimate is, however, constrained by the limited number of bromoform measurements globally. Sunlight and oxidative stress have been shown to result in the formation of bromoform in macro- and microalgae. This formation of bromoform is thought to involve the reduction of H_2O_2 by means of the bromoperoxidase enzyme found in most macro- and microalgae. Though it should be noted that the exact mechanisms of bromoform production, especially in microalgae, are not fully understood or characterised, it is generally thought that the bromoperoxidase enzyme plays a central role. While this study presented a prime opportunity to investigate the potential role of haloperoxidase in the formation of bromoform in microalgae, the resources available did not allow for further investigation. A more in-depth investigation of the potential role of haloperoxidase enzymes on the formation of bromoform in microalgae should be performed.

The research described here examined three key areas (described below) regarding the quantitative detection of bromoform in the marine boundary layer surrounding Cape Point and the role of nutrient limitation in the production of bromoform from diatom species. A GC-ECD system with a custom-built developed thermal desorption unit was developed at the University of Cape Town for the detection and quantification of bromoform in environmental air samples. Using this system, measurements of

bromoform were taken at Cape Point during the austral spring of 2011. This dataset represents the first extended dataset made at this location or in southern Africa. The changes in the bromoform production rate by diatom species were measured under potentially climate-relevant nutrient limitations. Nutrient limitation has been shown to induce oxidative stress in microalgae.

6.1.1 GC system and method

A gas chromatography system and method were developed for the detection and quantification of bromoform at environmental concentrations. A pre-existing GC-ECD was used as the core of the system. The GC oven was able to achieve the temperatures required to efficiently separate bromoform from a mixed sample. A maximum rate of heating of 65 °C min^{-1} meant that the oven was heated to fixed temperatures at predefined times to form a temperature programme. The electron capture detector (ECD) was maintained at 300 °C and supplied with nitrogen make-up gas at 30 m*l* min^{-1}. A DB-624 capillary column was used with helium carrier gas maintained at a flow rate of 5 m*l* min^{-1}. This achieved a bromoform retention time of approximately 14 minutes.

Samples were introduced to the GC from the custom-built thermal desorption unit (TDU) by means of a manual six-port selection valve. The TDU housed a glass tube into which adsorbents (9 mg Carboxen 1016 and Carbopack X) were packed, which when cooled trapped halocarbons from the passing air stream. This had the effect of pre-concentrating bromoform from the air prior to analysis. The flow rate through the TDU for sampling was regulated to 100 m*l* min^{-1} by an ASM mass flow controller for 15 minutes, resulting in 1.5 *l* sample volumes. This is smaller than the breakthrough volume on this system and therefore these samples sizes are suitable for the trapping of air samples. Air samples were drawn in by means of a piston pump and chemically dried before passing onto the pre-concentration trap.

Injected samples were re-focused at the head of the column in order to achieve high quality chromatography. A 'freeze-out' loop was immersed in liquid nitrogen for the duration of the desorption of the sample from the TDU. A custom computer graphical user interface (GUI) was developed for the import of data to the computer from the analogue output of the ECD. The data were displayed in real-time and stored for later analysis. Calibration of the system was performed by permeation oven. Fixed volume aliquots of bromoform in nitrogen were introduced to the GC via the TDU. Repeated injection of aliquots from the permeation oven prior to injection into the GC allowed a range of mixing ratios to be tested. The resulting peak area was integrated by the trapezium method in MATLAB. A precision of 12.7 % and limit of detection of 0.73 ± 0.09 ppt were found for the system.

6.1.2 Bromoform detection and quantification at Cape Point

The GC system described above was deployed to Cape Point in austral spring to quantify bromoform from environmental air samples. The measurements recorded at Cape Point represent the first extended series of bromoform measurements taken in this region. During the experimental period (October / November 2011), bromoform mixing ratios were detected ranging from 2.29 to 84.7 ppt with a mean of 24.7 ppt.

Episodic extremes resulted in bromoform mixing ratios above 60 ppt at detected at Cape Point and are probably driven by the simultaneous influence of multiple sources, something which uniquely happens at this location. It is suggested that the dominant source at Cape Point was from the extensive local macroalgae beds and results in mixing ratios that are consistent with recently published reports for similar regions (Pyle et al., 2011; Zhou et al., 2008).

Air masses arriving at Cape Point from the southern Benguela, the Southern Ocean and local macroalgae beds make this a unique location to sample for atmospheric trace gases. Variations in the bromoform source associated with wind speed and direction may be the dominant driver of the observed variability in mixing ratios at Cape Point. Two dominant wind directions prevailed during the sampling period: north-westerly and south-easterly winds bringing air from the southern Benguela and Southern Ocean, respectively. Changes in the sea-air flux and accumulation rate in the atmosphere are associated with wind speed, with low gas exchange at low wind speed but high accumulation rates. Low wind speeds have been suggested to result in local sources dominating due to the smaller fetch (Quack and Suess, 1999).

The variability observed in the bromoform mixing ratio measurements could not be explained by any single variable. The testing of hypotheses of known drivers of bromoform variability failed to yield a clear understanding of the fluctuations in the mixing ratios observed. Some hypotheses explored known stimuli of bromoform production at varying lags, while others examined sinks. Neither the production nor destruction processes were able to suitably explain the variability in bromoform mixing ratios observed at Cape Point. It is possible that an, as yet, unidentified mechanism is responsible for the fluctuations in bromoform mixing ratios observed at Cape Point. Back trajectories highlight the complex factors at play in this region and an extended dataset might reveal the processes resulting in the elevated mixing ratios and variability observed.

6.1.3 Laboratory culture experiments

Nitrate and carbon limitation were used to induce an oxidative stress in the axenic marine diatoms *Phaeodaytlum tricornutum* and *Chaetoceros neogracile_cf* in order to asses the effect of this stress. The cultures were grown under a continuous cool white light (180 μmol photons m^{-2} s^{-1}) at approximately 21 °C. An f/2 medium made up from filtered and sterilised False Bay seawater was used as the base substrate for the cultures. Axenicity within the cultures was maintained through the use of a regularly sterilised laminar flow hood and equipment. The absence of bacteria was assessed by testing aliquots of culture medium in bactopeptone. The measurement of bromoform was performed at discrete points in the exponential growth and nutrient limited phases.

Gaseous bromoform was extracted from aliquots of culture medium by sparging in glass 'cold-traps' with nitrogen (Grade 5.0) for 5 minutes at 100 m*l* min^{-1}. The exhaust of the sparged gas was trapped on TDU adsorbent beds maintained at laboratory temperature. Samples were stored in the dark at 4 °C and analysed on the GC-ECD system described above within 6 hours. Elevated bromoform concentrations

were recorded in the seawater controls. It is hypothesised that this bromoform originates from the False Bay collection site. This introduced a great deal of uncertainty into the measurements. The mean of the blank was removed from the measurement of bromoform from the culture and if this calculated value was smaller than the confidence interval (95 %) of the blanks then the value was discarded.

A per cell increase in bromoform concentrations was recorded in both diatom species during the exponential growth phase. However, in both experiments and for both species, per cell concentrations of bromoform showed a statistically significant decrease after the initiation of oxidative stress. The decrease in bromoform production may be a result of decreased activity in the BrPO enzyme due to nutrient limitation. The BrPO enzyme is expensive in both carbon and nitrate and may be cut off under nutrient limitation. The requirement of nitrogen for the full functioning of this enzyme suggests that under nitrate limitation it was shut down. Alternate anti-oxidant systems such as iodine and DMSP, that are less dependent on nitrogen, may be utilised in this case. Understanding the effect of climate relevant oxidative stress pathways on the production of bromoform by diatoms might enable a greater insight into likely consequences under climate change scenarios. This might be particularly important in coastal upwelling regions that are dominated by diatoms.

6.2 Recommendations

The project described here lends itself to a number of possible future projects, which would each contribute greatly to the global understanding of bromoform mixing ratios in the atmosphere. Improvements to the infrastructure to facilitate an increased concentration of measurements over longer time spans could shed light on important processes within the southern African and Southern Ocean environments. This section outlines a number of possible areas that would advance the global knowledge of bromoform in the southern African environment.

6.2.1 GC system and method

The infrastructure and expertise developed in this project provides the mechanism to begin addressing further questions regarding halocarbons at Cape Point and in the southern African atmosphere. These questions are likely to be interesting to scientists and the public. Addressing these questions might lead to a greater understanding of climate related processes surrounding halocarbons, which is potentially of global importance. To really address questions relating to halocarbon or bromoform fluctuations within the atmosphere at Cape Point, a continuation of the development of the GC system should be performed. The GC system should be automated to ensure a discrete measurement time series is produced. This should include all phases of the method and process, which might necessitate further development of the TDU. An automated GC system could then be used to collect data over longer time periods with precise spaces in the sampling time.

A commercially available TDU with sample rosette might be purchased. A sampling rosette coupled with numerous TD adsorbent traps could lead to field campaigns addressing many specific questions without having to move the GC, thereby saving cost and effort. Once the GC system is able to run autonomously an expansion of the detectable halocarbons would be insightful. This expansion of detectable halocarbons might illuminate not only interactions between halocarbons but local driving mechanisms of bromoform variability. The permeation oven was designed with redundant capacity to easily be expanded to calibrate mixed and multiple gases.

Of considerable importance, especially in this region, is the training of future scientists. This might be achieved using the GC-ECD system described here as a training platform in the background to a commercially purchased system. The use of the GC developed here would allow students to develop the skills required to develop new components as needed, while the data from a newer system might be used for training in analytical techniques relating to atmospheric chemistry.

6.2.2 Cape Point

There are many projects that are worthy of examining further as they could each lead to a greater understanding of the dynamics of climate change, achieved through the understanding of the variability of bromoform in the atmosphere at Cape Point. A longer time series of discrete bromoform mixing ratio measurements at Cape Point would be of great value to scientists globally. Such a time series would lead to a greater understanding of the mechanisms of variability found at Cape Point. Utilising this understanding of the variability and driving mechanisms found at Cape Point could contribute to the identification of a number of key processes. The diurnal cycle, interactions between local and anthropogenic sources, and the role of the Benguela and the Southern Ocean on mixing ratios measured at Cape Point might all be unravelled. Examination of the diurnal and seasonal cycles could be of great interest, highlighting sources and strengths. Changes in these patterns over time might indicate a shift in source and therefore have an impact on climate change. This change in climate could be through a decrease in tropospheric ozone depletion or through a change in a source of bromoform. Changes on a diurnal scale might indicate changes in weather patterns or longer-term climate shifts. Local variability may result in a larger signal than global or regional climate change, thus suppressing the longer-term signal.

To date no study has a been made on the production rates of halocarbons by the species of macroalgae found around Cape Point. Extracting information regarding the conditions and rates at which these species produce halocarbons could lead to a greater understanding of the proportion of local sources on total halocarbon measurement. Understanding the rate and variability of local bromoform production could lead to a deeper understanding of the influence of the Benguela and Southern Ocean on halocarbon mixing ratios at Cape Point and consequently globally. These mixing ratios might play a significant, as yet undetermined role in climate change. Of particular importance might be the quantification of the mean release rate of bromoform from the decay of these macroalgae species. During the winter months a great deal of macroalgae is washed ashore and left to decay along the beaches surrounding Cape Point.

The decay of macroalgae and subsequent bromoform release might be an unrecognised source to the atmosphere. It is likely only to operate on a very local scale, but may still make a significant contribution to the atmospheric loading of bromoform at Cape Point. On this note, the measurement of other halocarbons such as dibromomethane might be of great interest. Nothing is known about the production mechanism of this halocarbon. It has come to light that subsequent to the completion of the work presented here the CO values used in the analysis had been cleaned of any anthropogenic influence. It is recommended that this new CO dataset be used in any further work or analysis of the bromoform measurements at Cape Point.

The regression model tested would be greatly enhanced by an extensive, discrete bromoform mixing ratio dataset (Chapter 4.5.5). This model might then be used in a predictive capacity to help identify new sources of bromoform to the atmosphere or changes in sources' strengths. Understanding the changes in the sources' strength might assist in understanding the southern African influence on bromine mediated stratospheric ozone depletion. With improvements the model could be used to provide a source strength parameterisation to larger global chemistry models.

Mercury depletion events have been noted at Cape Point and in the Antarctic (Brunke et al., 2010). It is thought that these depletion events may be triggered by short-lived halocarbons in the atmosphere; however, this is not necessarily the dominant process at Cape Point (Brunke et al., 2010). Concomitant decreases in ozone and mercury are not observed at Cape Point as they are in the polar regions. This suggests that an alternate chemistry process is involved in the mercury depletion events at Cape Point. Data here suggest that this uncharacterised chemistry process may be initiated by halogen and bromine chemistry. A better understanding of the dynamics and fluctuations of bromoform in the atmosphere at Cape Point might identify some of the processes which result in these mercury depletion events. Coupled with this, a study of the mercury speciation at Cape Point may provide an understanding of the atmospheric chemistry leading to the mercury depletion events.

6.2.3 Laboratory culture experiments

The scope of this project was restricted to the testing of only two species of diatoms under two nutrient limited oxidative stresses. An expansion of the number of species tested and the extent of oxidative stresses used could lead to interesting insights. It may be particularly important to use climate relevant limitations in order to fully understand possible future changes in bromoform production rates. Variations in the nutrient limited oxidative stresses may elicit differing responses in alternate microalgal species. Different species of microalgae may produce bromoform or other halocarbons as a consequence of anti-oxidative capacity. It would be of great benefit to examine numerous anti-oxidant systems known to exist in microalgae, such as iodine or DMS. This testing for other anti-oxidants along with a greater suite of short-lived biogenic halocarbons may illustrate the preferred 'coping mechanism' of phytoplankton when faced with these stresses. Understanding the possible response of microalgae to certain naturally occurring conditions may lead to a better forecast of climate change or biotic response to changes.

It is estimated that half the global bromoform source strength is from the release by microalgae. Any variations in the rate of production could therefore have significant ramifications. By examining the response mechanism of microalgae to various nutrient limited oxidative stresses, the complete processes of bromoform production may be identified. The understanding of these processes, coupled with global measurements could shed light on the global contribution by microalgae to the source strength.

6.2.4 Closing remarks

The recommendations described above encompass a large scope of work that can be achieved with this system and should be investigated. The first step should either be to automate the GC system used for bromoform measurement or replace it with a newer device capable of automated measurement. This would ensure that a longer and more consistent data set of measurements could be achieved. The quantitative detection of bromoform at Cape Point in air samples is of great importance and should continue. An extensive dataset would be invaluable. Furthermore, understanding the strength of the local macroalgal source and a better means of separating sources should be explored. A greater understanding of the local sources and their strengths would feed back into a better estimate of the global source strength and therefore its impact on the climate and ozone concentrations. It would be of of great interest to know what percentage, if any, of the bromoform and other halocarbons released from around southern Africa reach the stratosphere. Understanding or establishing the nature of anti-oxidant pathway(s) utilised for different species of microalgae is probably the most important thing that should be achieved. It should be a priority to determine if any species of microalgae produce bromoform when exposed to nitrate limitation. Given that the ocean might experience increasing nitrate limitation due to climate change, it may be of great interest to know the probable microalgal response and hence possible feedbacks into said climate change.

References

Abrahamsson, K., Choo, K.-S., Pedersén, M., Johansson, G., and Snoeijs, P. (2003). Effects of temperature on the production of hydrogen peroxide and volatile halocarbons by brackish-water algae. *Phytochemistry*, 64:725–734.

Abrahamsson, K., Lorén, A., Wulff, A., and Wängberg, S.-Å. (2004). Air-sea exchange of halocarbons: the influence of diurnal and regional variations and distribution of pigments. *Deep Sea Research Part II*, 51(22-24):2789–2805.

Alonso-Sáez, L., Waller, A. S., Mende, D. R., Bakker, K., Farnelid, H., Yager, P. L., Lovejoy, C., Tremblay, J.-É., Potvin, M., Heinrich, F., Estrada, M., Riemann, L., Bork, P., Pedrós-Alió, C., and Bertilsson, S. (2012). Role for urea in nitrification by polar marine archaea. *Proceedings of the National Academy of Sciences*, 109(44):17,989–17,994.

Andreae, M. O., Atlas, E. L., Harris, G. W., Helas, G., de Kock, A., Koppmann, R., Maenhaut, W., Manø, S., Pollock, W. H., J, R., Scharffe, D., Schebeske, G., and Welling, M. (1996). Methyl halide emissions from savanna fires in southern Africa. *Journal of Geophysical Research*, 101(D19):23,603–23,613.

Andrews, S. J., Jones, C. E., and Carpenter, L. J. (2013). Aircraft measurements of very short-lived halocarbons over the tropical Atlantic Ocean. *Geophysical Research Letters*, 40(5):1005–1010.

Aschmann, J., Sinnhuber, B.-M., Chipperfield, M. P., and Hossaini, R. (2011). Impact of deep convection and dehydration on bromine loading in the upper troposphere and lower stratosphere. *Atmospheric Chemistry and Physics*, 11(6):2671–2687.

Asher, W. and Wanninkhof, R. (1998). Transient tracers and air-sea gas transfer. *Journal of Geophysical Research*, 103(C8):15,939–15,958.

Barrie, L. A., Bottenheim, J. W., Schnell, R. C., Crutzen, P. J., and Rasmussen, R. A. (1988). Ozone destruction and photochemical reaction at polar sunrise in the lower arctic atmosphere. *Nature*, 334:138–141.

Barrie, L. A. and Platt, U. (1997). Arctic tropospheric chemistry: an overview. *Tellus*, 49(B):450–454.

Bartual, A., Gálvez, J. A., and Ojeda, F. (2008). Phenotypic response of the diatom *Phaeodactylum tricornutum* bohlin to experimental changes in the inorganic carbon system. *Botanica Marina*, 51:350–359.

Behrenfeld, M. J., O'Malley, R. T., Siegel, D. A., McClain, C. R., Sarmiento, J. L., Feldman, G. C., Milligan, A. J., Falkowski, P. G., Letelier, R. M., and Boss, E. S. (2006). Climate-driven trends in contemporary ocean productivity. *Nature*, 444:752–755.

Berg, W. W., Heidt, L. R. E., Pollock, W. H., Sperry, P. D., Cicerone, R. J., and Gladney, E. S. (1984). Brominated organic species in the Arctic atmosphere. *Geophysical Research Letters*, 11(5):429–432.

Branch, G. M., Griffiths, C. L., Branch, M. L., and Beckley, L. E. (2010). *Two Oceans - A guide to the marine life of southern Africa*. Struik Nature, 80 McKenzie St, Cape Town 8001.

Bravo-Linares, C. M. and Mudge, S. M. (2008). Temporal trends and identification of the sources of volatile organic compounds in coastal seawater. *Journal of Environmental Monitoring*, 11:628–641.

Bridgeman, C. H., Pyle, J. A., and Schallcross, D. E. (2000). A three-dimensional model calculation of the ozone depletion potential of 1-bromopropane (1-C_3H_7Br). *Journal of Geophysical Research*, 105(D21):26,493–26,502.

Brunke, E. G., Labuschagne, C., Ebinghaus, R., Kock, H. H., and Slemr, F. (2010). Gaseous elemental mercury depletion events observed at Cape Point during 2007-2008. *Atmospheric Chemistry and Physics*, 10:1121–1131.

Brunke, E. G., Labuschagne, C., Parker, B., Scheel, H. E., and Whittlestone, S. (2004). Baseline air mass selection at Cape Point, South Africa: application of ^{222}Rn and other filter criteria to CO_2. *Atmospheric Environment*, 38(33):5693–5702.

Bucciarelli, E. and Sunda, W. G. (2003). Influence of CO_2, nitrate, phosphate, and silicate limitation on intracellular dimethylsulfoniopropionae in batch cultures of the coastal diatom *Thalassiosira pseudonana*. *Limnology and Oceanography*, 48(6):2256–2265.

Bucciarelli, E., Sunda, W. G., Belviso, S., and Sarthou, G. (2007). Effect of the diel cycle on production of dimethlysulfoniopropionate in batch cultures of *Emiliania huxleyi*. *Aquatic Microbiala Ecology*, 48:73–81.

Butler, J. H., King, D. B., Lobert, J. M., Montzaka, S. A., Yvon-Lewis, S. A., Hall, B. D., Warwick, N. J., Mondeel, D. J., Aydin, M., and Elkins, J. W. (2007). Oceanic distributions and emissions of short-lived halocarbons. *Global Biogeochemical Cycles*, 21(1):1–11.

Carpenter, L. J., Archer, S. D., and Beale, R. (2012). Ocean-atmosphere trace gas exchange. *Chemical Society Reviews*, 41(19):6473–6506.

Carpenter, L. J., Fleming, Z. L., Read, K. A., Lee, J. D., Moller, S. J., Hopkins, J. R., Purvis, R. M., Lewis, A. C., Müller, K., Heinold, B., Herrmann, H., Fomba, K. W., Pinxteren, D., Müller, C., Tegen, I., Wiedensohler, A., Müller, T., Niedermeier, N., Achterberg, E. P., Patey, M. D., Kozlova, E. A., Heimann, M., Heard, D. E., Plane, J. M. C., Mahajan, A. S., Oetjen, H., Ingham, T., Stone, D., Whalley, L. K., Evans, M. J., Pilling, M. J., Leigh, R. J., Monks, P. S., Karunaharan, A., Vaughan, S., Arnold, S. R.,

Tschritter, J., Pöhler, D., Frieß, U., Holla, R., Mendes, L. M., Lopez, H., Faria, B. V. E., Manning, A. J., and Wallace, D. W. R. (2011). Seasonal characteristics of tropical marine boundary layer air measured at the Cape Verde Atmospheric Observatory. *Journal of Atmospheric Chemistry*, 67(2-3):87–140.

Carpenter, L. J., Jones, C. E., Dunk, R. M., Hornsby, K. E., and Woeltjen, J. (2009). Air-sea fluxes of biogenic bromine from the tropical North Atlantic Ocean. *Atmospheric Chemistry and Physics*, 9:1805–1816.

Carpenter, L. J. and Liss, P. S. (2000). On temperate sources of bromoform and other reactive organic bromine gases. *Journal of Geophysical Research*, 105(D16):20,539–20,547.

Carpenter, L. J., Malin, G., Liss, P. S., and Küpper, F. C. (2000). Novel biogenic iodine-containing trihalomethanes and other short-lived halocarbons in the coastal East Atlantic. *Global Biogeochemical Cycles*, 14(4):1191–1204.

Carpenter, L. J., Sturges, W. T., Penkett, S. A., Liss, P. S., Alicke, B., Hebestreit, K., and Platt, U. (1999). Short-lived alkyl iodides and bromides at Mace Head, Ireland: Links to biogenic sources and halogen oxide production. *Journal of Geophysical Research*, 104(D1):1679–1689.

Carpenter, L. J., Wevill, D. J., Hopkins, J. R., Dunk, R. M., Jones, C. E., Hornsby, K. E., and McQuaid, J. B. (2007a). Bromoform in tropical Atlantic air from 25°N to 25°S. *Geophysical Research Letters*, 34(L11810):1–5.

Carpenter, L. J., Wevill, D. J., Palmer, C. J., and Michels, J. (2007b). Depth profiles of volatile iodine and bromine-containing halocarbons in Antarctic waters. *Marine Chemistry*, 103:227–236.

Chatfield, C. (2003). *The Analysis of Time Series: An introduction, Sixth Edition*. Chapman & Hall/CRC, Boca Raton London New York Washington, D.C.

Chin, M., Jacob, D. J., Munger, J. W., Parrish, D. D., and Doddridge, B. G. (1994). Relationship of ozone and carbon monoxide over North America. *Journal of Geophysical Research*, 99(D7):14,565–14,573.

Christie, W. W. (1989). *Gas Chromatography and Lipids*. Oily Press Ltd.

Chuck, A. L., Turner, S. M., and Liss, P. S. (2005). Oceanic distributions and air-sea fluxes of biogenic halocarbons in the open ocean. *Journal of Geophysical Research*, 110(C10):C10022.

Class, T. and Ballschmiter, K. (1987). Chemistry of organic traces in air IX*: evidence of natural marine sources for chloroform in regions of high primary production. *Analytical Chemistry*, 327:40–41.

Class, T. H. and Ballschmiter, K. (1988). Chemistry of organic traces in air. *Journal of Atmospheric Chemistry*, 6:35–46.

Collén, J., Ekdahl, A., Abrahamsson, K., and Pedersén, M. (1994). The involvement of hydrogen peroxide in the production of volatile halogenated compounds by *Meristiella gelidium*. *Phytochemistry*, 36(5):1197–1202.

Colomb, A., Yassaa, N., Williams, J., Peeken, I., and Lochte, K. (2008). Screening volatile organic compounds (VOCs) emissions from five marine phytoplankton species by head space gas chromatography/mass spectrometry (HS-GC/MS). *Journal of Environmental Monitoring*, 10(3):325–330.

Cota, G. F. and Sturges, W. T. (1997). Biogenic bromine production in the Arctic. *Marine Chemistry*, 56:181–192.

Cowling, R. M. and Pressey, R. L. (2003). Introduction to systematic conservation planning in the cape floristic region. *Biological Conservation*, 112(1-2):1–13.

Cox, M. L., Sturrock, G. A., Fraser, P. J., Siems, S. T., and Krummel, P. B. (2005). Identification of regional sources of methyl bromide and methyl iodide from AGAGE observations at Cape Grim, Tasmania. *Journal of Atmospheric Chemistry*, 50:59–77.

Crutzen, P. J. (2006). Albedo enhancement by stratospheric sulphur injections. a contribution to resolve a policy dilemma? an editorial essay. *Climatic Change*, pages 211–219.

Dienért, F. and Wandenbulcke, F. (1923). On the determination of silica in water. *Comptes Rendus Chimie*, 176:1478–1480.

Douglas, T. A., Domine, F., Barret, M., Anastasio, C., Beine, H. J., Bottenheim, J., Grannas, A., Houdier, S., Netcheva, S., Rowland, G., Staebler, R., and Steffen, A. (2012). Frost flowers growing in the Arctic ocean-atmosphere-sea ice-snow interface: 1. Chemical composition. *Journal of Geophysical Research*, 117(D00R09).

Dvortsov, V. L., Geller, M. A., Solomon, S., Schauffler, S. M., Atlas, E. L., and Blake, D. R. (1999). Rethinking reactive halogen budgets in the midlatitude lower stratosphere. *Geophysical Research Letters*, 26(12):1699–1702.

Ekdahl, A., Pedersén, M., and Abrahamsson, K. (1998). A study of the diurnal variation of biogenic volatile halocarbons. *Marine Chemistry*, 63:1–8.

Emmert, G., Brown, M., Simone Jr, P., Geme, G., and Cao, G. (2007). *Methods for Real-Time Measurement of THMs and HAAs in Distribution Systems, Part 2*. IWA Publishing.

Farman, J. C., Gardiner, B. G., and Shanklin, J. D. (1985). Large losses of total ozone in Antarctica reveal seasonal ClO_x/NO_x interaction. *Nature*, 315:207 – 210.

Fawcett, A., Pitcher, G. C., Bernard, S., Cembella, A. D., and Kudela, R. M. (2007). Contrasting wind patterns and toxigenic phytoplankton in the southern benguela upwelling system. *Marine Ecology Progress Series*, 348:19–31.

Fuhlbrügge, S., Krüger, K., Quack, B., Atlas, E. L., Hepach, H., and Ziska, F. (2013). Impact of the marine atmospheric boundary layer conditions on vsls abundances in the eastern tropical and subtropical north atlantic ocean. *Atmospheric Chemistry and Physics*, 13:6345–6357.

Galbally, I. E., Bentley, S. T., and Meyer, C. P. M. (2000). Mid-latitude marine boundary-layer ozone destruction at visible sunrise observed at cape grim, tasmania, 41°S. *Geophysical Research Letters*, 27(23):3841–3844.

Goldman, J. C., Azov, Y., Riley, C. B., and Dennett, M. R. (1982). The effect of ph in intensive microalgal cultures. i. biomass regulation. *Journal of Experimental Marine Biology and Ecology*, 57(1):1–13.

Goodwin, K. D., North, W. J., and Lidstrom, M. E. (1997). Production of bromoform and dibromomethane by giant kelp: Factors affecting release and comparison to anthropogenic bromine sources. *Limnology and Oceanography*, 42(8):1725–1734.

Google (2014). Cape point, satellite imagery. https://maps.google.com/maps?q=Cape+Point,+Cape+Town,+South+Africa&hl=en&ll=-34.350239,18.481064&spn=0.379255,0.614548&sll=-34.32756,18.660278&sspn=1.517424,2.458191&oq=Cape&t=h&hnear=Cape+Point,+Cape+Town,+Western+Cape,+South+Africa&z=11.

Granier, C., Pétron, G., Müller, J.-F., and Brasseur, G. (2000). The impact of natural and anthropogenic hydrocarbons on the tropospheric budget of carbon monoxide. *Atmospheric Environment*, 34:5255–5270.

Grasshoff, K., Ehrhardt, M., and Kremling, K. (1983). *Methods of seawater analysis*. Verlag Chemie, Weinheim, Germany.

Grasshoff, K., Kremling, K., and Ehrhardt, M., editors (2009). *Methods of Seawater Analysis*. Wiley-VCH.

Greenfield, L. J. and Kalbar, F. A. (1954). Inorganic phosphate measurements in sea water. *Bulletin of Marine Science*, 4(4):323–335.

Gregory, G. L., Fuelberg, H. E., Longmore, S. P., Anderson, B. E., Collins, J. E., and Blake, D. R. (1996). Chemical characteristics of tropospheric air over the tropical South Atlantic Ocean: Relationship to trajectory history. *Journal of Geophysical Research*, 101:23–23.

Gschwend, P. M., MacFarlane, J. K., and Newman, K. A. (1985). Volatile halogenated organic compounds released to seawater from temperate marine macroalgae. *Science*, 227(4690):1033–1035.

Guillard, R. R. L. (1975). *Culture of marine invertebrate animals*, chapter Culture of phytoplankton for feeding marine invertebrates, pages 29–60. Plenum Publishers.

Guillard, R. R. L. and Ryther, J. H. (1962). Studies of marnie plankton diatoms. I. *Cycltella nana* hustedt and *Detonula confervacea* cleve. *Canadian Journal of Microbiology*, 8:229–239.

Hense, I. and Quack, B. (2009). Modelling the vertical distribution of bromoform in the upper water column of the tropical Atlantic Ocean. *Biogeosciences*, 6:535–544.

Hill, V. and Manley, S. L. (2009). Release of reactive bromine and iodine from diatoms and its possible role in halogen transfer in polar and tropical oceans. *Limnology and Oceanography*, 54(3):812–822.

Ho, D. T., Law, C. S., Smith, M. J., Schlosser, P., Harvey, M., and Hill, P. (2006). Measurements of air-sea gas exchange at high wind speeds in the Southern Ocean: Implications for global parameterizations. *Geophysical Research Letters*, 33(16):L16611.

Hossaini, R., Chipperfield, M. P., Monge-Sanz, B., Richards, N. A. D., Atlas, E. L., and Blake, D. R. (2010). Bromoform and dibromomethane in the tropics: a 3-D model study of chemistry and transport. *Atmospheric Chemistry and Physics*, 10:719–735.

Hossaini, R., Mantle, H., Chipperfield, M. P., Montzaka, S. A., Hamer, P., Ziska, F., Quack, B., Krüger, K., Tegtmeier, S., Atlas, E. L., Sala, S., Engel, A., Bönisch, H., Keber, T., Oram, D. E., Mills, G., Ordonez, C., Saiz-Lopez, A., Warwick, N. J., Liang, Q., Feng, W., Moore, F., Miller, B. R., Marécal, V., Richards, N. A. D., Dorf, M., and Pfeilsticker, K. (2013). Evaluating global emission inventories of biogenic bromocarbons. *Atmospheric Chemistry and Physics*, 13:11819–11838.

Hughes, C., Chuck, A. L., Rossetti, H., Mann, P. J., Turner, S. M., Clarke, A. D., Chance, R., and Liss, P. S. (2009). Seasonal cycle of seawater bromoform and dibromomethane concentrations in a coastal bay on the western Antarctic Peninsula. *Global Biogeochemical Cycles*, 23(2):GB2024.

Hutchings, L., van der Lingen, C., Shannon, L. J., Crawford, R. J. M., Verheye, H. M. S., Bartholomae, C. H., van der Plas, A. K., Louw, D., Ostrowski, M., Fidel, Q., Barlow, R. G., Lamont, T., Coetzee, J., Shillington, F. A., Veitch, J., Currie, J. C., and Monteiro, P. M. S. (2009). The benguela current: An ecosystem of four components. *Progress in Oceanography*, 83:15–32.

Itoh, N. and Shinya, M. (1994). Seasonal evolution of bromomethanes from coralline algae (Corallinaceae) and its effect on atmospheric ozone. *Marine Chemistry*, 45:95–103.

Jacob, D. J. (1999). *Introduction to Atmospheric Chemistry*. Princeton University Press.

Jennings, S., Kaiser, M. J., and Reynolds, J. D. (2001). *Marine Fisheries Ecology*. Blackwell Scientific Publishers.

Johnson, T. L., Palenik, B., and Brahamsha, B. (2011). Characterization of a functional vanadium-dependent bromoperoxidase in the marine cyanobacterium *Synechococcus* sp. CC9311. *Phycological Society of America*, 42:792–801.

Jones, C. E., Andrews, S. J., Carpenter, L. J., Hogan, C., Hopkins, F. E., Laube, J. C., Robinson, A. D., Spain, T. G., Archer, S. D., Harris, N. R. P., Nightingale, P. D., O'Doherty, S. J., Oram, D. E., Pyle, J. A., Butler, J. H., and Hall, B. D. (2011). Results from the first national UK inter-laboratory calibration for very short-lived halocarbons. *Atmospheric Measurement Techniques*, 4(5):865–874.

Jury, M. R. (1984). *Wind shear and differential upwelling along the S W tip of Africa*. PhD thesis, University of Cape Town.

Kasibhatla, P., Chameides, W. L., Saylor, R. D., and Olerud, D. (1998). Relationships between regional ozone pollution and emissions of nitrogen oxides in the eastern United States. *Journal of Geophysical Research*, 103(D17):22,663–22,669.

Khalil, M. A. K., Rasmussen, R. A., and Hoyt, S. D. (1983). Atmospheric chloroform ($CHCl_3$): ocean-air exchange and global mass balance. *Tellus*, 35B:266–274.

Kim, P. S., Jacob, D. J., Warner, J. X., Yang, K., and Chance, K. (2013). Global ozone-CO correlations from OMI and AIRS: constraints on tropospheric ozone sources. *Atmospheric Chemistry and Physics*, 13:8901–8937.

Kolb, B. (1999). Headspace sampling with capillary columns. *Journal of Chromatography A*, 842:163–205.

Krysell, M. (1991). Bromoform in the Nansen Basin in the Arctic Ocean . *Marine Chemistry*, 33:187–197.

Kudela, R., Pitcher, G., Probyn, T., Figueiras, F., Moita, T., and Trainer, V. (2005). Harmful algal blooms in coastal upwelling systems. *Oceanography*, 18(2):184–197.

Kuilman, T., Michaloglou, C., Mooi, W. J., and Peeper, D. S. (2010). The essence of senescence. *Genes & Development*, 24:2463–2479.

Küpper, F. C., Carpenter, L. J., McFiggans, G. B., Palmer, C. J., Waite, T. J., Boneberg, E.-M., Woitsch, S., Weiller, M., Abela, R., Gromlimund, D., Potin, P., Butler, A., Luther, III, G. W., Kroneck, P. M. H., Meyer-Klaucke, W., and Feiters, M. C. (2008). Iodine accumulation provides kelp with an inorganic antioxidant impacting atmospheric chemistry. *Proceedings of the National Academy of Sciences*, 105(19):6954–6958.

Kuyper, B., Labuschagne, C., Philibert, R., Moyo, N., Waldron, H., Reason, C., and Palmer, C. (2012). Development of a Simplified, Cost Effective GC-ECD Methodology for the Sensitive Detection of Bromoform in the Troposphere. *Sensors*, 12(10):13583–13597.

Laturnus, F. (1996). Volatile halocarbons released from Arctic macroalgae. *Marine Chemistry*, 55:359–366.

Lee, K.-J., Pyo, H., Park, S.-J., Yoo, E.-A., and Lee, D.-W. (2001). A study on purge efficiency in purge and trap analysis of VOCs in water. *Bulletin-Korean Chemical Society*, 22(2):171–178.

Lin, C. Y. and Manley, S. L. (2012). Bromoform production from seawater treated with bromoperoxidase. *Limnology and Oceanography*, 57(6):1857–1866.

Liss, P. S. and Merlivat, L. (1986). *The role of air-sea exchange in geochemical cycling*, chapter Air-sea gas exchange rates: Introduction and synthsis, pages 113–127. Springer, New York.

Liss, P. S. and Slater, P. G. (1974). Flux of gases across the air-sea interface. *Nature*, 247:181–184.

Littlechild, J., Rodriguez, E. G., and Isupov, M. (2009). Vanadium containing bromoperoxidase - Insights into the enzymatic mechanism using X-ray crystallography. *Journal of Inorganic Biochemistry*, 103:617–621.

Liu, Y., Yvon-Lewis, S. A., Hu, L., Salisbury, J. E., and O'Hern, J. E. (2011). $CHBr_3$, CH_2Br_2, and $CHClBr_2$ in U.S. coastal waters during the Gulf of Mexico and east coast carbon cruise. *Journal of Geophysical Research*, 116(C10):1–10.

Lovelock, J. E. (1959). Gas chromatography of hydrocabons using capillary columns and ionising detectors. *Analytical Chemistry*, 31(4):619–621.

Lovelock, J. E. (1963). Electron absorption detectors and technique for use in quantitative and qualitative analysis by gas chromatography. *Analytical Chemistry*, 35(4):474–481.

Manley, S. L. and Barbero, P. (2001). Physiological constraints on bromoform ($CHBr_3$) production by *Ulva lactuca* (Chlorophyta). *Limnology and Oceanography*, 46(6):1392–1399.

Manley, S. L., Goodwin, K. D., and North, W. J. (1992). Laboratory production of bromoform, methylene bromide, and methyl iodide by macroalgae and distribution in nearshore southern California waters. *Limnology and Oceanography*, 38(8):1652–1659.

Marécal, V., Pirre, M., Krysztofiak, G., Hamer, P. D., and Josse, B. (2012). What do we learn about bromoform transport and chemistry in deep convection from fine scale modelling? *Atmospheric Chemistry and Physics*, 12(14):29561–29600.

Martens-Habbena, W., Berube, P. M., Urakawa, H., de la Torre, J. R., and Stahl, D. A. (2009). Ammonia oxidation kinetics determine niche separation of nitrifying archaea and bacteria. *Nature*, 461:976–979.

Mattsson, E. (2013). *On biogenic halocarbons in Antarctic waters*. PhD thesis, University of Gothenburg.

McGivern, W. S., Francisco, J. S., and North, S. W. (2002). Investigation of the atmospheric oxidation pathways of bromoform: Initiation via OH/Cl reactions. *The Journal of Physical Chemistry*, 103(26):6395–6400.

Molina, M. J. and Rowland, F. S. (1974). Stratospheric sink for chlorofluromethanes: chlorine atomc-atalysed destruction of ozone. *Nature*, 249:810 – 812.

Monson, R. K., Stidham, M. A., Williams III, G. J., Edwards, G. E., and Uribe, E. G. (1982). Temperature dependence of photosynthesis in *Agropyron smithii* Rydb. *Plant Physiology*, 69:921–928.

Moore, R. M. (2003). Marine sources of volatile organohalogens. *The Handbook of Environmental Chemistry*, 3(P):85–101.

Moore, R. M. and Groszko, W. (1999). Methyl iodide distribution in the ocean and fluxes to the atmosphere. *Journal of Geophysical Research*, 104(C5):11.163–11.171.

Moore, R. M., Webb, M., Tokarczyk, R., and Wever, R. (1996). Bromoperoxidase and iodoperoxidase enzymes and production of halogenated methanes in marine diatom cultures. *Journal of Geophysical Research*, 101(C9):20,899–20,908.

Moyo, N. C. (2010). Links between fynbos biomass burning and release of bromoform ($CHBr_3$) Into the atmosphere. Master's thesis, University of Cape Town.

Mtolera, M. S. P., Collén, J., Pedersén, M., Ekdahl, A., Abrahamsson, K., and Semesi, A. K. (1996). Stress-induced production of volatile halogenated organic compounds in *Eucheuma denticulatum(Rhodophyta)* caused by elevated pH and high light intensities. *European Journal of Phycology*, 31(1):89–95.

Murphy, J. and Riley, J. (1958). A single-solution method for the determination fo soluble phosphate in sea water. *Journal of the Marine Biological Association of the United Kingdom*, 37(1):9–14.

Nguvava, M. (2012). The effect of nutrient limitation and oxidative stress on bromoform production from axenic cultures of marine diatoms. Master's thesis, University of Cape Town.

Nic, N., Jirat, J., and Kosata, B. (1997). *IUPAC Compendium of Chemical Technology*. Blackwell Scientific Publishers, Oxford, UK.

Nielsen, J. E. and Douglass, A. R. (2001). A simulation of bromoform's contribution to stratospheric bromine. *Journal of Geophysical Research*, 106(D8):8089–8100.

Nightingale, P. D. (2009). *Surface Ocean-Lower Atmopshere Processes*, chapter Air-Sea Gas Exchange, pages 69–98. American Geophysical Union.

Nightingale, P. D., Malin, G., Law, C. S., Watson, A. J., Liss, P. S., Liddicoat, M. I., Boutin, J., and Upstill-Goddard, R. C. (2000). In situ evaluation of air-sea gas exchange parameterizations using novel conservative and volatile tracers. *Global Biogeochemical Cycles*, 14(1):373–387.

Nightingale, P. D., Malin, G., and Liss, P. S. (1995). Production of chloroform and other low-molecular-weight halocarbons by some species of macroalgae. *Limnology and Oceanography*, 40(4):680–689.

Novelli, P. C., Masarie, K. A., and Lang, P. M. (1998). Distributions and recent changes of carbon monoxide in the lower troposphere. *Journal of Geophysical Research*, 103(D15):19,015–19,033.

Oatley, T. B. and Underhill, L. G. (2001). Distances moved and elapsed times between ringing and recovery for three *Ploceus* weavers in southern Africa. *Ostrich*, 72(1-2):41–44.

O'Brien, L. M., Harris, P., Robinson, A. D., Gostlow, B., Warwick, N. J., Yang, X., and Pyle, J. A. (2009). Bromocarbons in the tropical marine boundary layer at the Cape Verde Observatory- measurements and modelling. *Atmospheric Chemistry and Physics*, 9(22):9083–9099.

Palmer, C. J. (2006). *A study of the distribution and origin of volatile halogenated organic compounds in the troposphere and oceans*. PhD thesis, University of York.

Palmer, C. J., Anders, T. L., Carpenter, L. J., Küpper, F. C., and McFiggans, G. B. (2005). Iodine and halocarbon response of *Laminaria digitata* to oxidative stress and links to new particle production. *Environmental Chemistry*, 2:282–290.

Palmer, C. J. and Reason, C. J. C. (2009). Relationships of surface bromoform concentrations with mixed layer depth and salinity in the tropical oceans. *Global Biogeochemical Cycles*, 23(GB2014):1–10.

Paul, C. and Pohnert, G. (2011). Production and role of volatile halogenated compounds from marine algae. *Natural Product Reports*, 28(2):186.

Pedersén, M., Collén, J., Abrahamsson, K., and Ekdahl, A. (1996). Production of halocarbons from seaweeds: an oxidative stress reaction? *Scientia Marina*, 60:257–263.

Peschak, T. P. (2005). *Currents of Contrast - life in southern Africa's two oceans*. Struik Nature, Cape Town, South Africa.

Philibert, R. (2010). Development of carbon adsorbents towards the quantitative measurement of bromoform concentrations in false bay air samples. Honour's Thesis, Department of Chemistry, Univeristy of Cape Town.

Pitcher, G., Brown, P. C., and Mitchell-Innes, B. A. (1992). Spatio-temporal variability of phytoplankton in the southern benguela upwelling system. *South African Journal of Marine Science*, 12(1):439–456.

Pitcher, G. and Calder, D. (2000). Harmful algal blooms of the southern benguela current: a review and appraisal of monitoring from 1989 to 1997. *South African Journal of Marine Science*, 22(1):255–271.

Plass-Dülmer, C., Michl, K., Ruf, R., and Berresheim, H. (2002). C_2-c_8 hydrocarbon measurement and quality control procedures at the global atmospheric watch observatory hohenpeissenberg. *Jounral of Chromatography A*, 953:175–197.

Poole, C. F. (2003). *The Essence of Chromatography*. Elsevier B.V., Sara Burgerhartsraat 25, Amsterdam, The Netherlands.

Probyn, T. A. (1992). The inorganic nitrogen nutrition of phytoplankton in the southern benguela: new production, phytoplankton size and implications for pelagic foodwebs. *South African Journal of Marine Science*, 12(1):411–420.

Pyle, J. A., Ashfold, M. J., Harris, N. R. P., Robinson, A. D., Warwick, N. J., Carver, G. D., Gostlow, B., O'Brien, L. M., Manning, A. J., Phang, S. M., Yong, S. E., Leong, K. P., Ung, E. H., and Ong, S. (2011). Bromoform in the tropical boundary layer of the Maritime Continent during OP3. *Atmospheric Chemistry and Physics*, 11(2):529–542.

Pyle, J. A., Harris, N. R. P., Robinson, A. D., Gostlow, B., O'Brien, L. M., Ashfold, M. J., Carver, G. D., Warwick, N. J., Manning, A. J., Yong, S. E., Peng, L. K., Ung, H. E., and Ong, S. (2010). Bromoform in the tropical boundary layer of the Maritime Continent during OP3: the contrast between coast and rainforest. *Atmospheric Chemistry and Physics Discussions*, 10(6):14969–14991.

Quack, B., Atlas, E. L., Petrick, G., Schauffler, S. M., and Wallace, D. W. R. (2004). Oceanic bromoform sources for the tropical atmosphere. *Geophysical Research Letters*, 31(L23S05):1–4.

Quack, B., Atlas, E. L., Petrick, G., and Wallace, D. W. R. (2007). Bromoform and dibromomethane above the Mauritanian upwelling: Atmospheric distributions and oceanic emissions. *Journal of Geophysical Research*, 112(D9):D09312.

Quack, B. and Suess, E. (1999). Volatile halogenated hydrocarbons over the western Pacific between 43° and 4°N. *Journal of Geophysical Research*, 104(D1):1663–1678.

Quack, B. and Wallace, D. W. R. (2003). Air-sea flux of bromoform: Controls, rates, and Implications. *Global Biogeochemical Cycles*, 17(1):1–27.

Read, K. A., Mahajan, A. S., Carpenter, L. J., Evans, M. J., Faria, B. V. E., Heard, D. E., Hopkins, J. R., Lee, J. D., Moller, S. J., Lewis, A. C., Mendez, L., McQuaid, J. B., Oetjen, H., Saiz-Lopez, A., Pilling, M. J., and Plane, J. M. C. (2008). Extensive halogen-mediated ozone destruction over the tropical Atlantic Ocean. *Nature*, 453:1232–1235.

Robarts, R. D. and Zohary, T. (1987). Temperature effects on photosynthetic capacity, respiration and growth rates of bloom-forming cyanobacteria. *New Zealand Journal of Marine and Freshwater Research*, 21:391–399.

Roy, R., Pratihary, A., Narvenkar, G., Mochemadkar, S., Gauns, M., and Naqvi, S. W. A. (2011). The relationship between volatile halocarbons and phytoplankton pigments during a *Trichodesmium* bloom in the coastal eastern Arabian Sea. *Estuarine, Coastal and Shelf Science*, 95(1):110–118.

Saiz-Lopez, A., Lamarque, J., Kinnison, D. E., Tilmes, S., Ordonez, C., Orlando, J. J., Conley, A. J., Plane, J. M. C., Mahajan, A. S., Sousa Santos, G., Atlas, E. L., Blake, D. R., Sander, S. P., Schauffler, S. M., Thompson, A. M., and Brasseur, G. (2012). Estimating the climate significance of halogen-driven ozone loss in the tropical marine troposphere. *Atmospheric Chemistry and Physics*, 12(9):3939–3949.

Saiz-Lopez, A., Plane, J. M. C., and Shillito, J. A. (2004). Bromide oxide in the mid-latitude marine boundary layer. *Geophysical Research Letters*, 31(L03111):1–4.

Sarthou, G., Timmermans, K. R., Blain, S., and Tréguer, P. (2005). Growth physiology and fate of diatoms in the ocean: A review. *Journal of Sea Research*, 53(1):25–42.

Scarratt, M. G. and Moore, R. M. (1996). Production of methyl chloride and methyl bromide in laboratory cultures of marine phytoplankton. *Marine Chemistry*, 54:263–272.

Schall, C., Heumann, K. G., De Mora, S., and Lee, P. A. (1996). Biogenic brominated and iodated organic compounds in ponds on the McMurdo Ice Shelf, Antarctica. *Antarctic Science*, 8(1):45–48.

Seibert, P., Beyrich, F., Gryning, S. E., Joffre, S., Rasmussen, A., and Tercier, P. (2000). Review and intercomparison of operational methods for the determination of the mixing height. *Atmospheric Environment*, 34(7):1001–1027.

Seidel, D. J., Ao, C. O., and Li, K. (2010). Estimating climatological planetary boundary layer heights from radiosonde observations: Comparison of methods and uncertainty analysis. *Journal of Geophysical Research*, 115(D16):D16113.

Shannon, L. and Nelson, G. (1996). *The South Atlantic: Present and Past Circulation*, chapter The Benguela: Large Scale Features and Processes and System Variability, pages 163–210. Springer-Verlag.

Shaw, M. (2011). *Sources of Organic and Inorganic Halogens to the Polar and Temperate Marine Boundary Layer*. PhD thesis, University of Chemistry.

Sherman, L. S., Blum, J. D., Douglas, T. A., and Steffen, A. (2012). Frost flowers growing in the Arctic ocean-atmosphere-sea ice-snow interface: 2. Mercury exchange between the atmosphere, snow, and frost flowers. *Journal of Geophysical Research*, 117:D00R10.

Simmonds, P. G., Fenimore, D. C., Pettitt, B. C., Lovelock, J. E., and Zlatkis, A. (1976). Design of a nickle-63 electron absorption detector and analytical significance of high temperature operation. *Analytical Chemistry*, 39(12):1428–1433.

Singleton, A. T. and Reason, C. J. C. (2007). Variability in the characteristics of cut-off low pressure systems over subtropical southern africa. *International Journal of Climatology*, 27:295 – 310.

Sinnhuber, B.-M. and Folkins, I. (2005). Estimating the contribution of bromoform to stratospheric bromine and its relation to dehydration in the tropical tropopause layer. *Atmospheric Chemistry and Physics Discussions*, 5:12,939–12,956.

Sinnhuber, B.-M. and Folkins, I. (2006). Estimating the contribution of bromoform to stratospheric bromine and its relation to dehydration in the tropical tropopause layer. *Atmospheric Chemistry and Physics*, 6:4755–4761.

Sorensen, A. L. (2011). *Gaseous mercury in the marine boundary layer: Measurements and modeling*. PhD thesis, National Environmental Research Institute.

Strickland, J. D. H. and Parsons, T. R. (1965). *A manual of sea water analysis. 2^{nd} ed.* Fisheries Research Board of Canada.

Sturges, W. T., Cota, G. F., and Buckley, P. T. (1992). Bromoform emission from Arctic ice algae. *Nature*, 358(6388):660–662.

Sturges, W. T., Cota, G. F., and Buckley, P. T. (1997). Vertical profiles of bromoform in snow, sea ice, and seawater in the Canadian Arctic. *Journal of Geophysical Research*, 102(C11):25,073–25,083.

Sturges, W. T., Oram, D. E., Carpenter, L. J., and Penkett, S. A. (2000). Bromoform as a source of stratospheric bromine. *Geophysical Research Letters*, 27(14):2081–2084.

Sturges, W. T., Sullivan, C. W., Schnell, R. C., Heidt, L. r. E., and Pollock, W. H. (1993). Bromoalkane production by Antarctic ice algae. *Tellus*, 45(B):120–126.

Sunda, W. G. and Huntsman, S. A. (1995). Iron uptake and growth limitation in oceanic and coastal phytoplankton. *Marine Chemistry*, 50:189–206.

Sunda, W. G., Kieber, D. J., Kiene, R. P., and Huntsman, S. (2002). An antioxidant function for DMSP and DMS in marine algae. *Nature*, 418:317–320.

Tanhua, T., Fogelqvist, E., and Bastürk, Ö. (1996). Reduction of volatile halocarbons in anoxic seawater, results from a study in the black sea. *Marine Chemistry*, 54:159–170.

Tegtmeier, S., Kruger, K., Quack, B., Pisso, I., Stohl, A., and Yang, X. (2012). Bridging the gap between bromocarbon oceanic emissions and upper air concentrations. *Atmospheric Chemistry and Physics Discussions*, 12(2):4477–4505.

Tokarczyk, R. and Moore, R. M. (1994). Production of volatile organohalogens by phytoplankton cultures. *Geophysical Research Letters*, 21(4):285–288.

Tyson, P. D. and Preston-Whyte, R. A. (2000). *The weather and climate of southern Africa*. Oxford University Press, Cape Town.

Underhill, L. G. and Bradfield, D. (2005). *Introstat*. Juta Academic, Cape Town, South Africa.

Urias, K. R. (2002). Experimental studies in temperature programmed gas chromatography. Master's thesis, Virginia Polytechnic Institute and State University, Blacksburg, VA.

van Hofsten, A. and Pedersén, M. (1978). Bromine in red algae. *Journal of Ultrastructural Research*, 63(1):108–109.

Vardi, A., Berman-Frank, I., Rozenberg, T., Hadas, O., Kaplan, A., and Levine, A. (1999). Programmed cell death of the dinoflagellate *Peridinium gatunense* is mediated by CO_2 limitation and oxidative stress. *Current Biology*, 9(18):1061–1064.

Vingarzan, R. (2004). A review of surface ozone background levels and trends. *Atmospheric Environment*, 38:3431–3442.

von Glasow, R. (2007). A look at the claw hypothesis from an atmospheric chemistry point of view. *Research Front*, 4:379–381.

von Glasow, R. (2008). Sun, sea and ozone destruction. *Nature*, 453:1195 – 1196.

von Glasow, R. and Crutzen, P. J. (2003). Tropospheric halogen chemistry. *Treatise on Geochemistry*, 4:21–64.

von Glasow, R., von Kuhlmann, R., Lawrence, M. G., Platt, U., and Crutzen, P. J. (2004). Impact of reactive bromine chemistry in the troposphere. *Atmospheric Chemistry and Physics*, 4:2481–2497.

Voulgarakis, A., Telford, P. J., Aghebo, A. M., Braesicke, P., Faluvegi, G., Abraham, N. L., Bowman, K. W., Pyle, J. A., and Shindell, D. T. (2011). Global multi-year O_3-CO correlation patterns from models and TES satellite observations. *Atmospheric Chemistry and Physics*, 11:5819–5838.

Wada, S. and Hama, T. (2012). *Advanced Gas Chromatography - Progress in Agricultural, Biomedical and Industrial Applications*, chapter Application of Gas Chromatography to Exuded Organic Matter Derived from Macroalgae, pages 307–322. InTech.

Wanninkhof, R. (1992). Relationship between wind speed and gas exchange. *Journal Geophysical Research*, 97(C5):737–782.

Wanninkhof, R. and McGillis, W. R. (1999). A cubic relationship between air-sea CO_2 exchange and wind speed. *Geophysical Research Letters*, 26(13):1889–1892.

Warwick, N. J., Pyle, J. A., Carver, G. D., Yang, X., Savage, N. H., O'Connor, F. M., and Cox, R. A. (2006). Global modeling of biogenic bromocarbons. *Journal of Geophysical Research*, 111(D24):D24305.

Weinberger, F., Coquempot, B., Forner, S., Morin, P., Kloareg, B., and Potin, P. (2007). Different regulation of haloperoxidation during agar oligosaccharide-activated defence mechanisms in two related red algae, *Gracilaria sp.* and *Gracilaria chilensis*. *Journal of Experimental Botany*, 58(15/16):4365–4372.

Wever, R., Tromp, M. G. M., Krenn, B. E., and Marjani, A. (1991). Brominating Activity of the Seaweed *Ascophyllum nodosum*: Impact on the Biosphere. *Environmental Science and Technology*, 25:446–449.

Wever, R. and Van der Horst, M. A. (2013). The role of vanadium haloperoxidases in the formation of volatile brominated compounds and their impact on the environment. *Dalton Transactions*, 42(33):11,778–11,786.

Wevill, D. J. and Carpenter, L. J. (2004). Automated measurement and calibration of reactive volatile halogenated organic compounds in the atmosphere. *Analyst*, 129:634–638.

Whittlestone, S. and Zahorowski, W. (1998). Baseline radon detectors for shipboard use: Development and deployment in the first aerosol characterization experiment (ACE 1). *Journal of Geophysical Research*, 103(D13):16,743–16,751.

WMO (2011). *Scientific Assessment of Ozone Depletion: 2010, Global Ozone Research and Monitoring Project-Report No. 52*. World Meteorological Organisation, Geneva, Switzerland.

Wuchter, C., Abbas, B., Coolen, M. J. L., Herfort, L., van Bleijswijk, J., Timmers, P., Strous, M., Teira, E., Herndl, G. J., Middleberg, J. J., Schouten, S., and Sinninghe Damsté, J. S. (2006). Archaeal nitrification in the ocean. *Proceedings of the National Academy of Sciences*, 103(33):12317–12322.

Yang, X., Cox, R. A., Warwick, N. J., Pyle, J. A., Carver, G. D., O'Connor, F. M., and Savage, N. H. (2005). Tropospheric bromine chemistry and its impacts on ozone: A model study. *Journal of Geophysical Research*, 110(D23311):1–18.

Yokouchi, Y., Hasebe, F., Fujiwara, M., Takashima, H., Shiotani, M., Nishi, N., Kanaya, Y., Hashimoto, S., Fraser, P. J., Toom-Sauntry, D., Mukai, H., and Nojiri, Y. (2005). Correlations and emission ratios among bromoform, dibromochloromethane, and dibromomethane in the atmosphere. *Journal of Geophysical Research*, 110(D23):D23309.

Yokouchi, Y., Mukai, H., Yamamoto, H., Otsuki, A., Saitoh, C., and Nojiri, Y. (1997). Distribution of methyl iodide, ethyl iodide, bromoform, and dibromomethane over the ocean (east and southeast Asian seas and the western Pacific). *Journal of Geophysical Research*, 102(D7):8805–8809.

Zhou, Y., Mao, H., Russo, R. S., Blake, D. R., Wingenter, O. W., Haase, K. B., Ambrose, J., Varner, R. K., Talbot, R. W., and Sive, B. C. (2008). Bromoform and dibromomethane measurements in the seacoast region of New Hampshire, 2002-2004. *Journal of Geophysical Research*, 113(D8):D08305.

Ziska, F., Quack, B., Abrahamsson, K., Archer, S. D., Atlas, E. L., Bell, T. G., Butler, J. H., Carpenter, L. J., Jones, C. E., Harris, N. R. P., Hepach, H., Heumann, K. G., Hughes, C., Kuss, J., Krüger, K., Liss, P. S., Moore, R. M., Orlikowska, A., Raimund, S., Reeves, C. E., Reifenhäuser, W., Robinson, A. D., Schall, C., Tanhua, T., Tegtmeier, S., Turner, S. M., Wang, L., Wallace, D. W. R., Williams, J., Yamamoto, H., Yvon-Lewis, S. A., and Yokouchi, Y. (2013). Global sea-to-air flux climatology for bromoform, dibromomethane and methyl iodide. *Atmospheric Chemistry and Physics*, 13:8915–8934.

Appendix A

Appendix

Reported here is the MATLAB GUI code to connect the ADAM units to the computer and read data into the computer in real time.

```
function varargout = chromat(varargin)
% chromat M-file for chromat.fig
%   chromat, by itself, creates a new chromat or raises the existing
%   singleton*.
%
%   H = chromat returns the handle to a new chromat or the handle to
%   the existing singleton*.
%
%   chromat('CALLBACK',hObject,eventData,handles,...) calls the local
%   function named CALLBACK in chromat.M with the given input arguments.
%
%   chromat('Property','Value',...) creates a new chromat or raises the
%   existing singleton*. Starting from the left, property value pairs are
%   applied to the GUI before chromat_OpeningFunction gets called. An
%   unrecognized property name or invalid value makes property application
%   stop. All inputs are passed to chromat_OpeningFcn via varargin.
%
%   *See GUI Options on GUIDE's Tools menu. Choose "GUI allows only one
%   instance to run (singleton)".
%
% See also: GUIDE, GUIDATA, GUIHANDLES


% Edit the above text to modify the response to help chromat
```

```
% Last Modified by GUIDE v2.5 20-Aug-2013 11:17:00

% Begin initialization code - DO NOT EDIT % This begins setting up the GUI
gui_Singleton = 1;
gui_State = struct('gui_Name',   mfilename, ...
          'gui_Singleton', gui_Singleton, ...
          'gui_OpeningFcn', @chromat_OpeningFcn, ...
          'gui_OutputFcn', @chromat_OutputFcn, ...
          'gui_LayoutFcn', [] , ...
          'gui_Callback', []);
if nargin && ischar(varargin1)
  gui_State.gui_Callback = str2func(varargin1);
end

if nargout
  [varargout1 nargout] = gui_mainfcn(gui_State, varargin:);
else
  gui_mainfcn(gui_State, varargin:);
end
% End initialization code - DO NOT EDIT


% — Executes just before chromat is made visible.
function chromat_OpeningFcn(hObject, eventdata, handles, varargin)
% This function has no output args, see OutputFcn.
% hObject   handle to figure
% eventdata reserved - to be defined in a future version of MATLAB
% handles   structure with handles and user data (see GUIDATA)
% varargin command line arguments to chromat (see VARARGIN)

% Choose default command line output for chromat
handles.output = hObject;

% Update handles structure
guidata(hObject, handles);

% UIWAIT makes chromat wait for user response (see UIRESUME)
% uiwait(handles.figure1);
```

```
% — Outputs from this function are returned to the command line.
function varargout = chromat_OutputFcn(hObject, eventdata, handles)
% varargout cell array for returning output args (see VARARGOUT);
% hObject   handle to figure
% eventdata reserved - to be defined in a future version of MATLAB
% handles   structure with handles and user data (see GUIDATA)

% Get default command line output from handles structure
varargout1 = handles.output;

%f = getimage(h0bject)
%print -deps2 myplot.eps



% — Executes on button press in connect_pushbutton.
function connect_pushbutton_Callback(hObject, eventdata, handles)
% hObject   handle to connect_pushbutton (see GCBO)
% eventdata reserved - to be defined in a future version of MATLAB
% handles   structure with handles and user data (see GUIDATA)
s=serial('/dev/ttyS0'); %open serial connection between PC and ADAM units
set(s,'Terminator','CR');
fopen(s);
fprintf(s,'%0202OB0600'); % connects the ADAM units and interacts settings to be used
% 02 is the hexidecimal address of the ADAM unit
% 02 is the new hexidecimal address of the ADAM unit
% OB is input type 500 mV, OA = 1 V, OC = 150 mV, 09 = 5 V
% 06 is the baud rate 9600
% 00 bit parameter data format

c = clock; % Sets date and time for record purposes
d = datestr(c);

g = get(s,'Status'); % Sets status of the GUI
n=cell2mat(g);

set(handles.time_text,'String',d);
set(handles.connect_pushbutton,'UserData',s);
set(handles.conn_ans_text,'String',n);
```

```
guidata(hObject, handles);

% — Executes on button press in disconn_pushbutton.
function disconn_pushbutton_Callback(hObject, eventdata, handles)
% hObject   handle to disconn_pushbutton (see GCBO)
% eventdata reserved - to be defined in a future version of MATLAB
% handles   structure with handles and user data (see GUIDATA)
s = get(handles.connect_pushbutton,'UserData');
fclose(s)

g = get(s,'Status'); % Gets the status of the connection
n=cell2mat(g);

set(handles.conn_ans_text,'String',n);
set(handles.rec_ans_text,'String','Stopped');

guidata(hObject, handles);

% — Executes on button press in start_pushbutton.
function start_pushbutton_Callback(hObject, eventdata, handles)
% hObject   handle to start_pushbutton (see GCBO)
% eventdata reserved - to be defined in a future version of MATLAB
% handles   structure with handles and user data (see GUIDATA)
s = get(handles.connect_pushbutton,'UserData');
axes(handles.axes1)

tic % Starts the timing clock for the length of the sample run
for j=1:5000
  fprintf(s,'#020'); %writes the command to the ADAM to send data from Channel 0
  x=fscanf(s,'%s'); % Reads the data as a string
  x=x(3:end); % Cuts the first two Characters and leaves the numbers
  out(1,j)=toc/60; % counts the number of loops as they pass
  out(2,j)=str2num(x); % converst the string to a number and saves to the second row of out
  plot(out(1,:),out(2,:),'LineWidth',2); %% Plot Data on fixed set of axies...
  xlim([0 30]); % Sets the x-axis limits
  ylim([0 500]); % Sets the y-axis limits
  set(gca,'XMinorTick','on');
  grid % Plots a grid
  datacursormode on; % Allows mouse clicks on the graph
```

```
  v = get(s,'ValuesReceived');
  m(1,j) = cell2mat(v);
    if length(m)>(length(m)-j)
      rec= 'Recording'; % Sets the status Display to Recording
    else
      rec = 'Stopped'; % Sets the status Display to Stopped
    end
  set(handles.rec_ans_text,'String',rec);
  set(handles.start_pushbutton,'UserData',out);
  cd /home/brett/matlab/data/eleven/
  fout = get(handles.time_text,'String');
  save(fout,'out'); % Saves the data in real-time with the date and time stamp as a file name
  pause(0.25) % Pauses the data collection loop for 0.25 seconds before the next iteration
end

set(handles.rec_ans_text,'String','Stopped');
guidata(hObject, handles);

% — Executes on button press in save_pushbutton. % Plots the data on a set of axes and saves the
figure and data
function save_pushbutton_Callback(hObject, eventdata, handles)
% hObject   handle to save_pushbutton (see GCBO)
% eventdata reserved - to be defined in a future version of MATLAB
% handles   structure with handles and user data (see GUIDATA)
fout = get(handles.time_text,'String');

out = get(handles.start_pushbutton,'UserData');
time = out(1,:);
data = out(2,:);
cd /home/brett/matlab/figures/eleven/
figure
b=plot(time,data);
xlabel('Time (minutes)')
ylabel('Voltage (mV)')
title(fout)
xlim([0 30])
ylim([0 500])
set(gca,'XMinorTick','on');
grid
```

```
% figure(1);text(f(:, 2),f(:, 3),num2str(f(:,1))) % Number the peaks found on the graph
%set(gca,'paperpositionmode','auto')
saveas(b,fout,'jpg');

close

s = get(handles.connect_pushbutton,'UserData');
fclose(s)

g = get(s,'Status');

n=cell2mat(g);

set(handles.conn_ans_text,'String',n);
set(handles.rec_ans_text,'String','Stopped');

guidata(hObject, handles);

% --- Executes on button press in clear_pushbutton.
function clear_pushbutton_Callback(hObject, eventdata, handles)
% hObject    handle to clear_pushbutton (see GCBO)
% eventdata reserved - to be defined in a future version of MATLAB
% handles    structure with handles and user data (see GUIDATA)
s = get(handles.connect_pushbutton,'UserData');
fclose(s)
clear time data j x b c fout f y out d n rec v m
cla
g = get(s,'Status');
n=cell2mat(g);

set(handles.conn_ans_text,'String',n);
set(handles.rec_ans_text,'String','Stopped');

guidata(hObject, handles);

% --- Executes on button press in intergrate_pushbutton.
function intergrate_pushbutton_Callback(hObject, eventdata, handles)
% hObject    handle to intergrate_pushbutton (see GCBO)
% eventdata reserved - to be defined in a future version of MATLAB
```

% handles   structure with handles and user data (see GUIDATA)

Appendix B

Appendix

Subsequent analysis of the relationship between CO, bromoform and radon, using an updated CO dataset, suggests that anthropogenically influenced air masses contribute 26.4 $\pm$ 16.4 ppt to the bromoform loading at Cape Point, compared to 24.0 $\pm$ 17.6 ppt from background air masses. The highest measurements of bromoform at Cape Point were all from background air mass sources. This suggests that anthropogenic influences may be quite large and should be carefully separated from marine air.

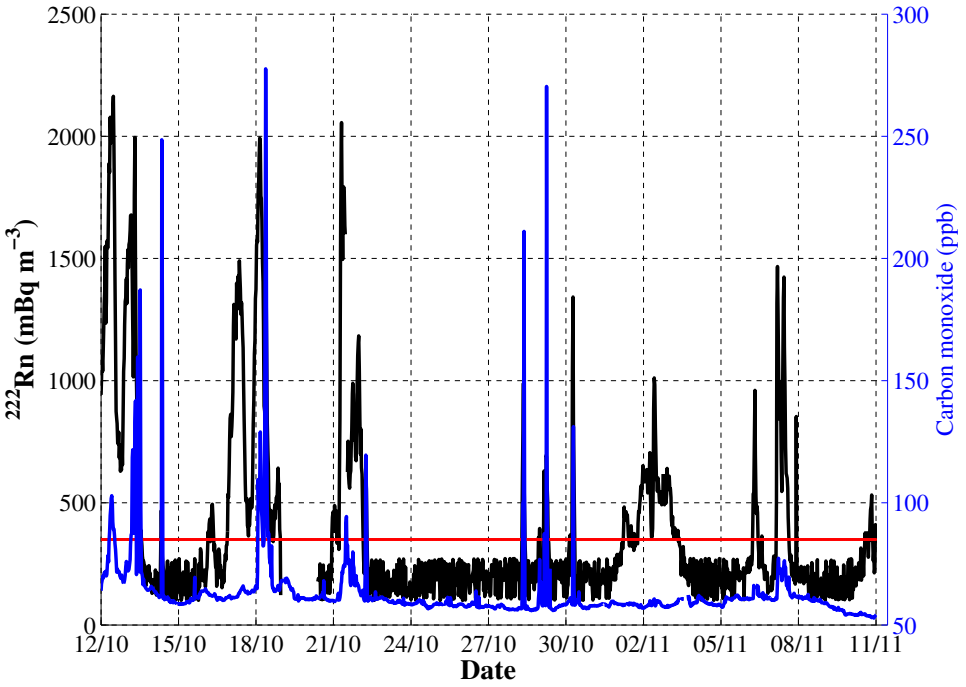

Figure B.1: The UPDATED time evolution of ^{222}Rn and CO measurements at Cape Point during the bromoform experimental period show concurrent elevation events, possibly the introduction of anthropogenically enhanced air masses. Gaps in both data sets are due to the removal of bad data through quality control checks applied by SAWS. Clean marine airs samples are shown by measurements occurring below red line (350 mBq m^{-3}).

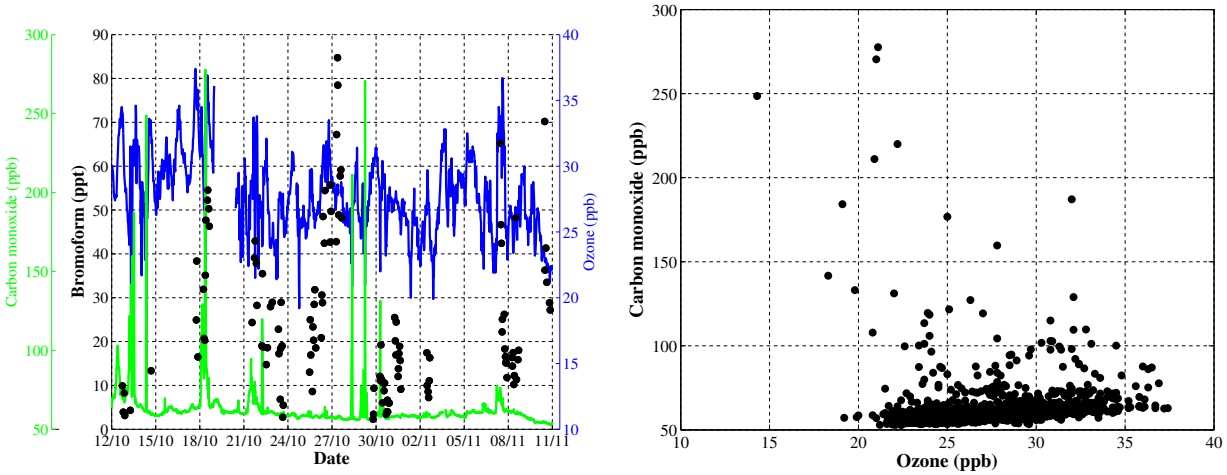

Figure B.2: The UPDATED comparative graphs of background CO (green) and O_3 (blue) (a) over time with bromoform indicated in black, and (b) correlation of CO and O_3 at Cape Point during the bromoform experimental period.